A PHOTOIONIZATION REFLECTRON TIME-OF-FLIGHT INVESTIGATION OF PHOSPHORUS CHEMISTRY IN EXTRATERRESTRIAL ICES

A DISSERTATION SUBMITTED TO THE GRADUATE DIVISION OF THE UNIVERSITY OF HAWAIʻI AT MĀNOA IN PARTIAL FULILLMENT OF THE REQUIREMENTS FOR THE DEGREE OF

DOCTOR OF PHILOSOPHY

IN

CHEMISTRY

MAY 2018

By
Andrew M. Turner

Dissertation Committee:

Ralf I. Kaiser, Chairperson
Joseph T. Jarrett
John Head
Ho Leung Ng
Jeffrey Gillis-Davis

DEDICATION

"non est ad astra mollis e terris via"
~Seneca, in *The Madness of Hercules*

To my grandfather, Hugh, a man of exemplary character and the first person I told that I wanted to grow up to be a scientist.

And to my niece, Lydia, representing future generations, may this dissertation inspire you to reach your full potential.

ACKNOWLEDGMENTS

This research was performed in collaboration of other scientists. The results of theoretical calculations by the group of Dr. Agnes H. H. Chang at the National Dong Hwa University in Taiwan (hhchang@mail.ndhu.edu.tw) are presented in this work, and gas chromatography experiments were performed by Dr. Cornelia Meinert at the Université Côte d'Azur in France (cornelia.meinert@unice.fr). Also, secondary-ion mass spectrometry analyses were carried out by TASCON-USA of New York. All other authors listed are at the University of Hawai'i and assisted me with the experiments described herein.

This dissertation represents the pinnacle of my academic development, and there are numerous people I would like to personally acknowledgment and thank for their assistance, encouragement, and support throughout the years. First and foremost, I want to thank my family, especially my parents, for their unwavering support, no matter which path in life I chose to follow.

During my K-12 years, I'm especially grateful to Bill Hutton and Brenda Wilson, my P.A.C.E. teachers, for nurturing my problem solving and critical thinking skills. My chemistry background began with Randy Sellers, a remarkable and caring teacher whose 6th grade lessons of the periodic table and ionic bonding are still memorable. My chemistry background expanded in high school by the excellent teacher Donald Julian, whose unusually strong background in chemistry enabled different chemistry course offerings during my sophomore, junior, and senior years of high school.

At DePauw University, Dr. Bridget Gourley was an excellent advisor who, along with Dr. Jeanette Pope (née Jerz), provided my first training as a research scientist. This research training was further developed by Dr. David Harvey, who also provided a strong foundation in analytical chemistry. Dr. Richard Martoglio also deserves acknowledgment as my physical chemistry instructor, and all four of these individuals were great mentors and resources for advice.

At Indiana University, I'm especially grateful for Dr. Cathrine Reck, who helped me through uncertain times. I'm also thankful to Dr. Ronald Hites for my first graduate school research experience.

At the University of Hawaii, I would first like to thank my dissertation committee for all their advice over the years: Dr. Jeffrey Gillis-Davis, Dr. John Head, Dr. Joseph Jarrett, and Dr. Ho Leung Ng. My advisor, Dr. Ralf Kaiser, deserves the greatest gratitude, and while he can be tough at times, I can understand the value of never accepting less than perfection. As a friend and colleague, I want to thank Matthew Abplanalp for 5+ years of teamwork and assistance, and Dr. Seol Kim for his initial experimental training. I would also like to thank Dr. Thomas Hemscheidt for all of his advice and patience with my questions. For financial support, I want to thank the University of Hawaii Department of Chemistry for their teaching assistantships and NASA for grant funding for my research assistantships.

Finally, I want to thank my friends during my graduate studies, including Reilly, Charito, Kristen, and Austin.

ABSTRACT

Multiple phosphorus-containing compounds have been detected in the Solar System (planetary atmospheres, comets, meteorites) along with interstellar and circumstellar environments. Of particular astrobiological interest are alkyl phosphonic acids (RH_2PO_3, R = methyl, ethyl, propyl, and butyl) extracted from the Murchison meteorite. These phosphonic acids are the only extraterrestrial phosphorus-containing organic compounds thus far discovered and offer a bioavailable and highly soluble form of phosphorus due to its reduced oxidation state. The research of this dissertation investigates the synthesis of phosphorus-containing products of electron-irradiated interstellar ice analogues containing phosphine (PH_3), water (H_2O), carbon dioxide (CO_2), and hydrocarbons such as methane (CH_4). Phosphine is known to exist in circumstellar envelopes (IRC +10216), is hypothesized to exist in comets (67P/Churyumov-Gerasimenko), and may serve as the phosphorus source of complex organic compounds such as the alkyl phosphonic acids. Utilizing *in situ* analysis techniques such as quadrupole mass spectrometry (QMS), tunable-photoionization reflectron time-of-flight mass spectrometry (PI-ReTOF-MS), and infrared spectroscopy (FTIR) in addition to *ex situ* analysis by secondary-ion mass spectrometry (SIMS) and two-dimensional gas chromatography mass spectrometry (GC×GC-TOF-MS), the intermediates and products of these irradiated ice analogues are characterized to demonstrate the potential to synthesize organic phosphine-containing molecules in astrophysical environments. Notable results include phosphanes (P_xH_{x+2}), methylphosphanes ($CH_3P_xH_{x+1}$), and phosphorus oxoacids (H_3PO_x, x=1–4, and pyrophosphoric acid ($H_4P_2O_7$)) along with their alkylated equivalents such as prebiotically significant methylphosphonic acid ($CH_3P(O)(OH)_2$) and methylphosphate ($CH_3OP(O)(OH)_2$).

TABLE OF CONTENTS

LIST OF TABLES

LIST OF FIGURES

LIST OF ABBREVIATIONS AND SYMBOLS

A/A_{exp} ..... absorption coefficient
ADP ..... adenosine diphosphate
amu ..... atomic mass unit
ATP..... adenosine triphosphate
C..... molar concentration, with units mol cm^{-3}
cm^{-1}..... wavenumber unit (equal to λ^{-1}, where λ is wavelength in cm)
d..... thickness (i.e. of ice)
δ..... deformation vibration
DNA..... deoxyribonucleic acid
eV..... electronvolt, ≈ 1.6×10^{-19} J
Gya..... billion years ago
GC×GC-TOFMS.....two-dimensional time-of-flight mass spectrometry
GCR..... galactic cosmic ray
HeNe..... helium neon (laser type)
FTIR ..... Fourier transform infrared spectroscopy
IE..... ionization Energy
k..... rate constant
L..... pathlength (i.e. of light beam through ice)
λ..... wavelength (i.e. of light)
m ..... number of fringes in interference pattern
M ..... molar mass, with units g mol^{-1}
MS..... mass spectrometry
m/z ..... mass-to-charge
n..... refractive index
N_A ..... Avogadro constant, ≈ 6.02×10^{23} mol^{-1}
Nd:YAG ..... neodymium: yttrium aluminum garnet (laser type)
$\tilde{\nu}$..... Wavenumber, with units cm^{-1} (equal to λ^{-1}, where λ is wavelength in cm)
ν..... normal mode; also stretching vibration
OFHC..... oxygen-free high conductivity (copper)
PI-ReTOF-MS... photoionization reflectron time-of-flight mass spectrometry
QMS..... quadrupole mass spectrometry
ReTOF ..... reflectron time-of-flight (mass spectrometry)
ρ..... density, with units g cm^{-3}
RGA ..... residual gas analyzer
SIMS..... secondary ion mass spectrometry
θ..... degrees of angle
T..... period of interference fringe
TOF-MS..... time-of-flight mass spectrometry
Torr..... a "Torr" is the symbol of "torr", a pressure unit ≈ 133.3 Pa
TPD..... temperature programmed desorption
UHV..... ultrahigh vacuum
UV ..... ultraviolet
VUV ..... vacuum ultraviolet
ω..... wagging vibration; also used for frequency of laser photons

CHAPTER 1
INTRODUCTION

1.1 The Phosphorus Problem

The six elemental building blocks of life include carbon, oxygen, hydrogen, nitrogen, sulfur, and phosphorus. The processes by which these elements first became abiotically incorporated into the first biomolecules have been an active area of research for decades, and while the ultimate destination may never be reached, the journey has continued to advance knowledge in science beyond just chemistry. A well-known pioneering study of abiogenesis was the Miller-Urey experiment,[1,2] which combined water (H_2O), methane (CH_4), ammonia (NH_3), and hydrogen (H_2)—plausible gases of the early Earth's atmosphere—and synthesized, among other products, amino acids via electric discharge. The addition of hydrogen sulfide (H_2S) in 1958 contributes a fifth element to the primordial mixture,[3] but a stable gaseous carrier of phosphorus eluded these early experiments. The phosphorus analogue to these reduced hydrogenated compounds, phosphine (PH_3), is spontaneously reactive with water and although suggested as constituent of the Earth's pre-oxidizing atmosphere from microbial activity,[4] phosphine is not known to significantly contribute in the prebiotic atmosphere.

However, phosphorus is a common terrestrial element with phosphate minerals, such as apatite ($Ca_5(PO_4)_3(F,Cl,OH)$), containing most of Earth's surface phosphorus. This leads to the assumption that phosphorus-containing biomolecules were first formed aqueously from dissolved phosphate minerals, but Gulick (1955)[5] points out that calcium phosphate ($Ca_3(PO_4)_2$) is sparingly soluble in pure water at 50 mg per kilogram water and thus calcium-rich natural waters would prevent the first organisms—which had not yet developed efficient means of concentrating phosphorus—from relying on dissolved phosphate as a nutrient source of phosphorus. Instead, Gulick suggested that reduced oxidation states of phosphorus, such as derivatives of H_3PO_3 (phosphorous/phosphonic acid) and H_3PO_2 (hypophosphorous/phosphinic acid), would provide a soluble and stable source of phosphorus under early Earth's non-oxidizing conditions. Gulick's hypothesis

was inconsistent with known geochemistry, but he noted that schreibersite—an iron-nickel phosphide ($(Fe,Ni)_3P$) that is rare on Earth but common in meteorites—should form phosphinic acid (H_3PO_2) by "minimal oxidation in a moist medium". Reasoning that meteorites are remnants of planet formation and that the early Earth would have similar geochemistry to these meteorites, this hypothesis assumes schreibersite was available on Earth and reacted with surface waters to produce reduced phosphorus oxoacids. While large amounts of schreibersite have not been found on Earth, phosphite ($H_2PO_3^-$) minerals have been identified in carbonaceous deposits from the early Archean Eon (2.5–4.0 billion years ago) suggesting that significant amounts of dissolved phosphites—perhaps from the oxidation of schreibersite—were present in Earth's oceans until about 3.5 billion years ago.[6]

1.2 Alkyl Phosphonic Acids

The reduced-phosphorus hypothesis remained relatively dormant in the literature until the discovery of alkyl phosphonic acids ($RP(O)(OH)_2$) in the Murchison meteorite in 1992.[7] The analysis revealed methylphosphonic acid ($CH_3P(O)(OH)_2$, 9 nmol g^{-1} meteorite), ethylphosphonic acid ($CH_3CH_2P(O)(OH)_2$, 6 nmol g^{-1} meteorite), and unquantified amounts of *n*-propylphosphonic acid ($CH_3CH_2CH_2P(O)(OH)_2$), isopropylphosphonic acid ($(CH_3)_2CHP(O)(OH)_2$), and an undetermined isomer of butylphosphonic acid ($C_4H_9P(O)(OH)_2$) (Figure 1.1). These alkyl phosphonic acids are significant as they are the only known phosphorus-containing organic compounds of extraterrestrial origin. Furthermore, the P(+III) oxidation state of the alkyl phosphonic acids provides a reduced oxidation state compound that is both soluble and contains organic carbon. Assuming these compounds were present on the meteorites impacting Earth during the Heavy Bombardment period (3.8–4.1 billion years ago), the discovery of alkyl phosphonic acids raises the possibility that these are prebiotic compounds that either chemically evolved into biomolecules or were utilized by early organisms as a source of biomolecular phosphorus. Research into exogenous sources of prebiotic phosphorus was thus refocused to explain the astrochemical origins of these compounds.

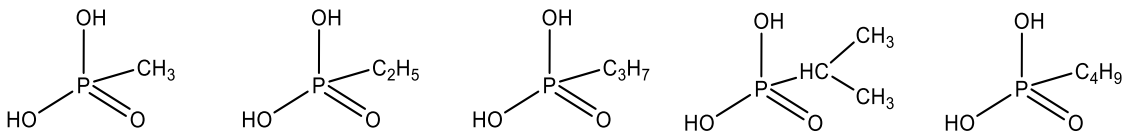

Figure 1.1. Alkyl phosphonic acids detected in the Murchison meteorite.

Attempts to explain the formation pathways of alkyl phosphonic acids began with de Graaf, Visscher, and Schwartz (1995),[8] who subjected aqueous solutions of sodium phosphite (Na_2HPO_2) with formaldehyde (CH_2O), and primary alcohols (RCH_2OH) to ultraviolet radiation and synthesized hydroxymethyl and 1-hydroxyethyl phosphonic acid. To obtain phosphonic acids found in the Murchison meteorite, e.g. methyl-phosphonic acid, a solution containing sodium phosphite and acetone—a source of methyl radicals—was irradiated for 8 hours and achieved 17 % yield of methyl-phosphonic acid. The same group (1997)[9] expanded the procedure to include sodium phosphite with acetylene (C_2H_2) and found vinyl phosphonic acid ($CH_2CHP(O)(OH)_2$) as the major product with a 4.4 % yield. A basic solution of vinyl phosphonic acid was then irradiated to produce phosphonoacetaldehyde ($HC(O)CH_2P(O)(OH)_2$) and 2-hydroxyethyl phosphonic acid ($HOCH_2CH_2P(O)(OH)_2$) as major products, although a smaller, but unquantified, amount of ethylphosphonic acid was also produced. While further research considered the aldol condensation of phosphonoacetaldehyde[10] using altered hydrotalcite minerals ($Mg_2Al(OH)_6Cl \bullet nH_2O$)[11] as a catalyst to produce dimers and its implications for producing the backbone of RNA,[12] the search for the origin of alkyl phosphonic acids remained unsolved. Research into the formation of the alkyl phosphonic acids continued with work by Pasek and Kee, which began by considering the carbon phosphide (CP) radical, which is the first interstellar molecular detected[13] containing a phosphorus-carbon bond. Kee modeled reactions of CP using theoretical calculations of water with phosphaethyne (HCP), which is the hypothesized parent molecule of CP and has itself since been discovered in the interstellar medium,[14] and synthesized in experiments using photolyzed solutions of 2,2-dimethylpropylidyne phosphine ($PCC(CH_3)_3$).[15] The calculations indicate that the reaction of HCP with water favorably produces

methylphosphonic acid (−400 kJ mol^{-1}), although significant energy barriers exist (150 kJ mol^{-1}) that limit this reaction to non-equilibrium chemistry. The photolysis of $PCC(CH_3)_3$ in water produced neopentylphosphonic acid ($(CH_3)_3CCH_2P(O)(OH)_2$), which suggests methylphosphonic acid might be produced from water processing of HCP.

Table 1.1. Percent phosphorus conversion yields for the UV irradiation of an aqueous suspension of iron phosphides (Fe_2P, Fe_3P, and schreibersite ($(Fe,Ni)_3P$) from the Nantan meteorite).[16]

Molecular Formula	Name	% yield from Fe_2P	% yield from Fe_3P*	% yield from Nantan meteorite
H_3PO_3	Phosphonic acid	69	59	86
H_3PO_4	Phosphoric acid	30	31	14
$H_4P_2O_6$	Hypophosphoric acid	1	2	n.d.
$H_4P_2O_7$	Pyrophosphoric acid	n.d.	1	n.d.

n.d. no detection, *reported values do not sum to 100 %

1.3 Schreibersite Research

From here, the research refocused once again away from interstellar chemistry to meteoritic chemistry by investigating reactions of schreibersite ($(Fe,Ni)_3P$). Using iron phosphides (Fe_nP) as a model for schreibersite, the UV irradiation of an aqueous suspension of Fe_2P produced evidence of phosphonic acid (H_3PO_3, 69 % yield), phosphoric acid (H_3PO_4, 30 %), and hypophosphoric acid ($H_4P_2O_6$, 1 %), while Fe_3P resulted in phosphonic acid (59 % yield), phosphoric acid (31 %), hypophosphoric acid (2 %), and pyrophosphoric acid ($H_4P_2O_7$, 1 %) (Table 1.1). To compare the model experiments, a sample of the Nantan meteorite, an iron-nickel meteorite with small quantities of schreibersite, was allowed to react in warm water for two months, after which time the solution was found to contain phosphonic acid (86 % yield) and phosphoric acid (14 %).[16] The meteorite sample was then brought to 77 K under vacuum and a layer of water and ethanol was condensed onto the sample. After UV irradiation, the reaction yielded 11 % phosphonic acid and, notably, 87 % phosphinic acid (H_3PO_2). These results demonstrate that the hydrolysis of schreibersite can form various phosphorus oxoacids, but especially the reduced oxidation state (H_3PO_2 and H_3PO_3) needed to provide soluble phosphorus in Earth's early oceans. Similar to the previous experiment by Kee, Pasek began by corroding Fe_3P in water or a solution of acetic acid/methanol/ethanol and found consistent results.[17] The corrosion in pure water produced derivatives of

phosphonic, phosphoric, hypophosphoric, and pyrophosphoric acid (H_3PO_3, H_3PO_4, $H_4P_2O_6$, $H_4P_2O_7$). Experiments studying the oxidation of phosphonic acid (H_3PO_3) using hydroxyl (OH) radicals generated by water and microwave discharge produced pyrophosphoric acid ($H_4P_2O_7$) and triphosphoric acid ($H_5P_3O_{10}$),[18] which indicates that iron is not necessary to catalyze the oxidation of phosphite (HPO_3^{2-}) to higher-order condensed phosphates. Higher-order phosphorus oxoacids were also found to form by heating solutions of phosphonic acid (H_3PO_3) to produce pyrophosphorous acid ($H_4P_2O_5$), which when added to phosphoric acid (H_3PO_4) reacts to hypophosphoric acid ($H_4P_2O_6$) and finally, when heated with additional phosphoric acid, achieves pyrophosphoric acid ($H_4P_2O_7$) with 7 % conversion yield.[19] These results demonstrate the facile synthesis of pyrophosphonic acid ($H_4P_2O_7$) from reduced oxidation state phosphorus (H_3PO_3), which is significant as $H_4P_2O_7$ represents a possible precursor to adenosine diphosphate/triphosphate (ADP/ATP), a molecule critical to intercellular energy transfer.

The fundamental role of schreibersite as a source of prebiotic phosphorus began by studying its surface corrosion and its matrix properties using samples from the Sikhote-Alin meteorite, which revealed that schreibersite is less susceptible to oxidation than its matrix.[20,21] This indicates that oxidation and weathering would remove the meteoritic matrix leaving behind a localized source of reactive phosphorus. As perspective, Pasek estimated that schreibersite—either from the delivery to Earth or from the reduction of phosphate (P(+V)) to phosphide (P(−III))—would contribute 1–10 % of Earth's surface phosphorus during the Hadean Eon.[22]

Of particular interest has been the phosphorylation (or, when considering reduced oxidation states of phosphorus, phosphonylation [P(+III)] or phosphinylation [P(+I)]) of prebiotic organic compounds by phosphorus-containing compounds that ultimately trace back to schreibersite. Given the ability for schreibersite to generate phosphorus oxoacids by hydrolysis, studies by Pasek and Kee have shown that phosphinic acid (H_3PO_2) can phosphinylate the metabolic intermediate pyruvic acid ($CH_3C(O)COOH$) to form R–P(O)OH–R (R = $C(CH_3)(OH)COOH$).[23] Furthermore, phosphoric acid (H_3PO_4) in a solution of urea ($(NH_2)_2CO$) and the biomolecule choline ($(CH_3)NCH_2CH_2OH^+$) yielded 99 % conversion to choline phosphate,[20] while the addition of organics such as glycerol

($CHOH(CH_2OH)_2$), ethanolamine ($NH_2CH_2CH_2OH$), glucose ($C_6H_{12}O_6$), and the nucleosides uridine ($C_9H_{12}N_2O_6$) and adenosine ($C_{10}H_{13}N_5O_4$) resulted in 10–99 % phosphorylation of the organics. The replacement of phosphoric acid (H_3PO_4) with phosphonic acid (H_3PO_3) in the mixture obtained 10–55 % phosphonylation. The investigation into uridine and adenosine was extended back to schreibersite using Fe_3P in aqueous solution with these nucleosides and, with heating, formed phosphorylated nucleosides with no greater than 6 % yield by adjusting for reaction time and pH.[24] This demonstrates that schreibersite, in the presence of nucleosides, can form precursors to RNA/DNA and ADP/ATP. In addition, various reagents including acetic acid (CH_3COOH), pyruvate ($CH_3C(O)COO^-$), acetaldehyde (CH_3COH), hydrogen peroxide (H_2O_2), ethylenediamine tetraacetic acid (EDTA, $C_{10}H_{16}N_2O_8$), acetonitrile (CH_3CN), ethanol (CH_3CH_2OH), and glycolaldehyde ($HOCH_2COH$) were added to the aqueous Fe_3P mixture to determine the amount of phosphorus oxoacids (H_3PO_3, H_3PO_4, $H_4P_2O_6$, and $H_4P_2O_7$) formed and any phosphorus-containing organic products.[25] Of note, EDTA and glycolaldehyde produced a tar from which no products were identified. The most phosphorus oxoacids were produced by acetic acid (11.7 mM), acetonitrile (6.4 mM), and hydrogen peroxide (5.3 mM), while ethanol (0.89 mM), pyruvate (0.66 mM), and acetaldehyde (0.4 mM) generated the least. In all solutions, $H_4P_2O_7$ was the least abundant oxoacid formed, followed by $H_4P_2O_6$, while either H_3PO_3 or H_3PO_4 was the most abundant. Notable products include numerous acetyl-phosphorus compounds, hydroxymethyl phosphonic acid ($HOCH_2P(O)(OH)_2$), diphosphonomethane ($(OP(OH)_2)_2CH_2$), formylphosphonic acid ($OP(OH)_2COOH$), and phosphinomethyl phosphate ($OP(OH)_2CH_2OP(O)(OH)_2$). Other research groups have also shown the potential for phosphoric acid and diamidophosphate ($(NH_2)_2PO_2^-$) to abiotically phosphorylate sugars, amino acids, and nucleotides.[26,27]

1.4 Dissertation Outline

While many of these publications acknowledge the discovery of alkyl phosphonic acids on the Murchison meteorite, they have ignored the words of Cooper et al. that "a current view of meteoric organic compounds is that they are closely related to interstellar molecules". At the time of discovery, few phosphorus-containing molecules were known in the interstellar medium, but Cooper et al. considered the implications of CP, which had

been discovered in the interstellar medium only a couple years prior.[7,13] Currently, seven phosphorus-containing molecules have been discovered in the interstellar medium (Figure 1.2): CP,[13] PO,[28] PN,[29-32] HCP,[14] CCP,[33] NCCP,[34] and PH_3.[35-37] The phosphorus monoxide (PO) molecule was detected toward the red supergiant star VY Canis Majoris while phosphorus nitride (PN) was first observed in the molecular clouds Orion KL and Sgr B2. The five other compounds, along with PN, were discovered in the circumstellar envelope of the carbon-rich star IRC+10216. Of these, phosphine (PH_3) shows the most promise as a prebiotic source of phosphorus as phosphine has been detected in the atmospheres of Jupiter[38] and Saturn,[39] has been hypothesized in Titan's atmosphere,[40] and has been assigned as the carrier for the phosphorus signal of comet 67P/Churyumov-Gerasimenko.[41] Phosphine is also present in trace amounts in Earth's atmosphere.[42,43]

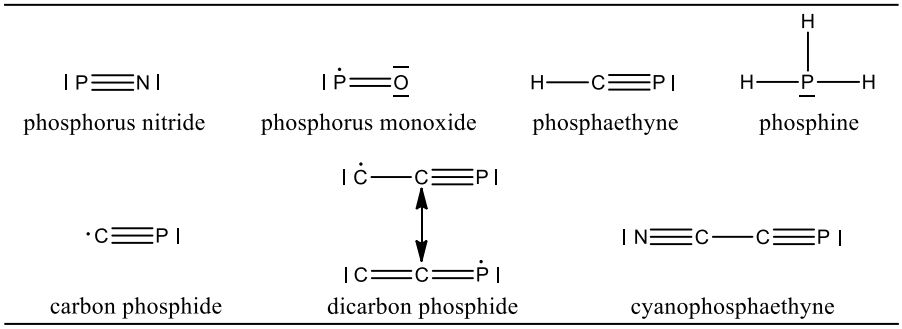

Figure 1.2. Phosphorus-containing molecules detected in the interstellar medium.

Thus, this dissertation investigates the possible formation of alkyl phosphonic acid under interstellar conditions rather than from meteoritic schreibersite. Not only would these results provide a plausible formation route to alkyl phosphonic acids, but they would help explain phosphorus chemistry in the interstellar medium and exhibit other potentially biorelevant molecules that could form under these conditions. Previous experiments have demonstrated the ability to synthesize biorelevant compounds such as amino acids,[44-48] glycerol,[49] glycolaldehyde,[50,51] and dipeptides,[52] in interstellar ice analogues at temperatures of 5–10 K. Detected ices in the interstellar medium relevant to the formation of alkyl phosphonic acids include methane (CH_4), water (H_2O), carbon dioxide (CO_2), carbon monoxide (CO), formaldehyde (H_2CO), and methanol (CH_3OH),

which form a thin layer of ice on small silicate and/or carbonaceous particles.[53] While no phosphorus-containing compounds have been detected on these interstellar icy grains, the gases of circumstellar envelopes become ejected into the interstellar medium and molecular clouds where they can condense onto the icy mantles of interstellar grains.[54] These mixtures of condensed molecules can be processed by galactic cosmic rays (GCRs) and UV photons to initiate chemistry that otherwise would not be possible at such low temperatures. Galactic cosmic rays also generate secondary electrons in their wake as they transverse the ice, and these secondary electrons are responsible for processing the bulk of the ice.[54] The cold molecular clouds provide the material of star systems, including our own solar system.

Along with phosphine, water and carbon dioxide have been chosen as sources of oxygen while methane was selected to provide organic carbon. Together, these compounds contain the components necessary to form alkyl phosphonic acids and potentially other biorelevant molecules. Phosphorus-containing biomolecules include ribonucleic acid (RNA), deoxyribonucleic acid (DNA), adenosine diphosphate/triphosphate (ADP/ATP), phospholipids, and as the mineral hydroxyapatite ($Ca_5(PO_4)_3OH$) found in bones and teeth (Figure 1.3). Using a step-wise approach starting from pure phosphine ices and then adding methane or water/carbon dioxide followed by the combination of these components, this research presents a systematic study of the phosphine chemistry in interstellar ice analogues (Appendix Table 1). By exploiting techniques such as photoionization reflectron time-of-flight mass spectrometry (PI-ReTOF-MS) and infrared spectroscopy (FTIR), but also to a lesser extent secondary ion mass spectrometry (SIMS), two-dimensional gas chromatography time-of-flight mass spectrometry (GC×GC-TOFMS), and quadrupole mass spectrometry (QMS) operating in residual gas analyzer (RGA) mode, the chemistry of these electron-irradiated ices were studied under ultrahigh vacuum (UHV) conditions and astrochemically relevant temperatures of 5–10 K. These ices are processed by energetic electrons that simulate the secondary electrons generated in the path of galactic cosmic rays. Infrared spectroscopy probes these ices *in situ* detecting functional groups, while PI-ReTOF-MS and QMS monitor molecules that sublime from the ices during temperature-programmed

desorption (TPD). The advantage of PI-ReTOF-MS over traditional QMS techniques include dramatically increased sensitivity as well as the ability to tune the ionization energy to selectively ionize only specific isomers. The solid residues that remain at room temperature can be analyzed *ex situ* using SIMS and GC×GC, which provides a wealth of data about the processes that occur within the ices during irradiation, the volatile molecules that form by non-equilibrium chemistry, and the thin film of less-volatile products that persist during heating. From these data, an understanding of phosphorus chemistry in the interstellar medium on the fundamental level can be elucidated and the potential formation of prebiotic molecules, such as the alkyl phosphonic acids, can be revealed.

The dissertation investigates first the formation of higher-order phosphanes in pure phosphine (PH_3) ices (Chapter 2), which serves as a foundation for the next studies by identifying signals, such as by mass spectrometry or infrared spectroscopy, that result only from phosphanes. Binary mixtures of phosphine with methane (CH_4, Chapter 3) along with phosphine with water/carbon dioxide (H_2O/CO_2, Chapter 5) build on this foundation by studying the formation of phosphorus-carbon and phosphorus-oxygen bond formation, respectively. In addition, experiments using deuterated methane (CD_4) with phosphine elucidate the formation routes toward higher-order methyl phosphanes, specifically whether insertion or radical recombination pathways dominate. Having established the nature of the P–P, P–C, and P–O bonds, a combined mixture of phosphine, methane, and water (Chapter 6) is capable of revealing biologically relevant compounds such as methyl phosphonic acid ($CH_3P(O)(OH)_2$) or methyl phosphoric acid ($CH_3OP(O)(OH)_2$). Also, a collective infrared spectroscopic study of all these ice mixtures, in addition to a more fundamental phosphine and dioxygen (O_2) mixture, is presented separately (Chapter 4) before a more detailed mass spectroscopic study involving phosphine with water or carbon dioxide. Each chapter, which represents a peer-reviewed publication (or one waiting peer review) begins with an abstract page followed by the chapter's introduction, and also includes supplementary information that is a component of the original publication and not an appendix solely contained in the dissertation.

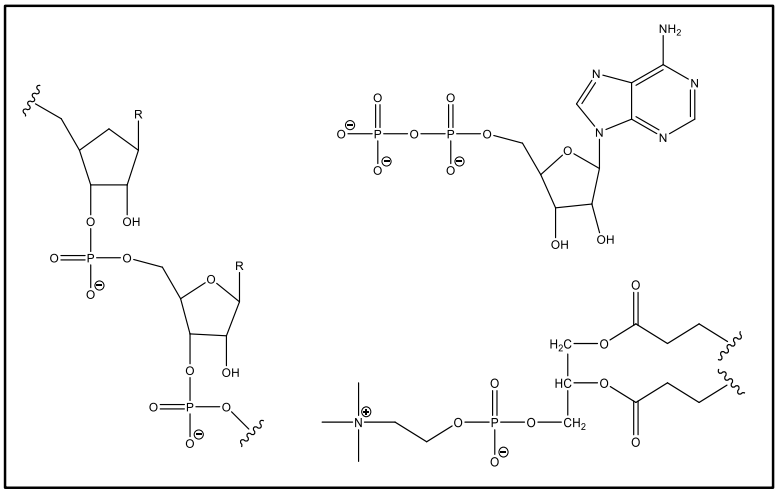

Figure 1.3. Representative examples of phosphorus-containing biomolecules: RNA backbone (left), hydrophilic head of a phospholipid (bottom right), ADP (top right).

CHAPTER 2
PURE PHOSPHINE ICES

This chapter is based on the paper: A. M. Turner, M. J. Abplanalp, S. Y. Chen, Y. T. Chen, A. H. H. Chang, R. I. Kaiser, "A Photoionization Mass Spectroscopic Study on the Formation of Phosphanes in Low Temperature Phosphine Ices", Phys. Chem. Chem. Phys. *17, 27281-27291 (2015)*

Isovalency rationalizes fundamental chemical properties of elements in the same group, but often fails to account for differences in the molecular structure due to the distinct atomic sizes and electron-pair repulsion of the isovalent atoms. With respect to main group V, saturated hydrides of nitrogen are limited to ammonia (NH_3) and hydrazine (N_2H_4) along with ionic and/or metal-bound triazene (N_3H_5) and potentially tetrazene (N_4H_6). Here, we present a novel approach for synthesizing and detecting phosphanes formed via non-classical synthesis exploiting irradiation of phosphine ices with energetic electrons, subliming the newly formed phosphanes via fractionated sublimation, and detecting these species via reflectron time-of-flight mass spectrometry (ReTOF) coupled with vacuum ultraviolet (VUV) single photon ionization. This approach is able to synthesize, to separate, and to detect phosphanes as large as octaphosphane (P_8H_{10}), which far out-performs the traditional analytical tools of infrared spectroscopy and residual gas analysis via mass spectrometry coupled with electron impact ionization that could barely detect triphosphane (P_3H_5) thus providing an unconventional tool to prepare complex inorganic compounds such as a homologues series of phosphanes, which are difficult to synthesize via classical synthetic methods.

2.1 Introduction

Ever since Langmuir devised the concept of isovalency in 1919,[55] this framework has presented a fundamental pillar of chemistry and elucidates the periodic property that elements in the same group with an identical valence electron configuration hold similar chemical properties. Isovalency has been exploited to understand the chemical formulas, reaction mechanisms, and even molecular geometries for a vast array of chemical compounds. For instance, the molecular formulas for hydrides of main group V elements —ammonia (NH_3), phosphine (PH_3), arsine (AsH_3), stibine (SbH_3), and bismuthine (BiH_3) —can be rationalized by the ns^2np^3 valence electron configuration of the central atoms. However, factors related to the atomic radius as well as bonding and non-bonding atomic orbitals have shown to result in distinct molecular structures.[56,57] These differences are most evident considering the elemental forms of the first two members of main group V: nitrogen and phosphorus. Molecular nitrogen exists as a diatomic molecule (N_2) in the gas phase, while white phosphorus is composed of P_4 tetrahedrons occurring in the liquid and gas phase and exists in equilibrium with diatomic phosphorus (P_2) at elevated temperatures above 1,070 K.[58] An evaluation of the molecular structures of the hydrides of nitrogen and phosphorus demonstrates simultaneously the validity, but also the shortcomings of the isovalency concept.

The two simplest azanes (N_nH_{n+2}; n = 1,2) and phosphanes (P_nH_{n+2}; n = 1,2) have been known for more than a century. The molecular formula of the most common and least toxic azane—ammonia (NH_3)—was determined in 1785[59] with phosphine (PH_3) being discovered in that same year.[60] These were followed by diphosphine (P_2H_4) in 1844,[61] which was surprisingly discovered 50 years before its nitrogen analogue, hydrazine (N_2H_4).[62] More complex molecules have proven to be more difficult to synthesize. Triazane (N_3H_5) was first reported as a silver-complex[63] and later monitored via its molecular ion exploiting microwave plasma discharge of hydrazine.[64] This study tentatively characterized tetrazane (N_4H_6), but only as a complex with lithium. Thus, free azanes heavier than hydrazine have been difficult to synthesize and require a metal-cation complex to stabilize the molecule in the gas phase or in zeolites. Despite the

isovalency between nitrogen and phosphorus, far larger hydrides of phosphorus have been detected.[65] Triphosphane (P_3H_5) was first probed via Raman spectroscopy as a transient species[66] and was also isolated for preparative studies.[67] Heated mixtures of diphosphine (P_2H_4) and triphosphane (P_3H_5) produced traces of tetraphosphane (P_4H_6), which could not be purified due to rapid disproportionation. Further heating led to the formation of poorly defined mixtures of pentaphosphane (P_5H_7), hexaphosphane (P_6H_8), and heptaphosphane (P_7H_9), which could not be separated due to the thermal instability of higher phosphanes. Octaphosphane (P_8H_{10}) and nonaphosphane (P_9H_{11}) were only identified tentatively.[11] The fact that phosphorus can form more complex hydrides than nitrogen illustrates that additional factors beyond isoelectronicity affect the chemistry of these elements, such as the established tendency of nitrogen to favor the formation of multiple bonds due to the smaller radius of the nitrogen atom (71 pm) compared to phosphorus (109 pm).[68] However, despite the tentative identification of higher phosphanes, their underlying synthetic pathways together with their explicit isolation and protocols to their clean preparation have not been established to date.

Here, we demonstrate that phosphanes up to octaphosphane (P_8H_{10}) can be efficiently prepared and thereafter separated via fractionated sublimation upon exposure of phosphine ices to energetic electrons at ultralow temperatures of 5.5 K. The low temperature was chosen to minimize thermal chemistry in the ice. Reflectron time-of-flight (ReTOF) mass spectroscopy coupled with 'soft' single vacuum ultraviolet (VUV) photon ionization at 10.49 eV is applied to explicitly identify the molecular formulas of the newly synthesized phosphanes on line and *in situ* upon their sublimation into the gas phase upon warming of the irradiated target to 300 K. Our study presents clear evidence of higher molecular mass phosphanes thus providing a clean route to their formation up to octaphosphane (P_8H_{10}) via exposure of phosphine ices to energetic electrons followed by fractionated sublimation of the phosphanes. This study further provides a proof of concept for a novel adaption of ReTOF mass spectroscopy coupled with VUV single-photon ionization to form and to identify inorganic molecules, which are difficult to synthesize via classical synthetic methods.

2.2 Experimental

The experiments were conducted in a contamination-free ultra-high vacuum stainless steel chamber evacuated to a few 10^{-11} Torr using oil-free turbomolecular pumps and dry scroll backing pumps, which has been described previously.[51,69-77] Briefly, a silver mirror substrate is mounted onto a rotatable cold finger made of oxygen-free high-conductivity copper (OFHC) cooled to 5.5 K ± 0.1 by a closed-cycle helium refrigerator (Sumitomo Heavy Industries, RDK-415E). Phosphine (Sigma-Aldrich, 99.9995%) was condensed onto the substrate through a glass capillary at a pressure of 5 × 10^{-8} Torr at thicknesses of 920 ± 20 nm[78-80] (Supplementary Information). The refractive index (n_{PH_3}) of solid phosphine necessary to calculate the thickness was experimentally determined exploiting laser interferometry by two helium-neon lasers[81] to be n_{PH_3} = 1.51 ± 0.04. The ices were isothermally irradiated with 5 keV electrons at fluxes as high as 2 × 10^{10} electrons s^{-1} cm^{-2} over an area of 1.0 ± 0.1 cm^2 at an angle of incidence of 70° relative to the substrate normal. The average absorbed dose per target molecule was determined from Monte Carlo (CASINO)[82] simulations using the density of 0.90 g cm^{-3} for solid phosphine[83] to be 0.17 ± 0.04 eV per molecule. The ices were monitored on line and *in situ* during the irradiation using a Fourier Transform Infrared Spectrometer (FTIR, Nicolet 6700) over a range of 6000 cm^{-1} to 500 cm^{-1} at 4 cm^{-1} resolution. One hour after the irradiation, a temperature programmed desorption (TPD) protocol heated the irradiated ices to 300 K at rates of 1 K min^{-1}. During the sublimation, the molecules were probed via reflectron time-of-flight mass spectrometry (Jordan TOF Products, Inc.) after photoionization (PI-ReTOF-MS) at 118.2 nm (10.49 eV).[69] Here, the pulsed (30 Hz) coherent vacuum ultraviolet (VUV) light was generated via four wave mixing using xenon (99.999 %) as a non-linear medium. The third harmonic (354.6 nm) of a high-power pulsed neodymium-doped yttrium aluminum garnet laser (Nd:YAG, Spectra Physics, PRO-250, 30 Hz) underwent a frequency tripling process ($\omega_{vuv} = 3\omega_1$) to obtain the 118.2 nm photons at levels of ~10^{14} VUV photons per pulse.[51] The xenon was

pulsed into an evacuated mixing chamber at an operating pressure of 3×10^{-4} Torr. The VUV light was separated from the fundamental using a lithium fluoride (LiF) plano-convex lens[84] (ISP Optics, LF-PX-38^{-1}50) based on distinct refractive indices of the lens material for different wavelengths and then directed 1 mm above the ice surface.[51] The photoionized molecules were then directed toward the focusing regions by a repeller plate (held at ground) and an extraction plate (−190 V) with the field between the repeller and extraction plates held at a voltage of −210 V. Mass-to-charge ratios were determined based on the arrival time of the ions at a multichannel plate; the signal was amplified with a fast preamplifier (Ortec 9305) and recorded using a bin width of 4 ns, which was triggered at 30 Hz (Quantum Composers, 9518).

2.3 Theoretical Methods

The structural isomers and adiabatic ionization energies from PH_3 to P_8H_{10} were investigated with *ab initio* electronic structure calculations. The optimized geometries and harmonic frequencies of the neutral and ionic species were obtained with the hybrid density functional theory, B3LYP/cc-pVTZ. [85-88] Their energies were refined further by utilizing the CCSD(T)/cc-pVTZ with B3LYP/cc-pVTZ zero-point energy corrections.[89-92] The adiabatic ionization energy of each species was then computed by taking the energy difference between the neutral and ionic counterparts; this procedure reproduced the ionization energies within ± 0.1 eV.[93,94] The GAUSSIAN 09 program was employed for the electronic structure calculations.[95]

2.4 Results & Discussion

2.4.1 Infrared Spectroscopy

During the irradiation, new absorption features emerged (Table 2.1, Figures 2.1 & 2.2). The absorptions at 1061 cm^{-1} and at 2294 cm^{-1}, which are easily recognizable in the post-irradiation infrared spectrum recorded at 5.5 K, could be assigned to diphosphine

Table 2.1. Infrared absorption assignments for phosphine ice at 5.5 K and the products of electron irradiation.

Phosphine ice, pre-irradiation (5.5 K)	
Assignment‡	Position (cm^{-1})
ν_2 (δ(HPP))	983
ν_4 (δ(HPP))	1097, 1108sh
$\nu_2 + \nu_4$	2067, 2083
$2\nu_4$	2195
ν_1 (ν(PH))	2303
ν_3 (ν(PH))	2316
$\nu_1/\nu_3 + \nu_L$	2376, 2426, 2461
$3\nu_2$	2905
$\nu_1 + \nu_2$	3288
$\nu_1 + \nu_4$	3392
$\nu_3 + \nu_4$	3405
$2\nu_1$	4536
$\nu_1 + \nu_3$	4621
New peaks from irradiation	
P_2H_4 (ν_{11}, δ(HPP))	1061
P_2H_4 (ν_5, ν(PH))	2294
P_3H_5 (ν(PH))	2264, 2288
P_3H_5 (δ(HPP))	1059

‡Assignments based on previous studies[96,97]

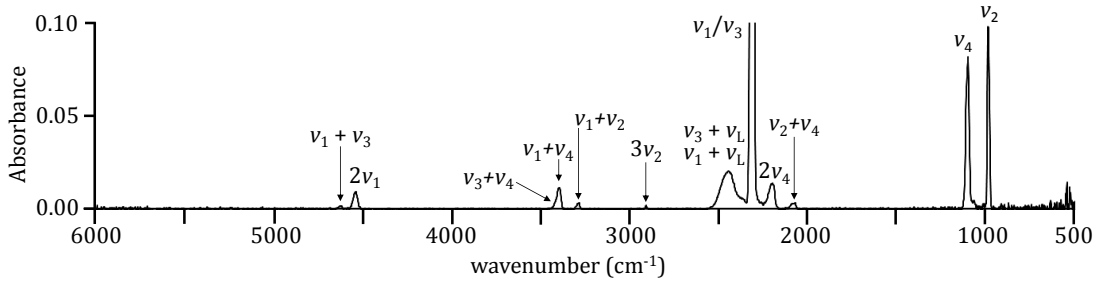

Figure 2.1. Infrared spectrum of pre-irradiated solid phosphine taken at 5.5 K.

(P_2H_4) (Figure 2.2 top); these data agree very well with previous literature data at 1052 cm^{-1} and 2299 cm^{-1}.[96] No additional new absorption features were observable at 5.5 K. Upon annealing the irradiated ices to 85 K, the phosphine ice (PH_3) fully sublimed, and the 1061 cm^{-1} and at 2294 cm^{-1} absorptions attributed to diphosphine (P_2H_4) became easily identifiable (Figure 2.2 center). Upon annealing to 130 K, diphosphine (P_2H_4) sublimed completely, and absorption features of triphosphane (P_3H_5) emerged at 1059 cm^{-1} (H–P–P bending), 2264 cm^{-1} (P–H stretching), and 2288 cm^{-1} (P–H stretching) (Figure 2.2 bottom).[97] After the sublimation of triphosphane (P_3H_5) at 165 K, a broad absorption from 2310 cm^{-1} to 2280 cm^{-1} characteristic of the P–H stretching in higher phosphanes remains. These spectra demonstrate the limitations of distinguishing higher molecular weight phosphanes exploiting infrared spectroscopy since the most intense absorption of all phosphanes—the P–H stretching mode—occurs over a narrow spectral range. For the remainder of the heating process, these absorptions slowly decayed into the baseline and disappeared near 300 K.

Having assigned the absorptions first qualitatively, we are now attempting to elucidate the underlying decomposition (reactant) and formation pathways of the product(s). For this, we traced the temporal profiles of the phosphine reactant and also of the deconvoluted bands of the products during the irradiation (Figure 2.3) and utilized a set of coupled differential equations to numerically fit these temporal profiles, i.e. the column density of the reactant/product(s) versus the irradiation time. To determine the column density of phosphine, the ν_2 fundamental at 983 cm^{-1} was exploited since the ν_1 and ν_3 modes overlap with the P–H stretching modes of the reaction product(s) (Supplementary Information). The ν_{11} fundamental at 1061 cm^{-1} was used to determine the column density of diphosphine (P_2H_4). Since this mode overlaps slightly with ν_4 mode of phosphine, the peak areas of the ν_{11} and ν_4 modes were determined by deconvoluting the spectra.[98] Two reaction schemes were explored to fit the column densities with the resulting rate constants listed in Table 2.2. Equation 2.1 proposes a first order decay of phosphine dimers $(PH_3)_2$ in the condensed phase leading to diphosphine (P_2H_4) plus atomic/molecular hydrogen followed by the subsequent reaction of diphosphine (P_2H_4) to

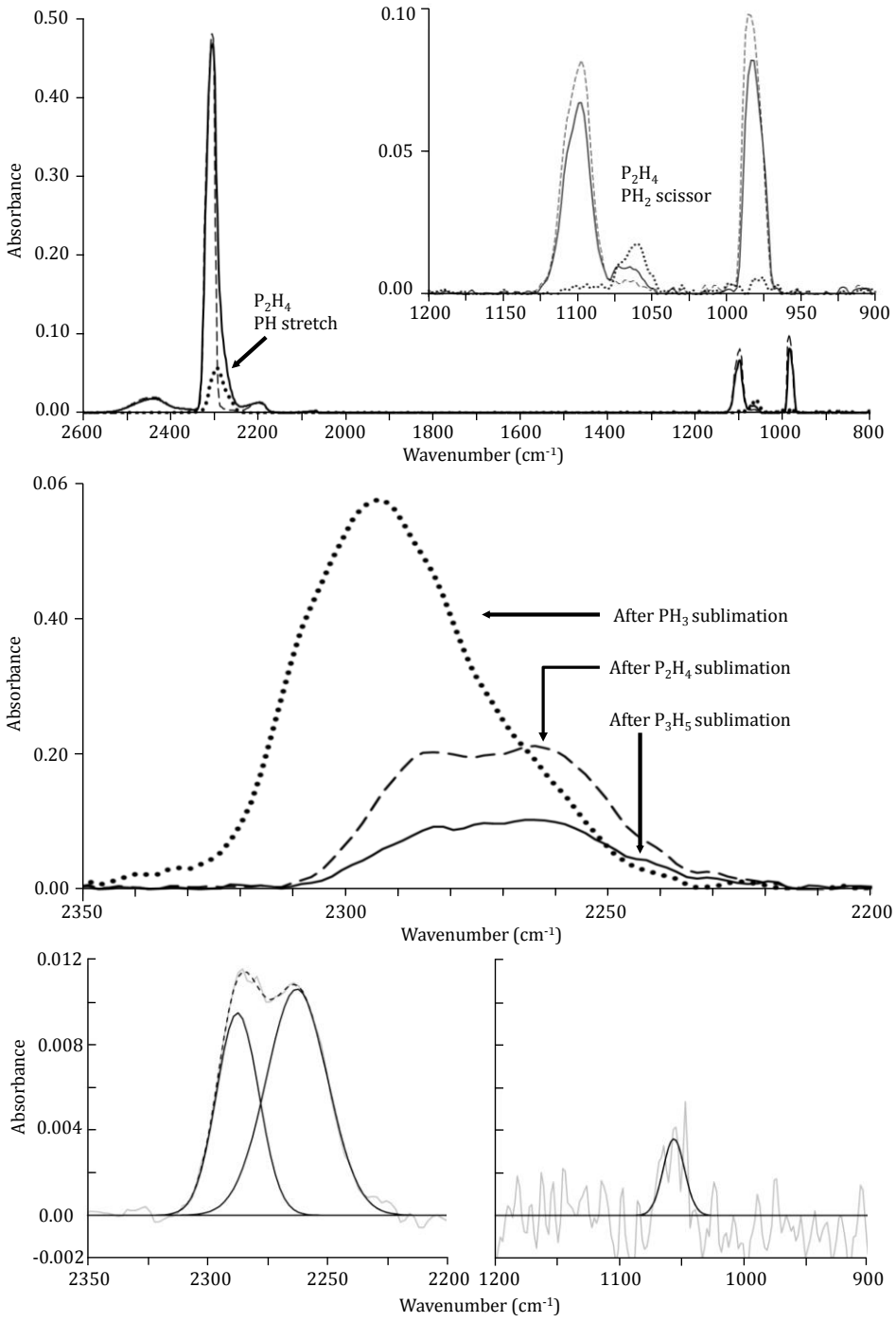

Figure 2.2. *(top)* Overlay of infrared spectra of solid PH_3 taken before (dashed line) and after (solid line) irradiation, with the spectrum after PH_3 sublimed (85 K, dotted line) emphasizing the products of irradiation. *(center)* Infrared spectra of the P-H stretching region after PH_3 (85 K, dotted line), P_2H_4 (130 K, dashed line), and P_3H_5 (165 K, solid line) sublime. *(bottom)* Infrared spectrum of P_3H_5 obtained by subtracting the post-P_3H_5 sublimation spectrum from its pre-sublimation spectrum. The peaks at 2264 cm^{-1} and 2288 cm^{-1} (*left*) result from P-H stretching while the peak at 1059 cm^{-1} (*right*) corresponds to H–P–P bending.

Table 2.2. Rate constants for reactions of PH_3 and P_2H_4.

Reaction	Reaction Order	k
$(PH_3)_2 \rightarrow P_2H_4 + 2H/H_2$	1	$4.8 \pm 0.1 \times 10^{-5}$ †
$P_2H_4 \rightarrow$ products	1	$8 \pm 3 \times 10^{-5}$ †
$2\ PH_3 \rightarrow P_2H_4 + 2H/H_2$	2	$8.2 \pm 0.1 \times 10^{-24}$ *
$P_2H_4 \rightarrow$ products	1	$6 \pm 2 \times 10^{-5}$ †

*units cm^2 $molecules^{-1}$ s^{-1}, †units s^{-1}

higher order phosphanes. Equation 2.2 probes the decomposition of second order decay of phosphine (PH_3) to diphosphine (P_2H_4) plus atomic/molecular hydrogen followed once again by the transformation of diphosphine (P_2H_4) to higher order phosphanes.

$$(PH_3)_2 \rightarrow P_2H_4 + 2H/H_2 \qquad (2.1)$$

$$P_2H_4 \rightarrow \text{products}$$

$$2\ PH_3 \rightarrow P_2H_4 + 2H/H_2 \qquad (2.2)$$

$$P_2H_4 \rightarrow \text{products}$$

The results as compiled in Figure 2.3 show that both reaction schemes fit the decay of phosphine (PH_3) and the rise profile of diphosphine (P_2H_4) equally well. Note that it was important to include a reaction pathway from diphosphine (P_2H_4) to higher order phosphanes to avoid an overproduction of diphosphine (P_2H_4) at longer irradiation times.

Considering the infrared absorption coefficients of $5.1 \pm 0.3 \times 10^{-19}$ cm $molecule^{-1}$ for the ν_2 band (983 cm^{-1}) for phosphine and of $7.0 \pm 0.4 \times 10^{-19}$ cm $molecule^{-1}$ for the ν_{11} band (1061 cm^{-1}) for diphosphine (P_2H_4) (Supplementary Information), $9.4 \pm 0.6 \times 10^{17}$ molecules cm^{-2} of phosphine and $4.6 \pm 0.3 \times 10^{17}$ molecules cm^{-2} of diphosphine were destroyed and produced, respectively, during the electron irradiation. This was derived based on a comparison of the infrared spectra taken before and after the electron irradiation. This leads to a production rate of $9.4 \pm 0.8 \times 10^{-2}$ molecules eV^{-1} at 5.5 K and a diphosphine yield of 6.9 ± 0.6 % with respect to phosphine. The formation of diphosphine accounts for 89 ± 4 % of the phosphorus from the destroyed phosphine reactant. Therefore, 11 ± 4 % of the phosphine has to be converted to hitherto unidentified higher order phosphanes containing more than two phosphorus atoms. The formation of higher phosphanes is in line with a destruction pathway of diphosphine to higher phosphanes required to avoid an overproduction of diphosphine at longer irradiation times.

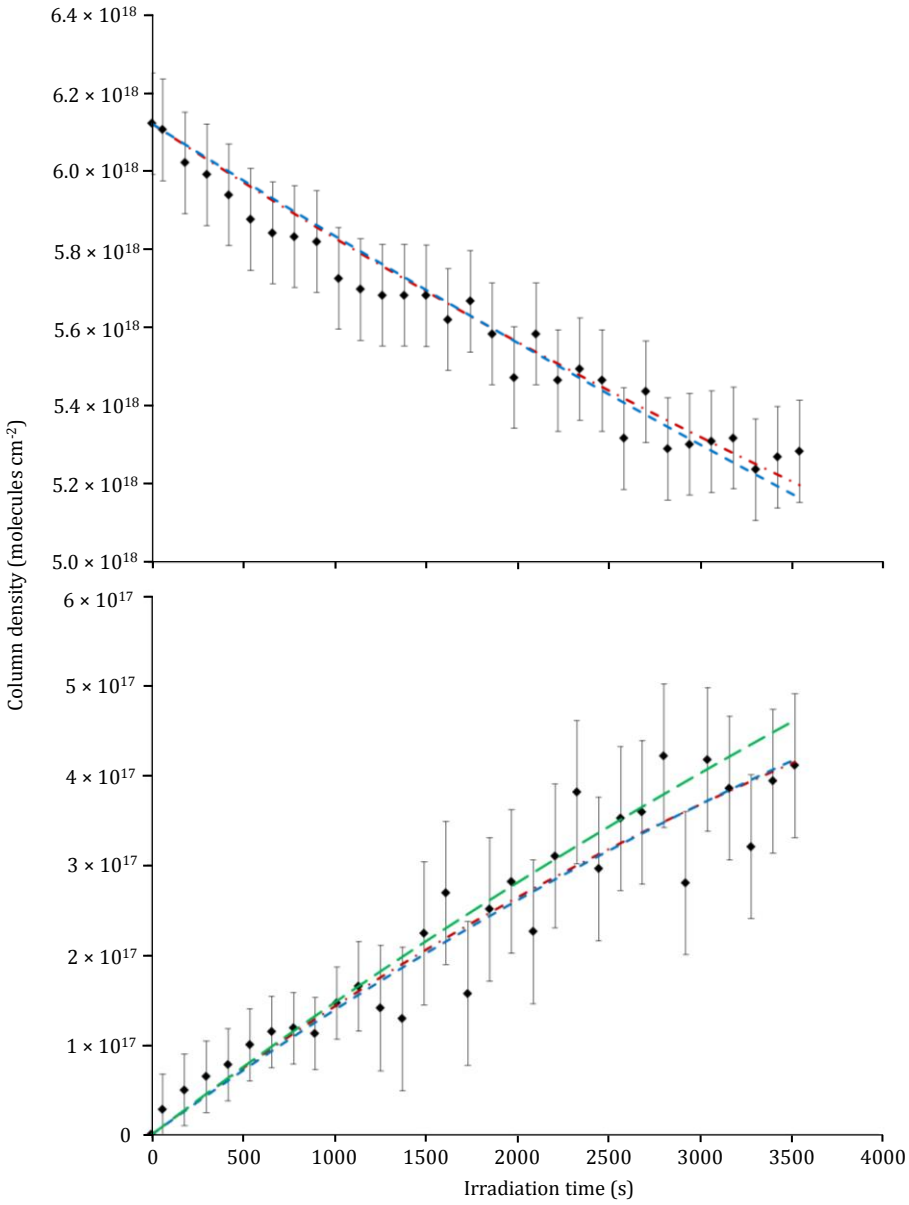

Figure 2.3. Temporal profiles of the decay of PH_3 (top) and production of P_2H_4 (bottom) during irradiation. The intensity of the PH_3 ν_2 vibrational mode at 983 cm^{-1} was used as a proxy for the abundance of PH_3 while the P_2H_4 ν_{11} vibrational mode at 1061 cm^{-1} was used to monitor P_2H_4. Fits for the second-order reaction of 2 PH_3 → P_2H_4 + H_2 (red) along with the first-order reaction $(PH_3)_2$ → P_2H_4 + H_2 (blue) are shown coupled with the reaction P_2H_4 → products. The green line indicates the total amount of P_2H_4 formed from PH_3 decay with the assumption that P_2H_4 does not further react.

2.4.2 Reflectron Time-of-Flight Mass Spectrometry (ReTOF-MS)

Despite the FTIR spectra, with the exception of diphosphine (P_2H_4), these data alone cannot identify individual higher phosphanes because the group frequencies, for instance of the P–H stretches and bending modes, overlap significantly. We thus turned to the complementary, highly sensitive PI-ReTOF-MS technique to identify *individual phosphanes* based on their mass-to-charge ratios and the sublimation temperatures upon annealing of the irradiated ices to 300 K. Figure 2.4 depicts the ReTOF mass spectra as a function of temperature during the warm up phase after irradiating the phosphine ices obtained by photoionizing the subliming molecules with 10.49 eV photons. The spectra display the intensity of the ion counts of the photoionized products subliming into the gas phase at well-defined temperatures. Here, ions with mass-to-charge ratios up to m/z = 225 are observable. The temperature programmed desorption (TPD) profiles of the individual ions are compiled in Figure 2.5; these TPD spectra are color coded to highlight to what extent ions at lower mass-to-charge ratios originate as fragment ions from corresponding higher mass species. Identical TPD profiles of ions at two distinct mass-to-charge ratios in a well-defined temperature range indicate that both species originate from a common parent and correspond to molecular fragment ions.

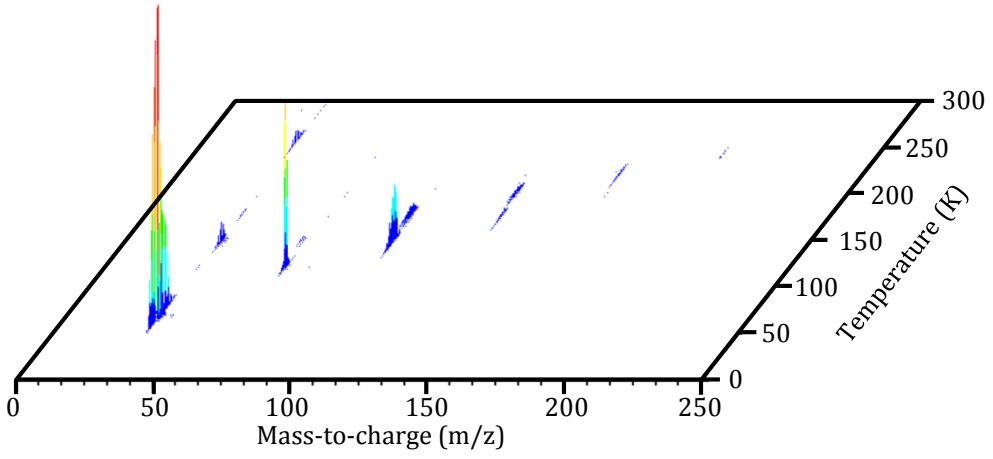

Figure 2.4. ReTOF mass spectrometry data as a function of sublimation temperature as irradiated phosphine ice was heated from 5.5 K to 300 K at 1 K min^{-1}.

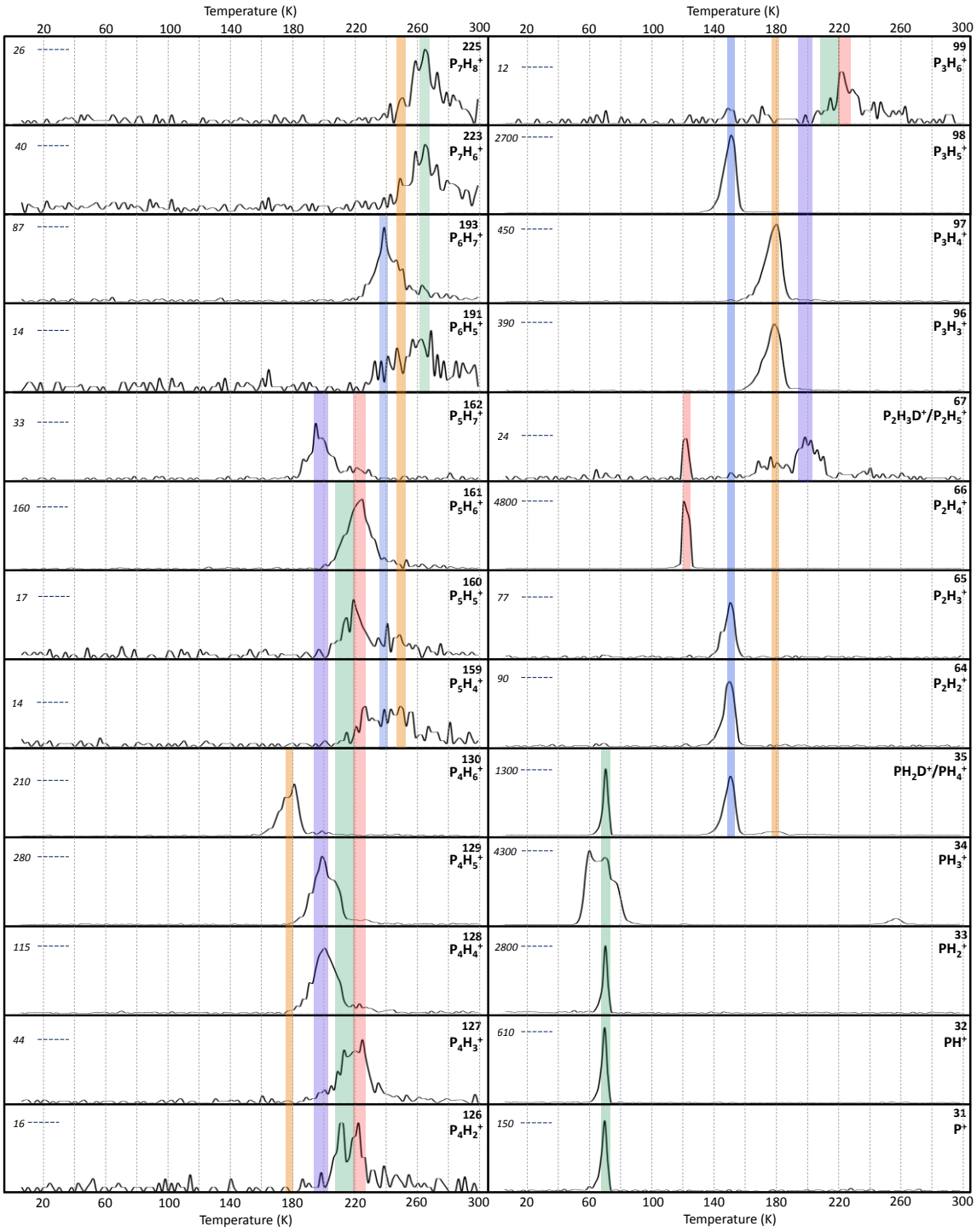

Figure 2.5. ReTOF data as a function of temperature for the indicated masses (top-right in bold with formula). The irradiated phosphine sample was heated from 5.5 K to 300 K at 1 K min^{-1}. The strongest peak intensity is shown on the left in italics, and colored lines trace sublimation events that occur at the same temperature. The peak shape of phosphine (m/z = 34) results from detector saturation.

As expected from the infrared data, phosphine (PH_3) and diphosphine (P_2H_4) can be identified with the PI-ReTOF-MS technique via their parent ions at m/z = 34 (PH_3^+) and 66 ($P_2H_4^+$) (Figure 2.5, Table 2.3). Here, phosphine (PH_3) can fragment to m/z = 33 (PH_2^+), 32 (PH^+), and 31 (P^+) as well, diphosphine (P_2H_4) does not fragment at all upon 10.49 eV photoionization, and the signal at m/z = 67 can originate from $P_2DH_3^+$ and/or $P_2H_5^+$ potentially formed via proton transfer from PH_4^+. Further, higher order phosphanes can be identified. These are triphosphane (P_3H_5) assigned via its parent peak at m/z = 98 ($P_3H_5^+$) and the fragments at m/z = 65 ($P_3H_3^+$), 64 ($P_3H_2^+$), and 35 (PH_4^+). It is important to note that as the molecular mass increases from 34 amu (PH_3) via 66 (P_2H_4) to 98 (P_3H_5), the onset of the sublimation also rises from 63 K via 99 K to 130 K (Figure 2.6). It is notable that beginning with tetraphosphane (P_4H_6), fragmentation of the parent upon photoionization becomes significant; the intensities of the fragment ions are always higher than the respective molecular parent ions. These fragmentation patterns become more pronounced at higher masses. While the singly ionized tetraphosphane (P_4H_6) (m/z = 130) holds an abundance of about 50 % with respect to the fragments at m/z = 96 ($P_3H_3^+$) and 97 ($P_3H_4^+$), the relative abundance of the parent ion of pentaphosphane (P_5H_7) depicts an intensity of only about 10 % compared to their most intense fragments at m/z =129 ($P_4H_5^+$). Beginning with hexaphosphane (P_6H_8), fragmentation occurs to such an extent that the molecular ion can no longer be directly observed. However, the characteristic phosphane fragmentation pattern of PH_2-loss, which produces the largest fragments of P_5H_7 and P_4H_6 and the second largest fragment, due to slightly more PH_3-loss fragmentation, of P_3H_5, continues with fragment ions m/z = 161 ($P_5H_6^+$), 193 ($P_6H_7^+$), and 225 ($P_7H_8^+$), which correlate to parent compounds hexaphosphane (P_6H_8), heptaphosphane (P_7H_9), and octaphosphane (P_8H_{10}). Since these larger phosphanes were not directly observed via their molecular ions, their fragments' sublimation temperatures were utilized to assign the sublimation temperature of their parent compounds. A regression curve (Figure 2.6) for the five phosphanes (PH_3 to P_5H_7) directly observed via their molecular parent ions was explored and extrapolated toward higher masses; these predictions depict an excellent agreement with the assigned sublimation temperatures for the high mass phosphanes from P_6H_8 through P_8H_{10} based on their fragments.

Table 2.3. Observed masses from the reflectron time-of-flight mass spectrometer.

Mass	Formula	Comments	Parent Compound
31	P^+	fragment	PH_3
32	PH^+	fragment	PH_3
33	PH_2^+	fragment	PH_3
34	PH_3^+	parent	PH_3
35	PH_2D^+	isotope	
	PH_4^+	protonated parent	PH_3
	PH_4^+	fragment	P_3H_5, P_4H_6
64	$P_2H_2^+$	fragment	P_3H_5
65	$P_2H_3^+$	fragment	P_3H_5
66	$P_2H_4^+$	parent	P_2H_4
67	$P_2H_3D^+$	isotope	
	$P_2H_5^+$	protonated parent	P_2H_4
	$P_2H_5^+$	fragment	P_4H_6, P_5H_7
96	$P_3H_3^+$	fragment	P_4H_6
97	$P_3H_4^+$	fragment	P_4H_6
98	$P_3H_5^+$	parent	P_3H_5
99	$P_3H_4D^+$	isotope	
	$P_3H_6^+$	protonated parent	P_3H_5
	$P_3H_6^+$	fragment	P_6H_8
126	$P_4H_2^+$	fragment	P_6H_8
127	$P_4H_3^+$	fragment	P_6H_8
128	$P_4H_4^+$	fragment	P_5H_7
129	$P_4H_5^+$	fragment	P_5H_7
130	$P_4H_6^+$	parent	P_4H_6
159	$P_5H_4^+$	fragment	P_7H_9
160	$P_5H_5^+$	fragment	P_6H_8, P_7H_9
161	$P_5H_6^+$	fragment	P_6H_8
162	$P_5H_7^+$	parent	P_5H_7
191	$P_6H_5^+$	fragment	P_7H_9, P_8H_{10}
193	$P_6H_7^+$	fragment	P_7H_9
223	$P_7H_6^+$	fragment	P_8H_{10}
225	$P_7H_8^+$	fragment	P_8H_{10}

Since traditional residual gas analyzers are utilized to detect newly synthesized molecules such as phosphanes in the gas phase, we compare the ReTOF data with those obtained by a residual gas analyzer (RGA; quadrupole mass spectrometer) in electron impact mode with 100 eV electrons at an emission current of 1 mA (Figure 2.7 & Table 2.4). The RGA data are consistent, but more limited than the data of the ReTOF mass spectrometer. The only products identified via the RGA are diphosphine (P_2H_4) and triphosphane (P_3H_5). Although the parent peak of the latter is tenuous in the RGA, it is notable that the signal for PH_4^+ (m/z = 35) occurred as a fragment ion of triphosphane upon ionization in both the RGA and the ReTOF. Therefore, our data demonstrate that a fractionated sublimation of synthesized phosphanes combined with photoionization mass spectrometry presents an ideal, unconventional tool to identify thermally labile molecules, which are difficult to synthesize by classical 'inorganic synthetic approaches'.

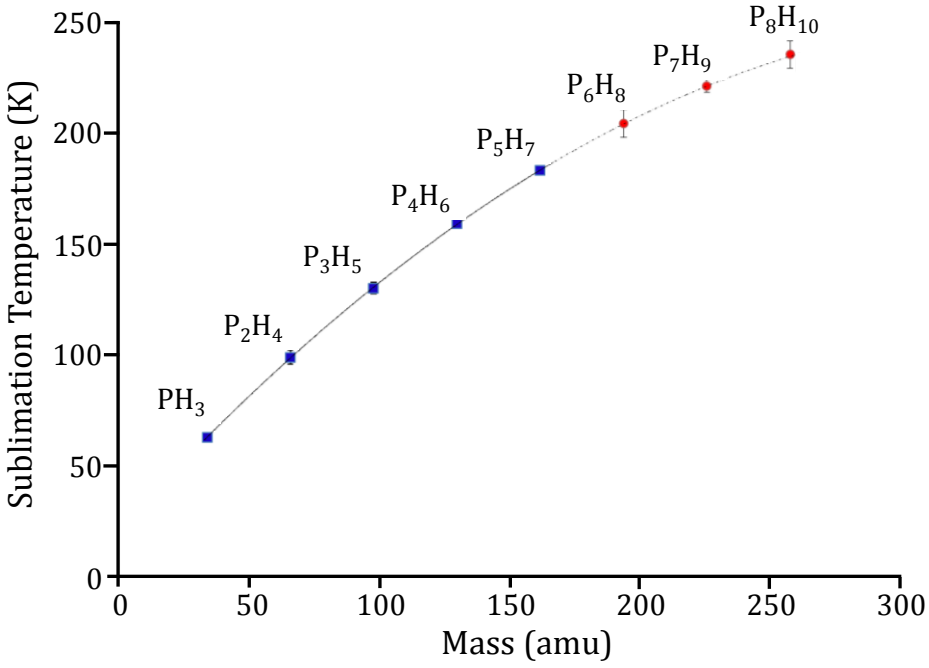

Figure 2.6. Sublimation temperatures as a function of mass observed using the ReTOF mass spectrometer. Blue squares represent phosphanes that were directly observed, while red circles represent phosphanes that were indirectly identified from predicted mass fragments. The five observed phosphanes were used to create the solid trend line, while the dashed line shows the projection of this trend line at higher masses.

Table 2.4. Observed masses from the residual gas analyzer (QMS).

Mass	Formula	Comments	Parent Compound
31	P^+	fragment	PH_3
32	PH^+	fragment	PH_3
33	PH_2^+	fragment	PH_3
35	PH_2D^+ PH_4^+	isotope protonated parent	PH_3
	PH_4^+	fragment	P_3H_5
62	P_2^+	recombination fragment	PH_3 P_2H_4
63	P_2H^+	fragment	P_2H_4
64	$P_2H_2^+$	fragment	P_2H_4
65	$P_2H_3^+$	fragment	P_2H_4, P_3H_5
66	$P_2H_4^+$	parent	P_2H_4
93	P_3^+	fragment	P_3H_5
97	$P_3H_4^+$	fragment	P_3H_5
98	$P_3H_5^+$	parent	P_3H_5

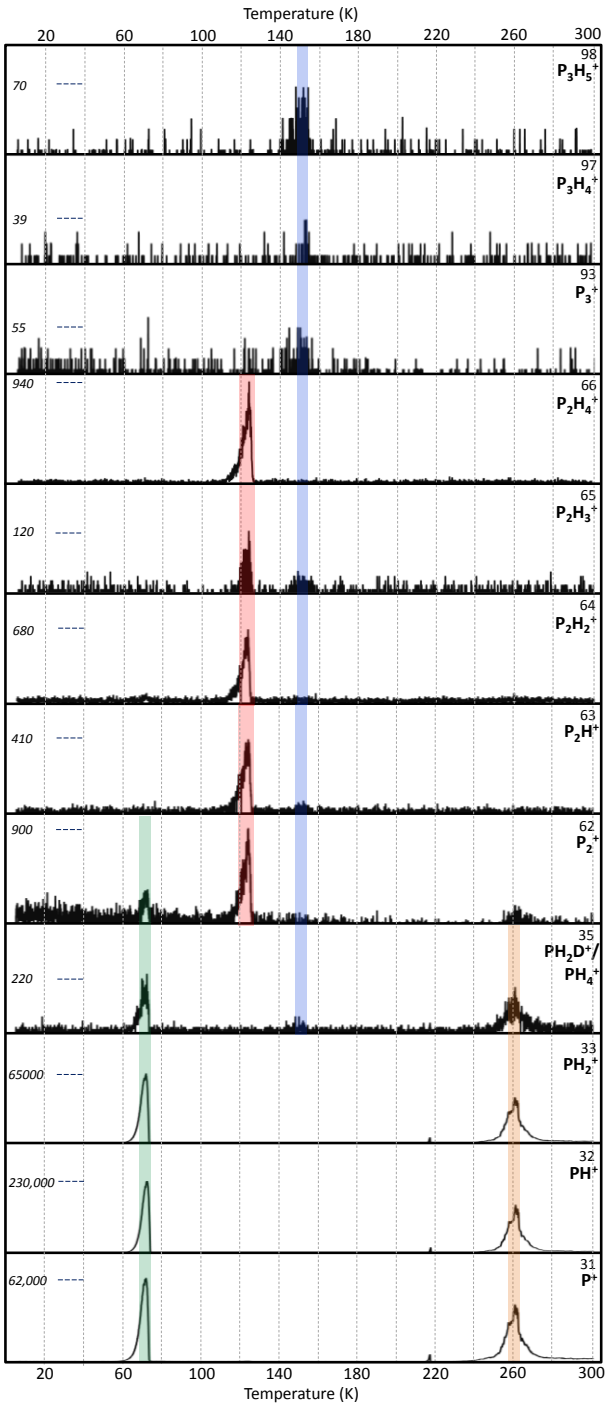

Figure 2.7. Residual gas analysis data (quadrupole mass spectrometry) plotted as a function of temperature for the indicated masses (top-right in bold with formula). The irradiated phosphine sample was heated from 5.5 K to 300 K at 1 K min^{-1}. The strongest peak intensity is shown on the left in italics, and colored lines trace sublimation events that occur at the same temperature. Molecular phosphine (m/z = 34) was not measured due to saturation concerns.

2.4.3 Theoretical Calculations

The optimized geometrical structures for distinct phosphanes and their isomers up to octaphosphane (P_8H_{10}) (Figures 2.8–2.10 & Table 2.5) indicate that the predicted phosphorus–hydrogen (P–H) bond lengths occur only in a narrow range from 142 to 143 pm across all compounds while the phosphorus-phosphorus (P-P) bond lengths vary from 223 to 227 pm with no significant correlation between the molecular size or primary, secondary, or tertiary phosphorus atoms. The H–P–H bond angles show little variation among molecules holding values from 92° to 95°. Similar values can be seen for the H–P–P bond angles, in particular when the molecule contains no branched moieties. However, in a few cases such as the P_6H_8-2 isomer, all branched P_7H_9 isomers, and several P_8H_{10} isomers, this bond angle increased to about 100° mainly when the central atom of the H–P–P moiety was a secondary phosphorus atom connected to a tertiary phosphorus. Two additional instances occurred with the central phosphorus attached to a terminal phosphorus atom in the P_8H_{10} isomers. Besides the bond lengths, it is interesting to investigate trends in the relative stabilities of the isomers. Here, the relative energies of the isomers clearly depicts that branched isomers are energetically preferred compared to the least stable chain isomer, in agreement with previous experimental abundances.[11] The relative energy difference between the straight-chain and the most highly branched isomers are 9 kJ mol^{-1} (P_4H_6), 6 kJ mol^{-1} (P_5H_7), 16 kJ mol^{-1} (P_6H_8), 19 kJ mol^{-1} (P_7H_9), and 29 kJ mol^{-1} (P_8H_{10}). As evident from Table 2.5, this energy difference becomes more pronounced for larger molecules. Finally, let us investigate the ionization energies of the phosphanes. Experimentally, the adiabatic ionization energies have only been reported for phosphine (PH_3),[99] diphosphine (P_2H_4),[100] and triphosphane (P_3H_5)[101] to be 9.9 eV, 8.8 eV, and 8.7 eV, respectively. Considering phosphine (PH_3) and diphosphine (P_2H_4), the computed adiabatic ionization energies at the CCSD(T)/cc-pVTZ level of theory are only lower by 0.13 eV and 0.04 eV, respectively. Note that the discrepancy of the computed and experimentally determined adiabatic ionization energy of triphosphane (P_3H_5) could be an artifact of only one experimental characterization, which exploited electron impact mass spectrometry, i.e. utilizing a 'broad' electron beam with poor resolution.

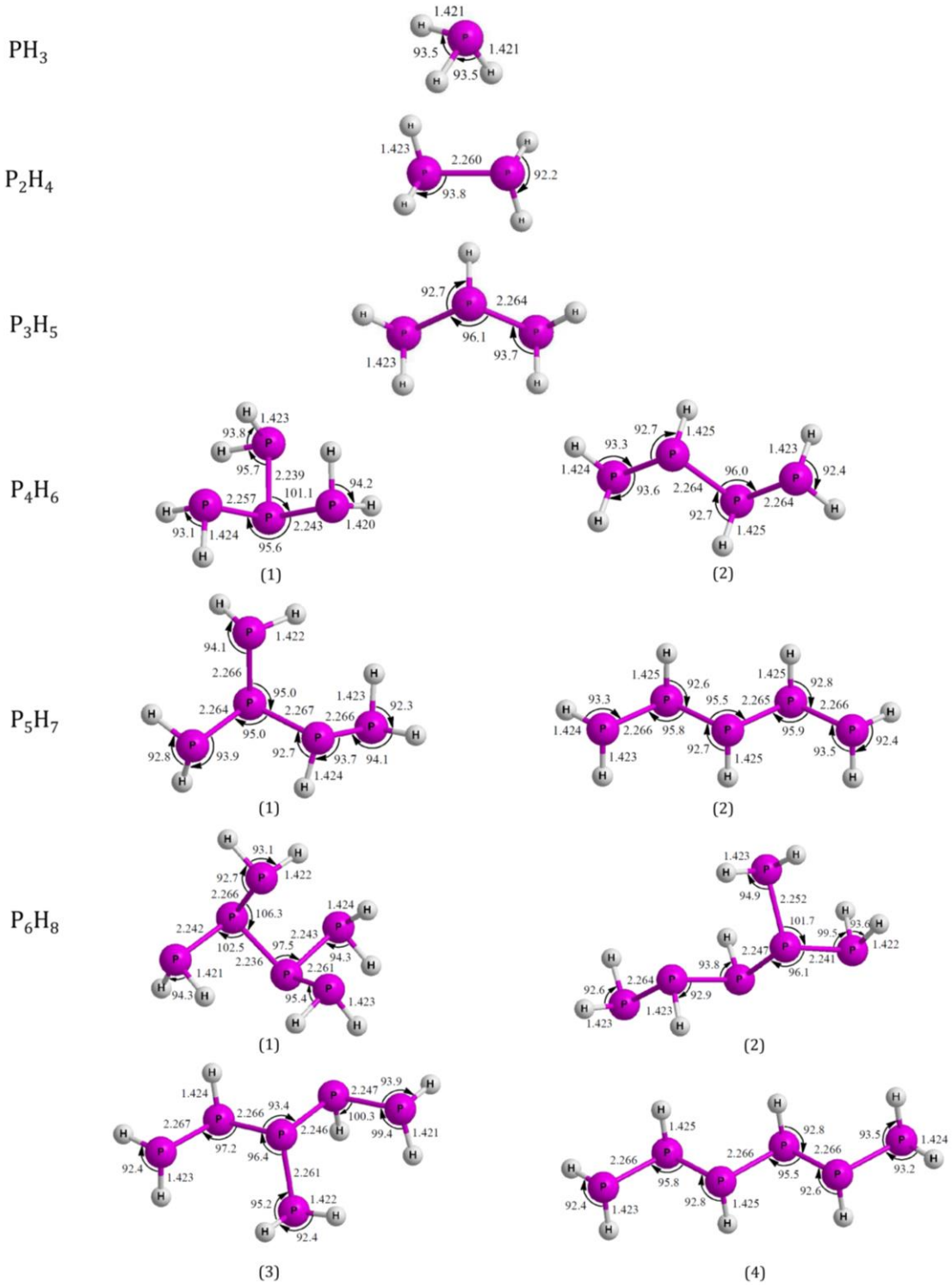

Figure 2.8. Calculated bond lengths and angles for isomers of PH_3 through P_6H_8.

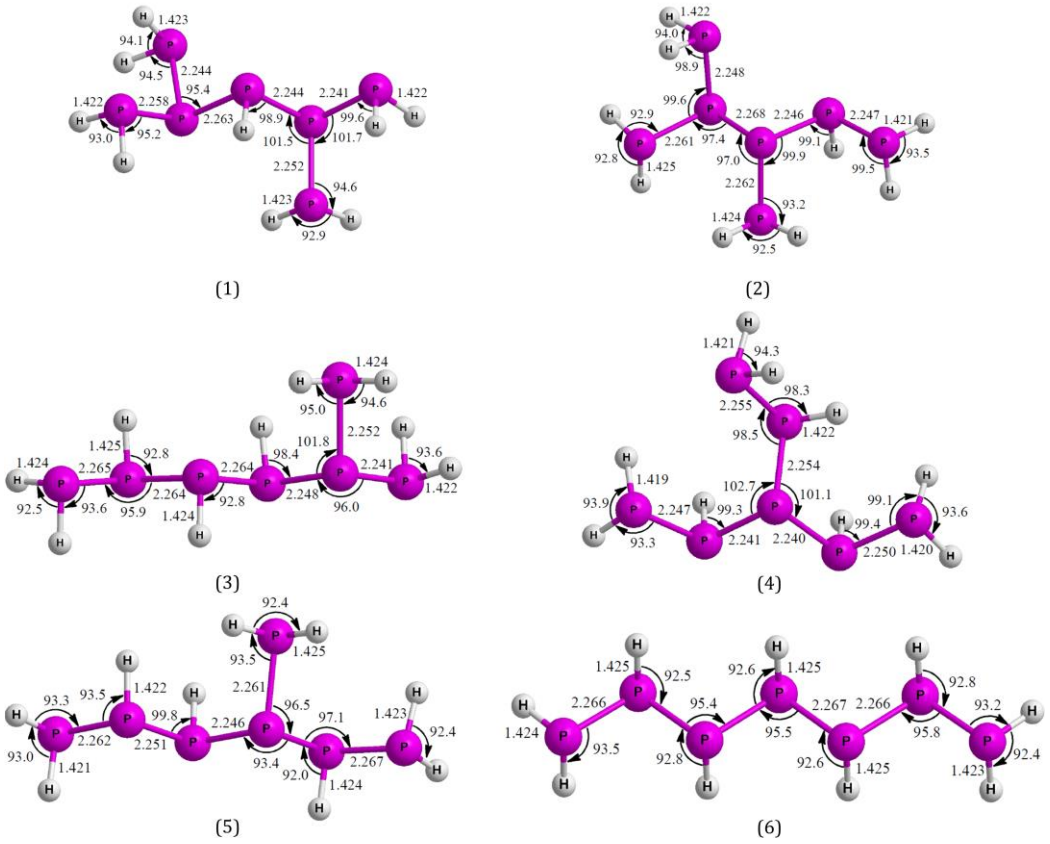

Figure 2.9. Calculated bond lengths and angles for isomers of P_7H_9.

Therefore, we can conclude that the computed ionization energies are about 0.1 eV lower when compared to the experimental predictions; this shift is in line with previous computations of adiabatic ionization energies of polyacetylenes[93] and nitrogen-terminated carbon clusters.[94] With respect to higher phosphanes, the calculated ionization energies decrease as the molecules become larger from 7.89 eV to 7.49 eV from tetraphosphane to octaphosphane, respectively. Interestingly, the ionization potentials for a set of isomers are similar to each other without a correlation to branching. The range of CCSD(T)/cc-pVTZ ionization energies are 7.89–8.00 eV (P_4H_6), 7.71–7.87 eV (P_5H_7), 7.60–7.79 eV (P_6H_8), 7.50–7.74 eV (P_7H_9), and 7.49–7.91 eV (P_8H_{10}). The ionization energies show little difference between P_7H_9 and P_8H_{10} isomers and this trend is expected to continue with higher-order phosphanes. Most importantly, all ionization energies are well below 10.49 eV—the energy of the VUV photon utilized to photoionize the subliming molecules in the present experiments.

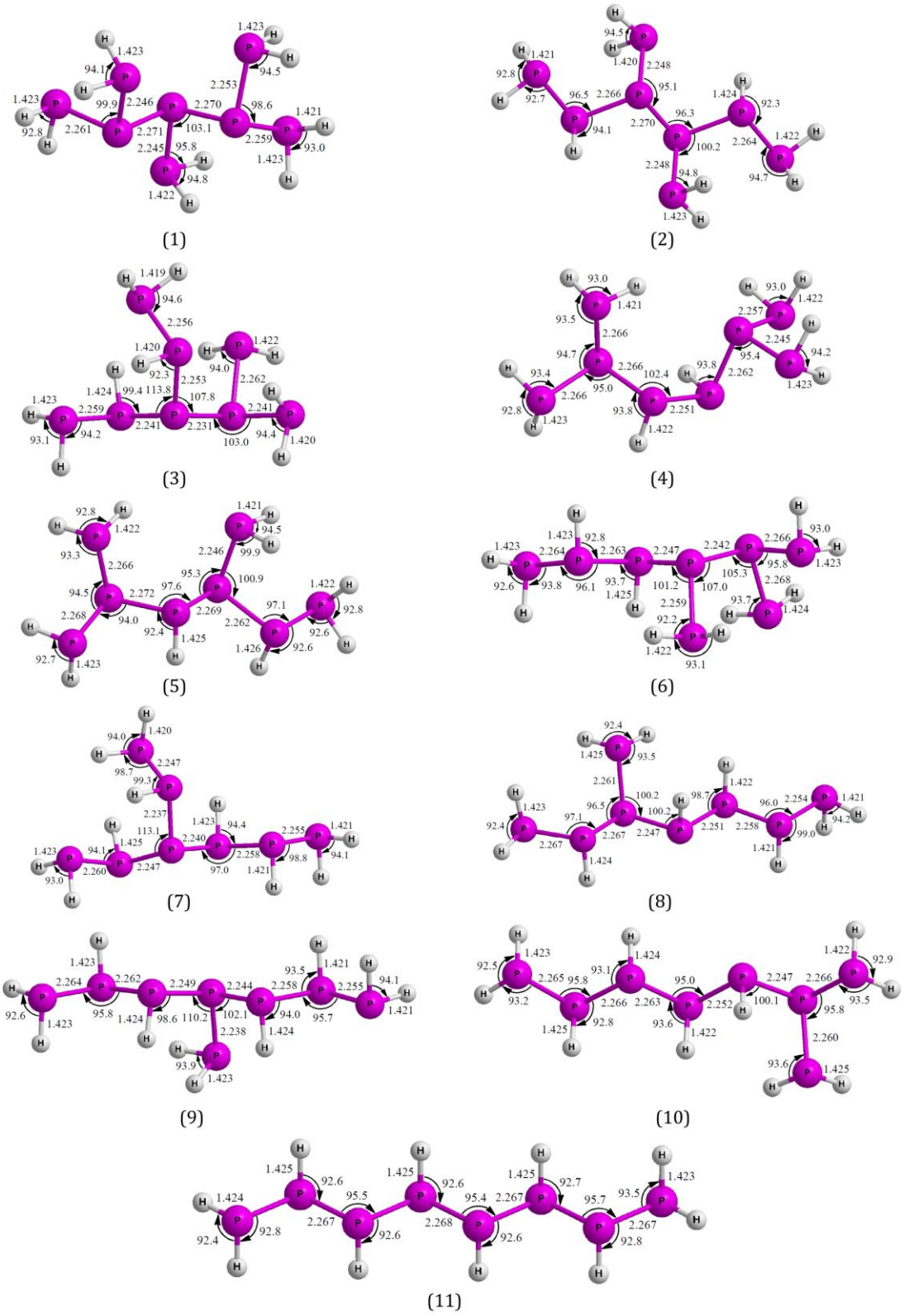

Figure 2.10. Calculated bond lengths and angles for isomers of P_8H_{10}.

Table 2.5. Calculated ionization energies and relative isomer energies for PH_3 to P_8H_{10}.

Isomer[a]	Ionization Energy (eV)[b]	Ionization Energy (eV)[c]	Ionization Energy (eV)[d]	Relative Energy (kJ mol^{-1})
PH_3	9.82	9.74	9.87	--
P_2H_4	8.68	8.76	8.8	--
P_3H_5	8.10	8.23	8.7	--
P_4H_6 (1)	7.74	7.89		0
P_4H_6 (2)	7.81	8.00		9
P_5H_7 (1)	7.52	7.71		0
P_5H_7 (2)	7.64	7.87		6
P_6H_8 (1)	7.62	7.76		0
P_6H_8 (2)	7.47	7.68		5
P_6H_8 (3)	7.39	7.60		7
P_6H_8 (4)	7.53	7.79		16
P_7H_9 (1)	7.45	7.69		0
P_7H_9 (2)	7.30	7.52		0.4
P_7H_9 (3)	7.44	7.69		9
P_7H_9 (4)	7.29	7.50		10
P_7H_9 (5)	7.34	7.55		11
P_7H_9 (6)	7.47	7.74		19
P_8H_{10} (1)	7.24	7.49		0
P_8H_{10} (2)	7.26	7.50		4
P_8H_{10} (3)	7.44	7.65		7
P_8H_{10} (4)	7.36	7.62		11
P_8H_{10} (5)	7.28	7.55		12
P_8H_{10} (6)	7.49	7.68		12
P_8H_{10} (7)	7.57	7.91		15
P_8H_{10} (8)	7.30	7.50		19
P_8H_{10} (9)	7.49	7.91		20
P_8H_{10} (10)	7.38	7.57		21
P_8H_{10} (11)	7.40	7.69		29

[a] The number in parentheses labels the isomer with the lowest energy isomer listed first (Figures 2.8–2.10)
[b] B3LYP/cc-pVYZ energy with zero-point correction
[c] CCSD(T)/cc-pVTZ with B3LYP/cc-pVTZ zero-point energy correction
[d] Reference ionization energies[99-101]

2.5 Conclusion

An exposure of phosphine (PH_3) ices to energetic electrons produced a homologues series of saturated phosphanes as complex as octaphosphane (P_8H_{10}). This finding is in quite contrast to isoelectronic ammonia (NH_3) systems,[102-106] leading only to hydrazine (N_2H_4) as the most complex hydrogenated nitrogen compound. Despite the isovalency, similar experimental conditions (temperature, radiation exposure) have been shown to produce far larger hydrides of phosphorus than those of isoelectronic nitrogen. Here, the smaller N-N bond distance (145 pm)[107] compared to typical P-P bonds (221 pm)[96] contributes to the decreased stability of complex nitrogen-based hydrides. The method of vacuum ultraviolet (VUV) single photon ionization to detect inorganic compounds synthesized through non-classical, radiation induced synthetic pathways

with the extremely sensitive PI-ReTOF-MS technique has proven to be far more illuminating than traditional experiments employing only FTIR and RGA mass spectroscopic analysis to identify complex phosphanes. The latter technique limited the observations to diphosphine (P_2H_4) and triphosphane (P_3H_5), while compounds as large as octaphoaphane (P_8H_{10}) could be monitored using PI-ReTOF-MS. Future experiments will be designed to identify *individual* isomers by selectively photoionizing these isomers with VUV photons exploring four-wave difference and sum mixing[84,108] ultimately exploring the complexity of novel inorganic molecules synthesized via non-traditional techniques such as low temperature electron irradiation of simple precursor ices.

2.6 Supplementary Information

2.6.1 Refractive index and ice thickness determination

The refractive index (n_{PH_3}) of solid phosphine and the experimental ice thickness were determined using laser interferometry. With this information, the absorption coefficients were obtained, and the details are presented below. Each laser interferogram was obtained by reflecting a HeNe laser at 632.8 nm (Melles Griot 25-LHP-213, 0.5 mW) off the silver substrate during phosphine deposition at angles shown in Figure 2.S1. The power of the reflected light was monitored using a photodiode interfaced connected to a picoammeter (Keithley 6485), which was GPIB-interfaced to a computer and recorded using LabVIEW. The interference pattern results from constructive and destructive interference between the portion of the laser that reflects off the ice surface with the portion that transmits through the ice and reflects off the silver substrate (Figure 2.S2). As the ice deposits, the optical path difference increases and the relative phase changes result, ideally, in a sinusoidal pattern. The refractive index was determined using a two-laser method[109] with the lasers at angles of incidence $\theta_1 = 20.0 \pm 0.1°$ and $\theta_2 = 57.0 \pm 0.1°$ and Equation 2.S1:

$$n_{PH_3}^2 = \frac{\frac{T_2^2}{T_1^2} sin^2\theta_2 - sin^2\theta_1}{\frac{T_2^2}{T_1^2} - 1} \quad (2.S1)$$

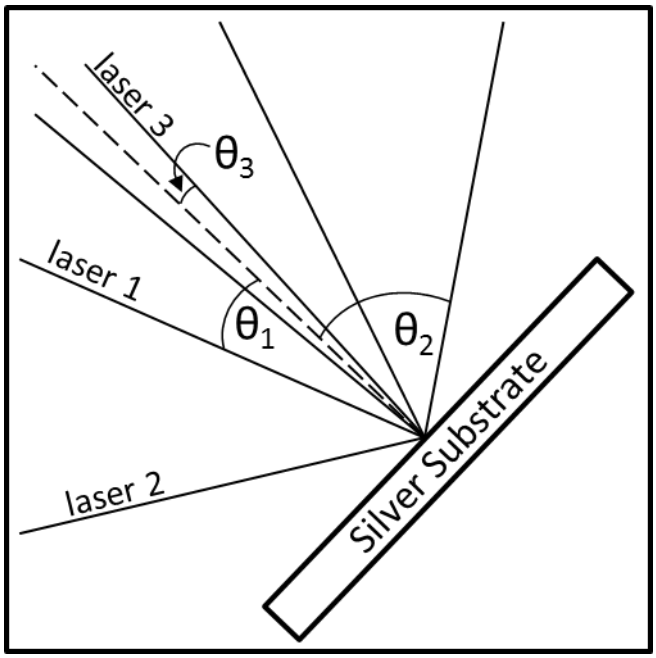

Figure 2.S1. Diagram showing the angles of incidence relative to the surface normal (dashed line) for the three 632.8 nm lasers. The angles at θ_1 = 20.0° and θ_2 = 57.0° were used for determining the refractive index, while θ_3 = 4° was used for calculating the thickness of the ice.

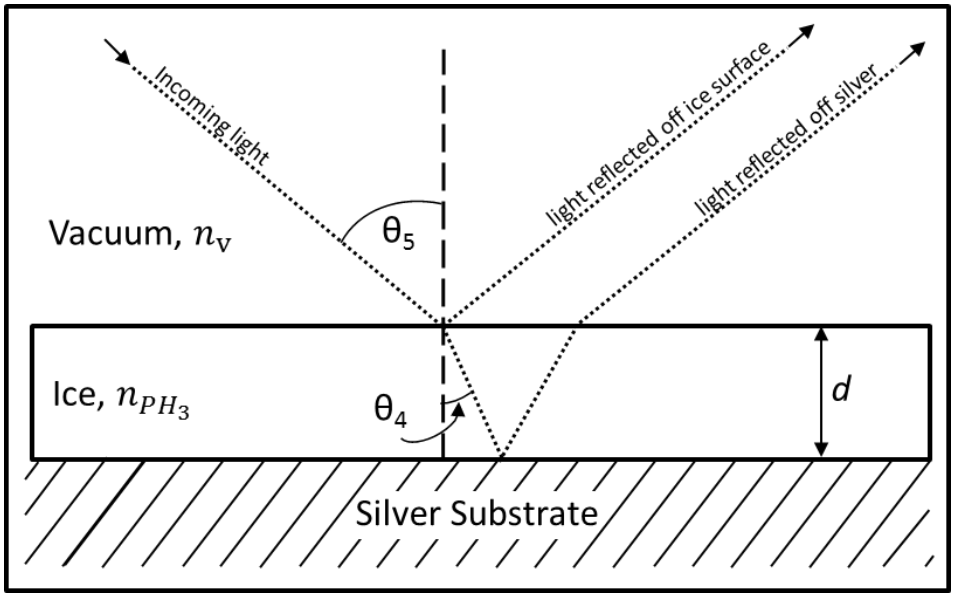

Figure 2.S2. Diagram showing that incoming light can either reflect off the surface of the ice or pass through the ice and reflect off the silver substrate before passing out of the ice. The notation for θ_4 and θ_5 is used for the incoming infrared beam (θ_4 = 43°) in the calculation of the absorption coefficients.

where T_1 and T_2 are the periods of the interference fringes for laser 1 and laser 2, respectively. A plot showing simultaneous data collection from both lasers during sample deposition is shown in Figure 2.S3.

Our experimentally obtained value for solid phosphine is n_{PH_3} = 1.51 ± 0.02. The refractive index was utilized in Equation 2.S2 to determine the thickness (d) of the ice using the interference pattern of one laser (λ = 632.8 nm) at an angle of incidence θ_3 = 4°:

$$d = \frac{m\,\lambda}{2\sqrt{n_{PH_3}^2 - sin^2\theta_3}} \tag{2.S2}$$

Here, the fringes of the interference pattern (m) are determined using a plot such as Figure 2.S4, which shows the interference pattern during ice deposition. Using 4.4 interference fringes, the ice was calculated to be 920 ± 20 nm thick.

2.6.2 Absorption coefficients.

The absorption coefficients (A_{exp}) for infrared peaks were experimentally determined starting with Equation 2.S3:

$$A_{exp} = \frac{\ln(10)\int_{\tilde{\nu}_1}^{\tilde{\nu}_2} A(\tilde{\nu})d\tilde{\nu}}{C\,L} \tag{2.S3}$$

where $\int_{\tilde{\nu}_1}^{\tilde{\nu}_2} A(\tilde{\nu})d\tilde{\nu}$ is the integrated peak area (measured in cm^{-1}), C is the concentration of the ice in mol cm^{-3}, and L is the pathlength of the infrared beam through the ice. The concentration is related to the density of the ice (ρ = 0.90 g cm^{-3}) and the molar mass (M = 34.00 g mol^{-1}) by Equation 2.S4:

$$C = \frac{\rho}{M} \tag{2.S4}$$

The density determination utilized x-ray diffraction data that four molecules of phosphine (5.646×10^{-22} g $molecule^{-1}$) are contained in a face-centered cubic unit cell with volume $2.51 \pm 0.01 \times 10^{-22}$ cm^3.[83] The density of this crystal lattice approximates the density of our ice with an unknown crystalline or amorphous phase. The pathlength of the infrared beam through the ice, L, can be solved geometrically using Equation 2.S5:

$$L = \frac{2d}{cos\,\theta_4} \tag{2.S5}$$

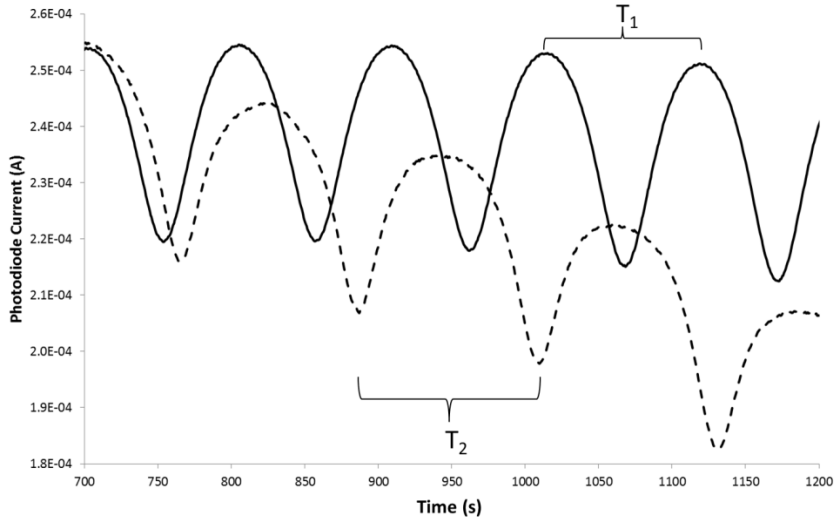

Figure 2.S3. Interference plot for two 632.8 nm lasers striking the surface at angles of incidence of 20.0° (solid line) and 57.0° (dashed line). The distance between two extrema, measured in time, is used for values of T_1 and T_2 to calculate the refractive index of the ice.

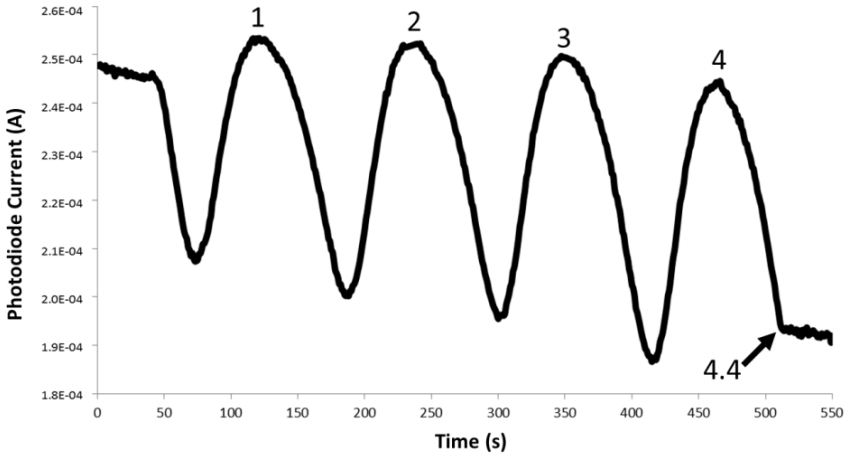

Figure 2.S4. Interference plot for one 632.8 nm laser recorded during ice deposition at an angle of incidence of 4°. Integer numbers of fringes are labeled above signal maxima, and at the deposition stop time, 4.4 fringes had accumulated.

where θ_4 is the angle at which the refracted light passes through the ice relative to the surface normal and the factor of 2 accounts for the incoming and outgoing beams. This can be related to the angle of incidence of the infrared beam (θ_5 = 43°) using Snell's Law (Equation 2.S6):

$$\theta_4 = sin^{-1} \frac{n_v}{n_{PH_3}} sin\, \theta_5 \tag{2.S6}$$

Noting that $cos\ sin^{-1} \frac{n_v}{n_{PH_3}} sin\, \theta_5 = \sqrt{1 - \frac{sin^2\theta_5}{n_{PH_3}^2}}$ and the refractive index in a vacuum (n_v) is 1, Equations 2.S4, 2.S5, and 2.S6 can be combined into Equation 2.S7:

$$A_{exp} = \frac{\ln(10) M \int_{\tilde{\nu}_1}^{\tilde{\nu}_2} A(\tilde{\nu}) d\tilde{\nu}}{2\, d\, \rho} \frac{\sqrt{n_{PH_3}^2 - sin^2\theta_5}}{n_{PH_3}} \tag{2.S7}$$

The experimentally determined intensities are compared with those from theoretical calculations, along with the observed and calculated peak positions, in Table 2.S1 and reported with units cm molecules^{-1} by introducing the Avogadro constant (N_A) into Equation 2.S8:

$$A_{exp} = \frac{\ln(10) M \int_{\tilde{\nu}_1}^{\tilde{\nu}_2} A(\tilde{\nu}) d\tilde{\nu}}{2\, N_A\, d\, \rho} \frac{\sqrt{n_{PH_3}^2 - sin^2\theta_5}}{n_{PH_3}} \tag{2.S8}$$

Compared to results for liquid[110] and gaseous[111] phosphine, P–H stretching vibrations (ν_1 and ν_3) show similar absorption coefficients with solid phosphine. However, the values for the solid phase deformation modes (ν_2 and ν_4) were approximately a third of their liquid and gas phase counterparts. The values obtained from theoretical calculations were higher than all experimental values. Specifically, solid phosphine's experimentally determined values were 30-40% of the theoretical values for P-H stretching modes and 15-20% for deformation modes.

Because the experimental absorption coefficients for diphosphine are unknown, the theoretical value was corrected using equivalent vibrations for phosphine. Phosphine's ν_4 mode at 1096 cm^{-1} has an experimental absorption coefficient that is 19% of the theoretical value, so 19% of diphosphine's ν_{11} theoretical value was used to approximate the experimental value of 7.0×10^{-17} cm molecule^{-1}.

Table 2.S1. Experimental and calculated infrared data for PH_3. Solid phase and calculated values were determined in this study. Absorption coefficients from liquid phosphine includes combined values for two fundamental modes.

Assignment	Experimental Frequency (cm^{-1})	Calculated Frequency (cm^{-1})	Scaling Factor	Absorption Coefficients (A_{exp}, × 10^{-18} cm molecule^{-1})			
				Solid[a]	Gas[b]	liquid[c]	Calculated[a]
v_2	982	1018	0.965	0.51	1.7	4.2	3.3
v_4	1096	1138	0.963	0.71	2.1		3.7
v_3	2303	2382	0.967	2.4	2.4	12	5.8
v_1	2308	2390	0.966	7.0	8.4		22

[a]This study
[b]Gas phase absorption coefficients[3]
[c]Liquid phase absorption coefficients[4]

CHAPTER 3
PHOSPHINE AND METHANE ICES

This chapter is based on the paper: A. M. Turner, M. J. Abplanalp, R. I. Kaiser, "Probing the Carbon-Phosphorus Bond Coupling in Low-Temperature Phosphine (PH_3)-Methane (CH_4) Interstellar Ice Analogues", The Astrophysical Journal*, 819, 97 (2016)*

Phosphine, which has now been confirmed around the carbon-rich star IRC+10216, provides the first example of a phosphorus-containing single bond in interstellar or circumstellar media. While four compounds containing both phosphorus and carbon have been discovered, none contain a carbon-phosphorus single bond. Here, we show that this moiety is plausible from the reaction of phosphine with methane in electron-irradiated interstellar ice analogues. Fractional sublimation allows for detection of individual products at distinct temperatures using reflectron time-of-flight mass spectrometry (ReTOF) coupled with vacuum ultraviolet (VUV) photoionization. This method produced phosphanes and methylphosphanes as large as P_8H_{10} and $CH_3P_8H_9$, which demonstrates that a phosphorus-carbon bond can readily form and that methylphosphanes sublime at 12 to 17 K higher temperatures than the non-organic phosphanes. Also, irradiated ices of phosphine with deuterated-methane untangles the reaction pathways through which these methylphosphanes were formed and identified radical recombination to be preferred over carbene / phosphinidene insertion reactions. In addition, these ReTOF results confirm that CH_3PH_2 and CH_6P_2 can form *via* insertion of carbene and phosphinidene and that the methylenediphosphine ($PH_2CH_2PH_2$) isomer forms in the ices, although methylphosphine ($CH_3P_2H_3$) is likely the more abundant isomer and that phosphanes and organophosphanes preferentially fragment via the loss of a phosphino group when photoionized. While the formation of methylphosphine is overall endoergic, the intermediates produced by interactions with energetic electrons proceed toward methylphosphine favorably and barrierlessly and provide plausible mechanisms toward hitherto unidentified interstellar compounds.

3.1 Introduction

The recent discovery of phosphine (PH_3) in the circumstellar envelope of the carbon-rich star IRC+10216 (CW Leonis)[35-37] at abundances of 10^{-8} compared to molecular hydrogen (H_2) has revitalized the interest in the interstellar phosphorus chemistry. Besides phosphine, only six phosphorus-bearing molecules have been discovered in interstellar and/or circumstellar environments (Figure 3.1). These are phosphorus nitride (PN),[29-32] carbon phosphide (CP),[13,31] phosphaethyne (HCP),[14,31] phosphorus monoxide (PO),[28] dicarbon phosphide (CCP),[33] and cyanophosphaethyne (NCCP).[34] Each of these, except for phosphorus monoxide (PO), has been detected along with phosphine (PH_3) in IRC+10216 with abundances compared to molecular hydrogen of 3×10^{-10} for phosphorus nitride (PN),[31] 5×10^{-9} for carbon phosphide (CP),[31] 3×10^{-8} for phosphaethyne (HCP),[31] 10^{-9} for dicarbon phosphide (CCP),[33] and an upper abundance of 3×10^{-8} for the tentative detection of cyanophosphaethyne (NCCP).[34] Furthermore, phosphaethyne (HCP) and phosphine (PH_3) account for 5% and 2%, respectively, of the total phosphorus budget around IRC+10216.[37] Given the carbon-rich nature of this circumstellar envelope, it is not surprising that four of the six phosphorus-bearing compounds around IRC+10216 also contain carbon. Using the phosphaethyne-to-hydrogen cyanide (HCN) ratio (HCP/HCN = 0.001, compared to the solar ratio of 0.003)[112] to estimate the phosphorus to nitrogen ratio, the relatively high abundance of nitrogen also rationalizes the presence of phosphorus nitride (PN) and cyanophosphaethyne (NCCP). Phosphorus monoxide (PO), on the other hand, was discovered in the oxygen-rich circumstellar envelop of the supergiant star VY Canis Majoris.[28] Unlike phosphine, these molecules are notable in that phosphorus is bonded only to elements of the second period of the periodic table of the elements and that each compound contains a strong double or triple bond with phosphorus holding bond energies between 510 kJ mol^{-1} and 620 kJ mol^{-1}.[113] In contrast, phosphine only contains phosphorus-hydrogen single bonds with a bond energy of only 343 kJ mol^{-1}.[114]

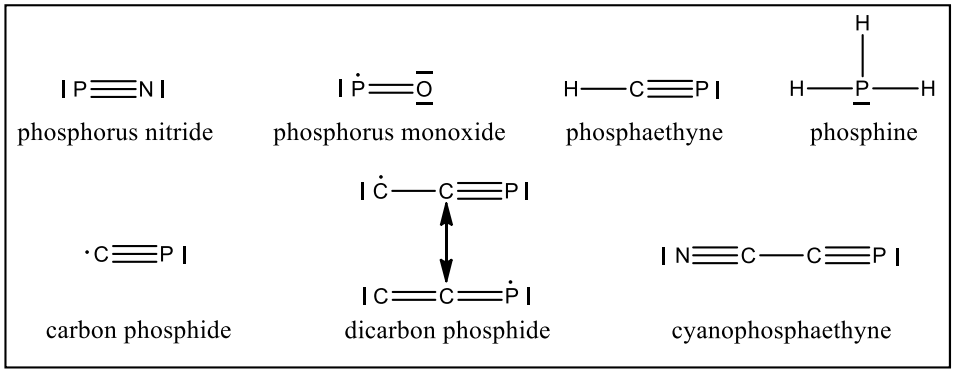

Figure 3.1. Phosphorus-bearing molecules detected in the interstellar medium.

It is not surprising that, with the exception of cyanophosphaethyne (NCCP), analogues to each of these compounds have been discovered in the interstellar medium in which phosphorus is substituted by its isovalent element: nitrogen. Given the discovery of phosphine, it follows that larger phosphorus-containing compounds analogous to those formed from isoelectronic ammonia should exist in interstellar environments. For example, methylamine (CH_3NH_2) was first discovered in the hot cores Sagittarius B2 and Orion A with abundances of 1×10^{-9} and 3×10^{-9}, respectively, compared to molecular hydrogen.[115,116] Recent laboratory experiments exposing ices of ammonia (NH_3) and C1 to C6 hydrocarbons[117] to energetic electrons, which mimicked the interaction of secondary electrons generated in the track of galactic cosmic rays while penetrating ice-coated interstellar grains, demonstrated that methylamine (CH_3NH_2) can be formed via the barrierless recombination of methyl radicals (CH_3) with amino radicals (NH_2) at 10 K. If ammonia is replaced by phosphine, the phosphorus analogue, methylphosphine (CH_3PH_2) is expected to form in interstellar analogue ices and predicted to exist toward Sagittarius B2 and Orion A along with methylamine.[118] However, as of today, interstellar methylphosphine (CH_3PH_2) has remained elusive.[119] In the present work, we investigate to what extent carbon-phosphorus bond coupling can lead to the formation of methylphosphine (CH_3PH_2) and potentially higher-order organophosphorus compounds in interstellar analogue ices of phosphine (PH_3) and methane (CH_4) upon interaction with energetic electrons generated in the track of galactic cosmic ray particles penetrating ice-coated particles in cold molecular clouds.

3.2 Experimental

The experiments were conducted in a stainless steel chamber operating under ultra-high vacuum pressures of 5 × 10^{-11} Torr by exploiting oil-free turbomolecular pumps and dry scroll backing pumps.[51,69-77] The ices were prepared on a reflective silver substrate mounted to a rotatable cold finger manufactured using oxygen-free high-conductivity copper capable of achieving temperatures as low as 5.5 ± 0.2 K by a closed-cycle helium refrigerator (Sumitomo Heavy Industries, RDK-415E). Methane (Advanced Specialty Gases, 99.999%) and phosphine (Sigma-Aldrich, 99.9995%) were premixed in a gas mixing chamber at 110 Torr each and then introduced into the main recipient with the help of a glass capillary at a pressure of 5 × 10^{-8} Torr for 8 minutes. A Nicolet 6700 Fourier Transform Infrared Spectrometer (FTIR) probed the deposited ices on the silver substrate on line and *in situ* from 6000 cm^{-1} to 500 cm^{-1} with 4 cm^{-1} resolution, and the integrated infrared peak areas ($\int_{\tilde{\nu}_1}^{\tilde{\nu}_2} A(\tilde{\nu})d\tilde{\nu}$) of the ν_2 band of phosphine (987 cm^{-1}) and ν_1 + ν_4 combination band of methane (4195 cm^{-1}) were used with their integrated absorption coefficients (A_{exp}) of 5.1 × 10^{-19} cm $molecule^{-1}$ and 3.5 × 10^{-19} cm $molecule^{-1}$, respectively,[109,120] in the following equation to determine the column density (N) of each reactant in the ice:

$$N = \frac{\ln(10) \int_{\tilde{\nu}_1}^{\tilde{\nu}_2} A(\tilde{\nu})d\tilde{\nu}}{2\, A_{exp}} \cos\left(\sin^{-1}\frac{\sin\alpha}{n_{ice}}\right) \quad (3.1)$$

The angle at which light passes through ice (β) is related to the angle of the incoming beam (α) by Snell's Law: $n_1 \sin\alpha = n_{ice} \sin\beta$. This was incorporated into Equation 3.1 along with a factor of 2 to account for the incoming and outgoing beams, by assigning the refractive index of vacuum to be $n_1 = 1$. To determine the refractive index of the ice mixture and the ice thickness, laser interferometry[78,79,120,121] was utilized during deposition by reflecting a helium-neon laser (λ = 632.8 nm) off the silver substrate and ice surfaces. The relative intensity between the maxima and minima of the interference fringes was used[121-123] to determine a refractive index of n_{ice} = 1.44 ± 0.04, which ranges between the refractive indices of pure phosphine (n_{PH_3}= 1.51)[120] and pure methane (n_{CH_4}= 1.33).[109] The column densities of 3.8 ± 0.3 × 10^{18} molecules cm^{-2} for phosphine

and 1.2 ± 0.1 × 10^{18} molecules cm^{-2} for methane indicate that the deposited ice mixture had a 3.2 ± 0.6 : 1.0 phosphine to methane ratio. The ice thickness (d) was measured using the equation:

$$d = \frac{m\,\lambda}{2\sqrt{n_{ice}^2 - sin^2\theta}} \tag{3.2}$$

Using the laser's angle of incidence (θ = 4 ± 1°) and by counting interference fringes (m = 4.45 ± 0.05 fringes), 980 ± 40 nm of ice was deposited. One hour after the deposition, the ice was irradiated with 5 keV electrons at a flux of 2 × 10^{10} electrons s^{-1} cm^{-2} at a 70° angle of incidence over an area of 1.0 ± 0.1 cm^2. Monte Carlo (CASINO)[82] calculations, which exploited the weighted averaged density of 0.78 g cm^{-3} from the phosphine (0.90 g cm^{-3})[83,120] and methane (0.47 g cm^{-3})[124] densities, were performed and determined the average absorbed dose with a 540 nm average penetration depth to be 3.5 ± 0.4 eV $molecule^{-1}$ for phosphine and 3.1 ± 0.3 eV $molecule^{-1}$ for methane. Note that the penetration depth is smaller than the thickness of the ices indicating that the electrons only interact with the ices but not the silver substrate. A temperature programmed desorption (TPD) protocol heated the irradiated ice to 300 K with a heating rate of 1 K min^{-1} and allowed the reactants and newly formed molecules to sublime. During the irradiation and heating, the FTIR monitored the ice on line and *in situ*. Also, two mass spectroscopic techniques analyzed the subliming species. A traditional quadrupole mass spectrometer (QMS) operating in residual gas analyzer (RGA) mode with 100 eV electrons at 1 mA emission current offered detection of molecules via electron impact ionization. A more sensitive reflectron time-of-flight (ReTOF) mass spectrometer (Jordan TOF Products, Inc.) utilizing single photon photoionization (118.2 nm, 10.49 eV)[69] was also used. The pulsed (30 Hz) coherent vacuum ultraviolet (VUV) light was generated via four wave mixing with xenon (99.999%) as the non-linear medium. The third harmonic (354.6 nm) of a pulsed neodymium-doped yttrium aluminum garnet laser (Nd:YAG, Spectra Physics, PRO-250, 30 Hz) underwent a frequency tripling process ($\omega_{vuv} = 3\omega_1$) to obtain the 118.2 nm light with about 10^{14} photons per pulse.[51] This light was spatially separated from the fundamental using a lithium fluoride (LiF) planoconvex lens[84] (ISP Optics, LF-PX-38^{-1}50) exploiting distinct refractive indices of LiF for different wavelengths of 1.40 and 1.59, respectively.[125] The VUV light was directed 1 mm above the

ice surface, and the photoionized molecules were mass analyzed with a reflectron time-of-flight (ReTOF) mass spectrometer. Here, the arrival time of the ions to a multichannel plate is based on the mass-to-charge ratio, and the signal was amplified with a fast preamplifier (Ortec 9305) and recorded with a bin width of 4 ns triggered at 30 Hz (Quantum Composers, 9518). Previous studies[120] have shown that the ionization energy of phosphanes range from 9.8 eV for PH_3 to 7.5 eV for P_8H_{10}, and thus the chosen photon energy (10.49 eV) is capable of ionizing each of the phosphanes to be observed. Also, methylphosphine (CH_3PH_2) ionizes at 9.1 eV,[126,127] and following trends of both phosphanes and alkanes that ionization energies decline with increasing molecular size, more complex alkylphosphanes are also expected to have ionization energies below 10.49 eV. To obtain mechanistic information, additional experiments were performed replacing methane with deuterated methane, CD_4 (CDN Isotopes, 99.9% D atom) under otherwise identical experimental conditions.

3.3 Results

3.3.1 Infrared Spectroscopy

During the irradiation, infrared spectra were recorded in two-minute intervals (Figure 3.2 and Table 3.1). Most notably, the strong phosphorus-hydrogen stretching modes of phosphine (PH_3) (ν_1 and ν_3) centered around 2310 cm^{-1} decreased and broadened due to the appearance of the ν_5 mode of diphosphine (P_2H_4) (2262 and 2287 cm^{-1}). Also, the ν_{11} mode of P_2H_4 emerged, albeit more subtly, at 1063 cm^{-1}.[96] Nearby, a tenuous peak at 1054 cm^{-1} was assigned to the deformation band of the methyl group in methylphosphine (CH_3PH_2),[128] while a more distinguishable peak appears at 2973 cm^{-1} caused by carbon-hydrogen stretching. Thus, only four new peaks emerged during irradiation and only two products, diphosphine and methylphosphine, could be assigned. A drawback of using infrared spectroscopy for methane-doped phosphine ices is that the most intense vibrations, the phosphorus-hydrogen stretching mode, occur in the same region of the spectrum for all products, i.e. typically from 2350 cm^{-1} to 2250 cm^{-1}. In addition, carbon-hydrogen stretching modes cannot be used to identify individual methylated phosphanes because the group frequencies overlap among each other in the range of 3000 cm^{-1} to 2950 cm^{-1}.

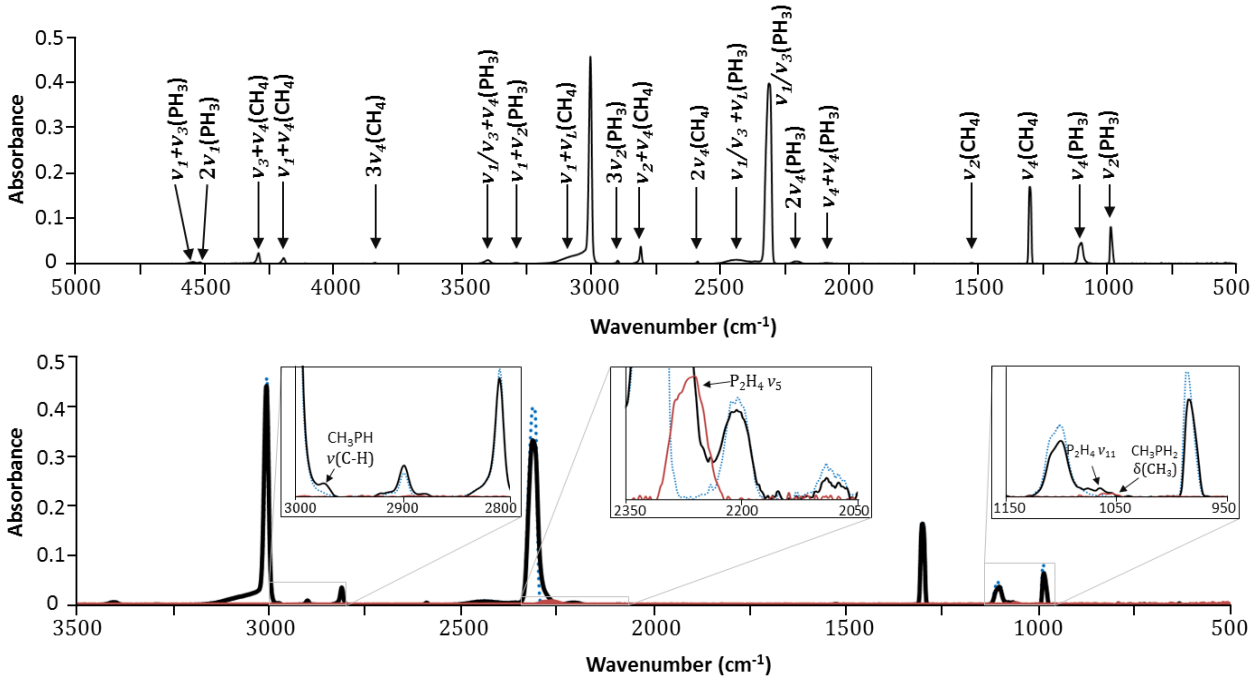

Figure 3.2. *(top)* Infrared spectrum of pristine methane-phosphine ice at 5.5 K. *(bottom)* Spectra of (PH_3) and methane (CH_4) ice before irradiation (blue dotted), after irradiation (black), and after methane and phosphine sublimed (90 K, red). New peaks seen from the irradiation are labeled.

After the sublimation of methane and phosphine (80 K), only the phosphorus-hydrogen stretches centered around 2295 cm^{-1} had significant intensity. Even after diphosphine sublimed (135 K), this peak slowly decreased in intensity and disappeared into the baseline as higher order products sublimed.

3.3.2 Reflectron Time-of-Flight Mass Spectrometry (ReTOF-MS)

The ReTOF data using a 10.49 eV photoionization energy provided the most useful and ample results for determining the products of irradiated ices of phosphine (PH_3) and methane (CH_4) (Figure 3.3, Tables 3.2 & 3.3), especially when compared to quadrupole mass spectrometry results (Supplementary Information). This highly sensitive technique allowed molecular identification exploiting unique mass-to-charge ratios and well-defined sublimation temperatures from heating the ices to 300 K at a rate of 1 K min^{-1}. Figure 3.4 depicts the ion count intensity for methane-doped phosphine ice as a function

Table 3.1. Infrared absorption assignments for phosphine (PH_3) and methane (CH_4) ice at 5.5 K and the irradiation products. ν_L defines the lattice mode.

Assignment	Compound	Position (cm^{-1})	References
ν_2	PH_3	983, 987	(1)
ν_4	PH_3	1099, 1100, 1110sh	(1)
ν_4	CH_4	1296, 1302	(2)
ν_2	CH_4	1526	(2)
$\nu_2 + \nu_4$	PH_3	2071, 2091	(1)
$2\nu_4$	PH_3	2193, 2209	(1)
ν_1	PH_3	2305	(1)
ν_3	PH_3	2313, 2326	(1)
$\nu_1/\nu_3 + \nu_L$	PH_3	2349, 2440, 2461	(1)
$2\nu_4$	CH_4	2589	(2)
$\nu_2 + \nu_4$	CH_4	2809, 2816	(2)
$3\nu_2$	PH_3	2899	(1)
ν_3	CH_4	3002, 3006, 3008	(2)
$\nu_3 + \nu_L$	CH_4	3029, 3074	(2)
$\nu_1 + \nu_2$	PH_3	3293	(1)
$\nu_1 + \nu_4$	PH_3	3402	(1)
$\nu_3 + \nu_4$	PH_3	3420	(1)
$3\nu_4$	CH_4	3841	(2)
$\nu_1 + \nu_4$	CH_4	4193, 4198	(2)
$\nu_3 + \nu_4$	CH_4	4291, 4296, 4306	(2)
$2\nu_1$	PH_3	4519	(1)
$\nu_1 + \nu_3$	PH_3	4547	(1)
New peaks from irradiation			
$\delta(CH_3)$	CH_3PH_2	1054	(3)
ν_{11}	P_2H_4	1063	(4)
ν_5	P_2H_4	2262, 2287	(4)
ν(C-H)	CH_3PH_2	2973	(3)

References: (1)[120], (2)[129], (3)[128], (4)[96]

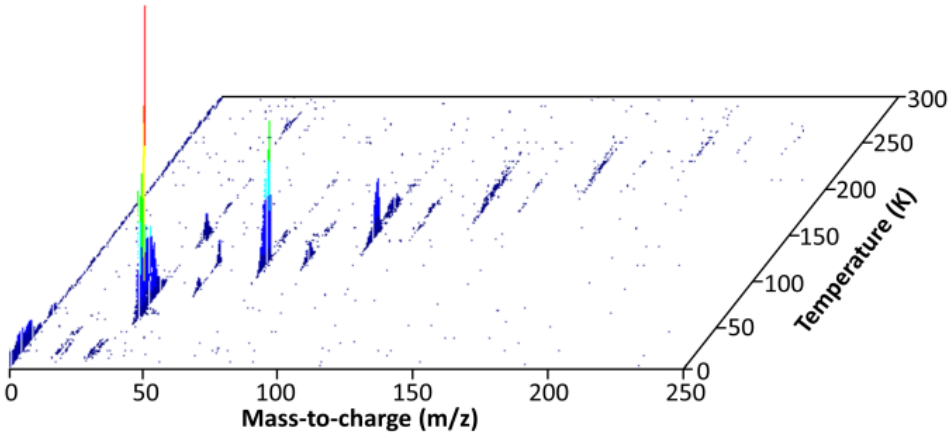

Figure 3.3. ReTOF mass spectrometry data as a function of sublimation temperature as irradiated phosphine (PH_3) and methane (CH_4) ice was heated from 5.5 K to 300 K at 1 K min^{-1}.

Table 3.2. Observed ions in the ReTOF mass spectrometer for the phosphine (PH_3) and methane (CH_4) irradiation.

Mass	Formula	Comments	Molecular Formula of Parent Compound
35	PH_4^+	fragment	P_3H_5, P_4H_6, $CH_3P_4H_5$
48	$PH_2CH_3^+$	parent	CH_3PH_2
49	$^{13}CH_3PH_2^+$	isotope	CH_3PH_2
	$CH_3PH_3^+$	fragment	$CH_3P_3H_4$, $CH_3P_4H_5$
66	$P_2H_4^+$	parent	P_2H_4
67	$P_2H_5^+$	protonated parent	P_2H_4
		fragment	P_4H_6, $CH_3P_4H_5$, P_5H_7, $CH_3P_4H_5$
78	$CH_3P_2H^+$	fragment	$CH_3P_3H_4$
79	$CH_3P_2H_2^+$	fragment	$CH_3P_3H_4$
80	$CH_3P_2H_3^+$	parent	$CH_3P_2H_3$
81	$^{13}CH_3P_2H_3^+$	isotope	$CH_3P_2H_3$
	$CH_3P_2H_4^+$	fragment	$CH_3P_5H_6$
96	$P_3H_3^+$	fragment	P_4H_6, $CH_3P_4H_5$
97	$P_3H_4^+$	fragment	P_4H_6, $CH_3P_4H_5$
98	$P_3H_5^+$	parent	P_3H_5
99	$P_3H_6^+$	protonated parent	P_3H_5
		fragment	P_6H_8, $CH_3P_6H_7$
110	$CH_3P_3H_2^+$	fragment	$P_4H_5CH_3$
111	$CH_3P_3H_3^+$	fragment	$CH_3P_4H_5$
112	$CH_3P_3H_4^+$	parent	$CH_3P_3H_4$
126	$P_4H_2^+$	fragment	P_6H_8, $P_6H_7CH_3$
127	$P_4H_3^+$	fragment	P_6H_8, $P_6H_7CH_3$
128	$P_4H_4^+$	fragment	P_6H_8, $P_6H_7CH_3$
129	$P_4H_5^+$	fragment	P_5H_7, $CH_3P_5H_7$, P_6H_8, $P_6H_7CH_3$
130	$P_4H_6^+$	parent	P_4H_6
143	$CH_3P_4H_4^+$	fragment	$CH_3P_5H_7$
144	$CH_3P_4H_5^+$	parent	$CH_3P_4H_5$
159	$P_5H_4^+$	fragment	P_7H_9, $CH_3P_7H_8$
160	$P_5H_5^+$	fragment	P_6H_8, $CH_3P_6H_7$, P_7H_9
161	$P_5H_6^+$	fragment	P_6H_8, $CH_3P_6H_7$
162	$P_5H_7^+$	parent	P_5H_7
175	$CH_3P_5H_5^+$	fragment	$CH_3P_6H_7$
191	$P_6H_5^+$	fragment	P_7H_9, $CH_3P_7H_8$, P_8H_{10}, $CH_3P_8H_9$
193	$P_6H_7^+$	fragment	P_7H_9, $CH_3P_7H_8$
207	$CH_3P_6H_6^+$	fragment	$CH_3P_7H_8$
225	$P_7H_8^+$	fragment	P_8H_{10}, $CH_3P_8H_9$
239	$CH_3P_7H_7^+$	fragment	$CH_3P_8H_9$

Table 3.3. Onset sublimation temperatures for the products of phosphine (PH_3) with methane (CH_4) irradiation and observed species (either molecular ions or fragments) that were assigned to each product. Because molecular ions for products larger than P_5H_7 and $CH_3P_4H_5$ were not observed, fragments were utilized to determine sublimation temperatures. The ratios of observed species assigned to each product are listed to illustrate the fragmentation patterns.

Compound	Sublimation Temperature	Species Detected by ReTOF-MS	Ratio of Species Detected (scaled to 100)
CH_3PH_2	87 K	$CH_3PH_2^+$	100
P_2H_4	98 K	$P_2H_5^+$, $P_2H_4^+$	0.75 : 100
$CH_3P_2H_3$	118 K	$CH_3P_2H_3^+$	100
P_3H_5	131 K	$P_3H_6^+$, $P_3H_5^+$, PH_4^+	0.3 : 100 : 34
$CH_3P_3H_4$	148 K	$CH_3P_3H_4^+$, $CH_3P_2H_2^+$, $CH_3P_2H^+$, $CH_3PH_3^+$	100 : 53 : 31 : 4
P_4H_6	160 K	$P_4H_6^+$, $P_3H_4^+$, $P_3H_3^+$, $P_2H_5^+$, PH_4^+	35 : 85 : 100 : 2 : 12
$CH_3P_4H_5$	175 K	$CH_3P_4H_5^+$, $CH_3P_3H_3^+$, $CH_3P_3H_2^+$, $CH_3PH_3^+$	29 : 100 : 16 : 7
P_5H_7	185 K	$P_5H_7^+$, $P_4H_5^+$, $P_4H_4^+$, $P_2H_5^+$	10 : 100 : 40 : 10
$CH_3P_5H_6$	197 K	$CH_3P_4H_4^+$, $CH_3P_2H_4^+$	100 : 10
P_6H_8	206 K	$P_5H_6^+$, $P_5H_5^+$, $P_5H_5^+$, $P_4H_3^+$, $P_4H_2^+$, $P_3H_6^+$	100 : 9 : 7 : 23 : 15 : 6
$CH_3P_6H_7$	218 K	$CH_3P_5H_5^+$	100
P_7H_9	231 K	$P_6H_7^+$, $P_6H_5^+$, $P_5H_5^+$, $P_5H_4^+$	100 : 17 : 10 : 31
$CH_3P_7H_8$	243 K	$CH_3P_6H_6^+$	100
P_8H_{10}	252 K	$P_7H_8^+$, $P_6H_5^+$	100 : 85
$CH_3P_8H_9$	264 K	$CH_3P_7H_7^+$	100

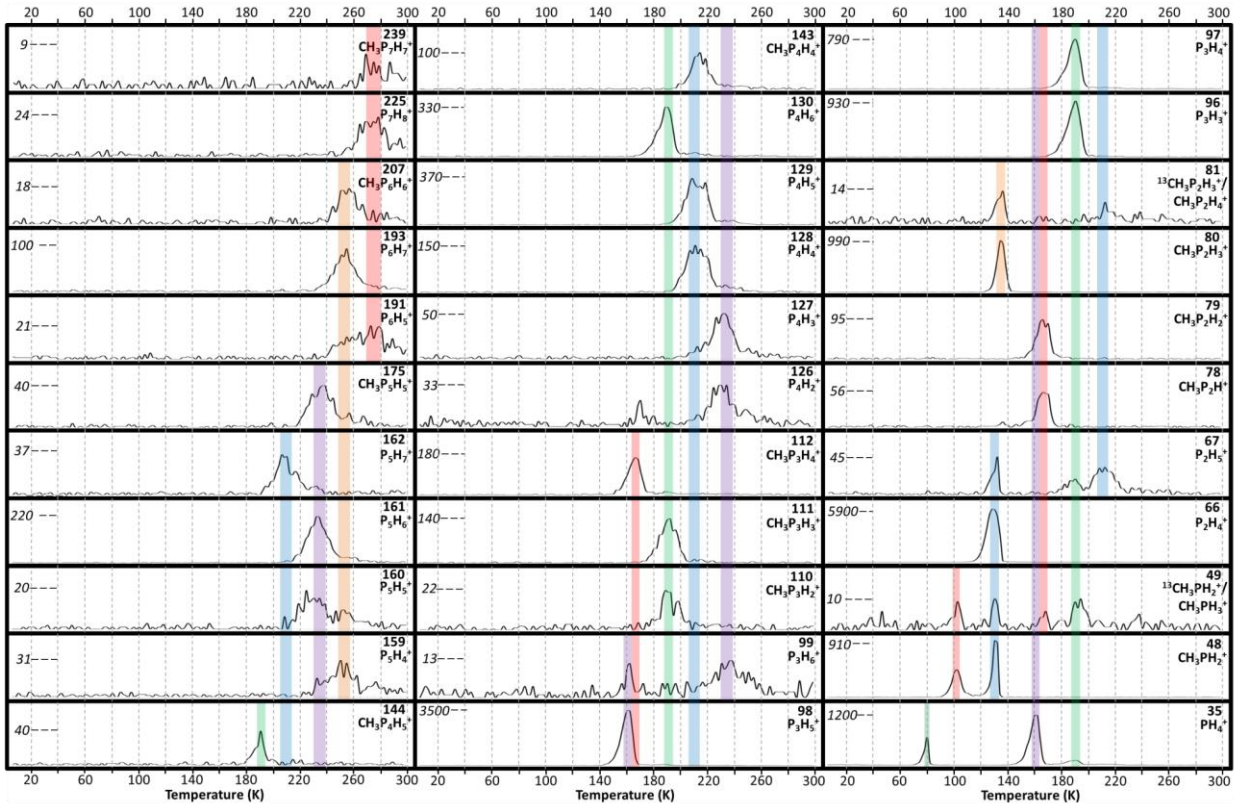

Figure 3.4. Time-of-flight mass spectra for the products of phosphine (PH_3) and methane (CH_4) irradiation as a function of temperature. Colored bands indicate sublimation events at similar temperatures. The intensity is listed on the left of each spectrum, while the mass-to-charge and ionic formula is on the right.

of temperature during warm-up of the irradiated ices to 300 K at all mass-to-charge ratios observed in the ReTOF. A few observations consistent with the irradiation of pure phosphine ice[120] can be highlighted. First, a series of saturated phosphanes including diphosphine (P_2H_4), triphosphane (P_3H_5), tetraphosphane (P_4H_6), and pentaphosphane (P_5H_7) were observed at progressively increasing sublimation temperatures via their parent ions that peaked at 130 K, 162 K, 190 K, and 208 K, respectively. Furthermore, the molecular ion counts for P_2H_4 and P_3H_5 were by far the highest of any product. Diphosphine showed no evidence of fragmentation, while triphosphane fragmented mostly into PH_4^+ at a third of the parent ion intensity and also to minor amounts of $P_2H_3^+$ and $P_2H_2^+$ through PH_2 and PH_3 loss. Beginning with P_4H_6, fragmentation became dominant and the parent ion was about five times less intense than the combined major PH_2 and PH_3 loss fragments: $P_3H_4^+$ and $P_3H_3^+$. Pentaphosphane (P_5H_7) showed that the extent of fragmentation increased with molecular size as the parent ion intensity was only 10% that of the PH_2 loss fragment, $P_4H_5^+$. A minor but notable protonated two-phosphorus fragment, $P_2H_5^+$, also occurred for P_5H_7. Starting with hexaphosphane (P_6H_8), fragmentation was quantitative so that the molecular ion could no longer be observed in the mass spectra, making $P_5H_7^+$ the largest observed parent ion. However, given the sequential order of sublimation temperatures as phosphanes increase in size along with the predictable pattern of fragmentation—predominately from PH_2 loss—fragments can be used to infer the presence of their parent compounds (Figure 3.4). Specifically, the intensity and sublimation temperature of fragment ions $P_5H_6^+$, $P_6H_7^+$, and $P_7H_8^+$ was exploited as a proxy for determination of hexaphosphane (P_6H_8), heptaphosphane (P_7H_9), and octaphosphane (P_8H_{10}). In summary, phosphine in the irradiated phosphine-methane ice reacted to form saturated phosphanes as complex as P_8H_{10}.

Further analysis revealed that each of the phosphanes observed in the ReTOF also correlated with an associated methylphosphane of the generic molecular formula $CH_3P_xH_{x+1}$, with x = 1 to 8. The most abundant products were molecules with the formula CH_3PH_2 and $CH_3P_2H_3$, which occurred in similar quantities, although CH_3PH_2 had two distinct sublimation events, which was unique among products, at 102 and 130 K. The first event was exploited to determine the onset sublimation temperature for

methylphosphine (CH_3PH_2), while the second peak occurred coincidentally with diphosphine (P_2H_4) sublimation. Here, a significant portion of CH_3PH_2 remained trapped in the P_2H_4 matrix, which was the most abundant product, and was released when P_2H_4 sublimed. Neither CH_3PH_2 nor $CH_3P_2H_3$ showed evidence of fragmentation. However, considering the next member, nearly half of the sublimed $CH_3P_3H_4$ fragmented into $CH_3P_2H_2^+$ and $CH_3P_2H^+$, which result from PH_2 and PH_3 loss. The heaviest molecular ion observed for methylphosphanes was $CH_3P_4H_5$, and the combined PH_2 and PH_3 loss fragments from $CH_3P_4H_5$ had a 4:1 ratio compared to the parent ion. All methylphosphanes including $CH_3P_4H_5$ and larger sublimed at similar temperatures as their non-methylated phosphane analogues, which complicates fragmentation analysis because $P_3H_3^+$ and $P_3H_4^+$ could be fragments from both $CH_3P_4H_5$ and P_4H_6. However, given the observed ratios of $P_2H_4^+$ to $CH_3P_2H_3^+$ (6:1) and $P_3H_5^+$ to $CH_3P_3H_4^+$ (20:1), it is likely that P_4H_6 formed in larger amounts than $CH_3P_4H_5$ and thus the $P_3H_4^+$ and $P_3H_3^+$ fragments originated predominately from P_4H_6, which itself had a parent ion ratio of 8:1 with $CH_3P_4H_5^+$. The parent ion for $CH_3P_5H_6$ was not observed, which is not surprising given the previously stated ratios between phosphanes and their methylated equivalents and that the intensity of $P_5H_7^+$ was diminished due to increased fragmentation. However, $CH_3P_5H_6$ can still be detected since it sublimed at a similar peak temperature of 212 K as P_5H_7 and the major PH_2 loss fragment, $CH_3P_4H_4^+$, was easily observed. This method also worked for the larger methylphosphanes $CH_3P_6H_7$, $CH_3P_7H_8$, and $CH_3P_8H_9$, which were identified using their fragments from PH_2 loss that appeared concurrently with the fragments from P_6H_8, P_7H_9, and P_8H_{10}, respectively. Thus, the irradiated methane-phosphine ices produced a series of phosphanes from P_2H_4 to P_8H_{10} and methylated phosphanes from CH_3PH_2 to $CH_3P_8H_9$. Notably, neither alkylphosphanes more complex than methylphosphanes nor pure hydrocarbons were detected, which was likely a result of the three-to-one phosphine-to-methane ratio in the ice mixture.

While the larger phosphanes showed similar *peak* sublimation temperatures with their methylated analogues, the temperature at the *onset* of sublimation was distinct. Figure 3.5 and Table 3.3 show how onset sublimation temperatures increase with atomic weight and how, from PH_3 to P_8H_{10} and from CH_3PH_2 to $CH_3P_8H_9$, the amount of

temperature increase declined with each successive member in the series. For PH_3 to P_3H_5, the onset sublimation temperatures were 17 to 20 K lower than their corresponding methylated form: 69 K vs. 87 K for PH_3/CH_3PH_2, 98 K vs. 118 for $P_2H_4/CH_3P_2H_3$, and 131 K vs. 148 K for $P_3H_5/CH_3P_3H_4$. The $P_4H_6/CH_3P_4H_5$ pair had a slightly lower difference of 15 K at 160 K vs. 175 K, while P_5H_8 (185 K), P_6H_8 (206 K), P_7H_9 (231 K), and P_8H_{10} (252 K) each began subliming 12 K below their methylated forms. Since higher order products were not observed via their parent ions, the fragments discussed previously were utilized to determine the onset sublimation temperature of the parent. The regression curves in Figure 3.5 used only the temperatures for directly observed ions, i.e. PH_3 through P_5H_7 and CH_3PH_2 through $CH_3P_4H_5$, and the curves were fit forward to higher order compounds. The regressions curves show good agreement with the assignments of parent ions from their fragments, which support the use of fragments when the intensity of parent ions is below the detection limit.

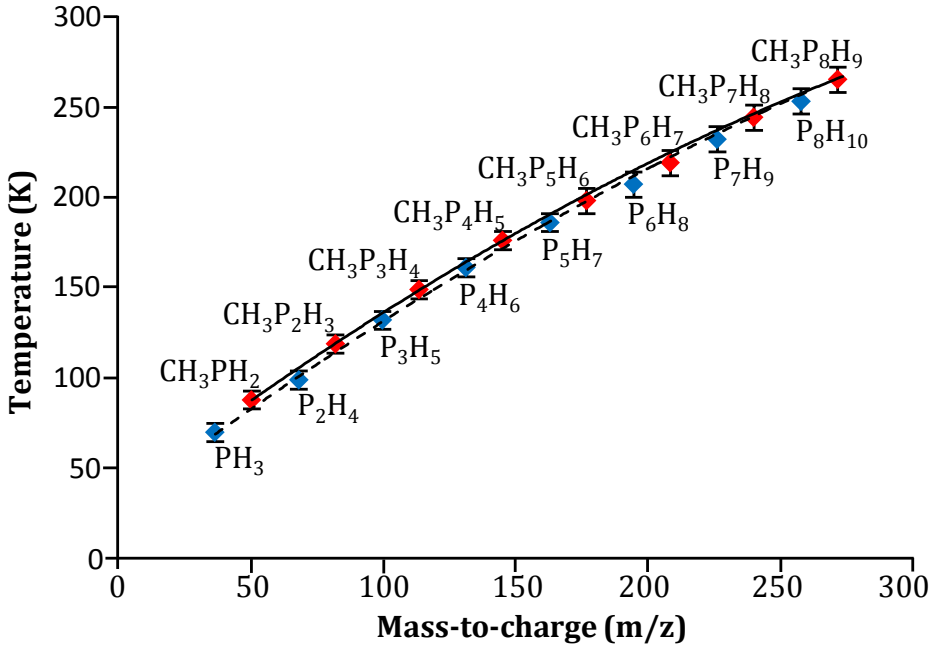

Figure 3.5. Onset sublimation temperatures for the phosphanes (blue) and alkylphosphanes (red) observed in the ReTOF mass spectrometer.

These ReTOF findings are consistent with the results when CH_4 was substituted with CD_4 in the phosphine ices (Figure 3.6 and Table 3.4) with the highest observed molecular ions at m/z = 147 ($CD_3P_4H_5^+$) and 162 ($P_5H_7^+$). Using the fragments at m/z = 210 ($CD_3P_6H_6^+$) and 225 ($P_8H_{10}^+$), we inferred the largest products formed in these ices were $CD_3P_7H_8$ and P_8H_{10}. However, additional mass-to-charge ratios appear associated with the various isotopologues of the methylphosphanes. For example with the simplest product, methylphosphine (CH_3PH_2), three isotopologues appeared in a 2:10:1 ratio: m/z = 50 (CHD_2PH_2), 51 (CD_3PH_3), and 52 (CD_3PHD).

3.4 Analysis

3.4.1 Quantitative Analysis: Mass Balance

Although the infrared results provide limited information about the identity of the products, the significant changes in the area of the reactant peaks gleans information about the amount of reactants destroyed and the rate of these reactions. Figure 3.7 compiles the column densities of phosphine and methane during irradiation utilizing the infrared peaks at 987 cm^{-1} and 4195 cm^{-1} with integrated absorption coefficients of 5.1 × 10^{-19} cm $molecule^{-1}$ and 3.5 × 10^{-19} cm $molecule^{-1}$.[109,120] These column densities were fitted with the following first order rate equations:

$$[PH_3]_t = [PH_3]_{t=0} e^{-k_1 t} \quad (3.3)$$

$$[CH_4]_t = [CH_4]_{t=0} e^{-k_2 t} \quad (3.4)$$

The rate at which phosphine and methane react are described by the rate constants k_1 = 4.7 ± 0.2 × 10^{-5} s^{-1} and k_2 = 3.8 ± 1.7 × 10^{-5} s^{-1}. In pure phosphine ices, the rate constant for the destruction of phosphine leading to the formation of diphosphine, which accounted for 89 ± 4 % of the products, was found to be k = 4.8 ± 0.1 × 10^{-5} s^{-1}, which is in agreement with the rate of destruction of phosphine in phosphine-methane ices.

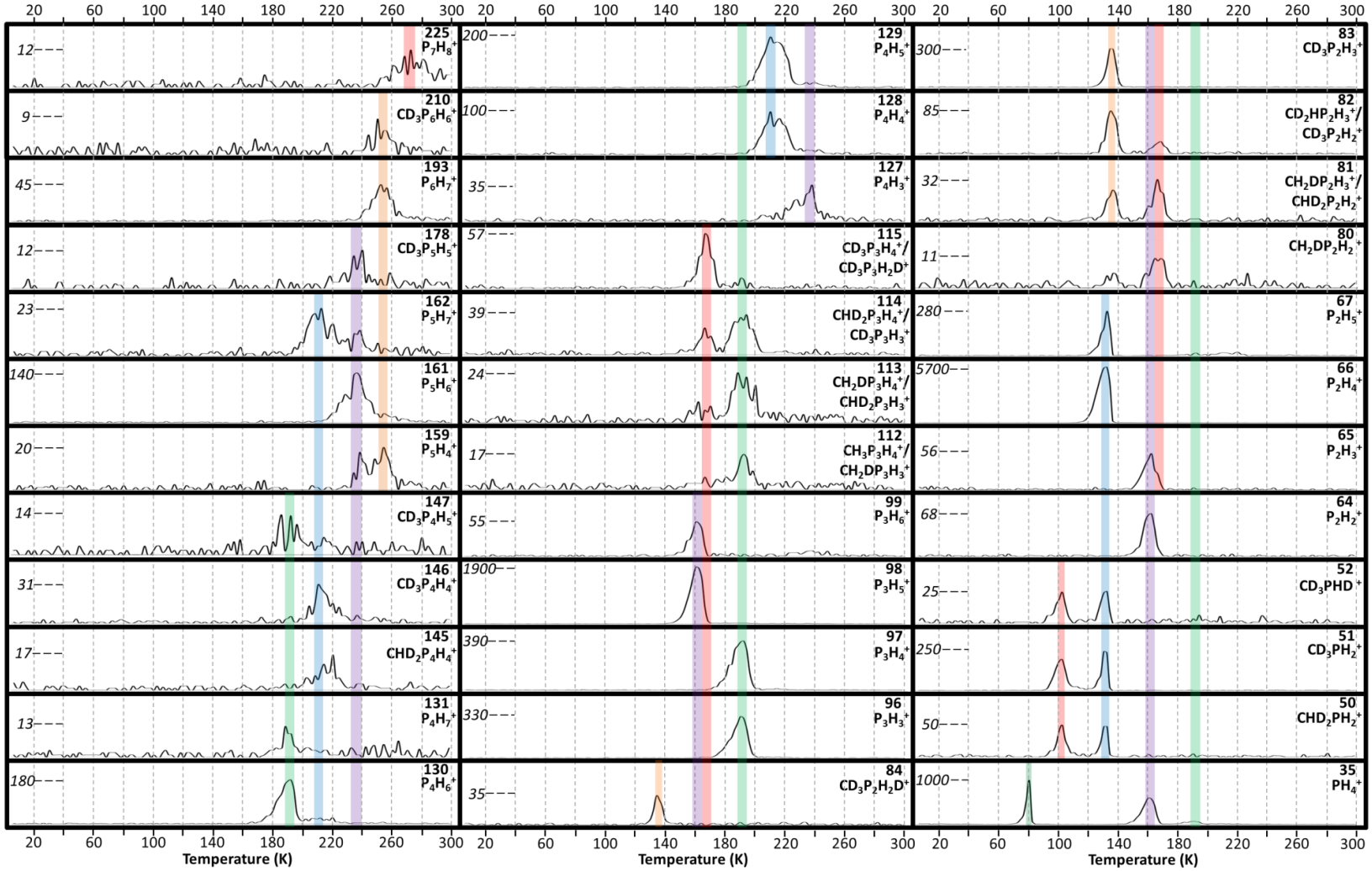

Figure 3.6. ReTOF mass spectra for phosphine (PH_3) and deuterated methane (CD_4) irradiation. Colored bands indicate sublimation events at similar temperatures. The intensity is listed on the left of each spectrum, while the mass-to-charge and ionic formula is on the right.

Table 3.4. Observed ions in the ReTOF mass spectrometer for the phosphine (PH_3) and deuterated methane (CD_4) irradiation.

Mass	Formula	Comments	Formula of Parent Compound
35	PH_4^+	fragment	P_3H_5, P_4H_6, $CD_3P_4H_5$
50	$CHD_2PH_2^+$	parent	CHD_2PH_2
51	$CD_3PH_2^+$	parent	CD_3PH_2
52	CD_3PHD^+	parent	CD_3PHD
64	$P_2H_2^+$	fragment	P_3H_5
65	$P_2H_3^+$	fragment	P_3H_5
66	$P_2H_4^+$	parent	P_2H_4
67	$P_2H_5^+$	protonated parent fragment	P_2H_4 P_5H_7
81	$CH_2DP_2H_3^+$ $CHD_2P_2H_2^+$	parent fragment	$CH_2DP_2H_3$ $CHD_2P_3H_4$
82	$CHD_2P_2H_3^+$ $CD_3P_2H_2^+$	parent fragment	$CHD_2P_2H_3$ $CD_3P_3H_4$
83	$CD_3P_2H_3^+$	parent	$CD_3P_2H_3$
84	$CD_3P_2H_2D^+$	parent	$CD_3P_2H_2D$
96	$P_3H_3^+$	fragment	P_4H_6
97	$P_3H_4^+$	fragment	P_4H_6
98	$P_3H_5^+$	parent	P_3H_5
99	$P_3H_6^+$	protonated parent	P_3H_5
111	$CH_3P_3H_3^+$	fragment	$CH_3P_4H_5$
112	$CH_3P_3H_4^+$ $CH_2DP_3H_3^+$	parent fragment	$CH_3P_3H_4$ $CH_2DP_4H_5$
113	$CH_2DP_3H_4^+$ $CHD_2P_3H_3^+$	parent fragment	$CH_2DP_3H_4$ $CHD_2P_4H_5$
114	$CHD_2P_3H_4^+$ $CD_3P_3H_3^+$	parent fragment	$CHD_2P_3H_4$ $CD_3P_4H_5$
115	$CD_3P_3H_4^+$ $CD_3P_3H_2D^+$	parent fragment	$CD_3P_3H_4$ $CD_3P_4H_4D$
126	$P_4H_2^+$	fragment	P_6H_8
127	$P_4H_3^+$	fragment	P_6H_8
128	$P_4H_4^+$	fragment	P_5H_7, P_6H_8
129	$P_4H_5^+$	fragment	P_5H_7, P_6H_8
130	$P_4H_6^+$	parent fragment	P_4H_6 P_5H_7
131	$P_4H_7^+$	protonated parent fragment	P_4H_6 P_5H_7
145	$CHD_2P_4H_4^+$	fragment	$CHD_2P_5H_6$
146	$CD_3P_4H_4^+$	fragment	$CD_3P_5H_6$
147	$CD_3P_4H_5^+$	parent	$CD_3P_4H_5$
159	$P_5H_4^+$	fragment	P_6H_8, P_7H_9
160	$P_5H_5^+$	fragment	P_6H_8
161	$P_5H_6^+$	fragment	P_6H_8
162	$P_5H_7^+$	parent fragment	P_5H_7 P_6H_8
177	$CHD_2P_5H_5^+$	fragment	$CHD_2P_6H_7^+$
178	$CD_3P_5H_5^+$	fragment	$CD_3P_6H_7^+$
193	$P_6H_7^+$	fragment	P_6H_8
210	$CD_3P_6H_6^+$	fragment	$CD_3P_7H_8$
225	$P_7H_8^+$	fragment	$P_8H_{10}^+$

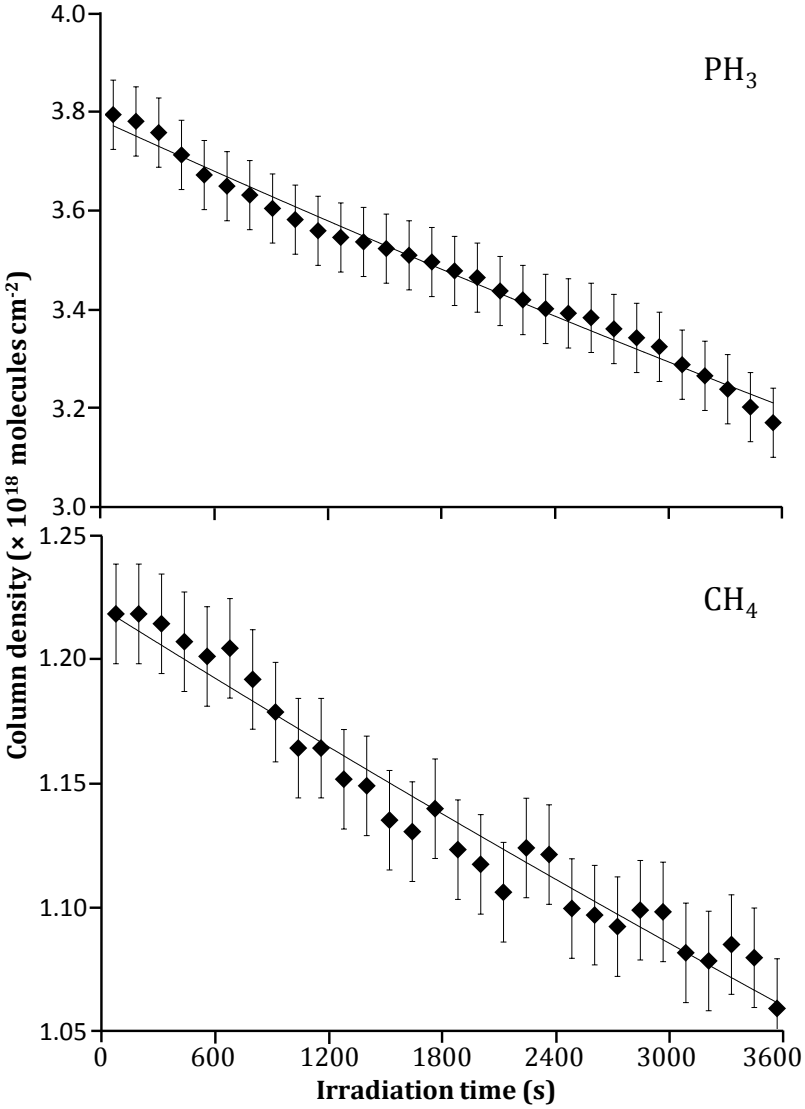

Figure 3.7. Column density of phosphine *(top)* and methane *(bottom)* as a function of irradiation time.

In total, 6.4 ± 1.6 × 10^{17} molecules cm^{-2} of phosphine were destroyed, which is a 17 ± 4 % loss. A lower percentage of the initial methane reacted, 13 ± 5 %, which is equivalent to 1.6 ± 0.6 × 10^{17} molecules cm^{-2}. This resulted in a loss rate of 0.11 ± 0.03 molecules eV^{-1} for phosphine and 0.09 ± 0.03 molecules eV^{-1} for methane. Since the ν_{11} band of diphosphine at 1063 cm^{-1} grew too subtly and was partially overlapped by the ν_4 band of phosphine, the temporal profile of diphosphine could not be monitored. However, the before- and after-irradiation spectra were compared to calculate this peak area and estimate the total diphosphine production. Using an integrated absorption coefficient of 7.0 × 10^{-19} cm $molecule^{-1}$,[120] 1.6 ± 0.4 × 10^{17} molecules cm^{-2} of diphosphine were produced. Thus, diphosphine accounted for 50 ± 13 % of the phosphorus from phosphine destruction. Given that the irradiated ice had a three-to-one phosphine-to-methane ratio and that diphosphine contained 89 % of the reacted phosphorus in pure phosphine ices, proportionally less diphosphine was formed in phosphine-methane ices, which indicates that either phosphine or diphosphine readily reacts with methane.

3.4.2 Reaction Pathways

The ReTOF results from irradiated phosphine and deuterated methane ice provide crucial information regarding the mechanism of formation for methylphosphanes by analyzing the intensities of various isotopologues. Figure 3.8 shows the possible formation routes that would lead to each of the three observed isotopologues of methylphosphine (CH_3PH_2). To obtain m/z = 50 (CHD_2PH_2), CD_4 has to decompose *via* the loss of molecular hydrogen or two deuterium atoms to form carbene (CD_2), which has been observed in previous irradiated ice studies,[45,130] and then insert into a phosphorus-hydrogen bond of phosphine (reaction 3.5). If the carbene is formed in its first excited singlet state (a^1A_1), the insertion is barrierless.[131] For m/z = 51 (CD_3PH_2), methane and phosphine each lost a hydrogen or deuterium atom, and the resulting methyl (CD_3)[132] and phosphino (PH_2) radicals recombined barrierlessly (reaction 3.6). Finally, the formation of m/z = 52 (CD_3PHD) mirrors that for CHD_2PH_2 but in this case phosphine lost two hydrogen atoms or molecular hydrogen to create the phosphinidene (PH) radical and then inserted into a carbon-deuterium bond of methane (reaction 3.7).

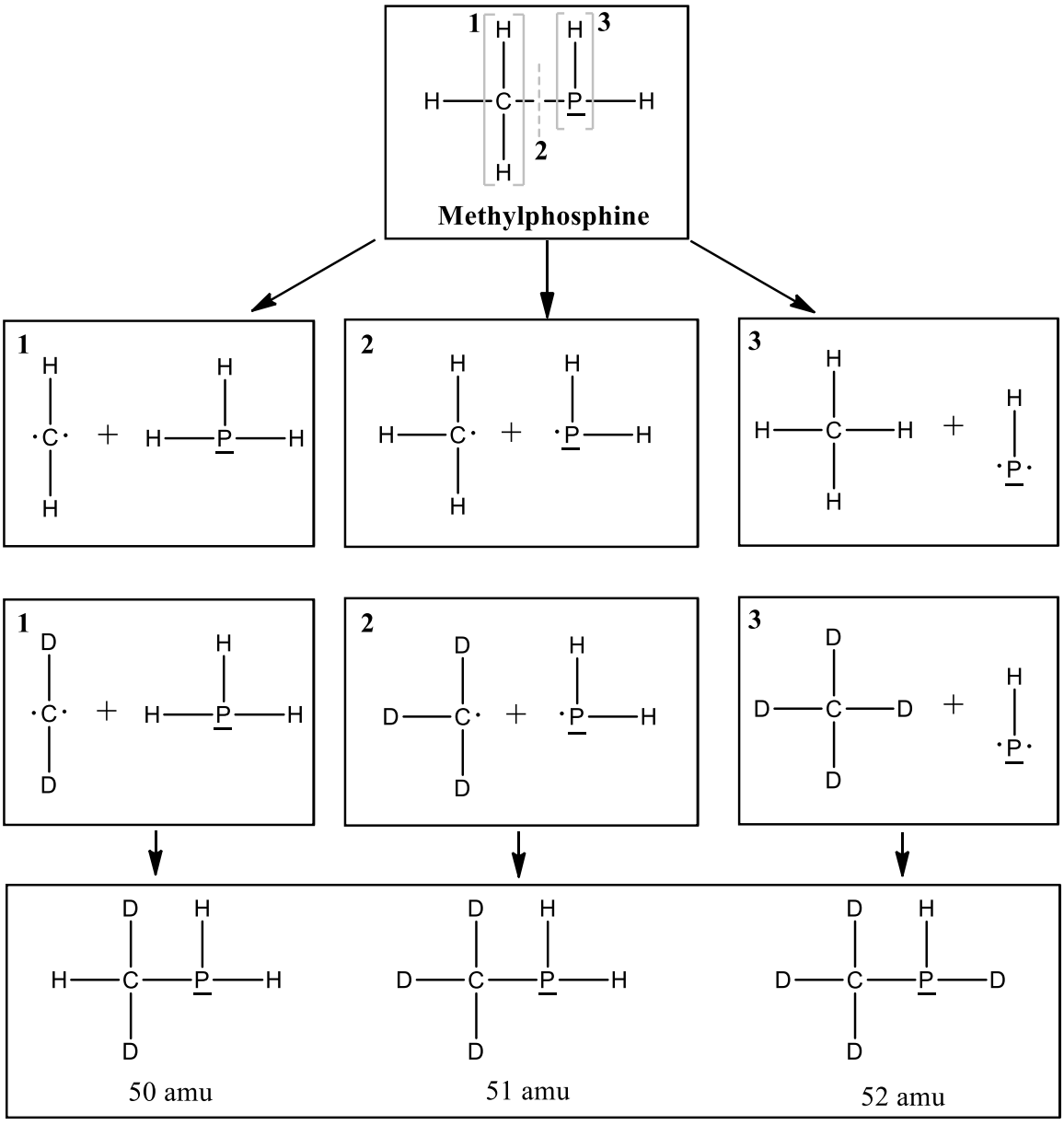

Figure 3.8. Retrosynthesis pathways from methylphosphine (CH_3PH_2) identifying the possible formulae from deuterated-methane substituted reactions. The masses shown were observed in the ReTOF.

Phosphinidene, like imidogen (NH),[133] is expected to insert barrierlessly in its first excited singlet state ($a^1\Delta$).

$$CD_4 \rightarrow CD_2 + 2D/D_2 \quad (3.5a)$$

$$CD_2 + PH_3 \rightarrow CHD_2PH_2 \quad (3.5b)$$

$$CD_4 \rightarrow CD_3 + D \quad (3.6a)$$

$$PH_3 \rightarrow PH_2 + H \quad (3.6b)$$

$$CD_3 + PH_2 \rightarrow CD_3PH_2 \quad (3.6c)$$

$$PH_3 \rightarrow PH + 2H/H_2 \quad (3.7a)$$

$$PH + CD_4 \rightarrow CD_3PHD \quad (3.7b)$$

Therefore, our results provide compelling evidence that methane decomposes not only to the methyl radical, but also to carbene. Likewise, phosphine was found to fragment to the phosphino radical and also to phosphinidene. The ratio of ion intensities for m/z = 50 : 51 : 52 is 2 : 10 : 1, indicating that radical recombination was the preferred formation pathway with CD_3PH_2 as the most abundant isotopologue. This could either be a result of the methyl and phosphino radicals reacting quickly or that more of these radicals were produced than carbene and phosphinidene.

The molecular formula CH_6P_2 can have two structural isomers: the carbon-terminated methyldiphosphine ($CH_3P_2H_3$) and also the carbon-bridging methylenediphosphine ($PH_2CH_2PH_2$). Figures 3.9 and 3.10 show the pathways by which each of these isomers could be formed using the intermediates from the irradiation of methane, phosphine, and methylphosphine. It was previously shown that the isotopologues of methylphosphine were CHD_2PH_2, CD_3PH_2, and CD_3PHD. Noting that non-deuterated CH_6P_2 has m/z = 80, the observed peak at m/z = 81 contained only one deuterium atom. Because the results indicate that the deuterated methylidyne radical (CD) was not formed, carbene (CD_2) must be involved and methylphosphine (CHD_2PH_2) would first be formed by reaction 3.5. Reaction 3.8 shows that the loss of a deuterium atom from CHD_2PH_2 formed the core one-deuterium radical compound that recombined with a phosphino radical (PH_2) to form the methylene-diphosphine isotopologue PH_2CHDPH_2. Given the starting materials and intermediates available, this is the only reaction pathway that can lead to m/z = 81 and thus the presence of methylenediphosphine is explicitly confirmed.

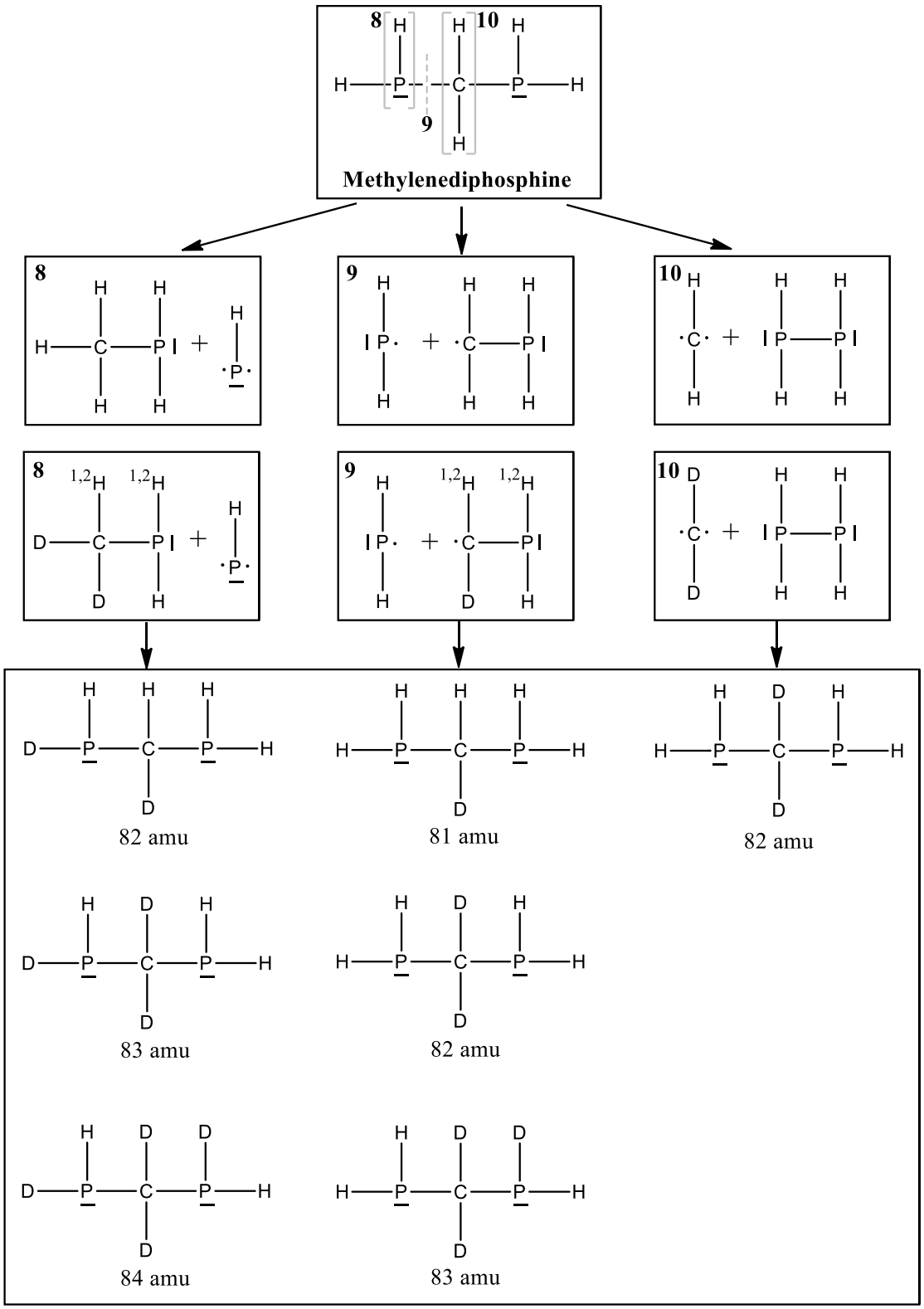

Figure 3.9. Retrosynthesis pathways from methylenediphosphine ($PH_2CH_2PH_2$) identifying the possible structures from deuterated-methane substituted reactions. The masses shown were observed in the ReTOF.

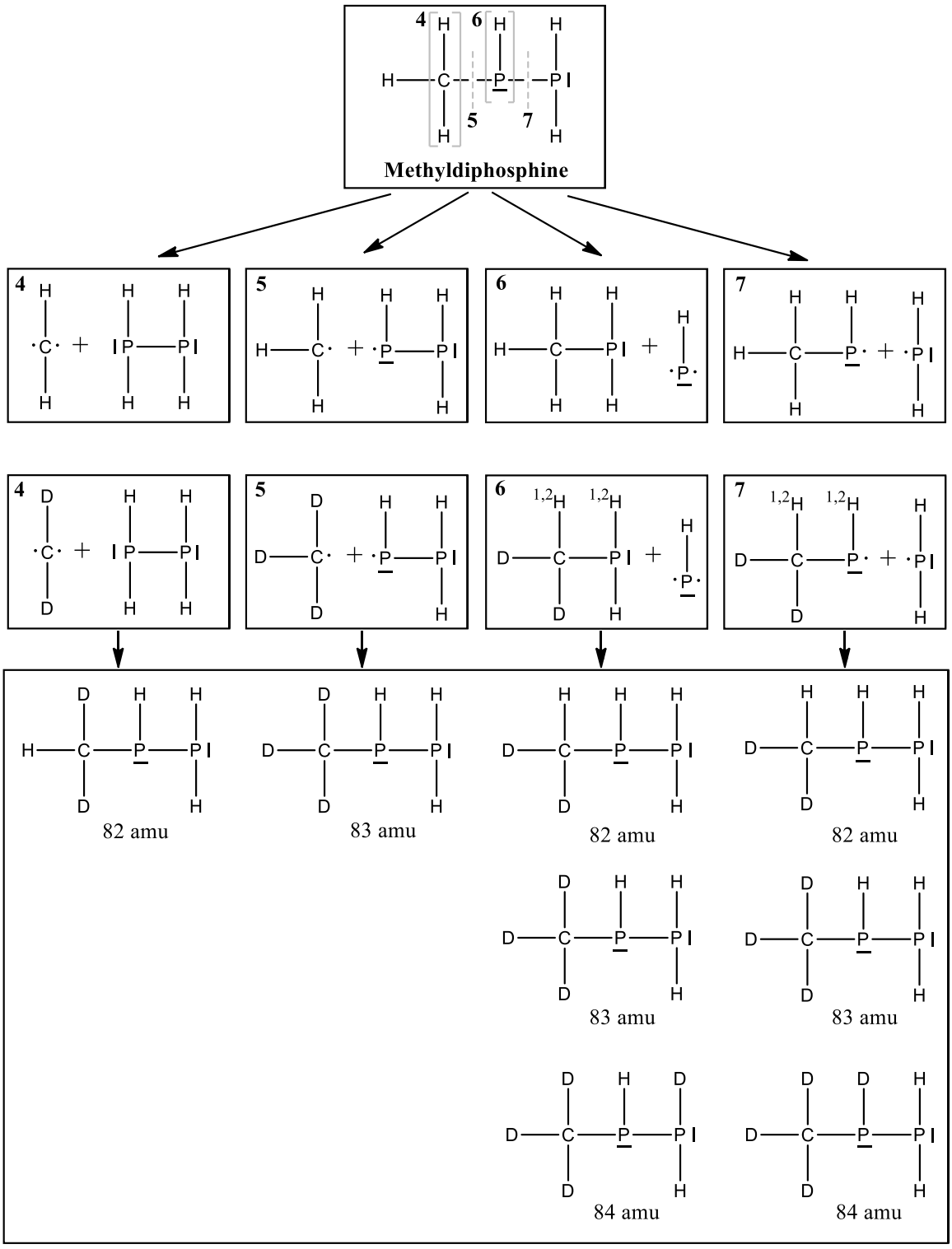

Figure 3.10. Retrosynthesis pathways from methyldiphosphine ($CH_3P_2H_3$) identifying the possible formulas from deuterated-methane substituted reactions. The masses shown were observed in the ReTOF.

$$CHD_2PH_2 \rightarrow CHDPH_2 + D \quad (3.8a)$$

$$CHDPH_2 + PH_2 \rightarrow PH_2CHDPH_2 \quad (3.8b)$$

The signal for m/z = 82 can be identified as three isotopomers ($PH_2CD_2PH_2$, $PHDCHDPH_2$, and $CHD_2P_2H_3$) with two deuterium atoms that can be formed through several pathways. Each of the three can be formed using CHD_2PH_2. Hydrogen loss from either the carbon or phosphorus atom in CHD_2PH_2 followed by recombination with the phosphino radical is shown in reaction 3.9 and reaction 3.10, respectively. Reaction 3.9 can also be completed by deuterium loss from CD_3PH_2.

$$CHD_2PH_2 \rightarrow CD_2PH_2 + H \quad (3.9a)$$

$$CD_3PH_2 \rightarrow CD_2PH_2 + D \quad (3.9b)$$

$$CD_2PH_2 + PH_2 \rightarrow PH_2CD_2PH_2 \quad (3.9c)$$

$$CHD_2PH_2 \rightarrow CHD_2PH + H \quad (3.10a)$$

$$CHD_2PH + PH_2 \rightarrow CHD_2P_2H_3 \quad (3.10b)$$

Also, insertion pathways involving CHD_2PH_2 are available in which the phosphinidene radical inserts into the phosphorus-hydrogen or carbon-phosphorus (reaction 3.11) bond, the carbon-hydrogen bond (reaction 3.12), or the carbon-deuterium bond (reaction 3.13) of CHD_2PH_2.

$$CHD_2PH_2 + PH \rightarrow CHD_2P_2H_3 \quad (3.11)$$

$$CHD_2PH_2 + PH \rightarrow PH_2CD_2PH_2 \quad (3.12)$$

$$CHD_2PH_2 + PH \rightarrow PHDCHDPH_2 \quad (3.13)$$

A final reaction that results in m/z = 82 has carbene (CD_2) inserting into a phosphorus-hydrogen (reaction 3.14) or phosphorus-phosphorus bond (reaction 3.15) of diphosphine.

$$P_2H_4 + CD_2 \rightarrow CHD_2P_2H_3 \quad (3.14)$$

$$P_2H_4 + CD_2 \rightarrow PH_2CD_2PH_2 \quad (3.15)$$

In summary, m/z = 82 can be assigned to two isotopomers of d_2-methylenediphosphine ($PH_2CD_2PH_2$ and $PHDCHDPH_2$) and one isotopologue of methyldiphosphine ($CHD_2P_2H_3$). We suggest that $PH_2CD_2PH_2$ through reaction 3.9b is the most abundant contributor to

m/z = 82 because CD_3PH_2 is the most abundant isotopologue of methylphosphine and phosphino radicals are readily available in irradiated phosphine-dominant ices.

Two isomers can contribute to m/z = 83: one for methylenediphosphine ($PHDCD_2PH_2$) and another for methyldiphosphine ($CD_3P_2H_3$). Irradiation of CD_3PH_2 and CD_3PHD followed by recombination with the phosphino radical can result in either of these isomers depending on which hydrogen or deuterium atom is lost. Reactions 3.16a and 3.16b show hydrogen and deuterium loss from the phosphorus atom on CD_3PH_2 and CD_3PHD, respectively, and in reaction 3.17 the deuterium atom can be lost from carbon on CD_3PHD.

$$CD_3PH_2 \rightarrow CD_3PH + H \quad (3.16a)$$

$$CD_3PHD \rightarrow CD_3PH + D \quad (3.16b)$$

$$CD_3PH + PH_2 \rightarrow CD_3P_2H_3 \quad (3.16c)$$

$$CD_3PHD \rightarrow CD_2PHD + D \quad (3.17a)$$

$$CD_2PHD + PH_2 \rightarrow PHDCD_2PH_2 \quad (3.17b)$$

The two isomers can also be formed via phosphinidene (PH) insertion into either a carbon-deuterium (reaction 3.18) or a phosphorus-carbon/hydrogen (reaction 3.19) bond of CD_3PH_2.

$$CD_3PH_2 + PH \rightarrow PHDCD_2PH_2 \quad (3.18)$$

$$CD_3PH_2 + PH \rightarrow CD_3P_2H_3 \quad (3.19)$$

The final reaction mechanism (reaction 3.20) involves the loss of a hydrogen atom from diphosphine (P_2H_4) and subsequent recombination with the methyl radical (CD_3).

$$P_2H_4 \rightarrow P_2H_3 + H \quad (3.20a)$$

$$P_2H_3 + CD_3 \rightarrow CD_3P_2H_3 \quad (3.20b)$$

Thus, the methylphosphines CD_3PH_2 and CD_2PHD are capable of producing both methylenediphosphine and methyldiphosphine at m/z = 83, while diphosphine can only lead to methyldiphosphine. The dominant isotopomer is likely $CD_3P_2H_3$ as due to reaction 3.16a and reaction 3.20. Not only are both radical recombination reactions, which have been shown to be the most favorable mechanism, but also reaction 3.16a begins with the

most abundant isotopologue of methylphosphine (CD_3PH_2), which then reacts with the radical from the most abundant reactant—the phosphino radical from phosphine. Similarly, reaction 3.20 shows the most abundant overall product, diphosphine, combining with a radical from the methane reactant.

Three isotopomers could be assigned to m/z = 84, and each originated from CD_3PHD: $PHDCD_2PHD$, CD_3PDPH_2, and CD_3PHPHD. The insertion of the phosphinidene radical (PH) into a carbon-phosphorus bond or phosphorus-deuterium bond of CD_3PHD is represented by reaction 3.21, while insertion into a carbon-deuterium or phosphorus-hydrogen bond is shown by reaction 3.22 and reaction 3.23, respectively.

$$CD_3PHD + PH \rightarrow CD_3PHPHD \quad (3.21)$$

$$CD_3PHD + PH \rightarrow PHDCD_2PHD \quad (3.22)$$

$$CD_3PHD + PH \rightarrow CD_3PDPH_2 \quad (3.23)$$

Thus, phosphinidene insertion can explain each of the possible isotopomers. However, one radical recombination pathway is also possible by hydrogen loss from CD_3PHD followed by recombination with a phosphino radical (reaction 3.24).

$$CD_3PHD \rightarrow CD_3PD + H \quad (3.24a)$$

$$CD_3PD + PH_2 \rightarrow CD_3PDPH_2 \quad (3.24b)$$

Reactions 3.21–3.24 provide little information about which product is most likely. While radical recombination has been previously identified as most probable, the low probability of hydrogen being removed from CD_3PHD makes this reaction unlikely. A comparison of the PH-insertion pathways shows that reaction 3.22 has three bonds available for insertion, reaction 3.21 has two bonds, and reaction 3.23 can only occur by insertion into only one bond. Thus, without further information about the ease at which the phosphinidene radical can insert into various bond types, $PHDCD_2PHD$ may be the most abundant product at m/z = 84.

To summarize, some important conclusions from the irradiation of phosphine-deuterated methane ices are as follows.

First, the methylphosphine isotopologues have ratios for m/z = 50 : 51 : 52 of 2: 10 : 1, indicating that radical recombination (CD_3PH_2) dominates and that carbene insertion (CHD_2PH_2) is twice as likely as phosphinidene insertion (CD_3PHD).

Second, the signals assigned to deuterated CH_6P_2 have ratios for m/z = 80 : 81 : 82 : 83 of 2 : 7 : 25 : 3. The most abundant product is thus $CD_3P_2H_3$ (at m/z = 83), which is formed by radical recombination of either CD_3PH with PH_2 (reaction 3.16) or CD_3 with P_2H_3 (reaction 3.20).

Third, the signal at m/z = 81 confirms that methylenediphosphine (PH_2CHDPH_2) must be present and that it formed via radical recombination of $CHDPH_2$ and PH_2 starting from CHD_2PH_2 and PH_3 (reaction 3.8). This provides further evidence of the formation of $CHDPH_2$ (m/z = 50) via carbene insertion into a phosphorus-hydrogen bond of phosphine (reaction 3.5).

Fourth, because the carbon-deuterium bond was cleaved in CHD_2PH_2, the decomposition of CHD_2PH_2 should also result in hydrogen loss to give CD_2PH_2, which can then recombine with the phosphino radical to form $PH_2CD_2PH_2$ (m/z = 82). Furthermore, carbon-deuterium bond cleavage should similarly occur in CD_3PH_2 and CD_3PHD, which when recombined with the phosphino radical would also form $PH_2CD_2PH_2$ (m/z = 82) in greater abundance than CHD_2PH_2 and also form $PHDCD_2PH_2$ (m/z = 83). Thus, compelling evidence exists for the formation three isotopologues of methylenediphosphine.

Fifth, all pathways forming m/z = 84 require CD_3PHD, which not only confirms this isotopologue of methylphosphine but also provides evidence that the phosphinidene radical inserts into a carbon-deuterium bond of methane.

3.4.3 Energetics

Using experimental reaction energies,[134,135] we now consider the energy necessary to form the observed products. The preferred pathway (reaction 3.6) toward formation of methylphosphine (CH_3PH_2) requires the recombination of the phosphino (PH_2) and methyl (CH_3) radicals. To remove one hydrogen from their parent compounds, 339 kJ mol^{-1} (3.51 eV) and 439 kJ mol^{-1} (4.55 eV) are needed, respectively (reactions 3.25a & 3.26a). This energy necessary for bond cleavage is supplied by the energetic electrons. The barrierless methyl and phosphino radical recombination (reaction 3.27) releases 291 kJ mol^{-1} (3.01 eV), and thus the reaction energy for bond cleavage followed by methyl and phosphino radical recombination (reaction 3.28) is +486 kJ mol^{-1} (5.04 eV). The overall reaction including molecular hydrogen formation (reaction 3.29) is endoergic by 50 kJ mol^{-1} (0.52 eV). Compared to removing the first hydrogen, only slightly more energy is necessary to remove a second hydrogen from phosphine or methane and form phosphinidene and carbene (reactions 3.25b & 3.26b). However, an additional 90 kJ mol^{-1} (0.94 eV) and 38 kJ mol^{-1} (0.39 eV), respectively, is necessary to promote these radicals to their first excited singlet state (reactions 3.25c & 3.26c), which allows them to insert barrierlessly. With minimal thermal energy available at 5.5 K, the reaction must involve non-equilibrium chemistry to proceed. Non-irradiated blank experiments showed that no reactions occurred, confirming that thermal chemistry cannot create these products at such low temperatures. Each of the three mechanisms shown to produce methylphosphine—radical recombination, phosphinidene insertion, and carbene insertion—is capable of barrierless methylphosphine formation. The endoergic nature of the reaction indicates that non-equilibrium chemistry initiated by high energy particles such as galactic cosmic rays are necessary in interstellar conditions, but once this initial energy is supplied the reaction proceeds favorably and barrierlessly. However, if these reaction intermediates are present in the first monolayer and within close proximity, they can spontaneously produce the products seen in this study without the need for ionizating radiation nor diffusion through the ice.

$PH_3 \rightarrow PH_2 + H$	+339 kJ mol^{-1}	(3.25a)
$PH_3 \rightarrow PH\ (X\,^3\Sigma^-) + 2H$	+684 kJ mol^{-1}	(3.25b)
$PH_3 \rightarrow PH\ (a^1\Delta) + H_2$	+339 kJ mol^{-1}	(3.25c)
$CH_4 \rightarrow CH_3 + H$	+439 kJ mol^{-1}	(3.26a)
$CH_4 \rightarrow CH_2\ (X\,^3B_1) + 2H$	+897 kJ mol^{-1}	(3.26b)
$CH_4 \rightarrow CH_2\ (a^1A_1) + H_2$	+499 kJ mol^{-1}	(3.26c)
$CH_3 + PH_2 \rightarrow CH_3PH_2$	−291 kJ mol^{-1}	(3.27)
$CH_4 + PH_3 \rightarrow CH_3PH_2 + 2H$	+486 kJ mol^{-1}	(3.28)
$CH_4 + PH_3 \rightarrow CH_3PH_2 + H_2$	+ 50 kJ mol^{-1}	(3.29)

3.5 Conclusion

Ices of phosphine with methane and deuterated methane that were irradiated with energetic electrons at 5.5 K produced a homologous series of phosphanes from P_2H_4 to P_8H_{10} and methylphosphanes from CH_3PH_2 to $CH_3P_8H_9$. All observed products were phosphorus-containing but the products that also contain carbon have exactly one carbon atom. Because the group frequencies of the products from phosphine and methane irradiation overlap significantly with the parent peaks, FTIR had limited use in this type of study and diphosphine was the only product that could be quantified. Furthermore, quadrupole mass spectrometry with electron impact ionization observed only diphosphine, methylphosphine, methyldiphosphine, and triphosphane. On the other hand, ReTOF mass spectrometry could observe molecular ions as large as $P_5H_7^+$ and $CH_3P_4H_5^+$, while P_8H_{10} and $CH_3P_8H_9$ could be identified from their fragments from PH_2 loss, which is the most common fragmentation pathway. Using deuterated methane results as evidence, a signal at m/z = 81 confirms the formation of methylenediphosphine (PH_2CHDPH_2) and, in addition to m/z = 51 (CHD_2PH_2), the formation of methylphosphine via carbene insertion. The signals at m/z = 52 (CD_3PHD) and m/z = 84 ($CD_4H_2P_2$) also confirm the formation of methylphosphine via phosphinidene insertion. However, radical recombination, which contributed to the intense signals at m/z = 51 (CD_3PH_2) and m/z = 83 ($CD_3P_2H_3$), was the most likely formation pathway. The overall reaction forming

methylphosphine (CH_3PH_2) is endoergic by +50 kJ mol^{-1} (0.52 eV), which makes this compound unlikely in cold environments that rely solely on thermal chemistry. However, our results show that energetic particles like galactic cosmic rays can induce non-equilibrium chemistry that not only forms methylphosphine but a suite of higher order phosphanes and methylphosphanes, and thus methylphosphine can be expected in cold interstellar environments with sufficient quantities of phosphine and methane. Methylphosphine contains a carbon-phosphorus single bond, which has yet to be observed in the interstellar medium but has been discovered in the C1 to C4 alkyl phosphonic acids contained in the Murchison meteorite,[7] which verifies that the carbon-phosphorus single bond can be produced in extraterrestrial environments, although their ultimate origins remain elusive. These results also have potential implications to the chemistry of planetary atmospheres, as phosphine[38,39] and methane[136] have been discovered on Jupiter and Saturn. Future work can look into the abundance of individual isomers, such as methylenediphosphine ($PH_2CH_2PH_2$) and methyldiphosphine ($CH_3P_2H_3$), by performing selective VUV photoionization experiments utilizing four-wave difference and sum mixing[84,108] to further investigate the most likely reaction pathways. Also, more complex mixtures, such as the addition of water or carbon dioxide, can be explored to synthesize potential interstellar compounds in more astrophysically relevant ices.

3.6 Supplementary Information

The use of a residual gas analyzer (RGA; QMS, quadrupole mass spectrometer) is common with experiments that detect products that sublime into the gas phase, and we utilize one in tandem with the ReTOF to compare the sensitivity of these techniques. It should be stressed that molecular sublimation and sputtering from the ice is negligible during the irradiation phase, and previous findings demonstrate that low currents of high energy electrons are inefficient at causing sputtering in low temperature ices at typically 5 K to 10 K[137,138].[137,138] During the TPD phase, diphosphine (P_2H_4) contributed the most interesting results in the RGA mass spectra for phosphine and methane irradiated ice (Figure 3.S1 and Table 3.S1). Unlike the ReTOF, P_2H_4 fragmented even down to P_2^+ via dissociative electron impact ionization. The other products seen, P_3H_5 and CH_3PH_2,

occurred at low intensities. The results for phosphine with deuterated methane (CD_4) (Figure 3.S2 and Table 3.S2) were identical for P_2H_4 and P_3H_5, and two isotopologues of CH_3PH_2 appeared: a strong m/z = 51 (CD_3PH_2) signal and an m/z = 50 (CHD_2PH_2) signal that barely appeared above background levels. Similar to the ReTOF results, CD_3PH_2 was the most abundant form of methylphosphine, although the RGA intensities are too small for a quantitative comparison. Small amounts of $CH_3P_2H_3$ and $CD_3P_2H_3$ were also seen at m/z = 80 and m/z = 83, respectively. Thus, the ReTOF was a far more sensitive mass spectrometry method, as it was capable of detecting 15 products for the phosphine and methane ice mixture compared to only four products using the RGA, and three isotopologues of methylphosphine were seen and quantitatively compared using the ReTOF, while the RGA detected only two isotopologues.

Table 3.S1. Observed ions in the quadrupole mass spectrometer for the phosphine (PH_3) and methane (CH_4) irradiation.

Mass	Formula	Comments	Formula of Parent Compound
35	PH_4^+	fragment	P_3H_5
48	$PH_2CH_3^+$	parent	PH_2CH_3
62	P_2^+	fragment	P_2H_4
63	P_2H^+	fragment	P_2H_4
64	$P_2H_2^+$	fragment	P_2H_4
65	$P_2H_3^+$	fragment	P_2H_4, P_3H_5
66	$P_2H_4^+$	parent	P_2H_4
93	P_3^+	fragment	P_3H_5
98	$P_3H_5^+$	parent	P_3H_5

Table 3.S2. Observed ions in the quadrupole mass spectrometer for the phosphine (PH_3) and deuterated methane (CD_4) irradiation.

Mass	Formula	Comments	Molecular Formula of Parent Compound
35	PH_4^+	fragment	P_3H_5
50	$CHD_2PH_2^+$	parent	CHD_2PH_2
51	$CD_3PH_2^+$	parent	CD_3PH_2
62	P_2^+	fragment	P_2H_4
63	P_2H^+	fragment	P_2H_4
64	$P_2H_2^+$	fragment	P_2H_4
65	$P_2H_3^+$	fragment	P_2H_4, P_3H_5
66	$P_2H_4^+$	parent	P_2H_4
98	$P_3H_5^+$	parent	P_3H_5

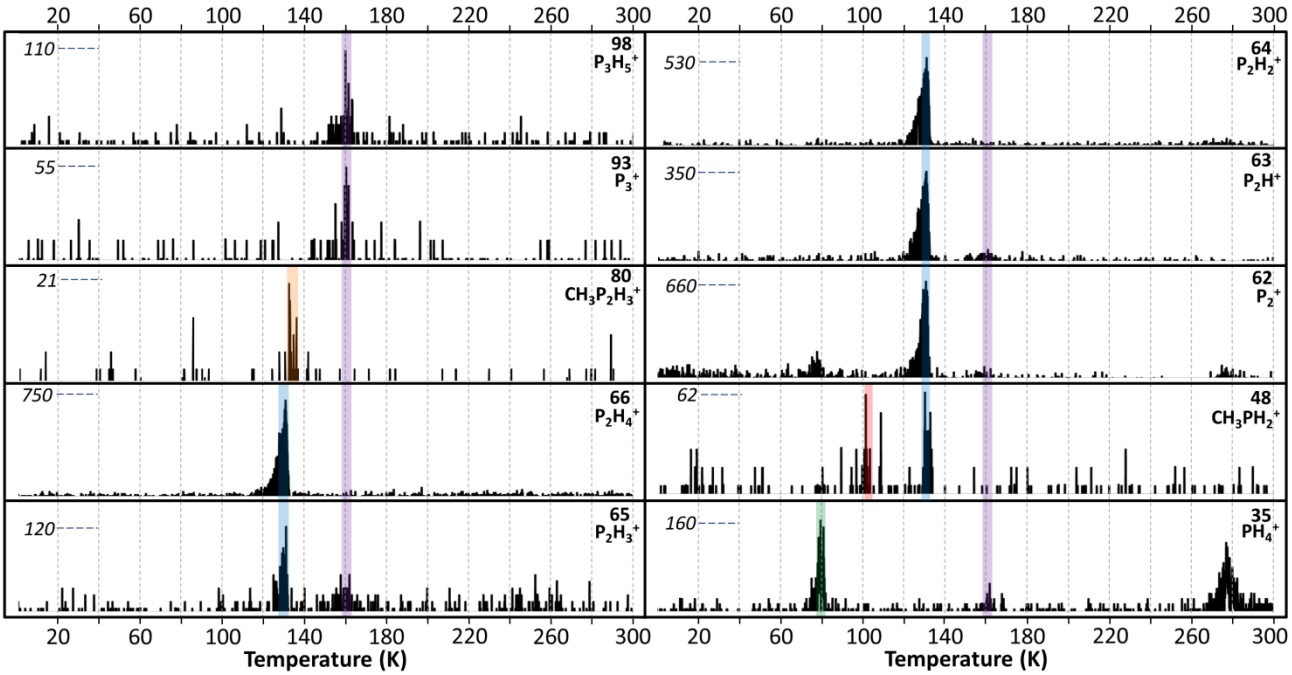

Figure 3.S1. Quadrupole mass spectra of the products from phosphine (PH_3) and methane (CH_4) irradiation. The intensity (in thousands) is listed on the left while the mass-to-charge and ionic formula are on the right.

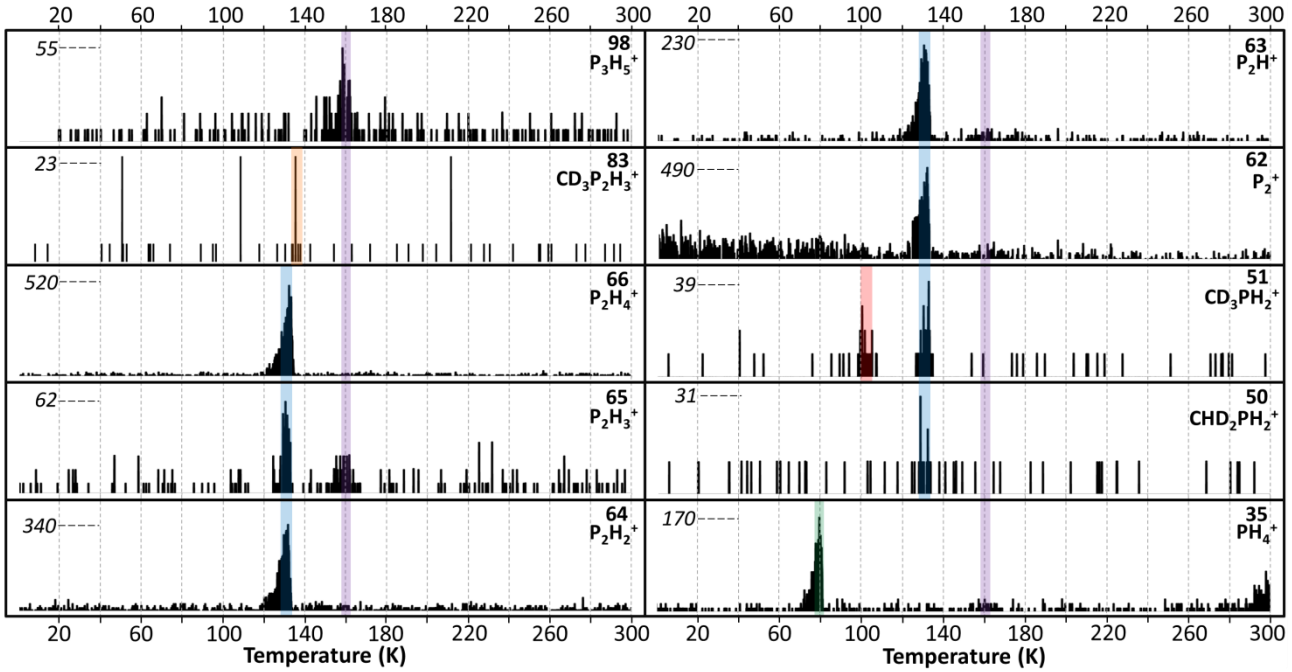

Figure 3.S2 Quadrupole mass spectra for the products of phosphine (PH_3) and deuterated methane (CD_4). The intensity (in thousands) is listed on the left while the mass-to-charge and ionic formula are on the right.

CHAPTER 4

INFRARED SPECTROSCOPY STUDIES OF PHOSPHINE-CONTAINING ICES

This chapter is based on the paper: A. M. Turner, M. J. Abplanalp, T. J. Blair, R. Dayuha, R. I. Kaiser, "An Infrared Spectroscopic Study Toward the Formation of Alkyl phosphonic Acids and Their Precursors in Extraterrestrial Environments", The Astrophysical Journal Supplement Series, *234, 6 (2018)*

The only known phosphorus-containing organic compounds of extraterrestrial origin, alkylphosphonic acids, were discovered in the Murchison meteorite and have accelerated the hypothesis that reduced oxidation states of phosphorus were delivered to early Earth and served as a prebiotic source of phosphorus. While previous studies looking into the formation of these alkylphosphonic acids have focused on the iron-nickel phosphide mineral schreibersite and phosphorous acid as a source of phosphorus, this work utilizes phosphine (PH_3), which has been discovered in the circumstellar envelope of IRC +10216, in the atmosphere of Jupiter and Saturn, and believed to be the phosphorus carrier in comet 67P/Churyumov-Gerasimenko. Phosphine ices prepared with interstellar molecules such as carbon dioxide, water, and methane were subjected to electron irradiation, which simulate the secondary electrons produced from galactic cosmic rays penetrating the ice, and probed using infrared spectroscopy to understand the possible formation of alkylphosphonic acids and their precursors on interstellar icy grains that could become incorporated into meteorites such as Murchison. We present the first study and results on the possible synthesis of alkylphosphonic acids produced from phosphine-mixed ices under interstellar conditions. All functional groups of alkylphosphonic acids were detected infrared spectroscopically suggesting that this class of molecules can be formed in interstellar ices.

4.1 Introduction

Alkyl phosphonic acids—organic compounds containing the $RPO(OH)_2$ functionality with R being an alkyl group—have been identified in the Murchison meteorite (Figure 4.1).[7] An understanding of the extraterrestrial origin and abiotic formation pathways of these alkyl phosphonic acids is of crucial importance to the astrobiology community on multiple levels. First, the Murchison meteorite can be seen as a benchmark for studies of carbonaceous chondrites. Carbonaceous chondrites are considered as the most primitive remnants from the formation of the Solar System and provide a singular record of the organic chemical evolution in the early Solar System.[139] Therefore, a better knowledge of the origin of astrobiologically relevant molecules in carbonaceous chondrites is vital because they resemble natural time capsules before life developed on Earth.[140] Hence, carbonaceous chondrites are important in their role as a repository of primitive organic material and are dubbed primordial fossils helping to understand the chemical makeup of the early Solar System. This is in particular true for key classes of astrobiologically important molecules detected in Murchison such as amino acids[141] and alkyl phosphonic acids.[7] Laboratory experiments provide compelling evidence that amino acids can be formed abiotically via the Strecker synthesis and also by photolysis and charged particle processing of low temperature interstellar ice analogues.[44-48] However, abiotic formation pathways leading to alkyl phosphonic acids in extraterrestrial low temperature environments have been elusive to date. A detailed knowledge of the formation routes of alkyl phosphonic acids in extraterrestrial ices can therefore help to shed light on the prebiotic phosphorus chemistry.

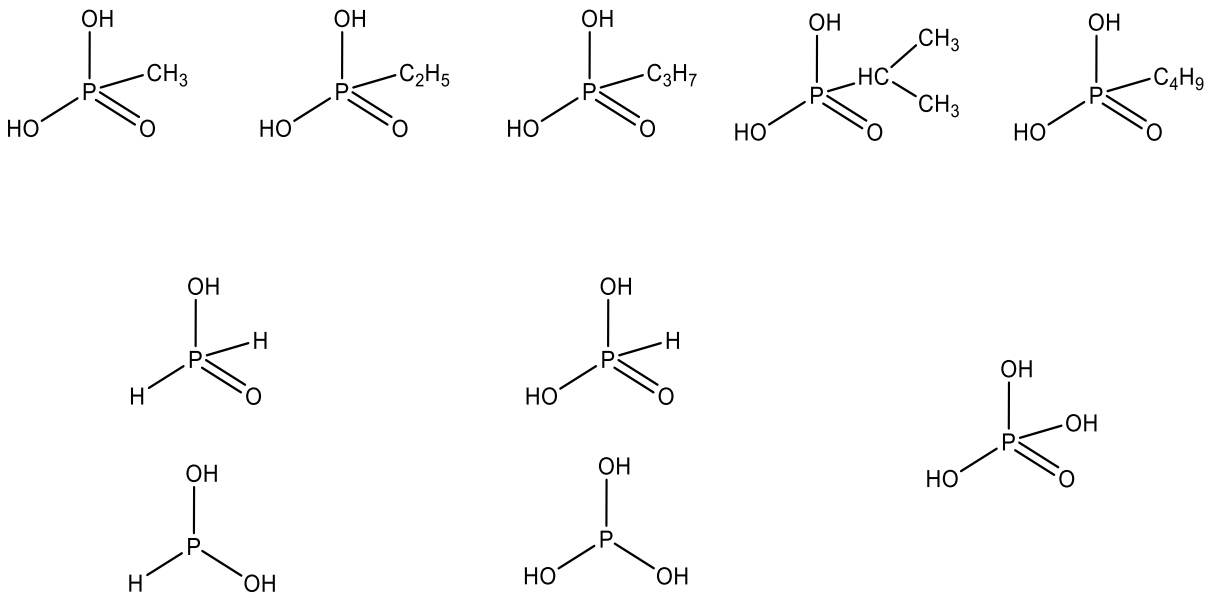

Figure 4.1. Five alkyl phosphonic acids (*top*) with methyl (CH_3), ethyl (C_2H_5), n-propyl (C_3H_7), isopropyl ($CH(CH_3)_2$), and n-butyl (C_4H_9) groups detected in the Murchison meteorite. Each gram of meteorite contained 9 nmole methylphosphonic acid and 6 nmole ethylphosphonic acid, although quantities of the remaining alkyl phosphonic acids were not determined. Possible products of oxidized phosphine are shown below as phosphorus oxoacids: H_3PO_2 (*left*, phosphinic acid and hypophosphorous acid), H_3PO_3 (*center*, phosphonic acid and phosphorous acid), and H_3PO_4 (*right*, phosphoric acid).

Second, although most phosphorus in meteorites is contained in phosphate minerals and schreibersite,[142] Murchison's homologous series of alkyl phosphonic acids (Figure 4.1), which comprises only 0.1 % of Murchison's phosphorus inventory,[143] represents a prototype class of astrobiologically important molecules and the *only* class of organic molecules containing phosphorus of extraterrestrial origin. Sophisticated $^{13}C/^{12}C$ and D/H isotope analyses of Murchison's organic matter strongly propose an interstellar origin,[144-146] which also implies that the organic chemistry characteristic of carbonaceous chondrites was of significance for the origin of terrestrial life. The interstellar origin of complex organic molecules has been linked to the processing of low temperature (10 K) ice-coated, carbonaceous- and/or silicate-based nanoparticles (interstellar grains) by ionizing radiation such as energetic galactic cosmic rays and the internal ultraviolet photon field[147] in cold molecular clouds—the nurseries of stars and planetary systems[148]—as well as by processes such as hydrogen-atom addition.[149,150] Laboratory studies provide compelling evidence that the interaction of ionizing radiation with

interstellar analogue ices can lead to a broad spectrum of astrobiologically important molecules including the sugar glycolaldehyde,[50,151] glycerol,[74] amino acids,[44-48] and even dipeptides.[52] The densest parts of these clouds eventually undergo gravitational collapse to form primitive material, which supplies the basic ingredients for planets, moons, asteroids, and cometary bodies. Therefore, at least part of the organic material such as alkyl phosphonic acids that initially formed in the molecular cloud could have been eventually incorporated into parent bodies of, for instance, the Murchison meteorite.[119,152] Consequently, the elucidation of synthetic routes leading to a key class of astrobiologically important molecules—alkyl phosphonic acids—will help to constrain fundamental processes that drive the hitherto poorly characterized interstellar phosphorus chemistry starting from the simplest closed-shell phosphorus-bearing molecule, phosphine (PH_3),[36,37] and leading to the abiotic synthesis of alkyl phosphonic acids in interstellar ices. Therefore, laboratory investigations are important to understand to what extent alkyl phosphonic acids might have been synthesized exogenously at a frozen stage prior to their delivery to early Earth.

Third, phosphorus in its highest oxidation state P(V) as found in the phosphate moiety (PO_4^{3-}) plays a central role in contemporary terrestrial biochemistry and presents one of the six elements that are biological building blocks along with carbon, hydrogen, oxygen, nitrogen, and sulfur. However, the low solubility of phosphates like calcium phosphate ($Ca_3(PO_4)_2$) in water presents a significant stumbling block in the chemistry for the origin of life.[5] The discovery of a reduced form of phosphorus(III) as present in highly water-soluble alkyl phosphonic acids in Murchison presents a compelling alternative starting point in the prebiotic phosphorus chemistry. It further suggests the possibility that these molecules were delivered by meteorites or even comets to early Earth.[152] This could have provided a supply of organic phosphorus molecules for the earliest stages of chemical evolution. Although probably not components of the first genetic systems, alkyl phosphonic acids might have been precursors to the first nucleic acids.[12] An understanding of the formation pathways of alkyl phosphonic acids in extraterrestrial environments provides a rigorous scientific background about how a class of water-soluble phosphorus-bearing molecules might have been synthesized abiotically.

Finally, our study might also assist in the understanding of the molecular composition and in particular the inventory of alkyl phosphonic acids on comet 67P/Churyumov-Gerasimenko, visited by the Rosetta spacecraft, which detected phosphorus that is believed to have originated from phosphine.[41] Comets are also regarded as leftover debris from gas, ice, rocks, and dust that formed the Solar System from interstellar matter about 4.6×10^9 years ago. Also, a recent analysis of samples of material from comet Wild2 collected by the Stardust mission implied that comets might be considered as one possible class of parent bodies of meteorites.[153,154] The *Rosetta* mission has provided the very first *in situ* exploration of a comet with its objective of characterizing the molecules in the coma of the comet and also on the comet's surface.[149,155-158] The *Philae* Lander landed and performed a detailed analysis of the comet's surface with the data analysis still ongoing. The COSAC (COmetary SAmpling and Composition) unit, a combined gas chromatograph and time-of-flight mass spectrometer, performed an analysis of soil samples and determined the content of volatile components. Hence, a comparison of the inventory of phosphorus-bearing molecules determined by *Rosetta* and *Philae* with predictions from our studies will be crucial in constraining the basic processes that might have led to the formation of compounds such as alkyl phosphonic acids on comets. Once formed abiotically, these alkyl phosphonic acids might have been delivered to early Earth, thus providing the feedstock of highly water-soluble organophosphorus molecules for the earliest stages of biochemical evolution.

Here, we explore experimentally in an ultra-high vacuum surface scattering machine the mechanisms involved in the formation of key functional groups related to the formation of alkyl phosphonic acids upon interaction of ionizing radiation with interstellar analogue ices from the 'bottom up' starting with simple precursor molecules. Our objectives are achieved by systematically replicating the conditions of phosphorus-bearing ice-coated interstellar grains as present in cold molecular clouds at 10 K in an ultra-high vacuum surface scattering machine through the exposure of interstellar analogue ices at relevant temperatures (10 K) to ionizing radiation in the form of energetic electrons, which mimics secondary electrons generated in the track of galactic cosmic ray particles penetrating interstellar ices. This is accomplished while probing

reaction intermediates and products *on line* and *in situ* via detection in the condensed phase by infrared spectroscopy. Infrared spectroscopy facilitates the identification of key functional groups of alkyl phosphonic acids such as C–P, P=O, and O=P–OH and their precursors in the ices as well as in the residues that remain after the ices have sublimed at room temperature.

4.2 Experimental

4.2.1 Experimental Protocol

The experiments were conducted in a contamination-free ultrahigh vacuum (UHV) chamber at pressures of typically 1×10^{-10} Torr achieved by magnetically suspended turbomolecular pumps (Osaka) backed by oil-free scroll pumps (Anest Iwata).[159-164] Briefly, a highly polished silver wafer is attached to an oxygen free high conductivity (OFHC) copper target, which in turn is connected to a two-stage closed-cycle helium refrigerator and programmable temperature controller capable of regulating temperatures between 10 and 330 K. High purity phosphine (PH_3), carbon dioxide (CO_2), methane (CH_4), ethane (C_2H_6), propane (C_3H_8), and butane (C_4H_{10}) premixed gas mixtures were prepared by mixing the individual components in a gas mixing chamber, while oxygen (O_2) and the vapors of ultra-high purity water were introduced to the UHV chamber separately due to their reactivity with phosphine. The preparation of the ices was controlled by a leak valve and introducing the gas mixture via a glass capillary array at 10 K at pressures of about 5×10^{-8} Torr in the main chamber. The ice thickness ranges from 910 $\pm$ 330 nm to 1500 $\pm$ 370 nm (Table 4.1) as determined by the integrated infrared absorption coefficients (Table 4.2), which we found to be constant among the deposited ice thickensses. Pure alkane samples were deposited to a thickness of 500 ± 20 nm using of laser interferometry[120,165,166] with a helium-neon (HeNe) laser operating at 632.8 nm in order to calculate their absorption coefficients[120] and precisely locate their absorption bands, which often lie near or overlap bands from other alkanes (Figure 4.2, Table 4.3).

Table 4.1. Composition of the eight ice mixtures utilized in this study, the average dose per molecule at 100 nA, 1000 nA, and 5000 nA irradiation current, the average thickness of the ice, and the calculated average electron penetration depth.

Ice number	Ice composition	Ratio of components	Dose (eV molecule^{-1})	Thickness (nm)	Average penetration depth (nm)
Ice I	PH_3		2.8 ± 0.6 28 ± 6 140 ± 30	1470 ± 280	480 ± 70
Ice II	$PH_3 – CH_4$	1.8 ± 0.4 : 1.0 ± 0.1	2.4 ± 0.5 24 ± 5 12 ± 25	1260 ± 300	640 ± 100
Ice III	$PH_3 – O_2$	2.5 ± 1.1 : 1.0 ± 0.6	2.1 ± 0.3 21 ± 3 100 ± 20	1050 ± 340	560 ± 80
Ice IV	$PH_3 – CO_2$	1.7 ± 0.1 : 1.0 ± 0.1	3.1 ± 0.7 31 ± 7 150 ± 30	1350 ± 200	460 ± 70
Ice V	$PH_3 – H_2O$	10 ± 0.4 : 1.0 ± 0.5	2.7 ± 0.6 27 ± 6 140 ± 30	1030 ± 160	480 ± 70
Ice VI	$PH_3 – CO_2 – CH_4$	3.1 ± 0.2 : 1.0 ± 0.8 : 2.4 ± 0.7	2.4 ± 0.5 24 ± 5 120 ± 30	910 ± 330	570 ± 90
Ice VII	$PH_3 – CO_2 – CH_4 –$ $C_2H_6 – C_3H_8 – C_4H_{10}$	3.8 ± 0.2 : 1.0 ± 0.5 : 2.0 ± 0.7 : 1.8 ± 0.2 : 1.7 ± 0.3 : 2.0 ± 0.2	3.4 ± 0.7 34 ± 7 170 ± 40	1500 ± 370	520 ± 80
Ice VIII	$PH_3 – H_2O – CH_4 –$ $C_2H_6 – C_3H_8 – C_4H_{10}$	11 ± 5 : 1.0 ± 0.4 : 3.4 ± 0.5 : 5.5 ± 1.9 : 5.8 ± 0.7 : 5.9 ± 1.5	3.5 ± 0.7 35 ± 7 180 ± 40	1320 ± 400	510 ± 80

Table 4.2. Integrated absorption coefficients (A), refractive indices (n), and ice densities (ρ) utilized to determine the thickness and mole ratio of each deposited ice sample.

Phosphine (PH_3)				
Assignment	Position (cm^{-1})	$A^{(1)}$ ($cm\ molec^{-1}$)	$n^{(1)}$	$\rho^{(2)}$ ($g\ cm^{-3}$)
ν_2	982	5.1×10^{-17}	1.51 ± 0.02	0.90
ν_4	1096	7.1×10^{-17}		
Water (H_2O)				
Assignment	Position (cm^{-1})	$A^{(3)}$ ($cm\ molec^{-1}$)	$n^{(4)}$	$\rho^{(5)}$ ($g\ cm^{-3}$)
ν_L	750	2.7×10^{-17}	1.29 ± 0.01	0.94
ν_2	1660	9.8×10^{-17}		
$\nu_1 + \nu_3$	3300	3.8×10^{-16}		
Carbon Dioxide (CO_2)				
Assignment	Position (cm^{-1})	$A^{(3)}$ ($cm\ molec^{-1}$)	$n^{(3)}$	$\rho^{(3)}$ ($g\ cm^{-3}$)
ν_2	660	1.4×10^{-17}	1.27 ± 0.02	1.11 ± 0.03
ν_4 ($^{13}CO_2$)	2283	7.3×10^{-17}		
$2\nu_2 + \nu_3$	3600	6.0×10^{-19}		
$\nu_1 + \nu_3$	3708	1.8×10^{-18}		
Methane				
Assignment	Position (cm^{-1})	$A^{(6)}$ ($cm\ molec^{-1}$)	$n^{(3)}$	$\rho^{(3)}$ ($g\ cm^{-3}$)
ν_4	1300	1.3×10^{-18}	1.34 ± 0.04	0.45 ± 0.03
ν_3	3008	6.6×10^{-18}		
$\nu_1 + \nu_4$	4204	2.9×10^{-19}		
$\nu_3 + \nu_4$	4303	4.2×10^{-19}		
Ethane				
Assignment	Position (cm^{-1})	$A^{(6)}$ ($cm\ molec^{-1}$)	$n^{(7)}$	$\rho^{(8)}$ ($g\ cm^{-3}$)
ν_{12}	819	2.2×10^{-19}	1.34	0.72 ± 0.07
$\nu_2 + \nu_6$	2736	1.4×10^{-19}		
$\nu_5 + \nu_9$	4066	1.4×10^{-19}		
$\nu_9 + \nu_{10}$	4163	1.7×10^{-19}		
$\nu_5 + \nu_8$	4323	1.9×10^{-19}		
$\nu_8 + \nu_{10}$	4401	1.8×10^{-19}		
Propane				
Assignment	Position (cm^{-1})	$A^{(6)}$ ($cm\ molec^{-1}$)	$n^{(6)}$	$\rho^{(9)}$ ($g\ cm^{-3}$)
ν_{26}	747	1.0×10^{-19}	1.36 ± 0.05	0.76
ν_6	1384	1.8×10^{-19}		
$2\nu_6$	2781	8.5×10^{-20}		
$\nu_1 + \nu_{19}$	4287	1.2×10^{-19}		
Butane				
Assignment	Position (cm^{-1})	$A^{(6)}$ ($cm\ molec^{-1}$)	$n^{(6)}$	$\rho^{(9)}$ ($g\ cm^{-3}$)
ν_{32}	1376	4.2×10^{-19}	1.38 ± 0.05	0.83
ν_{13}	2923	3.3×10^{-18}		

Note. Molecular oxygen was not observed in the infrared, but a density of 1.542 g cm^{-1} was used for calculation.[167]

References. (1)[120], (2)[83], (3)[168] , (4)[80] , (5)[169], (6) this study, (7)[170], (8)[171], (9)[172]

Table 4.3. Infrared band positions for methane (CH_4), ethane (C_2H_6), propane (C_3H_8), and butane (C_4H_{10}) observed for 500 nm thick pure ices at 10 K.

Position (cm^{-1})	Assignment
Methane (CH_4)[120]	
1300	ν_4
2814	$\nu_2 + \nu_4$
3008	ν_3
4204	$\nu_1 + \nu_4$
4303	$\nu_3 + \nu_4$
4531	$\nu_2 + \nu_3$
Ethane (C_2H_6)[175]	
819	ν_{12}
1371	ν_6
1461	ν_{11}
2646	$\nu_8 + \nu_{12}$
2736	$\nu_2 + \nu_6$
2878	ν_5
2910	$\nu_8 + \nu_{11}$
2941	$\nu_8 + \nu_{11}$
2969	ν_{10}
4066	$\nu_5 + \nu_9$
4130	$3\nu_6$
4163	$\nu_9 + \nu_{10}$
4323	$\nu_5 + \nu_8$
4401	$\nu_8 + \nu_{10}$
Butane (C_4H_{10})[174,176]	
730	ν_{17}
963	ν_{35}
1288	ν_{33}
1376	ν_{32}
1465	ν_{14}
2636	$\nu_{14} + \nu_{24}$
2727	$2\nu_{32}$
2859	ν_{29}
2871	ν_{28}
2923	ν_{13}
2955	ν_{12}
4335	$\nu_{12} + \nu_6$
Propane (C_3H_8)[173,174]	
747	ν_{26}
867	ν_8
919	ν_{21}
1049	ν_{20}
1156	ν_7
1185	ν_{25}
1333	ν_{19}
1369	ν_{18}
1384	ν_6
1451	ν_5
1466	ν_4
2650	$\nu_4 + \nu_6/\nu_{18}$
2729	$2\nu_{18}$
2781	$2\nu_6$
2869	ν_3
2891	$2\nu_5$
2933	$2\nu_4$
2957	ν_1/ν_2
4024	$\nu_1 + \nu_7$
4054	$\nu_3 + \nu_{25}$
4116	$2\nu_4 + \nu_6/\nu_{18}$
4145	$\nu_1 + \nu_{25}$
4205	$\nu_3 + \nu_{19}$
4241	$\nu_3 + \nu_{18}$
4287	$\nu_1 + \nu_{19}$
4327	$\nu_1 + \nu_4$
4383	$2\nu_4 + \nu_5$

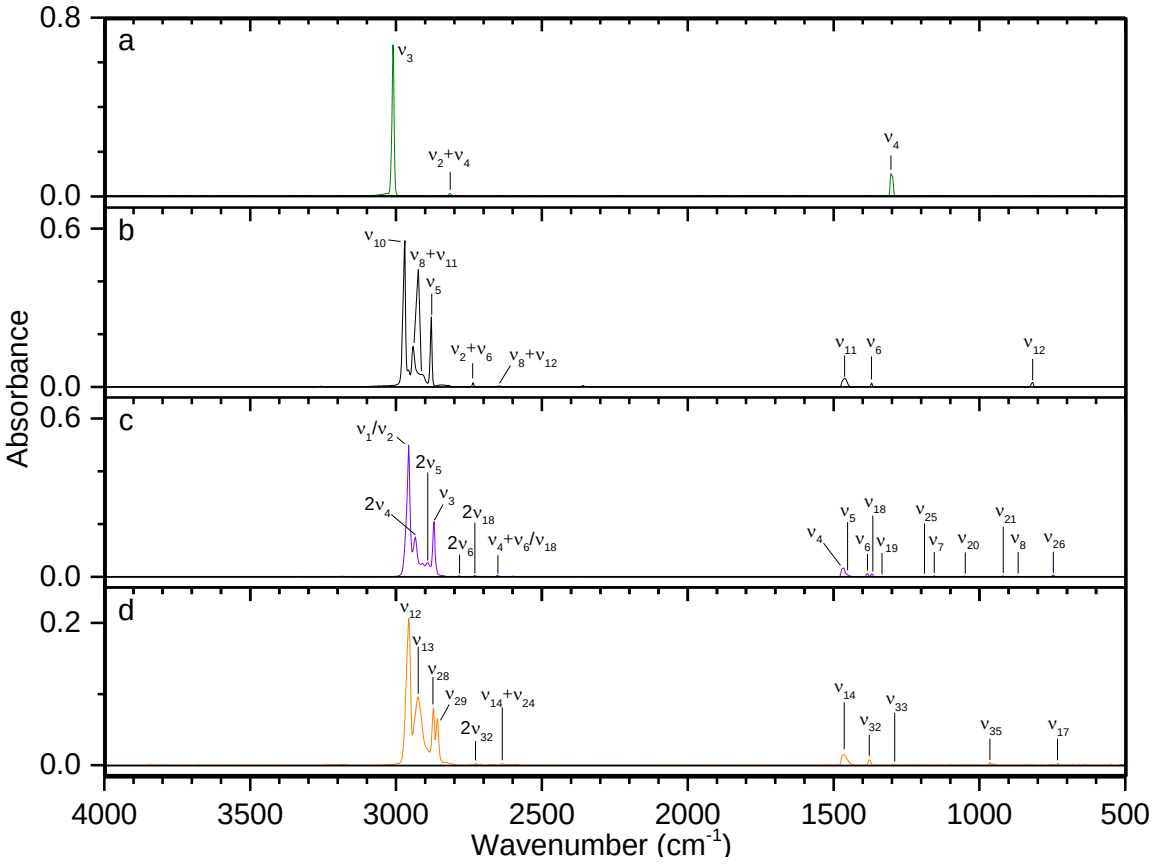

Figure 4.2. Infrared spectra (a) methane, (b) ethane, (c) propane and (d) butane taken at 10 K.

The ice mixtures were then irradiated for 60 minutes with 5 keV electrons at a current of 0 nA (blank), 100 nA, 1000 nA, and 5,000 nA from a Specs EQ 22-35 electron gun. The electron beam exposed an area of 3.2 $\pm$ 0.3 cm^2 at an angle of 15° relative to the surface normal with an actual extraction efficiency of 78.8 % of the electrons by scanning the beam over the ice surface. The electron trajectories and energy losses inside the ices were simulated by the CASINO code.[82] These simulations yielded average penetration depths from 460 $\pm$ 70 nm to 640 $\pm$ 100 nm translating to average doses between 2.1 $\pm$ 0.3 eV and 3.5 $\pm$ 0.7 eV absorbed per molecule at 100 nA irradiation current in the deposited ices (Table 4.1), which scales to between 21 $\pm$ 3 eV and 35 $\pm$ 7 eV at 1000 nA and between 100 $\pm$ 20 eV and 180 $\pm$ 40 eV at 5000 nA. For an interstellar ice grain, these doses correspond to a range of approximately 10^6 to 5 × 10^7 years, which approaches the lifetime for a interstellar molecular cloud.[177] It is important to note that the penetration depths of the electrons are less than the thickness of the ices ensuring that the electrons interact only with the ices, but not with the silver target. After the irradiation, the irradiated ices remained at 10 K for an additional 60 minutes before being heated to 300 K at a rate of 1 K min^{-1}. *In situ* infrared data were collected by a Nicolet 6700 Fourier Transform Infrared Spectrometer at 4 cm^{-1} resolution throughout the irradiation and temperature programmed desorption (TPD).

4.2.2 Ice Composition

In order to synthesize phosphorus-bearing molecules—including alkyl phosphonic acids—in interstellar analogue ices, appropriate precursor molecules that have been detected or predicted to exist on low temperature grains must be utilized; these precursor molecules must also contain carbon (C), hydrogen (H), oxygen (O), and phosphorus (P) as present in alkyl phosphonic acids. First, in astrophysically relevant ices, water (H_2O) presents the dominating component and can provide the required oxygen and hydrogen.[53] Second, oxygen can be also provided by carbon dioxide (CO_2), which has been detected on interstellar grains at levels of 19–28 % the abundance of water ice.[53] Goldsmith, et al. detected molecular oxygen toward Orion and at levels suggesting O_2 comprises at most 1% of interstellar oxygen,[179] and laboratory experiments have verified that molecular oxygen

most likely represents a radiolysis product of water ice.[162,180] The reaction of phosphine with these free oxygen atoms is expected to form, e.g., the phosphorus oxoacids H_3PO_2, H_3PO_3, and H_3PO_4 (Figure 4.1), whose infrared spectra have been investigated by Chapman, et al., Brun, and Ahmadi, et al., respectively.[178-180] Third, considering the molecular structure of the alkyl phosphonic acids and the existence of an alkyl moiety (Figure 4.1), astrophysically relevant alkanes shall also be a component of the analogue ices. Here, methane (CH_4) has been detected in interstellar ices at levels of up to 5 % the abundance of water.[53] Ethane (C_2H_6) has never been detected in interstellar ices, but based on laboratory experiments, it presents the principal alkane, along with propane (C_3H_8) and butanes (C_4H_{10}), formed upon radiolysis of methane ices at 10 K.[129,181] Finally, a carrier of phosphorus is needed. Astrochemical models of interstellar clouds suggest that phosphorus should be depleted onto interstellar grains as phosphine (PH_3) at levels below the current detection limit via infrared spectroscopy.[182-184] Note that phosphine was identified in the circumstellar envelope of IRC+10216[36,37] as well as in the atmospheres of Jupiter[38] and Saturn.[185] Since the initial atmospheric makeup is generally related to the chemistry of the local solar nebula during planetary formation and molecular clouds provide the material for planetary formation, phosphine is expected to be present in molecular clouds and hence also on interstellar grains. Based on these considerations, we select eight sets of phosphine-rich model ices with rising complexity. Here, ice I helps to unravel the basic processes on the decomposition of phosphine in irradiated ices, whereas ice II probes potential carbon-phosphorus bond couplings. Ices III to V elucidate the reactivity of oxygen atoms released from molecular oxygen, carbon dioxide, and water with phosphine and the inherent formation of oxygen-phosphorus bonds as present in (alkyl)phosphonic acids. Eventually ices VI to VIII explore the formation of all functional groups of alkyl phosphonic acids by adding the C1 to C4 alkanes to the phosphine-water and phosphine-carbon dioxide ices.

4.3 Results & Discussion

4.3.1 Ice I (PH_3)

Pure phosphine (PH_3) ice (Figures 4.3—4.5, Table 4.4) displayed the distinct peaks for ν_2 (985 cm^{-1}) and ν_4 (1097 cm^{-1}) as well as an intense peak centered at 2305 cm^{-1} resulting from the unresolved bands of ν_1 and ν_3. The irradiated ice produced mostly diphosphine (P_2H_4), which was easily identified at 100 nA irradiation and consistent with previous results.[120] For all irradiations, the ν_1 (2280 cm^{-1}), ν_2 (2225 cm^{-1}), and ν_3 (1056 cm^{-1}) normal modes were observed, while additional vibrations of ν_5 (648 cm^{-1}), ν_8 (2289 cm^{-1}), ν_{11} (870 cm^{-1}), ν_{12} (632 cm^{-1}), $2\nu_2$ (4467 cm^{-1}), and $2\nu_1$ (4520 cm^{-1}) were observed at higher doses. In addition, triphosphane (P_3H_5) was observed at higher doses, with the δ(HPP) stretches observed at 721 and 778 cm^{-1}. The phosphorus-hydrogen stretching vibration for triphosphane and higher order phosphanes is likely present but obscured by the more intense stretches of phosphine and diphosphine. Not surprisingly, the residues that remained after the ice sublimed contained phosphorus-hydrogen stretching and, to a lesser extent, δ(PH_2), which suggest the residue consists of large molecular weight phosphanes that do not sublime at room temperature even under ultra-high vacuum. This experiment shows that phosphine molecules readily react to produce more complex phosphanes and provides the first piece of the puzzle in unraveling the capabilities of phosphine to react with neighboring constituents in ices.

4.3.2 Ice II (PH_3/CH_4)

The addition of methane (CH_4) to phosphine ices (Figures 4.6—4.8, Table 4.5) was observed through the ν_3 (3002 cm^{-1}) and ν_4 (1302 cm^{-1}) fundamentals, as well as a small peak for the infrared inactive ν_2 (1525 cm^{-1}) vibration. Upon irradiation, phosphine produced diphosphine and triphosphane in a similar manner to ice I, while the only hydrocarbon seen at all irradiations was ethane (C_2H_6), which displayed peaks for ν_5 (2880 cm^{-1}), ν_6 (1370 cm^{-1}), ν_{10} (2968 cm^{-1}), ν_{11} (1461 cm^{-1}), ν_{12} (821 cm^{-1}), and $\nu_8 + \nu_{11}$ (2936 cm^{-1}). At higher doses, two bands were seen for propane (C_3H_8), the ν_1 (2956 cm^{-1}) and ν_{21} (912 cm^{-1}) vibrations, while at 5000 nA the only unsaturated compound produced, ethylene (C_2H_4), was observed at ν_7 (947 cm^{-1}) and ν_9 (3087 cm^{-1}).

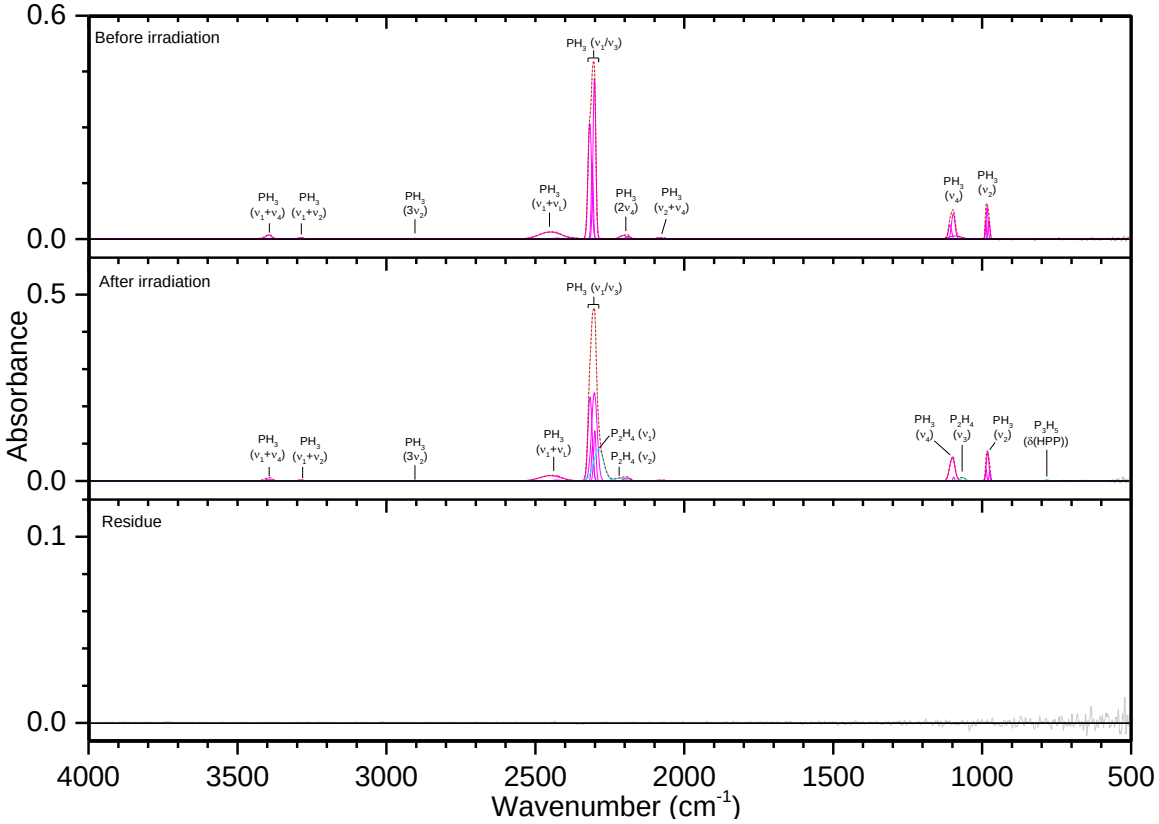

Figure 4.3. Infrared spectra of ice I at 10 K taken before (top) and after (middle) irradiation with 100 nA irradiation current for one hour. The remaining residue at 300 K after sublimation of the irradiated ice is shown in the bottom spectrum. The original spectrum (gray) is deconvoluted showing peaks assigned to phosphine (pink) and new peaks from irradiation (cyan), which sum to create a peak-fitted spectrum (red dashed).

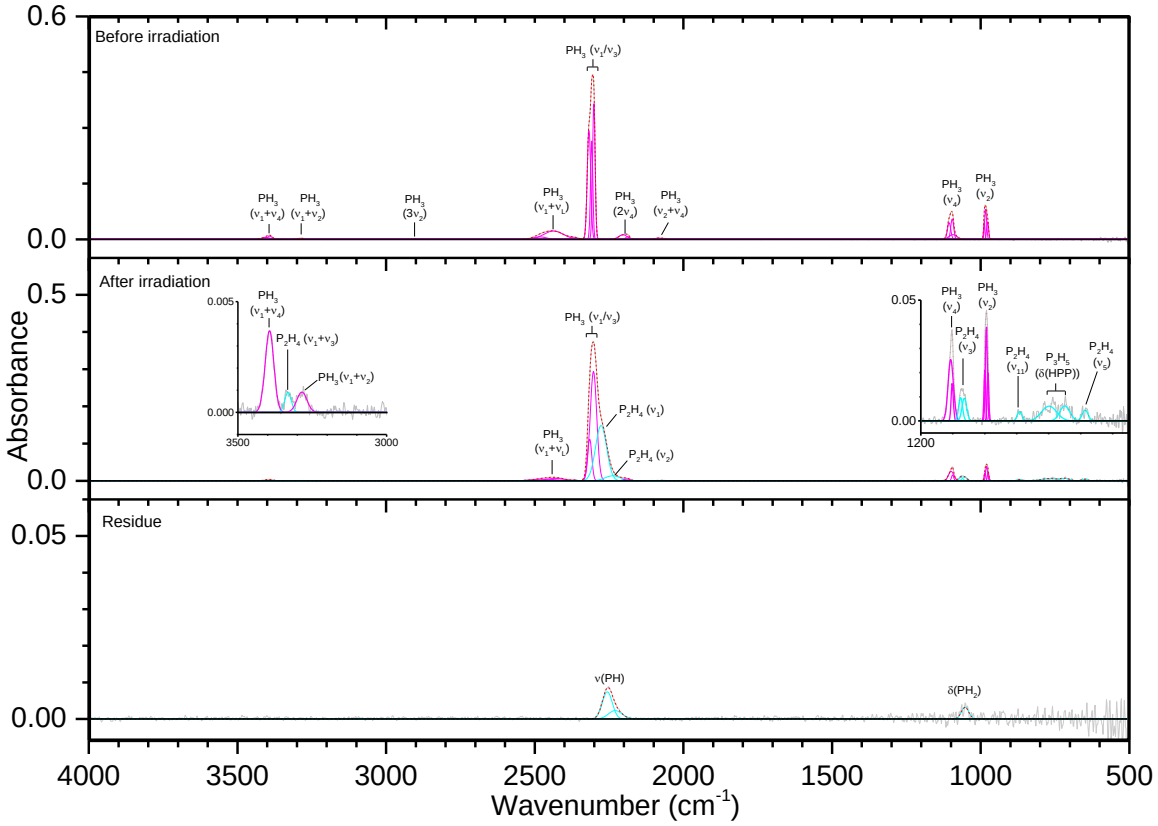

Figure 4.4. Infrared spectra of ice I at 10 K taken before (top) and after (middle) irradiation with 1000 nA irradiation current for one hour. The remaining residue at 300 K after sublimation of the irradiated ice is shown in the bottom spectrum. The original spectrum (gray) is deconvoluted showing peaks assigned to phosphine (pink) and new peaks from irradiation (cyan), which sum to create a peak-fitted spectrum (red dashed). The insets expand low-intensity regions of the spectrum.

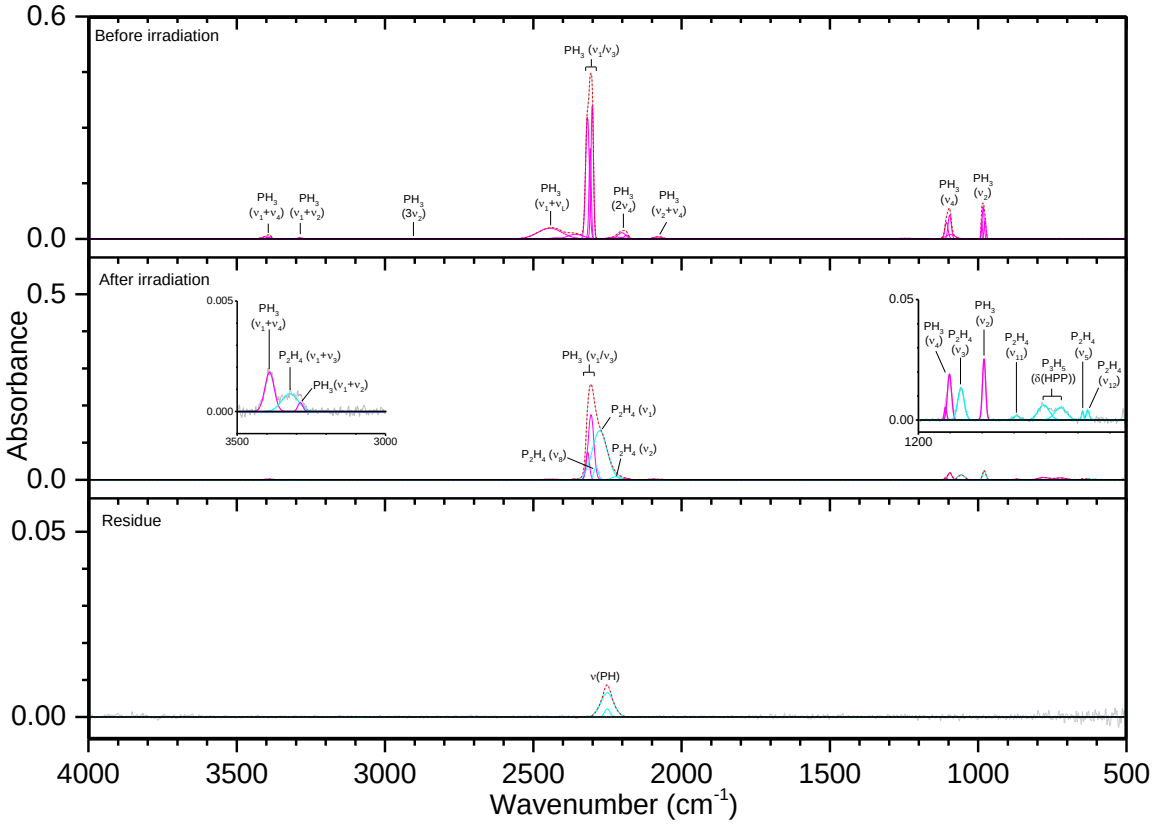

Figure 4.5. Infrared spectra of ice I at 10 K taken before (top) and after (middle) irradiation with 5000 nA irradiation current for one hour. The remaining residue at 300 K after sublimation of the irradiated ice is shown in the bottom spectrum. The original spectrum (gray) is deconvoluted showing peaks assigned to phosphine (pink) and new peaks from irradiation (cyan), which sum to create a peak-fitted spectrum (red dashed). The insets expand low-intensity regions of the spectrum.

Table 4.4. Infrared absorption assignments for ice I at 10 K, the products of irradiation at different doses, and the residue that remained at 300 K after the ice fully sublimed.

Pristine ice, before irradiation (10 K)			
Assignment	Compound	Position (cm^{-1})	Reference
ν_2	PH_3	985	(1)
ν_4	PH_3	1097	(1)
$\nu_2 + \nu_4$	PH_3	2068, 2082	(1)
$2\nu_4$	PH_3	2200	(1)
ν_1/ ν_3	PH_3	2302, 2309, 2317	(1)
$\nu_1 + \nu_L$	PH_3	2350–2450	(1)
$3\nu_2$	PH_3	2903	(1)
$\nu_1 + \nu_2$	PH_3	3287	(1)
$\nu_1 + \nu_4$	PH_3	3392	(1)
$\nu_1 + 2\nu_4$	PH_3	4536	(1)
$\nu_3 + 2\nu_4$	PH_3	4550	(1)
$2\nu_1$	PH_3	4619	(1)

New peaks after irradiation (10 K)				
Assignment	Compound	Position (cm^{-1})	Irradiation (nA)	Reference
ν_{12}	P_2H_4	632	5000	(2)
ν_5	P_2H_4	648	1000, 5000	(2)
δ(HPP)	P_3H_5	721	1000, 5000	(3)
δ(HPP)	P_3H_5	778	100, 1000, 5000	(3)
ν_{11}	P_2H_4	870	1000, 5000	(2)
ν_3	P_2H_4	1059	100, 1000, 5000	(2)
ν_2	P_2H_4	2225	100, 1000, 5000	(2)
ν_1	P_2H_4	2280	100, 1000, 5000	(2)
ν_8	P_2H_4	2289	5000	(2)
$2\nu_2$	P_2H_4	4467	1000, 5000	(4)
$2\nu_1$	P_2H_4	4520	1000, 5000	(4)

Residue (300 K)			
Assignment	Position (cm^{-1})	Irradiation (nA)	Reference
$\delta(PH_2)$	1052	1000	(5)
ν(PH)	2229, 2251	1000, 5000	(5)

Note. ν_L defines the lattice mode.
References. (1)[120], (2)[96] , (3)[97] , (4) This study, (5)[186]

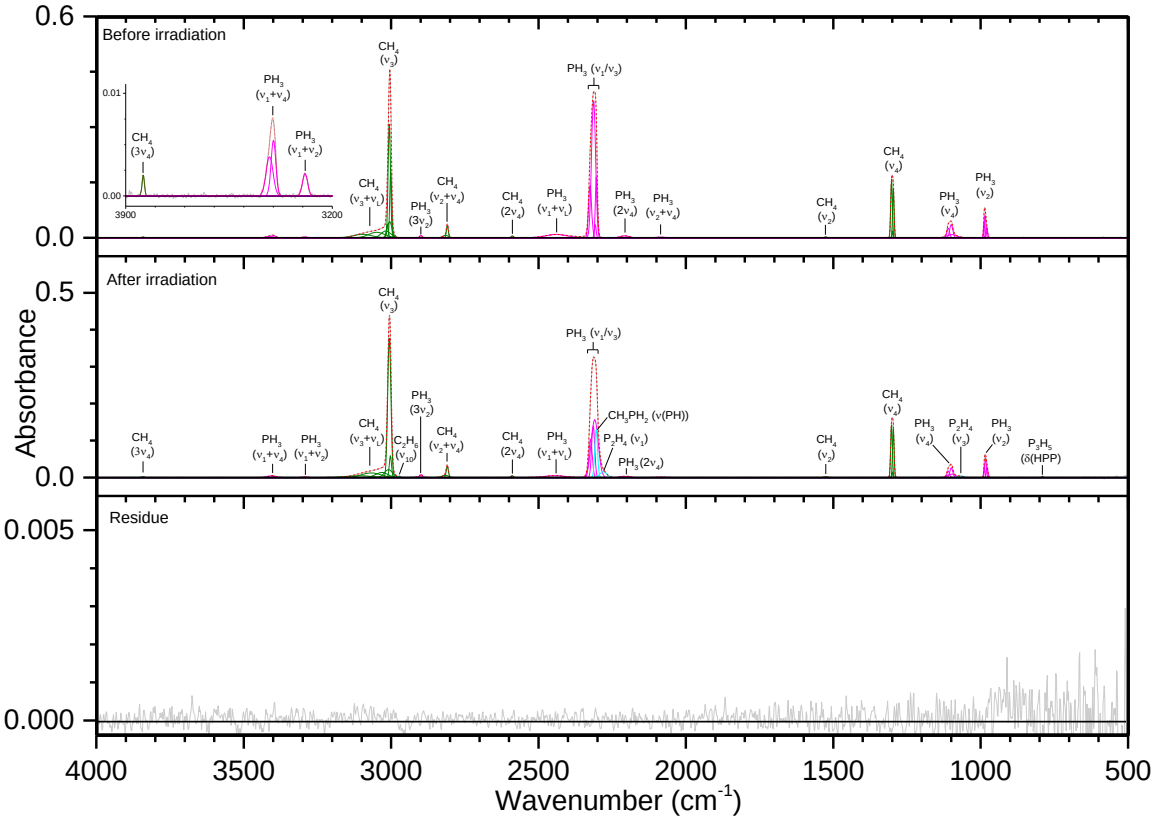

Figure 4.6. Infrared spectra of ice II at 10 K taken before (top) and after (middle) irradiation with 100 nA irradiation current for one hour. The remaining residue at 300 K after sublimation of the irradiated ice is shown in the bottom spectrum. The original spectrum (gray) is deconvoluted showing peaks assigned to phosphine (pink), methane (green), and new peaks from irradiation (cyan), which sum to create a peak-fitted spectrum (red dashed). The inset expands low-intensity regions of the spectrum.

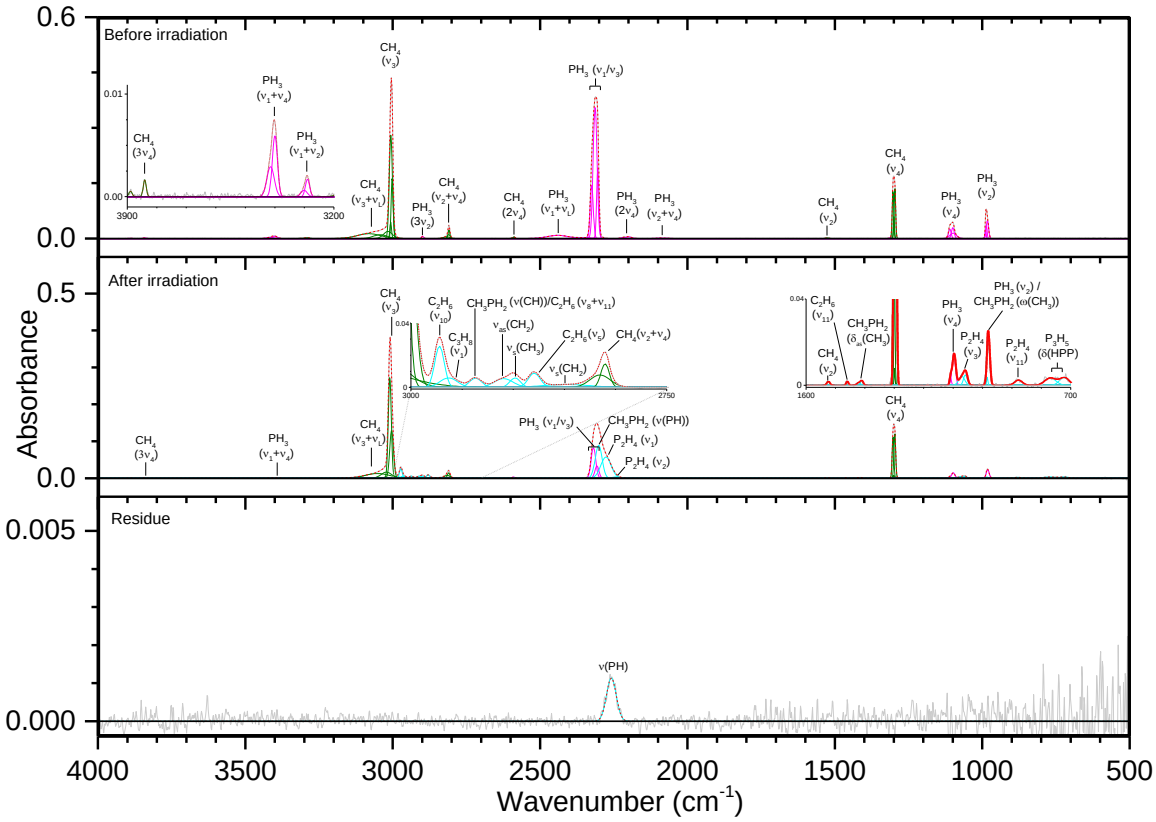

Figure 4.7. Infrared spectra of ice II at 10 K taken before (top) and after (middle) irradiation with 1000 nA irradiation current for one hour. The remaining residue at 300 K after sublimation of the irradiated ice is shown in the bottom spectrum. The original spectrum (gray) is deconvoluted showing peaks assigned to phosphine (pink), methane (green), and new peaks from irradiation (cyan), which sum to create a peak-fitted spectrum (red dashed). The insets expand low-intensity regions of the spectrum.

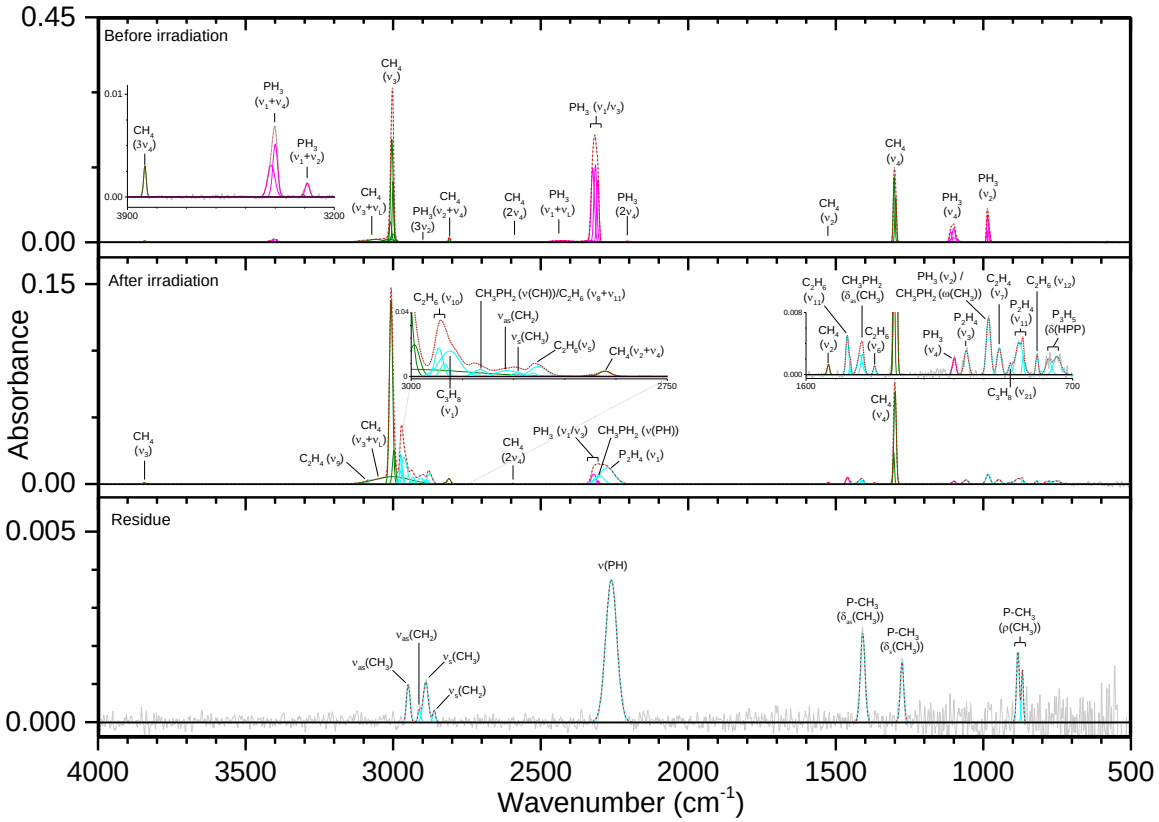

Figure 4.8. Infrared spectra of ice II at 10 K taken before (top) and after (middle) irradiation with 5000 nA irradiation current for one hour. The remaining residue at 300 K after sublimation of the irradiated ice is shown in the bottom spectrum. The original spectrum (gray) is deconvoluted showing peaks assigned to phosphine (pink), methane (green), and new peaks from irradiation (cyan), which sum to create a peak-fitted spectrum (red dashed). The insets expand low-intensity regions of the spectrum.

Table 4.5. Infrared absorption assignments for ice II at 10 K, the products of irradiation at different doses, and the residue that remained at 300 K after the ice fully sublimed.

Pristine ice, before irradiation (10 K)				
Assignment	Compound	Position (cm^{-1})		Reference
ν_2	PH_3	986		(1)
ν_4	PH_3	1104		(1)
ν_4	CH_4	1302		(2)
ν_2	CH_4	1525		(2)
$\nu_2 + \nu_4$	PH_3	2080		(1)
$2\nu_4$	PH_3	2204		(1)
$\nu_1/\ \nu_3$	PH_3	2306, 2315, 2323		(1)
$\nu_1 + \nu_L$	PH_3	2350-2450		(1)
$2\nu_4$	CH_4	2590		(2)
$\nu_2 + \nu_4$	CH_4	2809		(2)
$3\nu_2$	PH_3	2899		(1)
ν_3	CH_4	3002		(2)
$\nu_3 + \nu_L$	CH_4	3015–3115		(2)
$\nu_1 + \nu_2$	PH_3	3292		(1)
$\nu_1 + \nu_4$	PH_3	3402		(1)
$3\nu_4$	CH_4	3841		(2)
$\nu_1 + \nu_4$	CH_4	4193		(2)
$\nu_3 + \nu_4$	CH_4	4292		(2)
$\nu_1 + 2\nu_4$	PH_3	4534		(1)
$\nu_3 + 2\nu_4$	PH_3	4550		(1)
$2\nu_1$	PH_3	4615		(1)
New peaks after irradiation (10 K)				
Assignment	Compound	Position (cm^{-1})	Irradiation (nA)	Reference
δ(HPP)	P_3H_5	753	1000, 5000	(3)
δ(HPP)	P_3H_5	782	100, 1000, 5000	(3)
ν_{12}	C_2H_6	821	5000	(4)
ν_{11}	P_2H_4	875	1000, 5000	(5)
ν_{21}	C_3H_8	912	5000	(6)
ν_7	C_2H_4	947	5000	(7)
$\omega(CH_3)$	CH_3PH_2	984	1000, 5000	(8)
ν_3	P_2H_4	1059	100, 1000, 5000	(5)
ν_6	C_2H_6	1370	5000	(4)
$\delta_{as}(CH_3)$	CH_3PH_2	1412	1000, 5000	(8)
ν_{11}	C_2H_6	1461	1000, 5000	(4)
ν_2	P_2H_4	2245	1000	(5)
ν_1	P_2H_4	2275	100, 1000, 5000	(5)
ν(PH)	CH_3PH_2	2300	100, 1000, 5000	(8)
$\nu_s(CH_2)$	$C_nH_{2n+2}(n \geq 3)$	2850	1000	(9)
ν_5	C_2H_6	2880	1000, 5000	(4)
$\nu_s(CH_3)$	$C_nH_{2n+2}(n \geq 3)$	2895	1000, 5000	(9)
$\nu_{as}(CH_2)$	$C_nH_{2n+2}(n \geq 3)$	2907	1000, 5000	(9)
ν(CH), $\nu_8 + \nu_{11}$	CH_3PH_2, C_2H_6	2936	1000, 5000	(8), (4)
ν_1	C_3H_8	2956	1000, 5000	(6)
ν_{10}	C_2H_6	2968	100, 1000, 5000	(4)
ν_9	C_2H_4	3087	5000	(4)
$2\nu_1$	P_2H_4	4520	1000	(5)

Table 4.5. **(Continued)** Infrared absorption assignments for ice II at 10 K, the products of irradiation at different doses, and the residue that remained at 300 K after the ice fully sublimed.

Residue (300 K)			
Assignment	Position (cm^{-1})	Irradiation (nA)	Reference
P-CH_3 ρ(CH_3)	867	5000	(9)
P-CH_3 ρ(CH_3)	883	5000	(9)
P-CH_3 δ_s(CH_3)	1275	5000	(9)
P-CH_3 δ_{as}(CH_3)	1409	5000	(9)
ν(PH)	2260	1000, 5000	(9)
CH_2 ν_s(CH)	2861	5000	(9)
CH_3 ν_s(CH)	2889	5000	(9)
CH_2 ν_{as}(CH)	2912	5000	(9)
CH_3 ν_{as}(CH)	2949	5000	(9)

Note. ν_L defines the lattice mode.
References. (1)[120], (2)[187], (3)[97], (4)[175], (5)[96], (6)[174], (7)[166], (8)[188] , (9)[186]

The reaction of phosphine and methane was limited compared to reactions with themselves, and the only product identified in the irradiated ices was methylphosphine (CH_3PH_2), for which the associated vibrations of ω(CH_3) (984 cm^{-1}), δ_{as}(CH_3) (1412 cm^{-1}), ν(PH) (2300 cm^{-1}), and ν(CH) (912 cm^{-1}) were observed. Methylphosphine is significant because it establishes that ices of phosphine and methane can lead to phosphorus-carbon bonding and with further oxidation, methylphosphine could be a precursor in the formation of methylphosphonic acid. Finally, the peaks in the residue fall into three general categories and mostly appear only after 5000 nA irradiation, which suggests that products of phosphine and methane have a sufficiently high vapor pressure to sublime below room temperature except at high irradiation doses. The first category is phosphorus-hydrogen stretching (2260 cm^{-1}) typical of a phosphine-containing ice and is the only infrared band that was seen at less than 5000 nA. Second is a group of four peaks associated with carbon-hydrogen stretching: ν_s(CH) on CH_2 (2861 cm^{-1}), ν_s(CH) on CH_3 (2889 cm^{-1}), ν_{as}(CH) on CH_2 (2912 cm^{-1}), and ν_{as}(CH) on CH_3 (2949 cm^{-1}). The third group of vibrations belongs to the P–CH_3 moiety: ρ(CH_3) (867 and 883 cm^{-1}), δ_s(CH_3) (1275 cm^{-1}), and δ_{as}(CH_3) (1409 cm^{-1}). Thus, these bands indicate the molecules in the residue contain phosphorus-hydrogen bonds, carbon-hydrogen bonds, and most significantly, carbon-phosphorus bonds. Here, a substantial step in the systematic untangling of the production of alkyl phosphonic acids is supplied as phosphorus-carbon bonds were observed from a simple binary ice mixture. These results show that the bottom-up approach for synthesis of the phosphorus-carbon bond is in fact feasible within interstellar ices.[187]

4.3.3 Ice III (PH_3/O_2)

Three sources of oxygen were chosen for this study: water (H_2O), carbon dioxide (CO_2), and dioxygen (O_2). While small amounts of O_2 have been detected in the interstellar medium, it largely serves as a good foundation for the study of reactions of atomic oxygen with phosphine and as a carbon-free reference for comparison with the carbon dioxide ices. Although previous studies[189,190] observed the O_2 fundamental stretch in pure oxygen ices at 1549 cm^{-1}, these mixed ices with phosphine show no features related to O_2 (Figures 4.9—4.11, Table 4.6). However, the phosphine bands are less intense, and upon irradiation with even 100 nA their intensities decline to approximately 10 %, which indicates irradiated dioxygen is much more efficient at reacting with phosphine than methane. After irradiation, a several oxidized phosphorus peaks were observed at the expense of phosphanes, as only two peaks for diphosphine (ν_1 (2284 cm^{-1}) and ν_3 (1060 cm^{-1})) were seen. Also, the irradiated oxygen produced ozone (O_3), observed at ν_3 (1040 cm^{-1}) and its overtone $2\nu_3$ (2108 cm^{-1}). In general, the broad absorption features assigned to phosphorus with oxygen are identified as function groups that could belong to several molecules and numerous combinations of phosphorus, oxygen, and hydrogen. At lower frequencies exists a complex of bands bounded by ν(P–O) with peak intensity between 930 and 1000 cm^{-1} and by ν(P=O) with peak intensity ranging from 1160 to 1270 cm^{-1}. Intermediate between these bounds exists $\delta(PH_2)$ bands near 1050 cm^{-1}, which includes the ν_3 fundamental seen in this and previous ices. The P–OH moiety is evident by the location of oxygen-hydrogen stretches around 2170 and 2700 cm^{-1}, and the band at 1680 cm^{-1} indicates that O=P–OH is also present. That the band at 2700 cm^{-1} is greater intensity than 2170 cm^{-1} suggests a high concentration of phosphoric acid for the 1000 nA residues, while the roughly equal intensities at 5000 nA indicate greater amounts of phosphonic acid.[186] However, this method is limited in the irradiated ices because the $\nu_4(H_2O)$ band contributes to the 1680 cm^{-1} absorption, thus complicating the comparison of peak intensities. Other water bands that formed from irradiation include ν_L (800 cm^{-1}) and the broad oxygen-hydrogen stretches of ν_1 and ν_3 between 3000 and 3600 cm^{-1}. While water is not unexpected from this experimental mixture, the ease at which phosphine is oxidized to form compounds similar to phosphonic and phosphoric acid with P=O, P–OH, and combined O=P–OH is promising for phosphine's potential as a precursor to alkyl phosphonic acids.

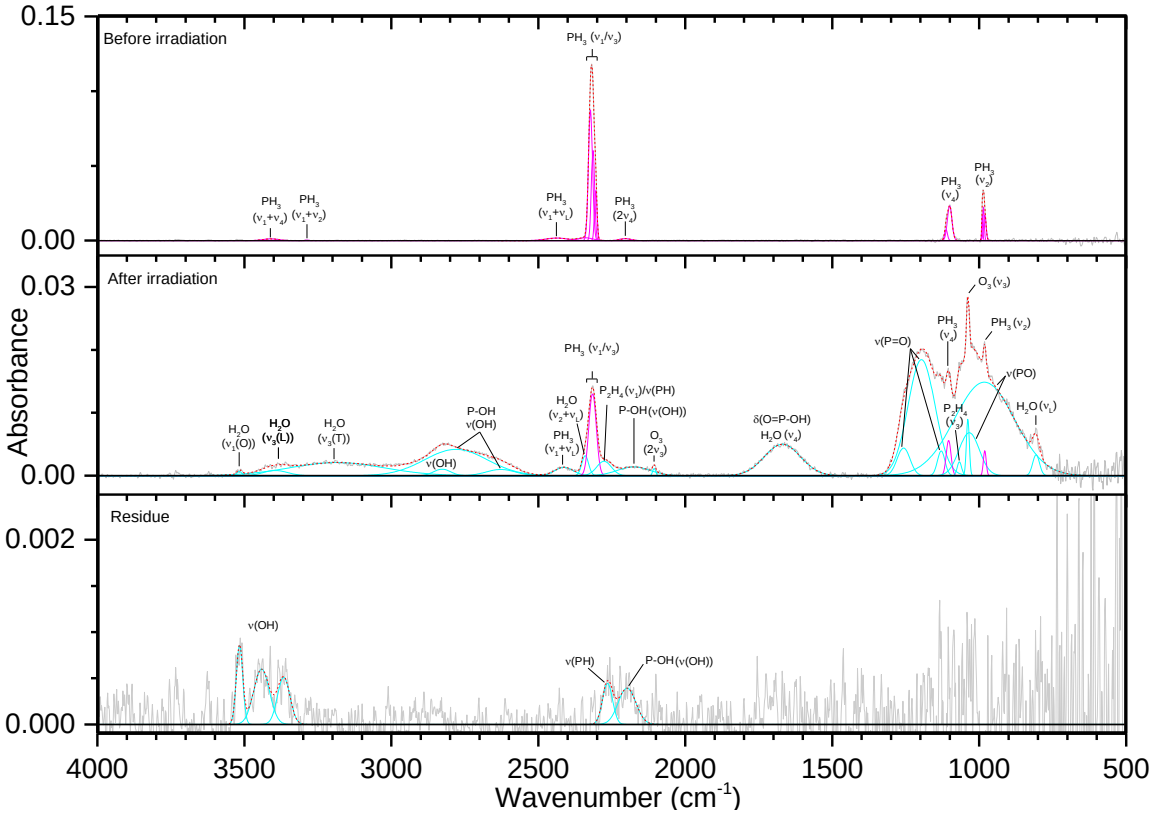

Figure 4.9. Infrared spectra of ice III at 10 K taken before (top) and after (middle) irradiation with 100 nA irradiation current for one hour. The remaining residue at 300 K after sublimation of the irradiated ice is shown in the bottom spectrum. The original spectrum (gray) is deconvoluted showing peaks assigned to phosphine (pink) and new peaks from irradiation (cyan), which sum to create a peak-fitted spectrum (red dashed). No molecular oxygen peaks were observed. The ν_1 and ν_3 vibration for water are labeled as "O" (out-of-phase with neighboring molecules), "L" (longitudinal), and "T" (transversal).

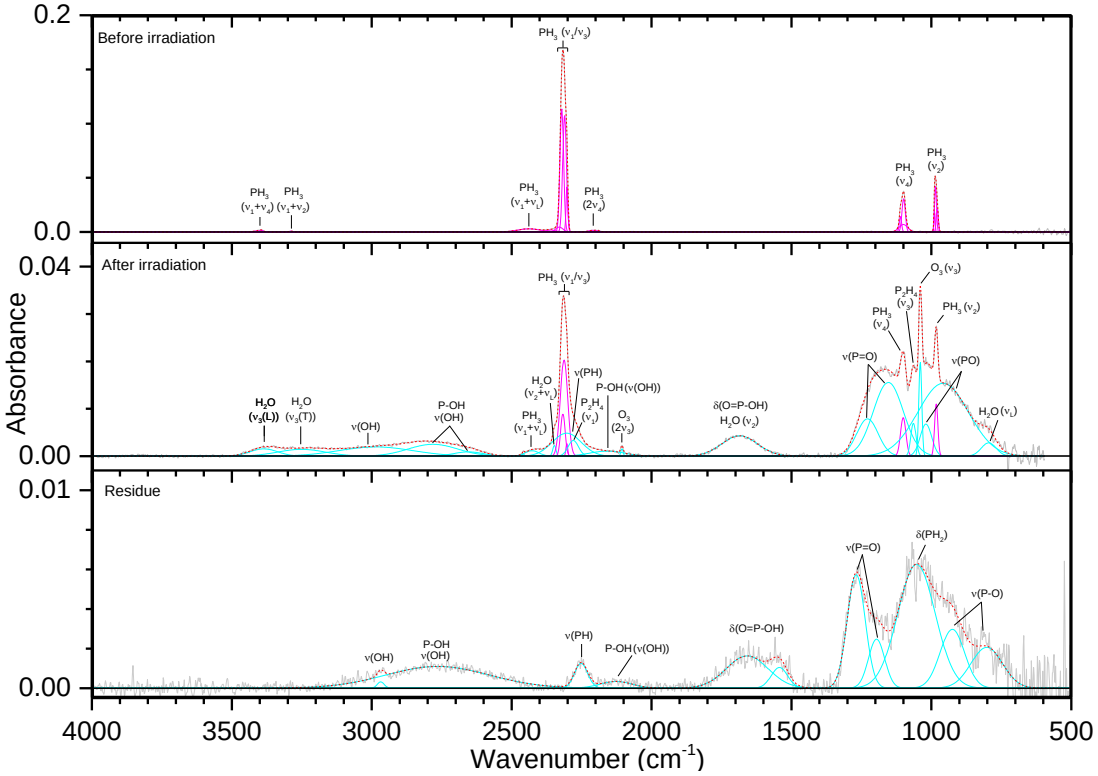

Figure 4.10. Infrared spectra of ice III at 10 K taken before (top) and after (middle) irradiation with 1000 nA irradiation current for one hour. The remaining residue at 300 K after sublimation of the irradiated ice is shown in the bottom spectrum. The original spectrum (gray) is deconvoluted showing peaks assigned to phosphine (pink) and new peaks from irradiation (cyan), which sum to create a peak-fitted spectrum (red dashed). No molecular oxygen peaks were observed. The ν_3 vibration for water is labeled as "L" (longitudinal) or "T" (transversal).

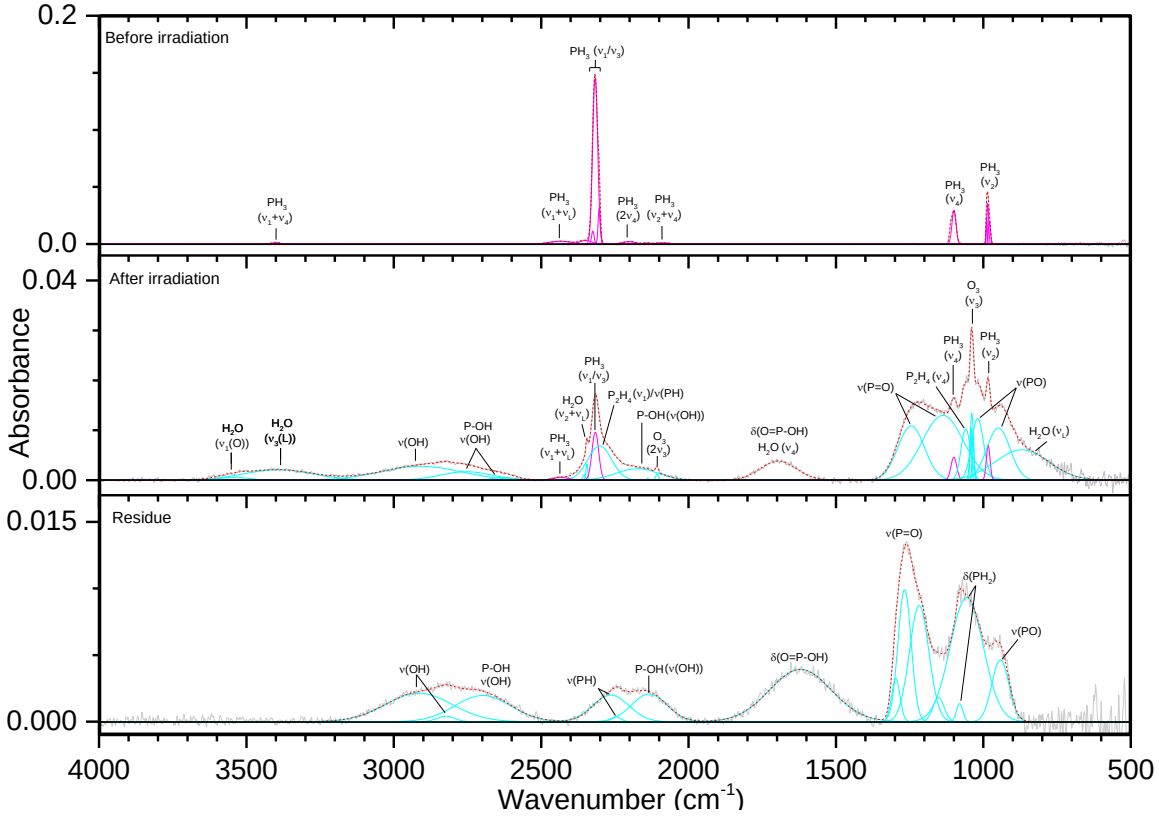

Figure 4.11. Infrared spectra of ice III at 10 K taken before (top) and after (middle) irradiation with 5000 nA irradiation current for one hour. The remaining residue at 300 K after sublimation of the irradiated ice is shown in the bottom spectrum. The original spectrum (gray) is deconvoluted showing peaks assigned to phosphine (pink) and new peaks from irradiation (cyan), which sum to create a peak-fitted spectrum (red dashed). No molecular oxygen peaks were observed. The ν_1 vibration for water are labeled as "O" (out-of-phase with neighboring molecules) while the ν_3 vibration is labeled as "L" (longitudinal).

Table 4.6. Infrared absorption assignments for ice III at 10 K, the products of irradiation at different doses, and the residue that remained at 300 K after the ice fully sublimed.

Pristine ice, before irradiation (10 K)				
Assignment	Compound	Position (cm^{-1})		Reference
ν_2	PH_3	987		(1)
ν_4	PH_3	1100		(1)
$\nu_2 + \nu_4$	PH_3	2087, 2143		(1)
$2\nu_4$	PH_3	2192, 2202		(1)
ν_1/ ν_3	PH_3	2303, 2317, 2324		(1)
$\nu_1 + \nu_L$	PH_3	2350-2450		(1)
$\nu_1 + \nu_2$	PH_3	3287		(1)
$\nu_1 + \nu_4$	PH_3	3399		(1)
$\nu_1 + 2\nu_4$	PH_3	4536		(1)
$\nu_3 + 2\nu_4$	PH_3	4550		(1)
New peaks after irradiation (10 K)				
Assignment	Compound	Position (cm^{-1})	Irradiation (nA)	Reference
ν_L	H_2O	790–870	100, 1000, 5000	(2)
ν(P-O)		900–1050	100, 1000, 5000	(3)
ν_3	O_3	1040	100, 1000, 5000	(4)
ν_3	P_2H_4	1059	100, 1000, 5000	(5)
ν(P=O)		1100–1300	100, 1000, 5000	(3)
δ(O=P-OH)		1630–1740	100, 1000, 5000	(3)
ν_4	H_2O			(2)
$2\nu_3$	O_3	2108	100, 1000, 5000	(4)
P-OH ν(OH)		2170	100, 1000, 5000	(3)
ν_1	P_2H_4	2279	100, 1000, 5000	(5)
ν(PH)		2270-2320	100, 1000, 5000	(3)
$\nu_2 + \nu_L$	H_2O	2345	100, 1000, 5000	(2)
P-OH ν(OH)		2600-2800	100, 1000, 5000	(3)
ν(OH)		2825-3000	100, 1000, 5000	(3)
ν_3 (transversal)	H_2O	3190-3250	100, 1000	(2)
ν_3 (longitudinal)	H_2O	3400	100, 1000, 5000	(2)
ν_1 (out of phase)	H_2O	3520-3550	100, 5000	(2)
Residue (300 K)				
Assignment	Position (cm^{-1})		Irradiation (nA)	Reference
ν(P-O)	800-950		1000, 5000	(3)
$\delta(PH_2)$	1030–1100		1000, 5000	(3)
ν(P=O)	1150–1300		1000, 5000	(3)
δ (O=P-OH)	1540–1660		1000, 5000	(3)
P-OH ν(OH)	2100–2190		100, 1000, 5000	(3)
ν(PH)	2260		100, 1000, 5000	(3)
P-OH ν(OH)	2700-2770		1000, 5000	(3)
ν(OH)	2820–3500		100, 1000, 5000	(3)

Note. ν_L defines the lattice mode and no absorption peaks were observed for molecular oxygen.
References. (1)[120], (2)[169], (3)[186], (4)[190], (5)[96]

4.3.4 Ice IV (PH_3/CO_2)

Carbon dioxide (CO_2) adds a level of complexity in that four elements are present in this ice (Figures 4.12–4.14, Table 4.7). Although carbon is again present in this system like in ice II, the purpose of adding carbon dioxide is as a source of oxygen from the decomposition of carbon dioxide to carbon monoxide (CO) and atomic oxygen, and thus the expected results are more similar to ice III. A downside to using carbon dioxide is that its most intense peak, ν_3 (2335 cm^{-1}) not only overlaps with ν_1/ν_3 of phosphine but dwarfs and obscures phosphine and some products with phosphorus-hydrogen bonding. Besides the ν_3 vibration and its carbon-13 isotopic peak (2274 cm^{-1}), the ν_2 band appears prominently at 665 cm^{-1}. The only carbon-containing compound detected in the irradiated was carbon monoxide at 2137 cm^{-1} and for ^{13}CO, 2092 cm^{-1}. The carbonyl functional group, ν(C=O), was also observed around 1765 cm^{-1}, but given its broad low intensity and overlapping neighboring peaks the specific nature of this carbonyl stretch cannot be ascertained. Other than these bands, the products were similar to the system of phosphine and oxygen. Water was observed at all irradiations through the ν_1, ν_2, ν_3, and ν_L bands. Similarly, the oxidized phosphorus functional groups of ν(P–O) (950 cm^{-1}), ν(P=O) (1150–1300 cm^{-1}), δ(O=P–OH) (1712 cm^{-1}), and P–OH ν(OH) (2170 and 2680 cm^{-1}) were observed at after irradiation and in the residues for the 1000 nA and 5000 nA experiments. Diphosphine was also detected after irradiation at 1000 nA, while the functional groups ν(PH) and δ(PH_2) were detected both after irradiation and in the residues. A comparison of the P–OH bands at 1712, 2170, and 2680 cm^{-1} indicates that for the 1000 and 5000 nA experiments, phosphonic acid is the dominant source of the P-OH moiety in the residue. The 5000 nA residue also has a band assigned to phosphorus-carbon stretching (745 cm^{-1}), although no other carbon stretches are available to help elucidate the nature of the compounds that might contain this bond. These results readily supply the next step in understanding the possible formation mechanism toward alkyl phosphonic acids as phosphonic acid vibrations are easily detected.

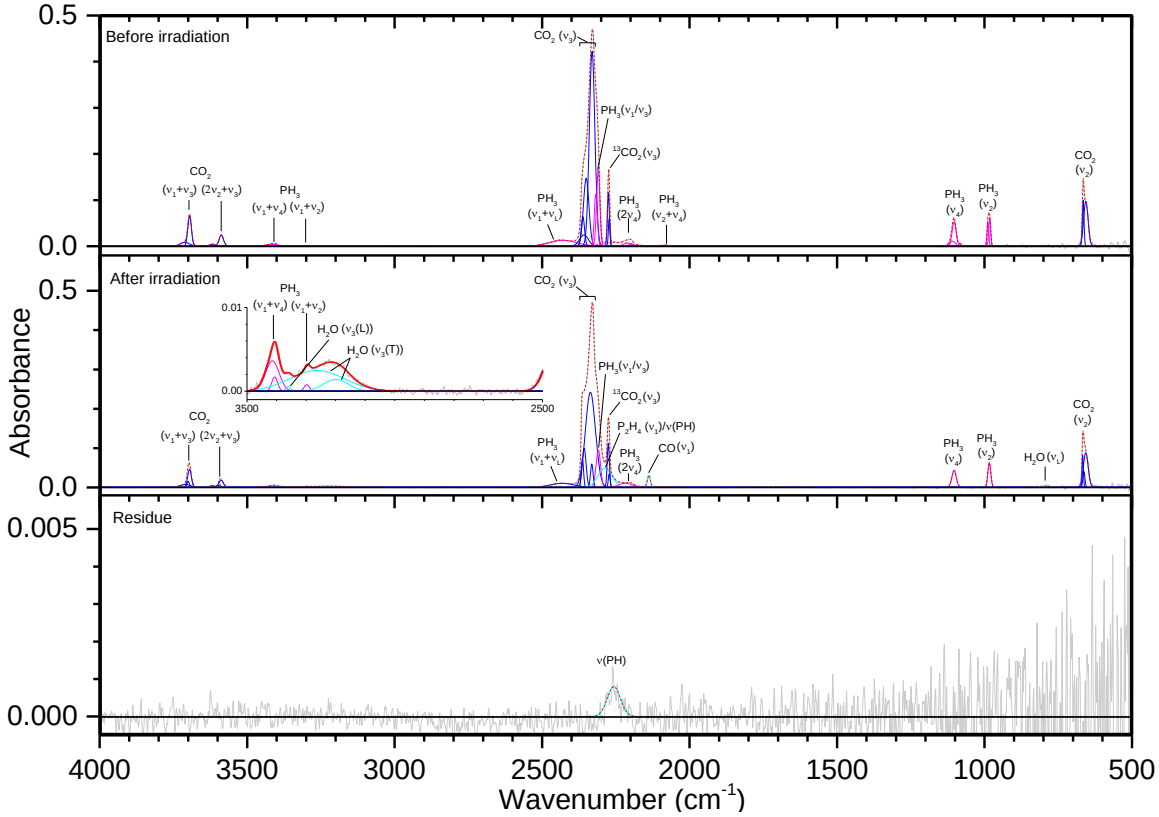

Figure 4.12. Infrared spectra of ice IV at 10 K taken before (top) and after (middle) irradiation with 100 nA irradiation current for one hour. The remaining residue at 300 K after sublimation of the irradiated ice is shown in the bottom spectrum. The original spectrum (gray) is deconvoluted showing peaks assigned to phosphine (pink), carbon dioxide (blue), and new peaks from irradiation (cyan), which sum to create a peak-fitted spectrum (red dashed). The ν_3 vibration for water is labeled as "L" (longitudinal) or "T" (transversal). The inset expands low-intensity regions of the spectrum.

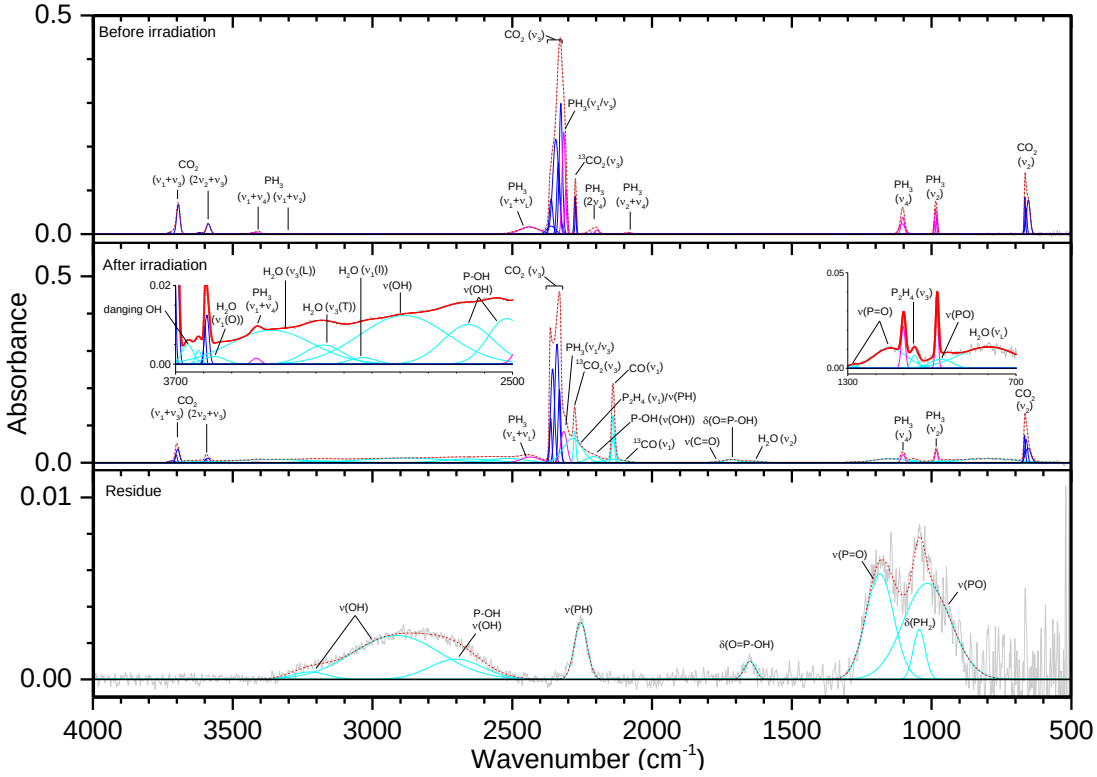

Figure 4.13. Infrared spectra of ice IV at 10 K taken before (top) and after (middle) irradiation with 1000 nA irradiation current for one hour. The remaining residue at 300 K after sublimation of the irradiated ice is shown in the bottom spectrum. The original spectrum (gray) is deconvoluted showing peaks assigned to phosphine (pink), carbon dioxide (blue), and new peaks from irradiation (cyan), which sum to create a peak-fitted spectrum (red dashed). The ν_1 and ν_3 vibration for water are labeled as "O" (out-of-phase with neighboring molecules), "I" (in-phase with neighboring molecules), "L" (longitudinal), and "T" (transversal). The insets expand low-intensity regions of the spectrum

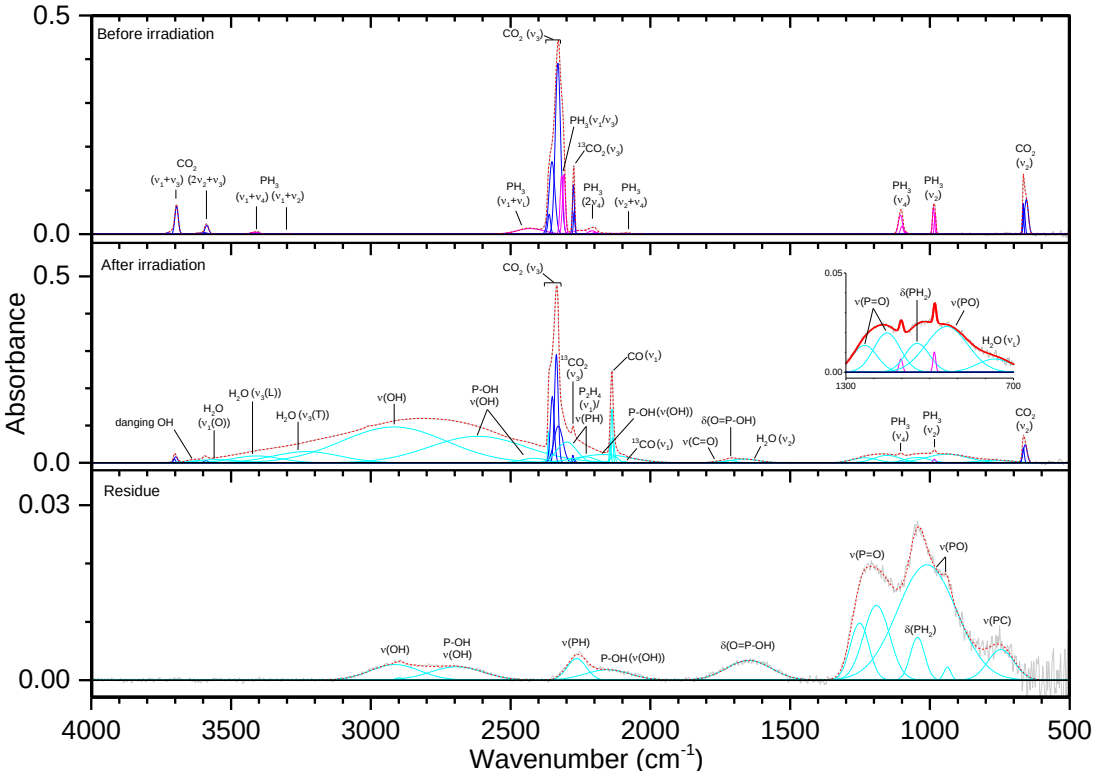

Figure 4.14. Infrared spectra of ice IV at 10 K taken before (top) and after (middle) irradiation with 5000 nA irradiation current for one hour. The remaining residue at 300 K after sublimation of the irradiated ice is shown in the bottom spectrum. The original spectrum (gray) is deconvoluted showing peaks assigned to phosphine (pink), carbon dioxide (blue), and new peaks from irradiation (cyan), which sum to create a peak-fitted spectrum (red dashed). The ν_1 and ν_3 vibration for water are labeled as "O" (out-of-phase with neighboring molecules), "L" (longitudinal), and "T" (transversal). The inset expands low-intensity regions of the spectrum.

Table 4.7. Infrared absorption assignments for ice IV at 10 K, the products of irradiation at different doses, and the residue that remained at 300 K after the ice fully sublimed.

Pristine ice, before irradiation (10 K)			
Assignment	Compound	Position (cm^{-1})	Reference
ν_2	CO_2	665	(1)
ν_2	PH_3	986	(2)
ν_4	PH_3	1103	(2)
$\nu_2 + \nu_4$	PH_3	2080	(2)
$2\nu_4$	PH_3	2203	(2)
ν_3	$^{13}CO_2$	2274	(1)
$\nu_1/\ \nu_3$	PH_3	2309, 2316	(2)
ν_3	CO_2	2325-2365	(1)
$\nu_1 + \nu_L$	PH_3	2435	(2)
$\nu_1 + \nu_2$	PH_3	3300	(2)
$\nu_1 + \nu_4$	PH_3	3407	(2)
$2\nu_2 + \nu_3$	CO_2	3588	(1)
$\nu_1 + \nu_3$	CO_2	3694	(1)
$\nu_1 + \nu_3$	PH_3	4554	(2)
$2\nu_3$	PH_3	4662	(2)

New peaks after irradiation (10 K)				
Assignment	Compound	Position (cm^{-1})	Irradiation (nA)	Reference
ν_L	H_2O	800	100, 1000, 5000	(3)
ν(P-O)		930-970	1000, 5000	(4)
$\delta(PH_2)$		1044	5000	(4)
ν_3	P_2H_4	1060	1000	(5)
ν(P=O)		1140–1300	1000, 5000	(4)
ν_2	H_2O	1630	1000, 5000	(3)
δ(O=P-OH)		1712	1000, 5000	(4)
ν(C=O)		1765	1000, 5000	(4)
ν_1	^{13}CO	2092	1000, 5000	(1)
ν_1	CO	2137	100, 1000, 5000	(1)
P-OH ν(OH)		2170	5000	(4)
ν_1	P_2H_4	2284	100, 1000, 5000	(5)
ν(PH)		2230-2330	100, 1000, 5000	(4)
P-OH ν(OH)		2400-2680	1000, 5000	(4)
ν(OH)		2850-2950	1000, 5000	(4)
ν_1(in phase)	H_2O	3037	1000	(3)
ν_3(transversal)	H_2O	3170-3270	100, 1000, 5000	(3)
ν_3(longitudinal)	H_2O	3360-3410	100, 1000, 5000	(3)
ν_1(out of phase)	H_2O	3557	1000, 5000	(3)
dangling OH	H_2O	3620–3670	1000, 5000	(6)

Residue (300 K)			
Assignment	Position (cm^{-1})	Irradiation (nA)	Reference
ν(PC)	745	5000	(4)
ν(P-O)	950–1010	1000, 5000	(4)
$\delta(PH_2)$	1045	1000, 5000	(4)
ν(P=O)	1180–1250	1000, 5000	(4)
δ(O=P-OH)	1647	1000, 5000	(4)
P-OH ν(OH)	2152	1000, 5000	(4)
ν(PH)	2250	100, 1000, 5000	(4)
P-OH ν(OH)	2690	1000, 5000	(4)
ν(OH)	2900-3250	1000, 5000	(4)

Note. ν_L defines the lattice mode.
References. (1)[160] , (2)[120], (3)[169], (4)[186], (5)[96], (6)[191]

4.3.5 Ice V (PH_3/H_2O)

While the irradiation of molecular oxygen and carbon dioxide produces a free reactive oxygen atom, reactions with water (Figures 4.15–4.17, Table 4.8) are expected to proceed differently as the hydroxyl radical (OH) is formed instead during irradiation. The unirradiated ice shows consistent features to the water produced in ices III and IV, including the broad ν_L band centered near 750 cm^{-1} and its small overtone at 1465 cm^{-1}, the asymmetric ν_2 band, the combination band of ν_L and ν_2 that falls in the ν(PH) region at 2335 cm^{-1}, and the complex of ν(OH) absorptions between 3000 and 3600 cm^{-1}. These broad absorptions include ν_1, which is split between vibrations that are in-phase and out-of-phase with its neighbors (3050 and 3500 cm^{-1}), and ν_3, which is also split between the transversal (3200 cm^{-1}) and longitudinal (3350 cm^{-1}) vibrations. The thickness of this ice is around 1 μm, which is sufficient for the transversal mode to be observed and not neutralized by the metal surface selection rule (MSSR).[192-194] The transversal mode, which arises from a transition dipole moment parallel to the surface and absorbs the s-polarized component of the infrared radiation, can be canceled out in much thinner films by the MSSR. Also, the notch seen in this peak can be attributed to coupling of the real refractive index (n) and the absorption index (k), resulting in a change of reflectivity that becomes more pronounced with increasing film thickness.[194] Furthermore, this complex includes a prominent absorption at 3570 cm^{-1} that was not seen in previous non-phosphorus containing ices. A similar spectral feature was seen by de Barros, et al.,[191] which they assigned to dangling OH bonds. The irradiated ice is comparatively simple, with the only non-oxygen-containing bands belonging to P_2H_4 (1060 and 2286 cm^{-1}), ν(PH) (2220-2300 cm^{-1}), and $\delta(PH_2)$ (1035 cm^{-1}). The latter two features are also observed in the residue. Compared to carbon dioxide and molecular oxygen, water reacted with phosphine less readily and produced fewer oxygenated phosphorus compounds. At 100 nA irradiation, the spectrum was nearly unchanged, and even at 1000 nA the only new phosphorus/oxygen bands were small signals for ν(P=O) (1135 cm^{-1}) and P-OH ν(OH) (2780 cm^{-1}). However, small signals for ν(P–O) and δ(O=P–OH) could be obscured by the ν_L and ν_2 bands of water, and ν(P–O) was visible in the residue. All of these vibrations were visible in the 5000 nA experiment, although still muted compared to the carbon dioxide ices. Missing from all irradiated ices was the P–OH ν(OH) at 2170 cm^{-1}, although a small peak appeared in the residue at 5000 nA. Unlike the carbon dioxide and molecular oxygen residues at 5000 nA,

these peaks from the water experiments indicate a low concentration of phosphonic acid and instead greater amounts of phosphoric and phosphinic acid (H_3PO_2). In summary, ices of phosphine with oxygen, carbon dioxide, and water each can produce, given sufficient irradiation, compounds that include a phosphorus-oxygen double bond (P=O), single bond (P–O), including to a hydroxyl group (P–OH), and the combination of these functional groups (O=P–OH). However, these signals were visible in the oxygen ices after just 100 nA irradiation, while carbon dioxide required 1000 nA and water needed the highest dose of 5000 nA for detection. These ice mixtures also contained phosphorus-hydrogen bonding that appeared comparatively more intense in the residues than they did in the irradiated ices, which suggests a large number of phosphorus-oxygen compounds were able to sublime from the ice while more phosphorus-hydrogen compounds remained in the residue. These results help to show possible barriers in the synthesis of the phosphonic acid group within water ice, which is the major component of interstellar ices.

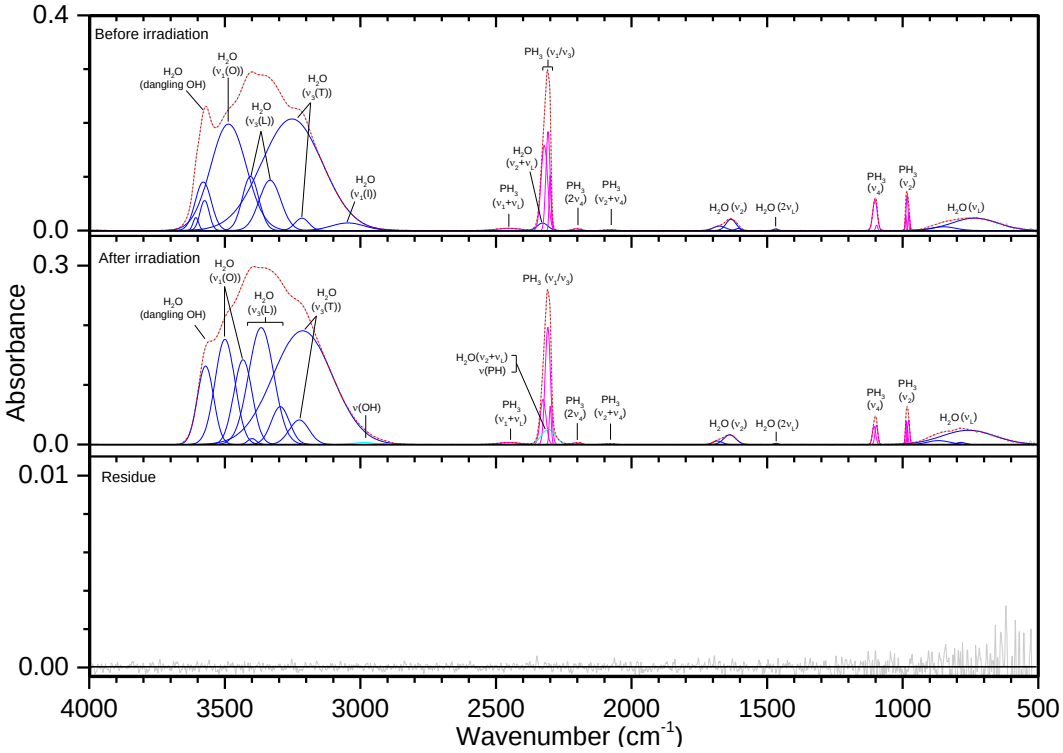

Figure 4.15. Infrared spectra of ice V at 10 K taken before (top) and after (middle) irradiation with 100 nA irradiation current for one hour. The remaining residue at 300 K after sublimation of the irradiated ice is shown in the bottom spectrum. The original spectrum (gray) is deconvoluted showing peaks assigned to phosphine (pink), water (blue), and new peaks from irradiation (cyan), which sum to create a peak-fitted spectrum (red dashed). The ν_1 and ν_3 vibration for water are labeled as "O" (out-of-phase with neighboring molecules), "I" (in-phase with neighboring molecules), "L" (longitudinal), and "T" (transversal).

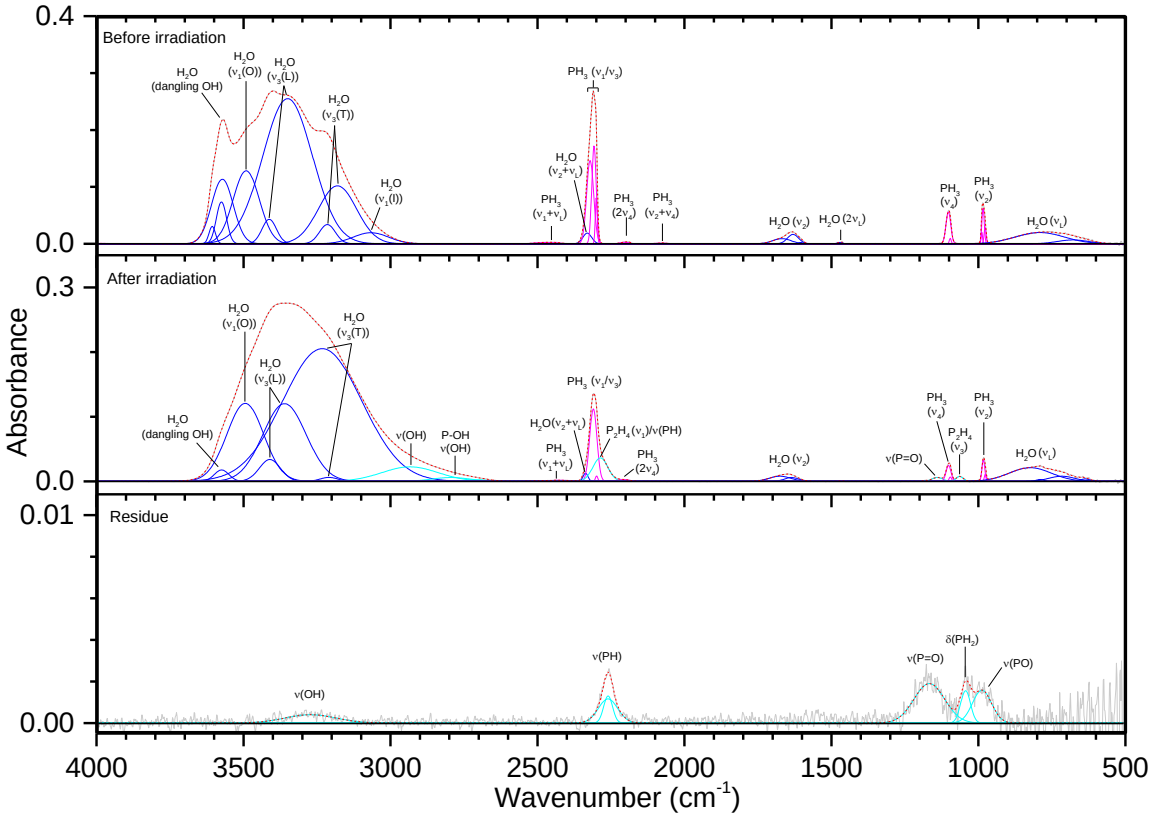

Figure 4.16. Infrared spectra of ice V at 10 K taken before (top) and after (middle) irradiation with 1000 nA irradiation current for one hour. The remaining residue at 300 K after sublimation of the irradiated ice is shown in the bottom spectrum. The original spectrum (gray) is deconvoluted showing peaks assigned to phosphine (pink), water (blue), and new peaks from irradiation (cyan), which sum to create a peak-fitted spectrum (red dashed). The ν_1 and ν_3 vibration for water are labeled as "O" (out-of-phase with neighboring molecules), "I" (in-phase with neighboring molecules), "L" (longitudinal), and "T" (transversal).

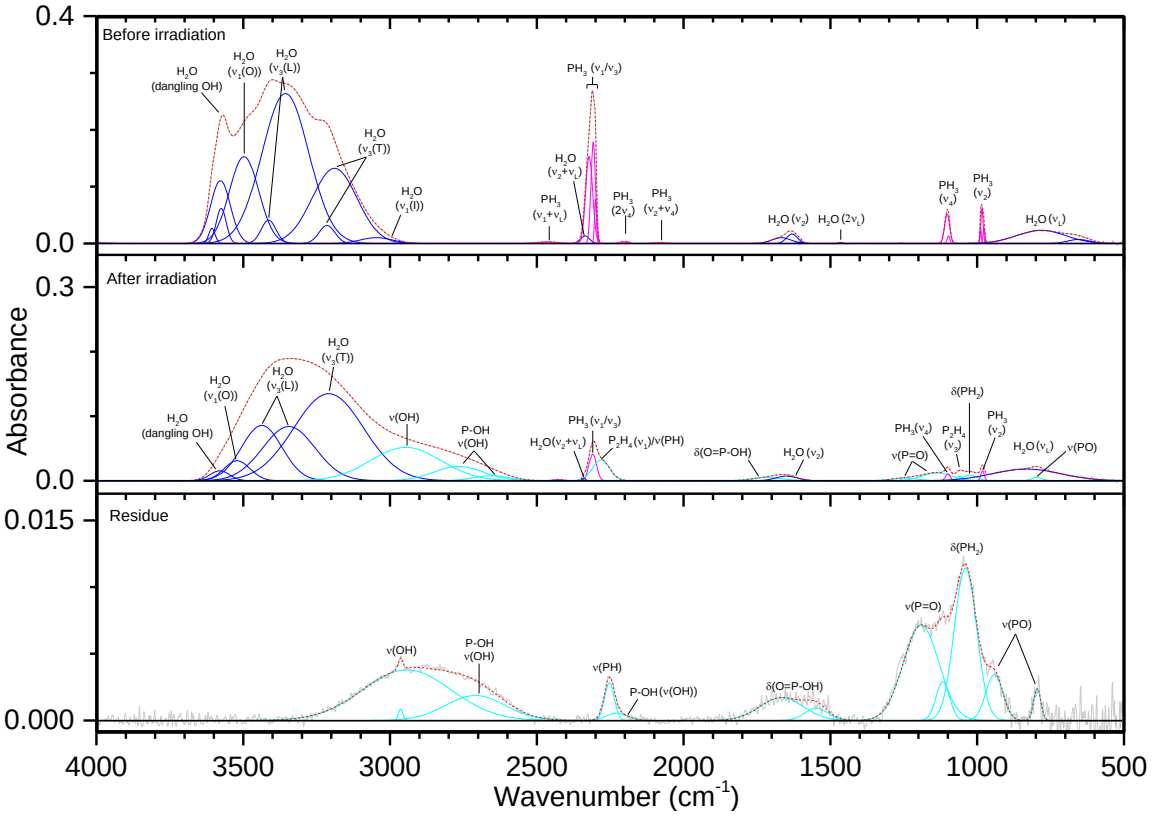

Figure 4.17. Infrared spectra of ice V at 10 K taken before (top) and after (middle) irradiation with 5000 nA irradiation current for one hour. The remaining residue at 300 K after sublimation of the irradiated ice is shown in the bottom spectrum. The original spectrum (gray) is deconvoluted showing peaks assigned to phosphine (pink), water (blue), and new peaks from irradiation (cyan), which sum to create a peak-fitted spectrum (red dashed). The ν_1 and ν_3 vibration for water are labeled as "O" (out-of-phase with neighboring molecules), "I" (in-phase with neighboring molecules), "L" (longitudinal), and "T" (transversal).

Table 4.8. Infrared absorption assignments for ice V at 10 K, the products of irradiation at different doses, and the residue that remained at 300 K after the ice fully sublimed.

Pristine ice, before irradiation (10 K)				
Assignment	Compound	Position (cm^{-1})		Reference
ν_L	H_2O	650–800		(1)
ν_2	PH_3	985		(2)
ν_4	PH_3	1101		(2)
$2\nu_L$	H_2O	1465		(1)
ν_2	H_2O	1600–1670		(1)
$\nu_2 + \nu_4$	PH_3	2075		(2)
$2\nu_4$	PH_3	2190, 2205		(2)
ν_1 / ν_3	PH_3	2300, 2308, 2321		(2)
$\nu_2 + \nu_L$	H_2O	2335		(1)
$\nu_1 + \nu_L$	PH_3	2431, 2471		(1)
ν_1 (in phase)	H_2O	3050		(1)
ν_3 (transversal)	H_2O	3150-3250		(1)
ν_3 (longitudinal)	H_2O	3320-3420		(1)
ν_1 (out of phase)	H_2O	3450-3520		(1)
dangling OH	H_2O	3550-3620		(3)
$2\nu_1$	PH_3	4532		(1)
$\nu_1 + \nu_3$	PH_3	4554		(1)
New peaks after irradiation (10 K)				
Assignment	Compound	Position (cm^{-1})	Irradiation (nA)	Reference
ν(P-O)		790	5000	(4)
$\delta(PH_2)$		1025	5000	(4)
ν_3	P_2H_4	1060	1000, 5000	(5)
ν(P=O)		1140–1250	1000, 5000	(4)
δ(O=P-OH)		1714	5000	(4)
ν_1	P_2H_4	2286	1000, 5000	(4)
ν(PH)			100, 1000, 5000	(5)
P-OH ν(OH)		2650–2780	1000, 5000	(4)
ν(OH)		2900–2950	100, 1000, 5000	(4)
Residue (300 K)				
Assignment	Position (cm^{-1})		Irradiation (nA)	Reference
ν(P-O)	790–1000		1000, 5000	(4)
$\delta(PH_2)$	1040		1000, 5000	(4)
ν(P=O)	1110–1250		1000, 5000	(4)
δ(O=P-OH)	1540–1670		5000	(4)
P-OH ν(OH)	2220		5000	(4)
ν(PH)	2220–2250		1000, 5000	(4)
P-OH ν(OH)	2710		5000	(4)
ν(OH)	2950-3275		1000, 5000	(4)

Note. ν_L defines the lattice mode.
References. (1)[169], (2)[120], (3)[191], (4)[186], (5)[96]

4.3.6 Ice VI ($PH_3/CO_2/CH_4$)

Ice VI (Figures 4.18–4.20, Table 4.9) represents the first of three ice mixtures capable of forming an alkyl phosphonic acid. Previous ices have shown that phosphine with methane is capable of forming the phosphorus-carbon bond, while phosphine with carbon dioxide results in functional groups present in a phosphonic acid. The unirradiated ice contained the expected peaks seen in ices II and IV, and the spectrum after 100 nA irradiated was fairly unremarkable with only small peaks for CO (2137 cm^{-1}), ν(PH) (2330 cm^{-1}), δ(O=P–OH) (1700 cm^{-1}), and ν(POC) (800 cm^{-1}), the latter which also remained in the residue. Increasing the current to 1000 nA provided more detailed results with the only compounds detected being CO, C_2H_6 (ν_{10}, ν_{11}, and ν_{12}), and H_2O (ν_2 and ν_3). The phosphorus-carbon bond was established by bands from ν(PC) (722 cm^{-1}), P–CH_3 ρ(CH_3) (875 cm^{-1}), and P–CH_3 δ_{as}(CH_3) (1419 cm^{-1}), with only the latter remaining in the residue. Absorptions of phosphorus and oxygen include ν(P–O) (955 cm^{-1}), ν(P=O) (1130–1360 cm^{-1}), δ(O=P–OH) (1720 cm^{-1}), and also in the residue P–OH ν(OH) (2790 cm^{-1}). This residue also contains carbon-hydrogen stretching at 2895 cm^{-1} (CH_3 ν_s(CH)) and 2977 cm^{-1} (CH_3 ν_{as}(CH)) and phosphorus-hydrogen vibrations at 1050 cm^{-1} (δ(PH_2)) and 2267 cm^{-1} (ν(PH)). The 5000 nA experiment shows similar and more intense results. Additional peaks for C_2H_6 (ν_5 and ν_6) appeared as did the P–OH ν(OH) stretch at 2130 cm^{-1}, although the broad H_2O ν_L band now masks many low frequency peaks. Notably, this is the first ice mixture in which diphosphine was not identified, which suggests that phosphine is sufficiently diluted by other compounds that it cannot react with itself to form a phosphorus-phosphorus bond. The residue spectrum has two new peaks of note: first is P–CH_3 (δ_s(CH_3)) at 1302 cm^{-1} and the second is P–O–CH_3 (δ(CH_3)) at 1456 cm^{-1}, which along with the ν(P–O–C) stretching seen at 1000 nA shows the potential for this ice mixture to form methyl ester phosphorus oxoacids. The degree to which these bands exist in the irradiated ice is hidden by CH_4 (ν_4) and C_2H_6 (ν_{11}), respectively. Also, the residue spectrum lacks the P–OH ν(OH) stretch at 2130 cm^{-1}, which indicates the residue has a higher concentration of phosphoric acid.

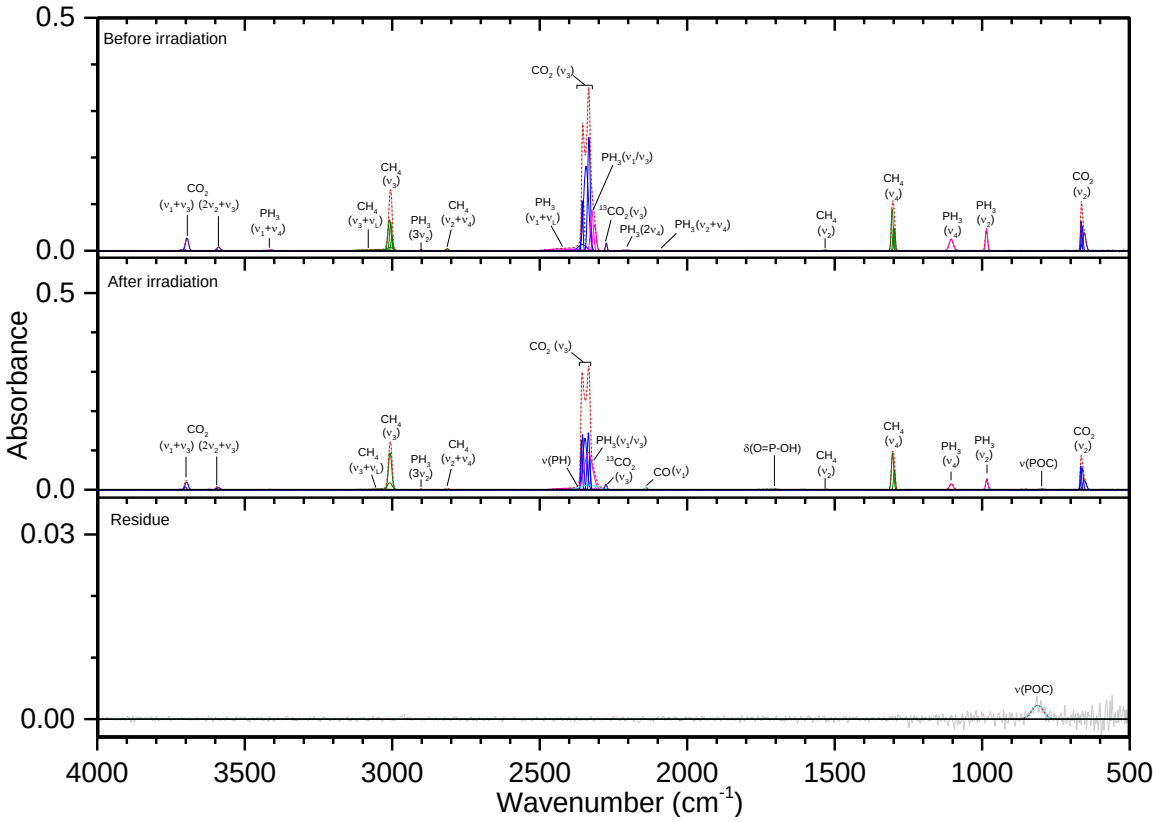

Figure 4.18. Infrared spectra of ice VI at 10 K taken before (top) and after (middle) irradiation with 100 nA irradiation current for one hour. The remaining residue at 300 K after sublimation of the irradiated ice is shown in the bottom spectrum. The original spectrum (gray) is deconvoluted showing peaks assigned to phosphine (pink), carbon dioxide (blue), methane (green), and new peaks from irradiation (cyan), which sum to create a peak-fitted spectrum (red dashed).

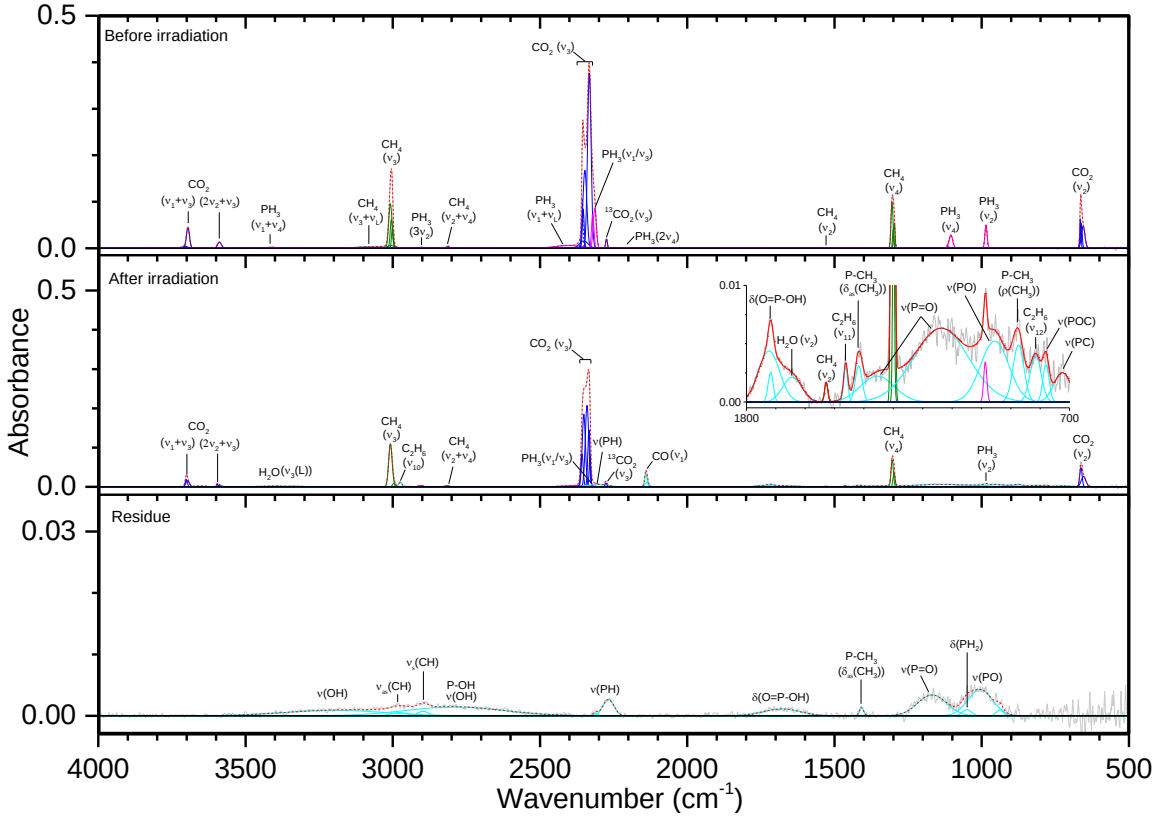

Figure 4.19. Infrared spectra of VI ice at 10 K taken before (top) and after (middle) irradiation with 1000 nA irradiation current for one hour. The remaining residue at 300 K after sublimation of the irradiated ice is shown in the bottom spectrum. The original spectrum (gray) is deconvoluted showing peaks assigned to phosphine (pink), carbon dioxide (blue), methane (green), and new peaks from irradiation (cyan), which sum to create a peak-fitted spectrum (red dashed). The inset expands low-intensity regions of the spectrum. The ν_3 vibration for water is labeled "L" for longitudinal.

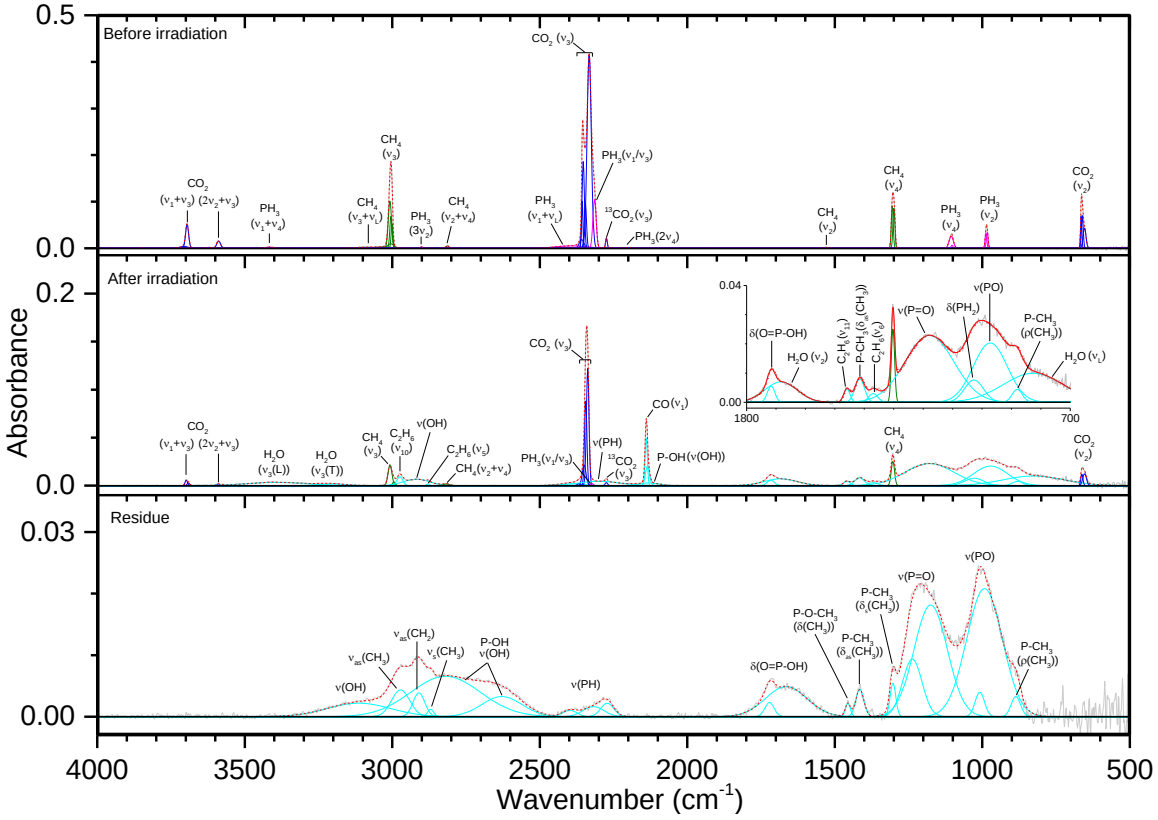

Figure 4.20. Infrared spectra of VI ice at 10 K taken before (top) and after (middle) irradiation with 5000 nA irradiation current for one hour. The remaining residue at 300 K after sublimation of the irradiated ice is shown in the bottom spectrum. The original spectrum (gray) is deconvoluted showing peaks assigned to phosphine (pink), carbon dioxide (blue), methane (green), and new peaks from irradiation (cyan), which sum to create a peak-fitted spectrum (red dashed). The inset expands low-intensity regions of the spectrum. The inset expands low-intensity regions of the spectrum. The ν_3 vibrations for water are labeled "L" for longitudinal and "T" for transversal.

Table 4.9. Infrared absorption assignments for ice VI at 10 K, the products of irradiation at different doses, and the residue that remained at 300 K after the ice fully sublimed.

Pristine ice, before irradiation (10 K)				
Assignment	Compound	Position (cm^{-1})		Reference
ν_2	CO_2	665		(1)
ν_2	PH_3	986		(2)
ν_4	PH_3	1103		(2)
ν_4	CH_4	1300		(3)
ν_2	CH_4	1530		(3)
$\nu_2 + \nu_4$	PH_3	2080		(2)
$2\nu_4$	PH_3	2203		(2)
ν_3	$^{13}CO_2$	2274		(1)
$\nu_1/\ \nu_3$	PH_3	2309, 2316		(2)
ν_3	CO_2	2325–2365		(1)
$\nu_1 + \nu_L$	PH_3	2435		(2)
$\nu_2 + \nu_4$	CH_4	2812		(3)
$3\nu_2$	PH_3	2901		(2)
ν_3	CH_4	3005		(3)
$\nu_3 + \nu_L$	CH_4	3070		(3)
$\nu_1 + \nu_4$	PH_3	3407		(2)
$2\nu_2 + \nu_3$	CO_2	3588		(1)
$\nu_1 + \nu_3$	CO_2	3694		(1)
$\nu_1 + \nu_4$	CH_4	4200		(3)
$\nu_3 + \nu_4$	CH_4	4296		(3)
New peaks after irradiation (10 K)				
Assignment	Compound	Position (cm^{-1})	Irradiation (nA)	Reference
ν(PC)		726	1000	(4)
ν(P-O-C)		790	100, 1000	(4)
ν_{12}	C_2H_6	814	1000	(5)
ν_L	H_2O	830	5000	(6)
P-CH_3 $\rho(CH_3)$		875	1000, 5000	(4)
ν(P-O)		950-975	1000, 5000	(4)
$\delta(PH_2)$		1030	5000	(4)
ν(P=O)		1140–1350	1000, 5000	(4)
ν_6	C_2H_6	1367	5000	(5)
P-CH_3 $\delta_{as}(CH_3)$		1416	1000, 5000	(4)
ν_{11}	C_2H_6	1460	1000, 5000	(5)
ν_2	H_2O	1640–1680	1000, 5000	(6)
δ(O=P-OH)		1710	100, 1000, 5000	(4)
P-OH ν(OH)		2120	5000	(4)
ν_1	CO	2137	100, 1000, 5000	(1)
ν(PH)		2250–2350	100, 1000, 5000	(4)
ν_5	C_2H_6	2877	5000	(5)
ν(OH)		2910	5000	(4)
ν_{10}	C_2H_6	2973	1000, 5000	(5)
ν_3(transversal)	H_2O	3210	5000	(6)
ν_3(longitudinal)	H_2O	3360–3410	1000, 5000	(6)

Table 4.9. **(Continued)** Infrared absorption assignments for ice VI at 10 K, the products of irradiation at different doses, and the residue that remained at 300 K after the ice fully sublimed.

Residue (300 K)			
Assignment	Position (cm^{-1})	Irradiation (nA)	Reference
ν(P-O-C)	810	100	(4)
P-CH_3 $\rho(CH_3)$	880	5000	(4)
ν(P-O)	940–1010	1000, 5000	(4)
$\delta(PH_2)$	1045	1000	(4)
ν(P=O)	1170–1250	1000, 5000	(4)
P-CH_3 $\delta_s(CH_3)$	1300	5000	(4)
P-CH_3 $\delta_{as}(CH_3)$	1410	1000, 5000	(4)
P-O-CH_3 $\delta_{as}(CH_3)$	1456	5000	(4)
δ(O=P-OH)	1640–1720	1000, 5000	(4)
ν(PH)	2250–2400	5000	(4)
P-OH ν(OH)	2630–2820	1000, 5000	(4)
$\nu_s(CH_2)$	2968	5000	(4)
$\nu_s(CH_3)$	2895	1000	(4)
$\nu_{as}(CH_2)$	2910	5000	(4)
$\nu_{as}(CH_3)$	2975	1000, 5000	(4)
ν(OH)	2900–3200	1000, 5000	(4)

Note. ν_L defines the lattice mode.
References. (1)[160], (2)[120], (3)[187], (4)[186], (5)[175], (6)[169]

4.3.7 Ice VII ($PH_3/CO_2/CH_4/C_2H_6/C_3H_8/C_4H_{10}$)

The alkyl phosphonic acids discovered in the Murchison meteorite not only included methylphosphonic acid but also contained C2 to C4 alkyl side chains. Because of this, the C2 to C4 alkanes—ethane (C_2H_6), propane (C_3H_8), and butane (C_4H_{10})—where added to the mixture of ice VI to study its potential to form each of the alkyl phosphonic acids (Figures 4.21–4.23, Table 4.10). These new alkanes are well-represented in the unirradiated ice with fundamentals for ethane (ν_5 (2878 cm^{-1}), ν_6 (1370 cm^{-1}), ν_{10} (2970 cm^{-1}), ν_{11} (1464 cm^{-1}), and ν_{12} (820 cm^{-1})), propane (ν_1/ ν_2 (2956 cm^{-1}), ν_3 (2871 cm^{-1}), ν_4 (1471 cm^{-1}), ν_6 (1383 cm^{-1}), ν_{18} (1370 cm^{-1}, with ethane ν_6), and ν_{25} (748 cm^{-1})), and butane (ν_{12} (2956 cm^{-1}, with propane ν_1/ ν_2), ν_{13} (2922 cm^{-1}), ν_{14} (1460 cm^{-1}), ν_{17} (728 cm^{-1}), ν_{29} (2860 cm^{-1}), and ν_{32} (1377 cm^{-1})) observed along with numerous overtones and combination bands. Despite the complex mixture, the irradiation products were straightforward. Water (ν_L, ν_1, ν_2, and ν_3) and CO were observed as expected, beginning with 100 nA, and like ice VI the residue of the 100 nA experiment was minimal. The phosphorus-oxygen double bond was already seen at 100 nA (ν(P=O) at 1170 cm^{-1} and δ(O=P=OH) at 1700 cm^{-1}), and although diphosphine was not detected again at any dose, ν(PH) appears at 100 nA irradiation.

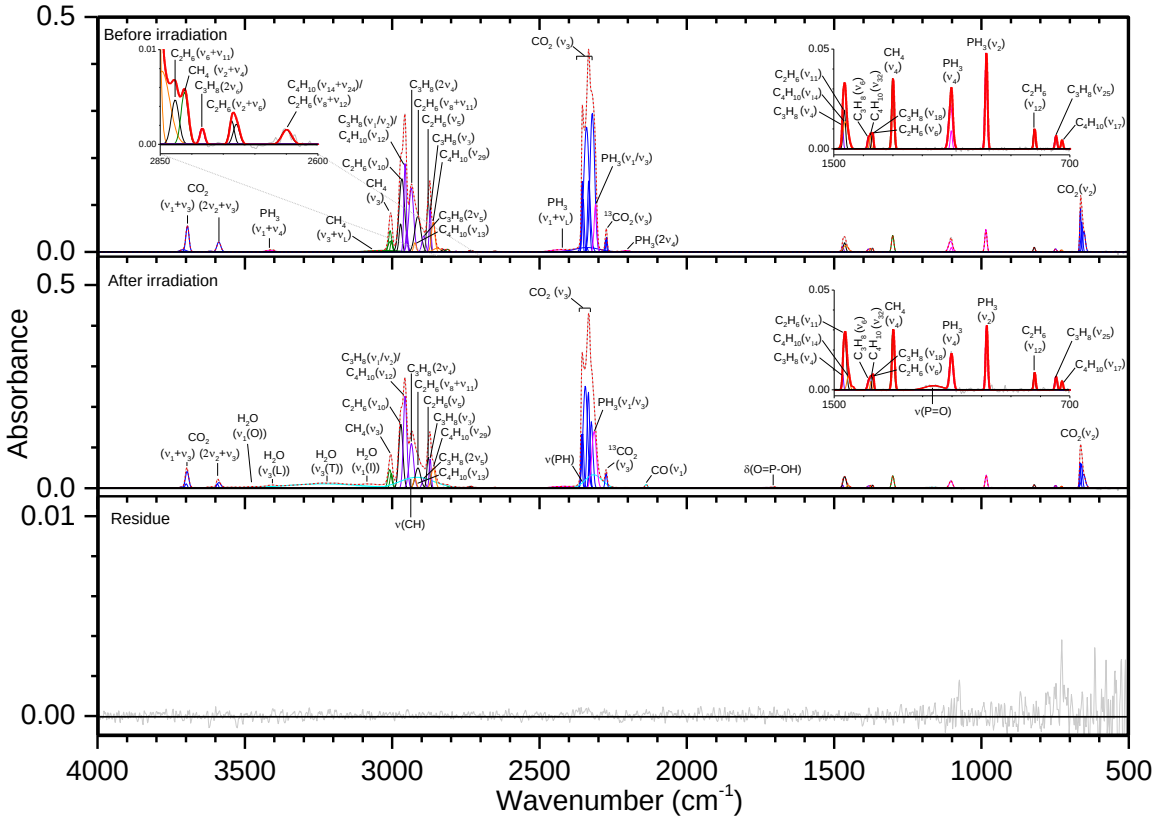

Figure 4.21. Infrared spectra of ice VII at 10 K taken before (top) and after (middle) irradiation with 100 nA irradiation current for one hour. The remaining residue at 300 K after sublimation of the irradiated ice is shown in the bottom spectrum. The original spectrum (gray) is deconvoluted showing peaks assigned to phosphine (pink), carbon dioxide (blue), methane (green), ethane (black), propane (violet), butane (orange), and new peaks from irradiation (cyan), which sum to create a peak-fitted spectrum (red dashed). The insets expand low-intensity regions of the spectrum. The ν_1 and ν_3 vibration for water are labeled as "O" (out-of-phase with neighboring molecules), "I" (in-phase with neighboring molecules), "L" (longitudinal), and "T" (transversal).

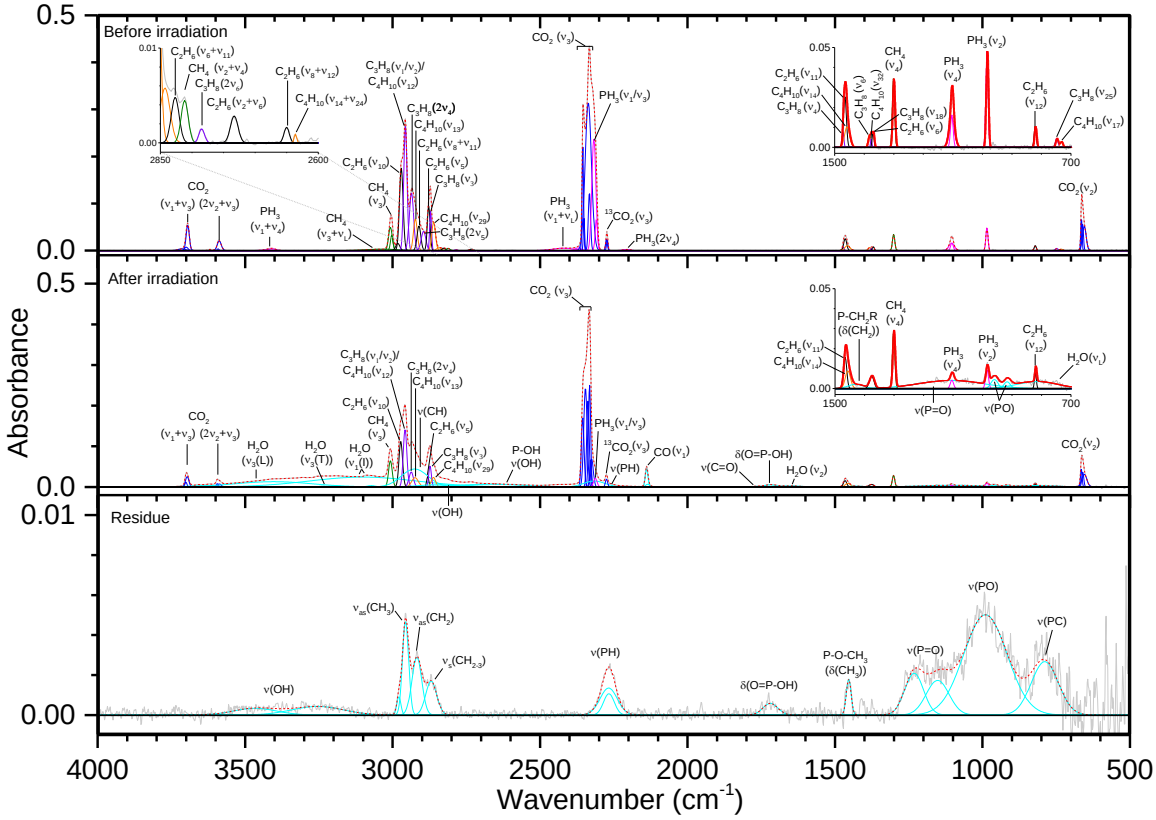

Figure 4.22. Infrared spectra of ice VII at 10 K taken before (top) and after (middle) irradiation with 1000 nA irradiation current for one hour. The remaining residue at 300 K after sublimation of the irradiated ice is shown in the bottom spectrum. The original spectrum (gray) is deconvoluted showing peaks assigned to phosphine (pink), carbon dioxide (blue), methane (green), ethane (black), propane (violet), butane (orange), and new peaks from irradiation (cyan), which sum to create a peak-fitted spectrum (red dashed). The insets expand low-intensity regions of the spectrum. The ν_1 and ν_3 vibration for water are labeled as "I" (in-phase with neighboring molecules), "L" (longitudinal), and "T" (transversal).

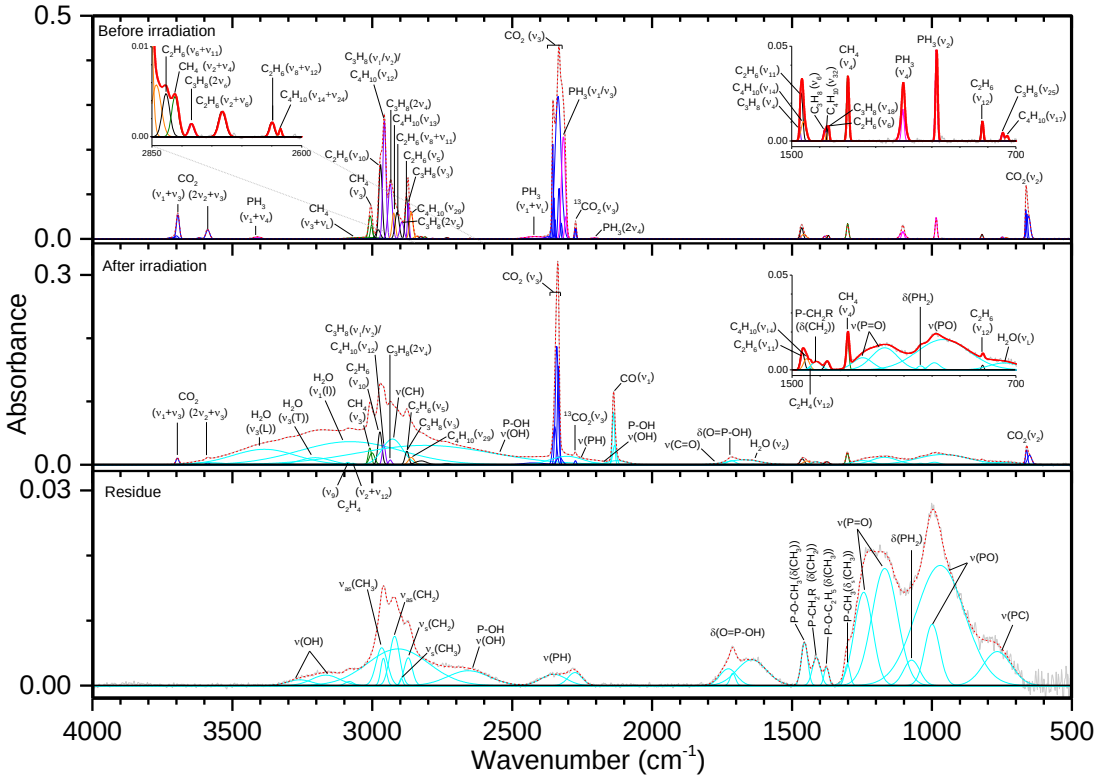

Figure 4.23. Infrared spectra of ice VII at 10 K taken before (top) and after (middle) irradiation with 5000 nA irradiation current for one hour. The remaining residue at 300 K after sublimation of the irradiated ice is shown in the bottom spectrum. The original spectrum (gray) is deconvoluted showing peaks assigned to phosphine (pink), carbon dioxide (blue), methane (green), ethane (black), propane (violet), butane (orange), and new peaks from irradiation (cyan), which sum to create a peak-fitted spectrum (red dashed). The insets expand low-intensity regions of the spectrum. The ν_1 and ν_3 vibration for water are labeled as "I" (in-phase with neighboring molecules), "L" (longitudinal), and "T" (transversal).

Table 4.10. Infrared absorption assignments for ice VII at 10 K, the products of irradiation at different doses, and the residue that remained at 300 K after the ice fully sublimed.

Pristine ice, before irradiation (10 K)			
Assignment	Compound	Position (cm^{-1})	Reference
ν_2	CO_2	663	(1)
ν_{17}	C_4H_{10}	728	(2)
ν_{25}	C_3H_8	748	(2)
ν_{12}	C_2H_6	820	(3)
ν_2	PH_3	986	(4)
ν_4	PH_3	1103	(4)
ν_4	CH_4	1300	(5)
ν_6	C_2H_6	1370	(3)
ν_{18}	C_3H_8		(2)
ν_{32}	C_4H_{10}	1377	(2)
ν_6	C_3H_8	1383	(2)
ν_{14}	C_4H_{10}	1460	(2)
ν_{11}	C_2H_6	1464	(3)
ν_4	C_3H_8	1471	(2)
$2\nu_4$	PH_3	2203	(4)
ν_3	$^{13}CO_2$	2274	(1)
$\nu_1/\ \nu_3$	PH_3	2310, 2317	(4)
ν_3	CO_2	2325–2365	(1)
$\nu_1 + \nu_L$	PH_3	2425	(4)
$\nu_{14} + \nu_{24}$	C_4H_{10}	2636	(2)
$\nu_8 + \nu_{12}$	C_2H_6	2650	(3)
$\nu_2 + \nu_6$	C_2H_6	2733	(3)
$2\nu_6$	C_3H_8	2784	(2)
$\nu_2 + \nu_4$	CH_4	2812	(5)
$\nu_6 + \nu_{11}$	C_2H_6	2826	(3)
ν_{29}	C_4H_{10}	2860	(2)
ν_3	C_3H_8	2871	(2)
ν_5	C_2H_6	2878	(3)
$2\nu_5$	C_3H_8	2892	(2)
$\nu_8 + \nu_{11}$	C_2H_6	2912	(3)
ν_{13}	C_4H_{10}	2922	(2)
$2\nu_4$	C_3H_8	2934	(2)
$\nu_1/\ \nu_2$	C_3H_8	2956	(2)
ν_{12}	C_4H_{10}		
ν_{10}	C_2H_6	2970	(3)
ν_3	CH_4	3005	(5)
$\nu_3 + \nu_L$	CH_4	3030	(5)
$\nu_1 + \nu_4$	PH_3	3407	(4)
$2\nu_2 + \nu_3$	CO_2	3588	(1)
$\nu_1 + \nu_3$	CO_2	3694	(1)
see table 4.3 for complete list		4000–4600	(2)

Table 4.10. **(Continued)** Infrared absorption assignments for ice VII at 10 K, the products of irradiation at different doses, and the residue that remained at 300 K after the ice fully sublimed.

New peaks after irradiation (10 K)				
Assignment	Compound	Position (cm^{-1})	Irradiation (nA)	Reference
ν_L	H_2O	730–815	1000, 5000	(6)
ν(P-O)		915-990	1000, 5000	(7)
$\delta(PH_2)$		1042	5000	(7)
ν(P=O)		1100–1250	100, 1000, 5000	(7)
P-CH_2R $\delta(CH_2)$		1415	1000, 5000	(7)
ν_{12}	C_2H_4	1436	5000	
ν_2	H_2O	1645	1000, 5000	(6)
δ(O=P-OH)		1710	100, 1000, 5000	(7)
ν(C=O)		1770	1000, 5000	(7)
ν_1	CO	2138	100, 1000, 5000	(1)
P-OH ν(OH)		2180	5000	
ν(PH)		2250-2350	100, 1000, 5000	(7)
P-OH ν(OH)		2500-2900	1000, 5000	(7)
ν(OH)		2855	1000	(7)
ν(CH)		2830-3000	100, 1000, 5000	(7)
$\nu_2 + \nu_{12}$	C_2H_4	3066	5000	(8)
ν_1 (in phase)	H_2O	3070	100, 1000, 5000	(6)
ν_9	C_2H_4	3087	5000	(8)
ν_3 (transversal)	H_2O	3230	100, 1000, 5000	(6)
ν_3 (longitudinal)	H_2O	3405	100, 1000, 5000	(6)
ν_1 (out of phase)	H_2O	3470	100	(6)

Residue (300 K)			
Assignment	Position (cm^{-1})	Irradiation (nA)	Reference
ν(PC)	765–795	1000, 5000	(7)
ν(P-O)	950–1010	1000, 5000	(7)
$\delta(PH_2)$	1070	5000	(7)
ν(P=O)	1150–1250	1000, 5000	(7)
P-CH_3 $\delta_s(CH_3)$	1300	5000	(7)
P-O-C_2H_5 $\delta(CH_3)$	1375	5000	(7)
P-CH_2R $\delta(CH_2)$	1410	5000	(7)
P-O-CH_3 $\delta(CH_3)$	1456	1000, 5000	(7)
δ(O=P-OH)	1640–1720	1000, 5000	(7)
ν(PH)	2270-2350	1000, 5000	(7)
P-OH ν(OH)	2650	5000	(7)
$\nu_s(CH_2)$	2968	1000, 5000	(7)
$\nu_s(CH_3)$	2895	1000, 5000	(7)
$\nu_{as}(CH_2)$	2918	1000, 5000	(7)
$\nu_{as}(CH_3)$	2970	1000, 5000	(7)
ν(OH)	2900–3450	1000, 5000	(7)

Note. ν_L defines the lattice mode.

References. (1)[160], (2)[174] and this work, (3)[175], (4)[120], (5)[187], (6)[169], (7)[186], (8)[195]

After 1000 and 5000 nA irradiation the residue spectra showed additional signs of interactions between phosphorus and carbon. The ν(PC) (770 cm^{-1}), P–CH_3 $\delta_s(CH_3)$ (1300 cm^{-1}), and P–CH_2R $\delta(CH_2)$ (1413 cm^{-1}, where R = alkyl group or H) vibrations confirm the phosphorus-carbon bond while P–O–CH_3 $\delta(CH_3)$ (1455 cm^{-1}) and P–O–C_2H_5 $\delta(CH_3)$ (1373 cm^{-1}) not only demonstrate methoxy linkages to phosphorus but also that larger alkanes, such as in this case the ethyl group, can be incorporated in alkoxy functional groups with phosphorus. Also of note in the 5000 nA irradiated ice is the detection of ethylene, first seen in ice II, at 1434 cm^{-1} (ν_{12}), 3068 cm^{-1} ($\nu_2 + \nu_{12}$), and 3086 cm^{-1} (ν_9). Similar to ice VI, ν(P–O) (970 cm^{-1}) and P-OH ν(OH) (2650 cm^{-1}) were detected while only a scarce amount of P-OH ν(OH) (2180 cm^{-1}) was observed—none of which remained in residues. Finally, as might be expected from the alkane mixture, the residues show a complex of carbon-hydrogen stretches from 2850 to 2990 cm^{-1}.

4.3.8 Ice VIII ($PH_3/H_2O/CH_4/C_2H_6/C_3H_8/C_4H_{10}$)

The final ice mixture replaces carbon dioxide in ice VII with water as the oxygen source (Figures 4.24–4.26, Table 4.11). The unirradiated ice is as reported in previous ice mixtures, and although the phosphorus-hydrogen stretching area is no longer overlapped with bands from carbon dioxide, it is immediately evident that small, low frequency bands are partially obscured by H_2O (ν_L) and that oxygen-hydrogen stretching will complicate the nearby overlapping carbon-hydrogen stretching region. Diphosphine, which was absent in the CO_2 ices VI and VII, returns at all irradiation doses, and this marks the only difference seen in the 100 nA ice other than a small amount of P–OH ν(OH) near 2740 cm^{-1}. The residue at 100 nA is more notable than in ices VI and VII and includes phosphorus-hydrogen, phosphorus-oxygen (perhaps as P–O–C), oxygen-hydrogen, and carbon-hydrogen bonds. At 1000 nA, the irradiated ice contains two additional peaks demonstrating that the phosphorus-carbon bond is formed: CH_3PH_2 $\omega(CH_3)$ at 985 cm^{-1} and P-CH_2R (where R is an alkyl group or H) $\delta(CH_2)$ at 1414 cm^{-1}. The residue includes oxygen-hydrogen stretches, including that for P–OH at 2640 cm^{-1}, as well as ν(PO), ν(P=O), and δ(O=P-OH). Besides P–H and C–H stretches, the residue also shows P-CH_2R $\delta(CH_2)$ and P-O-CH_3 $\delta(CH_3)$ at 1452 cm^{-1}. A small peak at 2140 cm^{-1}, which is normally associated with the broad P–OH ν(OH) vibration, appears in the 5000 nA irradiated ice and likely belongs to

CO, and this peak does not remain in the residue, leading again to the conclusion that phosphoric acid contributes mostly to the ν(OH) stretching. The P–CH_3 $\rho(CH_3)$ vibration (880 cm^{-1}) and ν(PH) stretch of CH_3PH_2 (2308 cm^{-1}) can also been seen in this ice, as well as the ν_{12} (1438 cm^{-1}), $\nu_2 + \nu_{12}$ (3066 cm^{-1}), and ν_9 (3084 cm^{-1}) bands of ethylene. The residue at 5000 nA shows P–O–C_2H_5 (1374 cm^{-1}), which was not seen at lower doses but again shows the capability for multi-carbon alkyl groups to create compounds with phosphorus and oxygen.

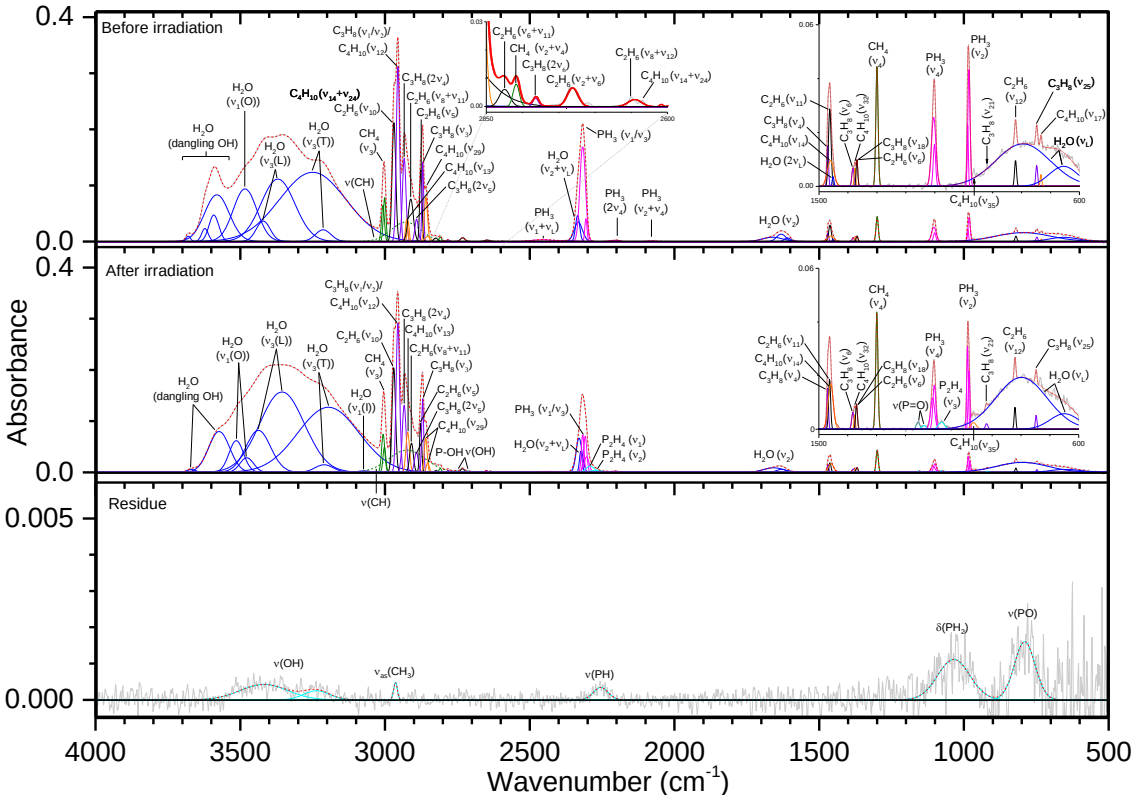

Figure 4.24. Infrared spectra of ice VIII at 10 K taken before (top) and after (middle) irradiation with 100 nA irradiation current for one hour. The remaining residue at 300 K after sublimation of the irradiated ice is shown in the bottom spectrum. The original spectrum (gray) is deconvoluted showing peaks assigned to phosphine (pink), water (blue), methane (green), ethane (black), propane (violet), butane (orange), and new peaks from irradiation (cyan), which sum to create a peak-fitted spectrum (red dashed). The insets expand low-intensity regions of the spectrum. The ν_1 and ν_3 vibration for water are labeled as "O" (out-of-phase with neighboring molecules), "I" (in-phase with neighboring molecules), "L" (longitudinal), and "T" (transversal).

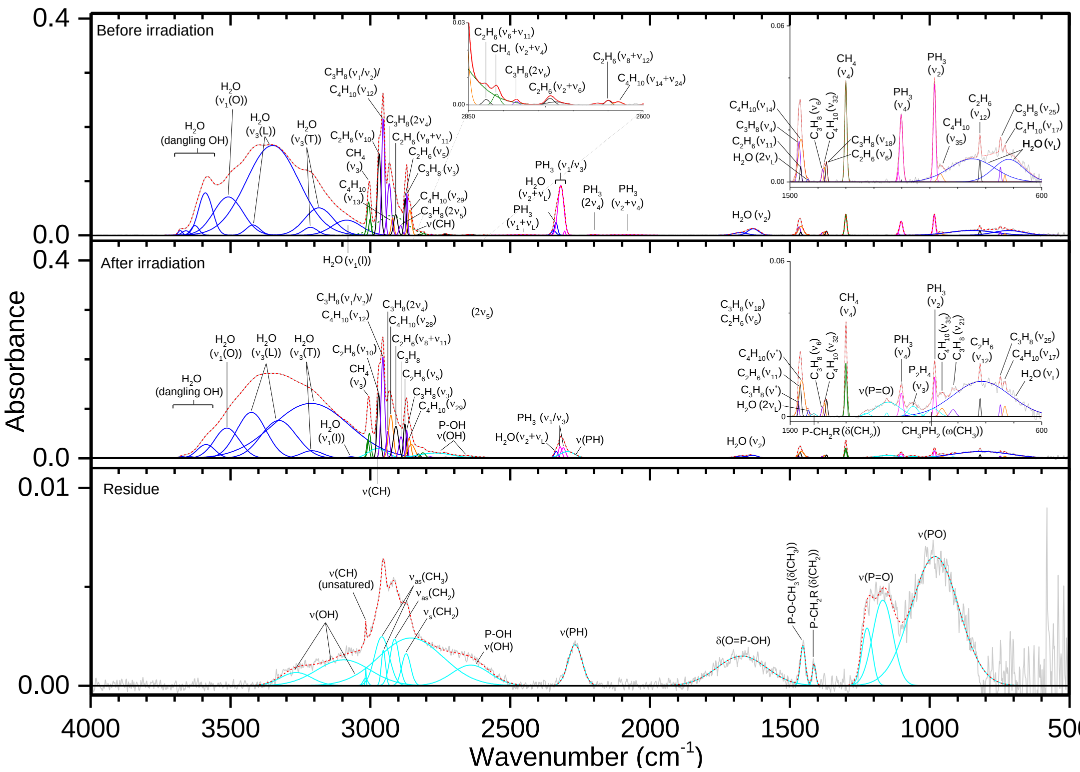

Figure 4.25. Infrared spectra ice VIII at 10 K taken before (top) and after (middle) irradiation with 1000 nA irradiation current for one hour. The remaining residue at 300 K after sublimation of the irradiated ice is shown in the bottom spectrum. The original spectrum (gray) is deconvoluted showing peaks assigned to phosphine (pink), water (blue), methane (green), ethane (black), propane (violet), butane (orange), and new peaks from irradiation (cyan), which sum to create a peak-fitted spectrum (red dashed). The insets expand low-intensity regions of the spectrum. The v_1 and v_3 vibration for water are labeled as "O" (out-of-phase with neighboring molecules), "I" (in-phase with neighboring molecules), "L" (longitudinal), and "T" (transversal).

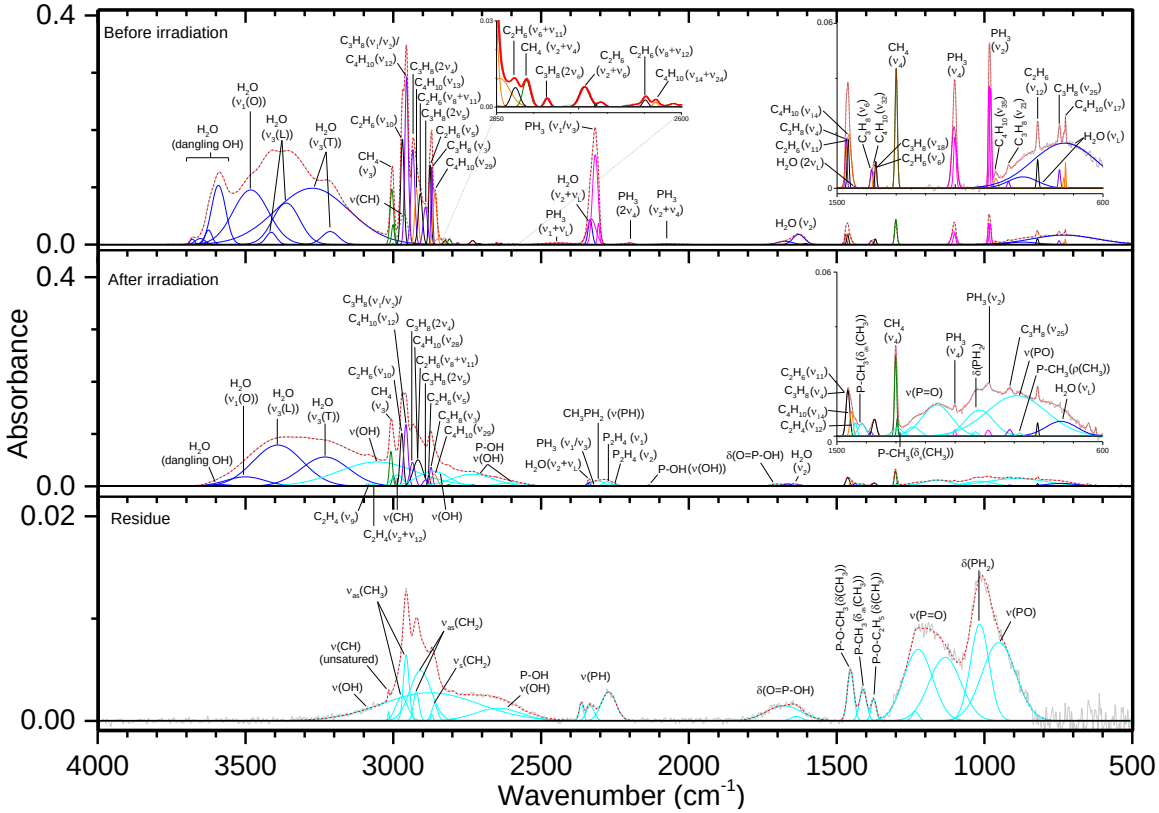

Figure 4.26. Infrared spectra of ice VIII at 10 K taken before (top) and after (middle) irradiation with 5000 nA irradiation current for one hour. The remaining residue at 300 K after sublimation of the irradiated ice is shown in the bottom spectrum. The original spectrum (gray) is deconvoluted showing peaks assigned to phosphine (pink), water (blue), methane (green), ethane (black), propane (violet), butane (orange), and new peaks from irradiation (cyan), which sum to create a peak-fitted spectrum (red dashed). The insets expand low-intensity regions of the spectrum. The ν_1 and ν_3 vibration for water are labeled as "O" (out-of-phase with neighboring molecules), "L" (longitudinal), and "T" (transversal).

Table 4.11. Infrared absorption assignments for ice VIII at 10 K, the products of irradiation at different doses, and the residue that remained at 300 K after the ice fully sublimed.

Pristine ice, before irradiation (10 K)			
Assignment	Compound	Position (cm^{-1})	Reference
ν_L	H_2O	600–900	(1)
ν_{17}	C_4H_{10}	733	(2)
ν_{25}	C_3H_8	747	(2)
ν_{12}	C_2H_6	819	(3)
ν_{21}	C_3H_8	918	(2)
ν_{35}	C_4H_{10}	962	(2)
ν_2	PH_3	986	(4)
ν_4	PH_3	1103	(4)
ν_4	CH_4	1300	(5)
ν_6	C_2H_6	1368	(3)
ν_{18}	C_3H_8		(2)
ν_{32}	C_4H_{10}	1375	(2)
ν_6	C_3H_8	1383	(2)
$2\nu_L$	H_2O	1451	(1)
ν_{14}	C_4H_{10}	1461	(2)
ν_{11}	C_2H_6	1463	(3)
ν_4	C_3H_8	1470	(2)
ν_2	H_2O	1630–1670	(1)
$\nu_2 + \nu_4$	PH_3	2078	(4)
$2\nu_4$	PH_3	2203	(4)
$\nu_1/\ \nu_3$	PH_3	2310, 2318	(4)
$\nu_2 + \nu_L$	H_2O	2333	(1)
$\nu_1 + \nu_L$	PH_3	2450	(4)
$\nu_{14} + \nu_{24}$	C_4H_{10}	2636	(2)
$\nu_8 + \nu_{12}$	C_2H_6	2650	(3)
$\nu_2 + \nu_6$	C_2H_6	2733	(3)
$2\nu_6$	C_3H_8	2784	(2)
$\nu_2 + \nu_4$	CH_4	2812	(5)
$\nu_6 + \nu_{11}$	C_2H_6	2825	(3)
ν(CH)	various	2850–3000	(6)
ν_{29}	C_4H_{10}	2860	(2)
ν_3	C_3H_8	2871	(2)
ν_5	C_2H_6	2878	(3)
$2\nu_5$	C_3H_8	2892	(2)
$\nu_8 + \nu_{11}$	C_2H_6	2912	(3)
ν_{13}	C_4H_{10}	2922	(2)
$2\nu_4$	C_3H_8	2934	(2)
$\nu_1/\ \nu_2$	C_3H_8	2955	(2)
ν_{12}	C_4H_{10}		
ν_{10}	C_2H_6	2969	(2)
ν_3	CH_4	3004	(5)
ν_1 (in phase)	H_2O	3085	(1)
ν_3 (transversal)	H_2O	3280–3250	(1)
ν_3 (longitudinal)	H_2O	3350–3420	(1)
ν_1 (out of phase)	H_2O	3480–3510	(1)
dangling OH	H_2O	3550–3700	(7)
see table 4.3 for complete list		4000–4600	(2)

Table 4.11. **(Continued)** Infrared absorption assignments for ice VIII at 10 K, the products of irradiation at different doses, and the residue that remained at 300 K after the ice fully sublimed.

New peaks after irradiation (10 K)				
Assignment	Compound	Position (cm^{-1})	Irradiation (nA)	Reference
P-CH_3 $\rho(CH_3)$		880	5000	(6)
ν(P-O)		886	5000	(6)
$\omega(CH_3)$	CH_3PH_2	984	1000	(8)
		1025	5000	(6)
ν_3	P_2H_4	1073	100, 1000	(9)
ν(P=O)		1130–1230	100, 1000, 5000	(6)
P-CH_2R $\delta(CH_2)$		1415	1000, 5000	(6)
ν_{12}	C_2H_4	1438		
δ(O=P-OH)		1704	5000	(6)
ν_1	CO	2140	5000	(8)
ν_2	P_2H_4	2260	100, 5000	(10)
ν_1	P_2H_4	2290	100, 5000	(10)
ν(PH)	CH_3PH_2	2303	5000	(9)
ν(PH)		2250–2350	1000	(6)
P-OH ν(OH)		2600–2800	100, 1000, 5000	(6)
ν(OH)		2850–3100	5000	(6)
ν(CH)		2850–3000	1000, 5000	(6)
$\nu_2 + \nu_{12}$	C_2H_4	3066	5000	(11)
ν_9	C_2H_4	3087	5000	(11)
Residue (300 K)				
Assignment		Position (cm^{-1})	Irradiation (nA)	Reference
ν(P-O)		790–980	100, 1000, 5000	(6)
$\delta(PH_2)$		1015–1030	100, 5000	(6)
ν(P=O)		1100–1250	1000, 5000	(6)
P-O-C_2H_5 $\delta(CH_3)$		1375	5000	(6)
P-CH_3 $\delta_{as}(CH_3)$		1410	1000, 5000	(6)
P-O-CH_3 $\delta_{as}(CH_3)$		1456	1000, 5000	(6)
δ(O=P-OH)		1650–1670	1000, 5000	(6)
ν(PH)		2250-2350	100, 1000, 5000	(6)
P-OH ν(OH)		2650	1000, 5000	(6)
$\nu_s(CH_2)$		2968	1000, 5000	(6)
$\nu_{as}(CH_2)$		2911	1000, 5000	(6)
$\nu_{as}(CH_3)$		2965	100, 1000, 5000	(6)
ν(CH) (unsaturated)		3015	1000, 5000	(6)
ν(OH)		2800–3450	100, 1000, 5000	(6)

Note. ν_L defines the lattice mode.

References. (1)[169] , (2) this work, see Table 3, (3)[175], (4)[120], (5)[187] (6)[186] (7)[191] , (8)[160], (9)[188], (10)[96], (11)[195]

4.3.9 Summary

Irradiated phosphine ices regularly form, with a few exceptions, diphosphine and residues with ν(PH) and $\delta(PH_2)$. The reaction of phosphine with methane and higher order alkanes can be seen with the low frequency phosphorus-carbon bond, the P-CH_3 $\rho(CH_3)$ vibration, the P-CH_2R $\delta(CH_2)$ band where R can be an alkyl group or hydrogen (if hydrogen, this band would be labeled P–CH_3 $\delta_{as}(CH_3)$ and occurs at the same frequency), the P–CH_3 $\delta_s(CH_3)$, and the vibrations of the compound methylphosphine (CH_3PH_2). The addition of oxygen to mixture via carbon dioxide, water, or dioxygen often results in residues with ν(P–O), ν(P=O), δ(O=P–OH), and two bands for P–OH ν(OH). When an alkane is present, P–O–CH_3 $\delta(CH_3)$ and P–O–C_2H_5 $\delta(CH_3)$ were also observed. This systematic study of the irradiation of interstellar ice analogues, from simple to complex, shows that not only can phosphine readily react to interstellar ices, but it is in fact capable of producing all of the necessary bonding to produce alkyl phosphonic acids. In conclusion, all functional groups necessary to form methylphosphonic acid are present (Figure 4.27), although whether they are present simultaneously in the same molecule cannot be ascertained using only infrared spectroscopy. However, more sensitive experiments are being designed to extract the true identity of these residues and the confirmation of alkyl phosphonic acids in phosphine-containing interstellar ices.

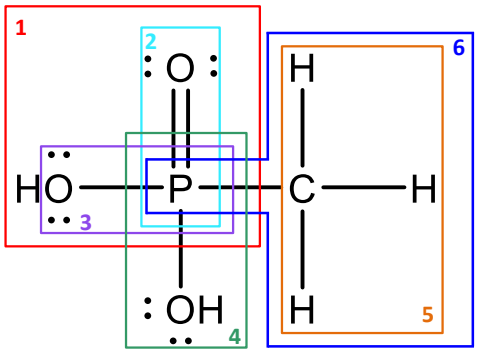

Figure 4.27. Structure of methylphosphonic acid indicating the functional groups observed in the irradiated ice samples and their residues. These functional group include (1) δ(O=P–OH) (1540–1720 cm^{-1}), (2) ν(P=O) (1100–1300 cm^{-1}), (3) ν(P–O) (800–1050 cm^{-1}), (4) P–OH ν(OH) (2100–2220 cm^{-1}, 2600–2800 cm^{-1}), (5) CH_3 ν(CH) (2850–3000 cm^{-1}), (6) P–CH_3 $\delta(CH_3)$ (1300, 1410 cm^{-1}) and P–CH_3 $\rho(CH_3)$ (875 cm^{-1}). Thus, the infrared spectra indicate that each functional group of methylphosphonic acid is present.

4.4 Astrophysical Implications

We would like to discuss these findings within the context of the *Origins of Life* theme. Phosphorus in its highest oxidation state P(V), as present in the phosphate moiety (PO_4^{3-}), plays a central role in contemporary terrestrial biochemistry.[143] The transmission of genetic information through self-replication (DNA/RNA), biochemical energy transfer processes (ATP/ ADP), cell bilayer materials (phospholipids), and structural building blocks like hydroxyapatite in teeth and bones all exploit the phosphate group (PO_4^{3-}). To this extent, our results provide evidence that the irradiation of our phosphine-rich ice mixtures can lead to P–O–C bond linkages, which are found in each non-structural biomolecules mentioned above. However, Gulick highlighted key problems with phosphates in prebiotic chemistry citing a poor water solubility of their metal salts and slow chemical reactivity in the absence of activating chemicals.[5] Therefore, the insolubility of phosphates in water presents a significant uncertainty in the chemistry for the origin of life. Gulick suggested that schreibersite ($(Fe,Ni)_3P$), a minor constituent of iron-nickel meteorites[196] that has been classified as one of the first phosphorus-bearing chemicals to condense from the early Solar Nebula[197], could have been oxidized in the presence of water to form phosphorus-bearing acids like hypophosphorous acid (H_3PO_2). The resulting acids would be more soluble than phosphate minerals and hence biologically available for early life forms under anoxic reducing atmospheric conditions. Therefore, despite the dominance of the phosphate moiety in contemporary biochemistry, there is growing evidence that nature exploited lower oxidations states of phosphorus such as P(III) as found in alkyl phosphonic acids during the early development of life on Earth. In fact, while most life on earth use P(V), P(III) compounds have been isolated from microorganisms while other microorganisms have developed the means to cleave the C–P bonds of organophosphonic acids to incorporate the phosphorus into phosphate moieties.[198] It is unknown if the first biomolecules maintained this P(III) oxidation state or contained fully oxidized phosphorus P(V) similar to current biomolecules. Alkyl phosphonic acids are stable under the high ultraviolet flux on early Earth, so they could have been utilized as prebiotic molecules with a reduced form of phosphorus. These biomolecules may have persisted until atmospheric oxygen began increasing thus favoring the oxidation state of P(V). But abiotic pathways to reduced forms of P(III) in alkyl phosphonic acids have been difficult to ascertain.[143]

Bryant and Kee[16] also suggested that schreibersite might act as a precursor to phosphorus-bearing acids in the early Earth ocean, and the authors hydrolyzed schreibersite in sulfuric acid and detected two phosphorus-bearing acids: phosphonic acid (H_3PO_3) and phosphoric acid (H_3PO_4). Schreibersite was also exposed in water ices at 77 K to ultraviolet light from a low pressure mercury arc tube in a photochemical reactor emitting mainly 254 nm and 185 nm. This experiment yielded phosphorus in more reduced oxidation states: phosphinic acid (H_3PO_2), phosphonic acid (H_3PO_3), as well as phosphoric acid (H_3PO_4). Finally, a dilute solution of sodium hypophosphite (NaH_2PO_2) was photolyzed in liquid water and ethanol. These results suggest that reduced organophosphorus compounds may have been formed upon photolysis in the presence of liquid water on early Earth. Bryant et al.[199] also proposed that phosphorus-bearing acids can be formed via electrochemistry of schreibersite. Here, schreibersite was pressed into a wafer and utilized as an anode in a galvanic cell containing an aqueous sodium chloride (NaCl) solution. The corrosion led to phosphonic acid (H_3PO_3) and phosphoric acid (H_3PO_4) at levels of a few percent. This study indicates that low-oxidation state phosphorus compounds can be formed from schreibersite in liquid water if an electric potential is present. Further, Bryant, et al. [21] exposed samples of the Sikhote-Alin iron meteorite with hydrochloric acid to simulate geothermal environments such as volcanically heated water. The results indicate that the iron-nickel matrix that surrounded schreibersite was preferentially corroded and allowed the phosphorus-bearing mineral to be converted to phosphites ($H_2PO_3^-$).

Pasek et al.[4,17,25,200] proposed an aqueous corrosion of meteoritic phosphide minerals followed by a radical-mediated phosphorus-carbon coupling as a source for organic phosphorus-bearing acids. In detail, iron phosphide (Fe_3P), which was used as an analogue for meteoric schreibersite, was corroded under oxygen gas in an aqueous buffer solution with additions of acetic acid (CH_3COOH) and ethanol (C_2H_5OH). The authors detected three classes of organic phosphorus bearing acids: i) organic acetyl phosphorus compounds [$(HO)_2OPCH_2COOH$], ii) methylenephosphorus compounds [$(HO)_2OPCH_2OH$; $(HO)_2OPCH_2PO(OH)_2$], and iii) phosphonoformates [$(HO)_2OPCOOH$] with molecules in brackets carrying C–P bonds. The high concentration of phosphite (HPO_3^{2-}) in Archean carbonates (3.5×10^9 years) may be explained by meteoric delivery of schreibersite.

Glycerol ($C_3H_8O_3$), a common organic molecule in Murchison, was found to react with schreibersite in water to yield glycerol-phosphate—a component of phospholipids.[201]

Further, de Graaf et al. investigated in laboratory experiments to what extent alkyl phosphonic acids can be synthesized from phosphonic acid (H_3PO_3) and organic compounds, thus benefitting from the fact that in both the phosphonic acid and the prospective alkyl phosphonic acids, phosphorus is in the same oxidation state, P(III), and hence no oxidation-reduction reaction needs to be considered.[8] Aqueous solutions of phosphonic acid (H_3PO_3) and formaldehyde (H_2CO) were photolyzed with a mercury vapor arc tube (254 nm; 185 nm) resulting in a 19 % conversion to hydroxymethyl phosphonic acid ($HOCH_2H_2PO_3$) and minor amounts of hydroxylethyl phosphonic acid ($HOCH_2CH_2H_2PO_3$). Reactions with methanol/ethanol also produced hydroxylmethyl phosphonic acid ($HOCH_2H_2PO_3$) and hydroxyethyl phosphonic acid ($HOCH_2CH_2H_2PO_3$). Exploiting acetone (CH_3COCH_3) resulted in a 17 % conversion to methylphosphonic acid (CH_3-H_2PO_3). In follow-up studies, the authors prepared dilute aqueous solutions of acetylene (C_2H_2) in the presence of sodium phosphite (Na_2HPO_3) and subjected this mixture to ultraviolet light.[9] This yielded vinylphosphonic acid ($C_2H_3H_2PO_3$). The authors speculated that if hydration of schreibersite yields phosphonic acid (H_3PO_3), and the latter is dissolved in water, organic phosphonic acids might have been formed with the help of ultraviolet radiation on early Earth.

Finally, Gorell et al. proposed an extraterrestrial route to the formation of alkyl phosphonic acids involving methinophosphide (HCP) and water.[15] Electronic structure calculations depicted that the multistep hydrolysis and oxidation processes can lead to methylphosphonic acid via hydrogen elimination pathways in an overall strongly exoergic reaction by about 400 kJ mol^{-1}. However, the authors highlighted the existence of significant entrance barriers (classical activation energies) of at least 40 kJ mol^{-1}. The involvement of these barriers prohibit the formation of methylphosphonic acid in liquid water thus effectively prohibiting this reaction without the presence of 'external' energy sources such as high energy photons or cosmic ray particles. Therefore, the author proposed the formation of alkyl phosphonic acids on interstellar grains exposed to high energy ionizing radiation.

To summarize, previous laboratory experiments focused essentially on the hydrolysis, photolysis, and galvanic corrosion of phosphides and an ultraviolet radiation mediated synthesis of organic phosphonic acids. These studies suggested that phosphonic acid together with organic phosphonic acids can be formed in the presence of liquid water. However, these simulation experiments failed to expose abiotic pathways leading to the formation of alkyl phosphonic acids on ices of interstellar grains at astrophysically relevant temperatures of 10 K, where liquid water does not exist. On the other hand, the present laboratory investigations provided compelling evidence on the formation of *key functional groups* present in alkyl phosphonic acids (Figure 4.27) by exploiting simple precursor molecules as present on interstellar grains in cold molecular clouds, which upon interaction with ionizing radiation form these *key functional groups* from the 'bottom up' incorporating phosphorus via phosphine (PH_3). These experiments revealed that oxygen sources readily react with phosphine to form both P–O and P=O bonds in all ice mixtures, while carbon-phosphorus bond coupling is more subtle and must rely on less intense peaks related to the effect of the phosphorus atom on the vibrations of, e.g., a methyl group. Future experiments shall focus on the identification of individual alkyl phosphonic acids on line and *in situ* utilizing sensitive mass spectrometry techniques, as well as ex situ analysis of the residual compounds that do not readily enter the gas phase. Further, the structural isomers—molecules with the same chemical formula but different connectivity of atoms—of the subliming species should be detected. This requires the exploitation of photoionization (PI) of the neutral subliming molecules via tunable vacuum ultraviolet (VUV) based on discrete ionization potentials and detecting the ions via a reflectron time-of-flight mass spectrometer (PI-ReTOF-MS). This method has been utilized previously in space simulation experiments[51,69,202,203] in the analysis of complex organic molecules (COMs) formed via interaction of ionizing radiation with low temperature interstellar analogue ices.

CHAPTER 5

PHOSPHORUS OXOACIDS FROM ICES OF PHOSPHINE, WATER, AND CARBON DIOXIDE

This chapter is based on the paper: A. M. Turner, A. Bergantini, M. J. Abplanalp, C. Zhu, S. Gobi, B.-J. Sun, K.-H. Chao, A. H. H. Chang, C. Meinert, R. I. Kaiser, "An Interstellar Synthesis of Phosphorus Oxoacids", Nature Communications*, submitted.*

Phosphorus signifies an essential element in molecular biology, yet given the limited solubility of phosphates on early Earth, alternative sources like meteoritic phosphides have been proposed to incorporate phosphorus into biomolecules under prebiotic terrestrial conditions. Here, we report on a previously overlooked source of prebiotic phosphorus from interstellar phosphine (PH_3) that produces key phosphorus oxoacids—phosphoric acid (H_3PO_4), phosphonic acid (H_3PO_3), and pyrophosphoric acid ($H_4P_2O_7$)—in interstellar analogue ices exposed to ionizing radiation at temperatures as low as 5 K. Since the processed material of molecular clouds eventually enters circumstellar disks and is partially incorporated into planetesimals like proto Earth, an understanding of the facile synthesis of oxoacids is essential to untangle the origin of water-soluble prebiotic phosphorus compounds and how they might have been incorporated into organisms not only on Earth, but potentially in our universe as well.

5.1 Introduction

The ubiquitous presence of the phosphorus (V) oxidation state in contemporary biomolecules found in phospholipids, ADP/ATP, and RNA/DNA represents a hitherto unresolved "phosphorus problem" as the deprived solubility of phosphate minerals such as apatite ($Ca_5(PO_4)_3(F,Cl,OH)$) limits bioavailable phosphorus for the first organisms on early Earth.[5,204] Efficient prebiotic mechanisms toward the formation of high-energy phosphates such as polyphosphates containing the repeating $(HPO_3)_n$ moiety and phosphate esters have remained elusive as well.[205] Phosphate diesters constitute the backbone of RNA and DNA—key molecules carrying the genetic information for the reproduction of all known living organisms—as well as the hydrophilic head of phospholipids, while monoesters of pyrophosphate ($P_2O_7^{4-}$) and triphosphate ($P_3O_{10}^{5-}$) play a critical role in cellular energy transfer as adenosine diphosphate (ADP) and triphosphate (ATP), respectively. To overcome this "phosphorus problem", soluble molecules carrying the phosphorus (III) oxidation state have been proposed with the alkyl phosphonic acids ($RP(O)(OH)_2$; R = methyl, ethyl, propyl, butyl) detected in the Murchison meteorite serving as soluble compounds of extraterrestrial origin.[7] Prebiotic phosphorus chemistry could have been initiated by phosphorus (III) or the first organisms might have oxidized bioavailable phosphorus (III) to (V). Yet, the underlying synthetic routes to these phosphorus-bearing biomolecules along with their precursors are still in their infancy. This fundamental knowledge on the origins of the phosphorus chemistry is critical to unravel how the phosphorus biochemistry and life itself might have emerged on early Earth.

In this *Communication*, we reveal a facile and versatile pathway toward the abiotic synthesis of phosphorus (III) and (V) oxoacids in phosphine (PH_3)-doped interstellar analogue ices of water (H_2O) and carbon dioxide (CO_2) upon interaction with ionizing radiation in the form of energetic electrons, which simulate secondary electrons generated in the track of galactic cosmic rays penetrating interstellar ices at temperatures as low as 5 K.[160] Phosphine has been observed in extraterrestrial environments such as in the circumstellar envelope of the carbon star IRC+10216[36,37] and also within our Solar System in the atmospheres of Jupiter and Saturn.[38,39] More recently, phosphine was attributed as the source of the phosphorus signal in comet 67P/Churyumov-Gerasimenko.[41] Surface

reactions involving schreibersite, an iron-nickel phosphide that along with phosphates compose the bulk of phosphorus in meteorites,[142] in aqueous solutions resembling conditions of early Earth have been suggested, but do not fully reproduce the synthesis of alkyl phosphonic acids,[6,8,17,20,143] although the phosphorylation of adenosine has been demonstrated.[24] Thus, the formation of biorelevant, phosphorus-bearing molecules on interstellar grains—silicate-based nanoparticles coated with a few hundred nanometers of water (H_2O), methanol (CH_3OH), carbon monoxide (CO), carbon dioxide (CO_2), methane (CH_4), formaldehyde (H_2CO), and ammonia (NH_3) ices[53]—in molecular clouds may represent a key process leading to a facile synthesis of phosphorus compounds of potential biological significance. Considering that molecular clouds constitute the nurseries of stars and planetary systems—including our own—the identification of phosphonic acid (H_3PO_3), phosphoric acid (H_3PO_4), and pyrophosphoric acid ($H_4P_2O_7$) in our ices suggests that these phosphorus oxoacids might have been at least partially incorporated into our Solar System from interstellar matter via circumstellar disks. Further, these compounds could have been delivered to early Earth by comets or meteorites such as Murchison as sources of phosphorus for biomolecules with both single phosphate groups (RNA/DNA, phospholipids) and phosphate chains (ADP/ATP). Our study defines the molecular complexity of phosphorus-bearing molecules synthesized in interstellar ices and unveils where in the universe discrete, phosphorus-containing molecular precursors relevant to the origins of life might have been synthesized and even incorporated into contemporary biomolecules.

5.2 Results & Discussion

In infrared spectra of irradiated, phosphine bearing ices, critical *functional groups* of phosphorus oxoacids were identified at 5 K and also in the residues that remained after annealing the exposed ices to 300 K (Tables 5.S1 and 5.S2).[206] These bands include stretching modes of phosphorus–oxygen single and double bonds [ν(P–O) (800–950 cm^{-1}), ν(P=O) (1140–1300 cm^{-1})], the deformation mode of the OPOH functional group [δ(O=P–OH) (1550–1710 cm^{-1})], and the P–OH moiety [ν(O–H) (2170 cm^{-1}, 2700 cm^{-1}). These findings suggest that *functional groups* linked to oxoacids of phosphorus are the results of

an exposure of the ices at temperatures as low as 5 K. The relative intensities of the δ(O=P–OH) and ν(P–OH) bands indicate that the acids remaining in the residues are phosphorous/phosphonic (H_3PO_3; $P(OH)_3/HPO(OH)_2$) and phosphoric acid (H_3PO_4).[186] To confirm these assignments, we exploited ^{18}O labeled ice constituents as well ($H_2{}^{18}O$, $C^{18}O_2$). These experiments match the isotopic shifts determined for redshifted ν(P–O) and ν(P=O) modes by approximately 30 cm^{-1}.[207-209] Therefore, the infrared analysis reveals the existence of *functional groups* [P–O, P=O, O=P–OH] present in phosphorus oxoacids; however, considering that the fundamentals of the oxoacids, such as of phosphonic and phosphoric acid, fall in the same range, *infrared spectroscopy does not allow an identification of individual oxoacids*.

To probe discrete molecular species, we exploited PI-ReTOF-MS during the annealing of the irradiated ices. The subliming products were photoionized in separate experiments with 10.86 eV and 9.93 eV photons to elucidate the nature of the oxoacid isomer(s) synthesized. Accounting for the adiabatic ionization energies (IE) of the oxoacids (H_3PO_x; x=1–4) (*Supplementary Information,* Table 5.1), the energy of the 10.86 eV photon is above the I.E. of each oxoacid; therefore, if formed *and* if subliming, all oxoacids can be ionized at this photoionization energy. The use of PI-ReTOF-MS necessitated isotopically labeled $H_2{}^{18}O$ and $C^{18}O_2$ reagents to distinguish between products formed at identical masses. Here, phosphinic acid and hypophosphorous acid (H_3PO_2) along with diphosphine (P_2H_4) have a molecular weight of 66 amu; on the other hand, ^{18}O substituted phosphinic acid and hypophosphorous acid ($H_3P^{18}O_2$) shifts the mass by 4 amu to 70 amu, thus discriminating these acids from diphosphine. At the photoionization energy of 10.86 eV, the temperature programmed desorption (TPD) profiles indicate that $H_3P^{18}O$ and $H_3P^{18}O_2$ oxoacids, which are associated with signal at m/z = 52 and 70, respectively, are formed in both PH_3–$H_2{}^{18}O$ and PH_3–$C^{18}O_2$ systems (Figure 5.1). As the irradiation current increases from 100 nA via 1,000 nA to 5,000 nA, the ion counts at m/z = 52 ($H_3P^{18}O^+$) decrease by a factor of about eight in the PH_3–$H_2{}^{18}O$ system; simultaneously, the signal at m/z = 70 ($H_3P^{18}O_2^+$), which is absent at 100 nA, arises.

Table 5.1. Calculated adiabatic ionization energies and relative energies of various phosphorus oxoacids.

Structure	Formula	Name	Ionization Energy (eV)[a]	Relative Energy (eV)
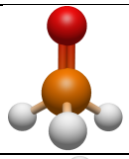	H_3PO	Phosphine oxide	10.71	0.00
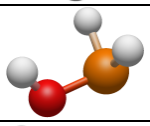	*cis*-H_2POH	*cis*-Hydroxyphosphine	9.22	0.03
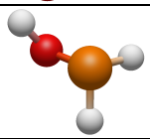	*trans*-H_2POH	*trans*-Hydroxyphosphine	9.23	0.03
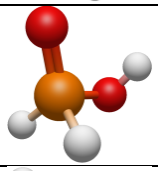	$H_2P(O)OH$	Phosphinic acid	10.71	0.00
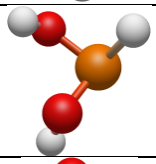	$HP(OH)_2$	Hypophosphorous acid	8.94	0.37
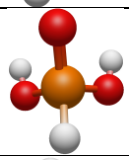	$HPO(OH)_2$	Phosphonic acid	10.83	0.00
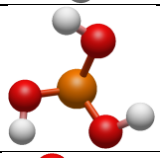	$P(OH)_3$	Phosphorous acid	8.68	0.52
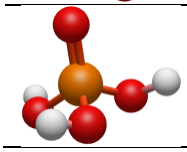	$PO(OH)_3$	Phosphoric acid[b]	10.69	0.00

[a] ionization potential by CCSD(T)/CBS with B3LYP/ccpVTZ zero-point energy correction

[b] in the ice, the C_3 symmetric phosphoric acid exists as two enantiomers:

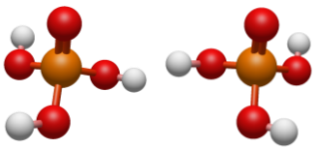

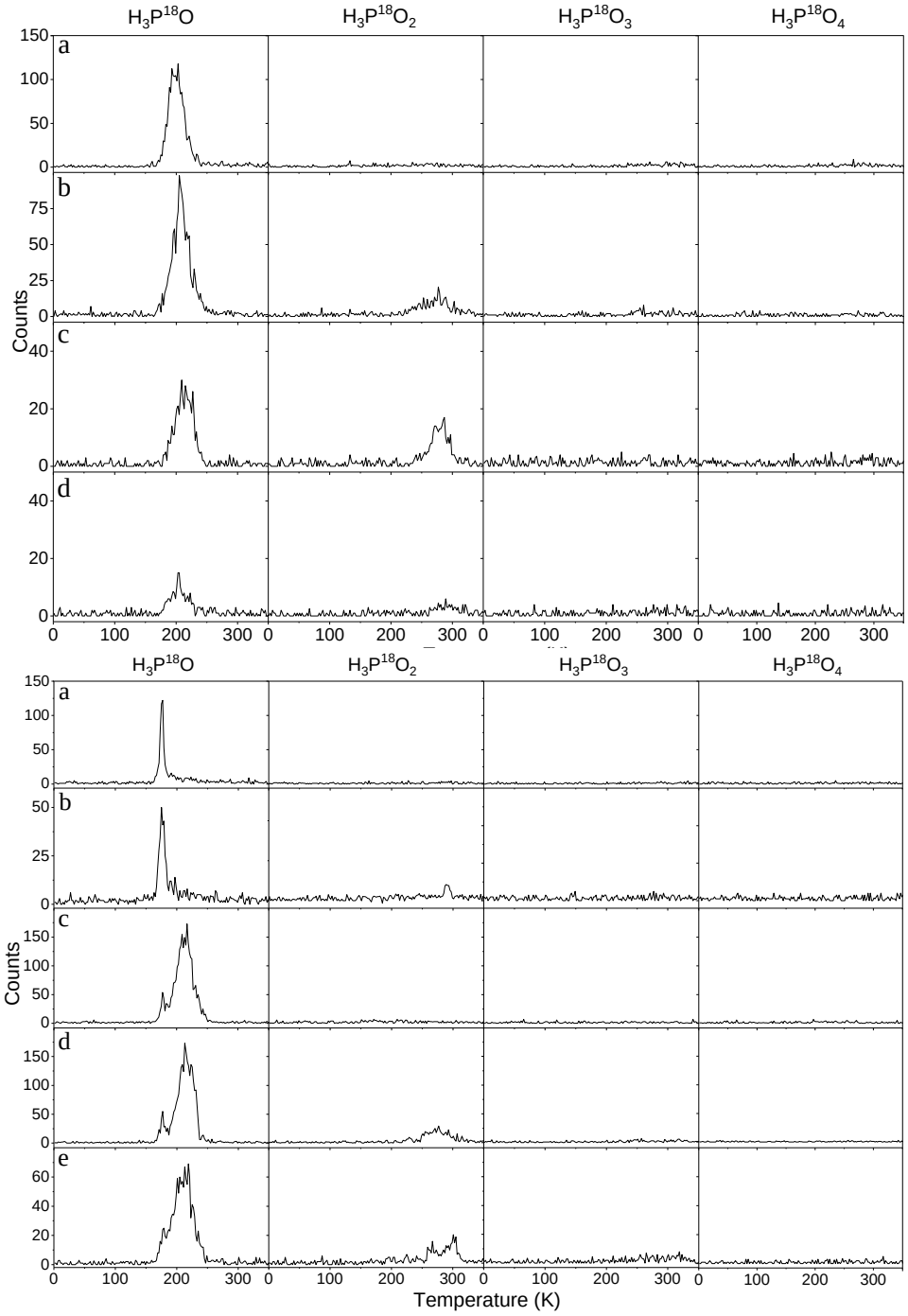

Figure 5.1. PI-ReTOF-MS data showing the temperature programmed desorption (TPD) profiles for m/z = 52 ($H_3P^{18}O$), m/z = 70 ($H_3P^{18}O_2$), m/z = 88 ($H_3P^{18}O_3$), and m/z = 106 ($H_3P^{18}O_4$). Top: Ices of phosphine (PH_3)–carbon dioxide ($C^{18}O_2$) at irradiation currents of a) 100 nA, 9.93 eV photoionization energy, b) 100 nA, 10.86 eV photoionization energy, c) 1,000 nA, 10.86 eV photoionization energy, and d) 5,000 nA, 10.86 eV photoionization energy. Bottom: Ices of phosphine (PH_3)–water ($H_2{}^{18}O$) at irradiations currents of a) 100 nA, 9.93 eV photoionization energy, b) 100 nA, 10.86 eV photoionization energy, c) 1,000 nA, 9.93 eV photoionization energy, d) 1,000 nA, 10.86 eV photoionization energy , and e) 5,000 nA, 10.86 eV photoionization energy.

This finding may suggest that phosphinic/hypophosphorous acid ($H_3P^{18}O_2$) is formed from phosphine oxide ($H_3P^{18}O$) likely via reaction with atomic oxygen. The analysis of the PH_3–$C^{18}O_2$ systems supports this conclusion: phosphinic/ hypophosphorous acid ($H_3P^{18}O_2$; 70 amu) is only detected at higher irradiation currents of 1,000 nA and 5,000 nA. On the other hand, PI-ReTOF-MS did not succeed in the detection of phosphorous/phosphonic acid ($H_3P^{18}O_3$; $P(^{18}OH)_3$/$HP^{18}O(^{18}OH)_2$) or phosphoric acid ($H_3P^{18}O_4$) due to their low volatility that limits their sublimation from the substrate. Considering the signals detected at m/z = 52 ($H_3P^{18}O^+$) and 70 ($H_3P^{18}O_2^+$) in the 10.86 eV experiment, we were interested in untangling the nature of the structural isomer(s) formed. Since the ionization energies of the $H_3P^{18}O$–$H_2P^{18}OH$ and $H_2P(^{18}O)(^{18}OH)$–$HP(^{18}OH)_2$ isomer pairs are separated by more than 1.5 eV (Table 5.1), a second set of experiments was carried out at a photoionization energy of 9.93 eV. This energy is *below* the ionization energies of the phosphine oxide ($H_3P^{18}O$) and phosphinic acid ($H_2P(^{18}O)^{18}OH$) isomers, but *above* the ionization energies of the hydroxyphosphine ($H_2P^{18}OH$) and hypophosphorous acid ($HP(^{18}OH)_2$) isomers. A close inspection of the TPD profiles of m/z = 52 (Figure 5.1) reveals that the TPD profiles are nearly identical at 10.86 eV and 9.93 eV suggesting that *at least* the thermodynamically less stable hydroxyphosphine isomer ($H_2P^{18}OH$) is formed; since the absolute photoionization cross sections of both isomers are unknown, the presence of phosphine oxide cannot be proven. However, Withnall & Andrews explored in previous matrix isolation experiments the chemistry of phosphine–molecular oxygen samples[207,208] and revealed the formation of hydroxyphosphine (H_2POH) with smaller contributions of the phosphine oxide isomer (H_3PO). Finally, we compare the TPD profiles of m/z = 70 recorded at 10.86 eV and 9.93 eV. Upon lowering the photon energy to 9.93 eV, the signal at m/z = 70 vanishes; therefore, we can conclude that only the thermodynamically preferred phosphinic acid isomer ($H_2P(^{18}O)^{18}OH$) is formed, but no hypophosphorous acid ($HP(^{18}OH)_2$). The higher molecular weight of phosphinic acid (70 amu) compared to hydroxyphosphine (52 amu) is also associated with an increase of the sublimation temperature in the range of 260 K to 300 K in contrast to 160 K to 240 K.

Having established the synthesis of at least two of the simplest phosphorus oxoacids (hydroxyphosphine and phosphinic acid) and possibly phosphine oxide by exploiting PI-

ReTOF-MS, we searched for higher molecular weight oxoacids in the residues of the annealed samples utilizing TOF-SIMS (*Supplementary Information*). TOF-SIMS facilitates the sputtering of the solid residues and detects the ions in both positive and negative ion detection modes (Figure 5.2). Since the sputtering might also fragment the phosphorus oxoacids, these fragmentation patterns have to be determined. This assists in an identification of well-defined mass-to-charge ratios unique to each of the oxoacids and also allows a quantification of the oxoacids formed. The results of the calibration of phosphonic acid (H_3PO_3), phosphoric acid (H_3PO_4), and pyrophosphoric acid ($H_4P_2O_7$) are compiled in Tables 5.S3 and 5.S4. The negative ion spectra are very sensitive to probe the oxoacids via their deprotonated parent molecules. Here, pyrophosphoric ($H_4P_2{}^{18}O_7$) and phosphonic acid ($H_3P^{18}O_3$) can be identified in all residues via their unique signals of $HP_2{}^{18}O_6{}^-$/ $H_3P_2{}^{18}O_7{}^-$ and $H_2P^{18}O_3{}^-$, respectively. While pyrophosphoric acid has a fragment of small intensity for $H_2P^{18}O_4{}^-$, the low quantity of $H_4P_2{}^{18}O_7$ in our residues contributes a minor amount to the moderately intense $H_2P^{18}O_4{}^-$ signal, which can be attributed to phosphoric acid ($H_3P^{18}O_4$). As a general trend, the yield of each of these oxoacids increases with the irradiation dose; significantly enhanced yields are seen in carbon dioxide bearing ices compared to water-rich ices especially at higher doses. Although phosphinic acid is subliming at T = 260 K to 300 K as verified in the PI-ReTOF-MS analysis, the SIMS analysis revealed a strong peak for $H_2P^{18}O_2{}^-$; this ion is not observed as a fragment from any calibration compound, but can be formally linked to phosphinic acid ($H_3P^{18}O_2$). A close look at the PI-ReTOF-MS data (Figure 5.1) indicates that the intensity of m/z = 70 ($H_3P^{18}O_2{}^+$) does not completely lead to zero at 300 K; therefore, a fraction of phosphinic acid ($H_3P^{18}O_2$) is likely to reside in the solid residue. Although holding a lower sensitivity, the positive ion spectra confirm the assignments derived from the negative ion mode. Pyrophosphoric acid ($H_4P_2{}^{18}O_7$), phosphonic acid ($H_3P^{18}O_3$), and phosphoric acid ($H_3P^{18}O_4$) could be detected via their protonated counterparts, i.e. $H_5P_2{}^{18}O_7{}^+$, $H_4P^{18}O_3{}^+$, and $H_4P^{18}O_4{}^+$.

Finally, the phosphorus oxoacids in the residues were also extracted, derivatized as trimethylsilyl (TMS) esters ($-OSi(CH_3)_3$), and analyzed via two-dimensional gas chromatography-time-of-flight mass spectrometry *(Supplementary Information*). A ReTOF-MS was exploited to record the retention times along with the mass spectra (Table 5.S5).

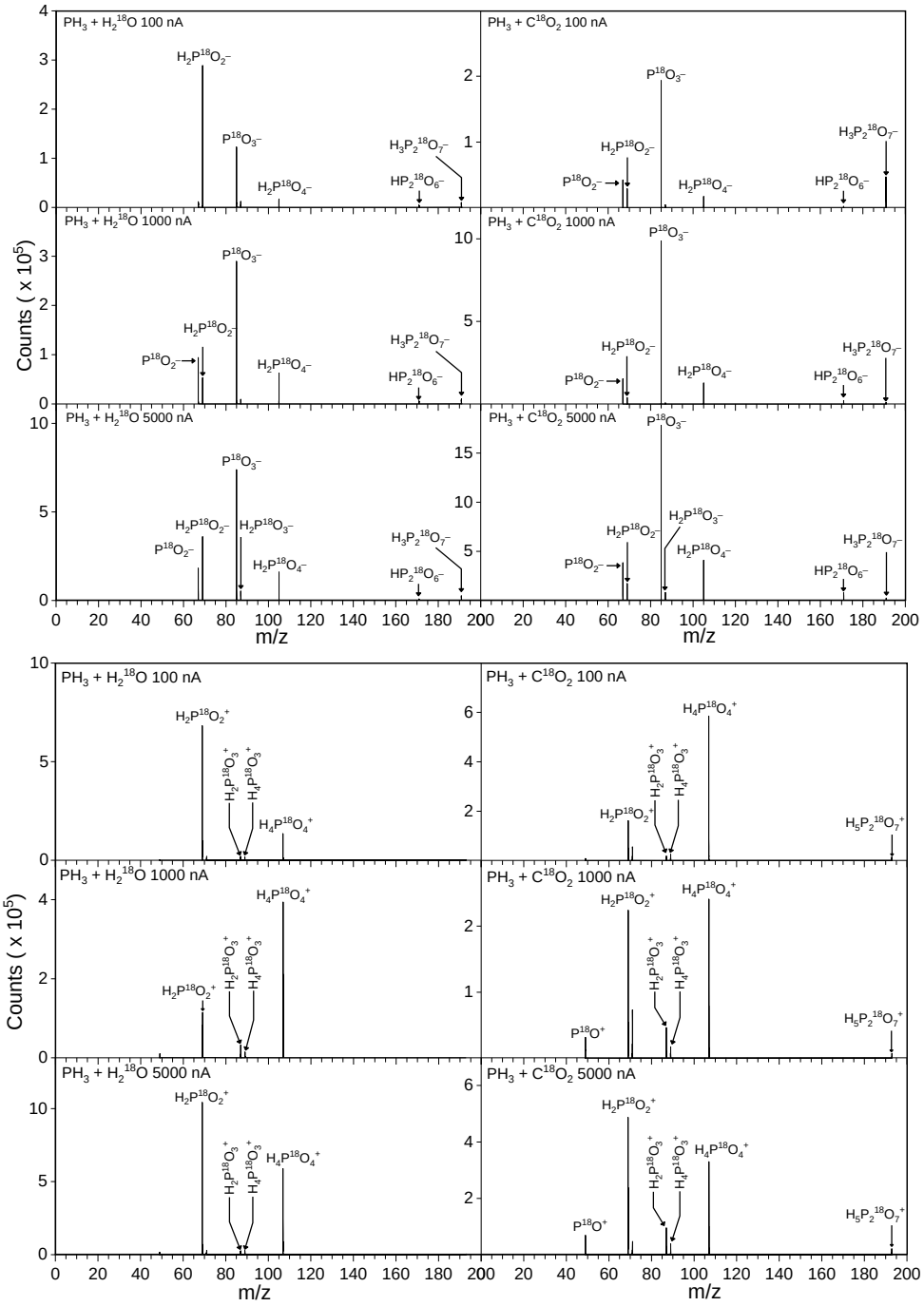

Figure 5.2. SIMS data recorded in the negative (top) and positive ion mode (bottom) correlated with the formation of ^{18}O-substituted oxoacids formed in irradiated phosphine (PH_3) - water ($H_2{}^{18}O$) and phosphine (PH_3) - carbon dioxide ($C^{18}O_2$) (left) ices.

This protocol led to the detection of three phosphorus oxoacids (Figure 5.3): phosphoric acid ($H_3P^{18}O_4$), phosphonic acid ($HP^{18}O(^{18}OH)_2$), and phosphinic acid ($H_2P^{18}O(^{18}OH)$). Phosphoric acid could be identified via the molecular ion of the tris(trimethylsilyl)ester ($^{18}OP(^{18}OSi(CH_3)_3)_3$) at m/z ($M^+$) = 322 and its fragment originating from the loss of a methyl group at m/z (M^+-15) = 307.[209] Phosphonic acid was detected via the molecular ion of the derivatized phosphorous acid tautomer in the form of its tris(trimethylsilyl)ester ($P(^{18}OSi(CH_3)_3)_3$) at m/z (M^+) = 304 and its fragment of the methyl group loss at m/z (M^+-15) = 304.[210] Finally, phosphinic acid could be sampled via its hypophosphorous acid tautomer as its bis(trimethylsilyl)ester ($HP(^{18}OSi\ (CH_3)_3)_2$) at m/z (M^+) = 214 and also by its fragment of the methyl group elimination at m/z (M^+-15) = 199. Derivatization as trimethylsilyl (TMS) esters shifts the tautomeric phosphonic-phosphorous and phosphinic-hypophosphorous acid equilibrium to the phosphorous and hypophosphorous acid esters (Figure 5.S1).[211] Calibration experiments suggest that the TMS derivative of pyrophosphoric acid as detected in small quantities via SIMS was found to be thermally unstable and decomposed on the GC columns.[212] Consequently, with the exception of pyrophosphoric acid, the GC×GC-TOF-MS analysis correlates exceptionally well with the SIMS data that detected key phosphorus oxoacids in the residues of the irradiated phosphine doped interstellar analogue ices.

To conclude, by exposing phosphine (PH_3) doped interstellar analogue ices to ionization radiation and exploiting an array of complementary *in situ* and *ex situ* analytical tools, the present study offers compelling evidence on a facile formation of distinct oxoacids of phosphorus: phosphinic acid (H_3PO_2) P(I), phosphonic acid (H_3PO_3) P(III), phosphoric acid (H_3PO_4) P(V), and pyrophosphoric acid ($H_4P_2O_7$) P(V). The formation of those oxoacids can be initiated via a radical-radical recombination between the hydroxy (OH) and phosphino (PH_2) radicals (reaction 5.1) or through insertion of electronically excited atomic oxygen, released by unimolecular decomposition of water and carbon dioxide, with phosphine forming phosphinic acid (PH_2OH) (reaction 5.2). Once phosphinic acid (PH_2OH) forms, successive addition and insertion of electronically excited oxygen atom to the phosphorus atom produce phosphonic acid (H_3PO_3) and phosphoric acid (H_3PO_4) (reaction 5.3).

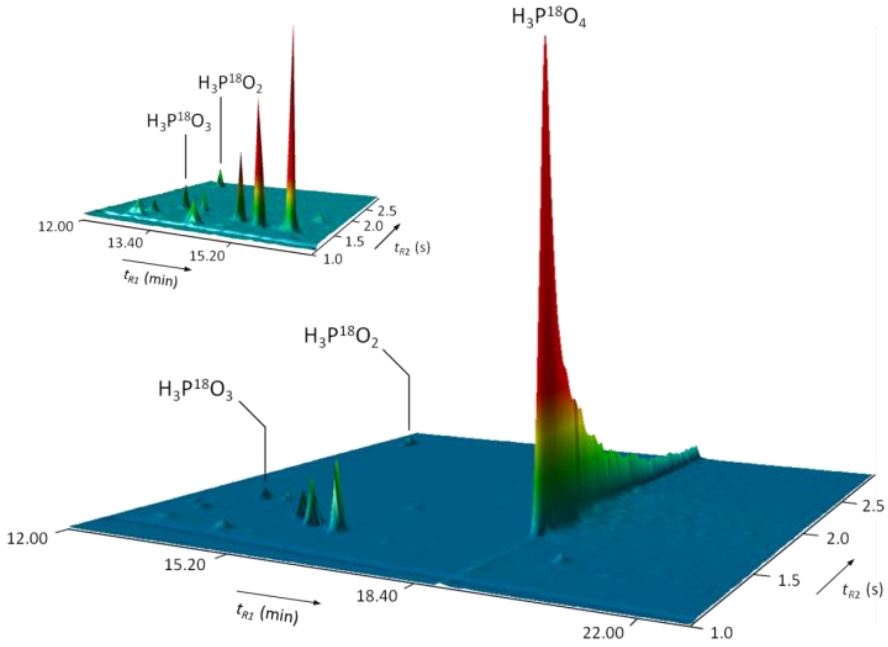

Figure 5.3. Multidimensional gas chromatogram showing ^{18}O labelled phosphorus oxoacids extracted from the residues. The atomic mass units 214 (×100) and 304 (×150) were selected for this multidimensional chromatographic representation. Partial GC×GC chromatogram of the separation of the two minor phosphorus oxoacids is shown top left.

Overall, up to four oxygen atoms are needed to oxidize phosphine to phosphoric acid; this requires up to about 30 eV. Hence, thermal reactions cannot form oxoacids at 5 K, but cosmic ray triggered non-equilibrium chemistry is required to supply the required oxygen atoms (and possibly the hydroxyl radicals) for the oxidation process. Whereas on Earth, phosphine is classified as highly toxic and only slightly soluble in water, the present work reveals interstellar phosphine as a critical precursor in the synthesis of highly water soluble phosphorus oxoacids prevalent in contemporary biochemistry. Phosphoric acid (H_3PO_4) in particular presents a soluble source of phosphorus in the phosphorus (V) oxidation state as found in RNA/DNA and ADP/ATP. The identification of pyrophosphoric acid ($H_4P_2O_7$)—a formal condensation product of phosphoric acid—is significant since our investigations expose that polyphosphates such as diphosphates found in ADP can be formed in interstellar ices upon interaction with ionizing radiation mimicking typical life times of molecular clouds of a few 10^6 years. The unsuccessful detection of triphosphoric acid ($H_5P_3O_{10}$)—a precursor to the phosphorus backbone of ATP—could indicate that the phosphorus chemistry in interstellar ices ceases with the synthesis of pyrophosphoric acid

over the lifetime of a molecular cloud, thus defining the molecular complexity of phosphorus-bearing oxoacids formed in extraterrestrial environments.

$$PH_2 + OH \rightarrow PH_2OH \quad (5.1)$$

$$PH_3 + O \rightarrow PH_2OH \quad (5.2)$$

$$PH_2OH \xrightarrow{+O} H_2P(O)OH \xrightarrow{+O} H_2P(O)(OH)_2 \xrightarrow{+O} H_3PO_4 \quad (5.3)$$

Finally, the synthesis of phosphonic acid (H_3PO_3) could support an alternative route to phosphorus (III) as found in alkyl phosphonic acids in the Murchison meteorite. As these alkyl phosphonic acids are of continued interest to the *Origins of Life* community, the incorporation of methane (CH_4) or more complex hydrocarbons to interstellar ices has the potential to yield a complex mixture of alkyl phosphonic acids as detected in Murchison and, with derivatives of phosphoric acid, biologically relevant phosphate esters. The phosphorus oxoacids detected in our experiments might have also been formed within the ices of comets such as 67P/Churyumov-Gerasimenko, whose phosphorus source is believed to derive from phosphine.[41] Since comets contain at least partially the remnants of the material of the protoplanetary disk that formed our solar system, these compounds might be traced back to the interstellar medium wherever sufficient phosphine in interstellar ices is available. Upon delivery to Earth by meteorites or comets, these phosphorus oxoacids would have been available for Earth's prebiotic phosphorus chemistry. For example, recent studies have shown phosphoric acid[26] and diamidophosphate—a possible derivative of trimetaphosphate[27]—can abiotically phosphorylate various prebiotic compounds such as sugars, amino acids, and nucleotides in aqueous solution to produce higher-order biologically-relevant molecules. Although future studies have to be conducted on the underlying formation mechanisms of these oxoacids (*Supplementary Information*), the present study embodies a significant first step toward elucidating possible abiotic pathways toward oxoacids of phosphorus resembling key molecular building blocks in contemporary biochemistry on Earth thus bringing us closer to eventually predicting where in the Galaxy molecular precursors linked to the *Origins of Life* might have been synthesized.

5.3 Experimental Summary

The experiments were conducted in an ultrahigh-vacuum surface chamber at pressures of few 10^{-11} Torr by depositing ices of phosphine with oxygen−18 labeled water ($H_2{}^{18}O$) or carbon dioxide ($C^{18}O_2$) onto a polished silver mirror that is attached to a cold finger capable of temperatures down to 5 K (*Supplementary Information*). The ices were irradiated with 5 keV electrons for 1 h and then heated at 1 K min^{-1} to 300 K, which simulate the processing of polar and apolar ices by galactic cosmic ray generated secondary electrons for a few 10^6 years over the typical life-time of cold molecular clouds. The exploitation of interstellar model ices—also called analogue ices—represents a validated methodology in the astrophysics community to elucidate the solid-state synthetic routes to molecules such as phosphorus-bearing oxoacids in deep space. The chemical modification of the ices was probed on line and *in situ* via Fourier transform infrared spectroscopy (FTIR) (Tables 5.S1–5.S2). After the irradiation, the ices were heated to 300 K to release the molecules via temperature programmed desorption (TPD) into the gas-phase while simultaneously monitoring the ices via infrared spectroscopy. During the TPD process, photoionization reflectron time-of-flight mass spectrometry (PI-ReTOF-MS) probed the subliming molecules using 9.93 and 10.86 eV vacuum ultraviolet (VUV) photoionization energy. The residues that remained on the silver substrates were first analyzed using SIMS-TOF utilizing 30 keV Bi_3^+ clusters and low-energy electron flood gun, where the positive and negative ion spectra were observed. The residues were then extracted, derivatized with *N*,*O*-bis(trimethylsilyl)trifluoro-acetamide (BSTFA) and trimethylsilyl chloride (TMCS), and, using helium as a carrier gas, passed through an Agilent J&W DB 5MS Ultra Inert primary column (30 m × 0.25 mm inner diameter (ID), 0.25 μm film thickness) connected to an Agilent DB Wax secondary column (1.40 m × 0.1 mm ID, 0.1 μm film thickness). This two-dimensional gas chromatography utilized TOF-MS for detection. We would like to stress that blank experiments were also conducted under identical conditions but without exposing the samples to ionizing radiation; no oxoacids were detected in these blank studies highlighting that ionizing radiation is critical to form the detected oxoacids (Figures 5.S2 and 5.S3). The theoretical calculations used the GAUSSIAN09 program to obtain the ionization energies, relative isomer energies (CCSD(T)/CBS with B3LYP/ccpVTZ), and enthalpies of formation.

5.4 Supplementary Information

5.4.1 Experimental Details

Ices of phosphine (Sigma Aldrich, 99.9995 %), carbon dioxide (Airgas, 99.999 %), and water (Fisher Scientific, HPLC grade), along with oxygen−18 labeled carbon dioxide (Sigma Aldrich, 95 atom % ^{18}O) and water (Sigma Aldrich, 99 atom % ^{18}O), were deposited onto a polished silver wafer. This silver substrate was mounted onto an oxygen-free high-conductivity copper cold head capable of achieving temperatures as low as 5 K by a closed-cycle helium refrigerator (Sumitomo Heavy Industries, RDK-415E) inside a contamination-free stainless steel chamber capable of pressures down to 5×10^{-11} Torr using magnetically suspended turbomolecular pumps (Osaka) and oil-free backing pumps (Anest Iwata).[69] Phosphine and carbon dioxide gases were premixed and deposited at 2×10^{-8} Torr via a glass capillary, while phosphine and water were deposited simultaneously using separate transfer mechanisms to avoid any pre-deposition reactions. Deposition continued until 750 nm of ice was deposited, which was measured *in situ* using laser interferometry by monitoring the interference fringes of a helium-neon laser (632.8 nm) that is reflected off the silver substrate.[120] The ice mixtures were found to be 10:1 water to phosphine and carbon dioxide to phosphine by using integrated infrared absorption coefficients.[168] The refractive index of the ice mixture, which is necessary for the thickness calculation, was determined to be the refractive index of the matrix (n_{CO_2} = 1.27,[168] n_{H_2O} = 1.29[80]) The ices were irradiated with 5 keV electrons at a 70° angle to the surface normal for one hour at currents of 100 nA, 1000 nA, and 5000 nA. Exploiting the CASINO simulation,[82] the average penetration depth was found to be 285 nm (H_2O/PH_3) and 300 nm (CO_2/PH_3), while the maximum penetration depth was 650 nm (H_2O/PH_3) and 700 nm (CO_2/PH_3), which is less than the 750 nm ice thickness. The average dose was calculated to be 2.8 ± 0.6 eV molecule^{-1} (CO_2/PH_3) and 2.4 ± 0.5 eV molecule^{-1} (H_2O/PH_3) for the 100 nA irradiation, and these values scale linearly to 1000 and 5000 nA. The density of the ice mixture used for the CASINO simulation was the weighted average to the ice components: 0.90 g cm^{-3} for PH_3,[83,120] 0.94 g cm^{-3} for H_2O,[169] and 1.11 g cm^{-3} for CO_2.[168] A Nicolet 6700 Fourier Transform Infrared Spectrometer monitored the ice during irradiation from 500 to 4000 cm^{-1} with 4 cm^{-1} resolution. Standard experiments utilized oxygen−18 labeled CO_2 and H_2O

and were repeated at 5000 nA irradiation with non-isotopically labeled CO_2 and H_2O in order to confirm the infrared assignments, and both isotopologues are presented in Tables 5.S1 and 5.S2.

5.4.2 PI-ReTOF-MS

After the irradiation, the ices were annealed at 1 K min^{-1} while any subliming molecules were detected using a reflectron time-of-flight (ReTOF) mass spectrometer (Jordon TOF Products, Inc.) with single photon ionization (PI).[69] This photoionization process utilizes difference four wave mixing to produce vacuum ultraviolet light ($\omega_{vuv} = 2\omega_1 - \omega_2$). These experiments were performed with 10.86 eV photoionization energy and repeated at 9.93 eV to distinguish between the isomers of the phosphorus oxoacids. To produce 10.86 eV, the second harmonic (532 nm) of a pulsed neodymium-doped yttrium aluminum garnet laser (Nd:YAG, Spectra Physics, PRO-270, 30 Hz) was used to pump a Rhodamine 610/640 dye mixture (0.17/0.04 g L^{-1} ethanol) to obtain 607 nm, which underwent a tripling process to achieve ω_1 = 202 nm. A second Nd:YAG laser pumped an LDS 867 (0.15 g L^{-1} ethanol) dye to obtain ω_2 = 890 nm, which when combined with $2\omega_1$, using krypton as a non-linear medium, generated ω_{vuv} = 114 nm (10.86 eV) at 10^{14} photons per pulse. The production of 9.93 eV occurred similarly except the second harmonic (532 nm) of the second Nd:YAG laser was used as ω_2. The VUV light was spatially separated from other wavelengths using a lithium fluoride (LiF) biconvex lens (ISP Optics) and directed 1 mm above the sample to ionize subliming molecules. The ionized molecules were mass analyzed with the ReTOF mass spectrometer where the arrival time to a multichannel plate is based on mass-to-charge ratios, and the signal was amplified with a fast preamplifier (Ortec 9305) and recorded with a bin width of 4 ns triggered at 30 Hz (Quantum Composers, 9518). The ReTOF recorded until the sample reached 300 K and held at constant temperature for one hour, after which an infrared spectrum of the resulting residue was recorded.

Table 5.S1. Infrared assignments for phosphine (PH_3)–carbon dioxide (CO_2) ices at 5 K prior to the irradiation, after the irradiation, and of the residues at 300 K.

Pristine ice, before irradiation (5 K)			
Assignment	Position with ^{16}O (cm^{-1})	Position with ^{18}O (cm^{-1})	Reference
CO_2 (ν_2)	651	638	160
PH_3 (ν_2)	985	985	187
PH_3 (ν_4)	1107	1107	187
CO_2 (ν_1)/CO_2 ($2\nu_2$)*	1226, 1336	1276, 1383	160
PH_3 ($2\nu_4$)	---	2207	187
$^{13}CO_2$ (ν_3)	2278	2245	160
PH_3 (ν_1/ ν_3)	2317	2314	187
CO_2 (ν_3)	2325	2292	160
CO_2 (ν_3 + ν_L)	2398–2440	2360–2390	160
PH_3 (ν_1 + ν_4)	3428	3428	187
CO_2 ($2\nu_2$ + ν_3)	3596	3511	160
CO_2 (ν_1 + ν_3)	3702	3622	160
New peaks after irradiation (5 K)			
Assignment	Position with ^{16}O (cm^{-1})	Position with ^{18}O (cm^{-1})	Reference
ν(P-O)	880–1010	850-950	186
O_3 (ν_3)	1040	975	190
δ(PH_2)	1030	1025	186
ν(P=O)	1180–1370	1150–1340	186
H_2O (ν_2)	1650	1630	169
δ(O=P-OH)	1730	1700	186
ν(C=O)	1780	1750	186
^{13}CO (ν_1)	2090	2042	160
CO (ν_1)	2140	2090	160
P-OH ν(OH)	---	2150	186
ν(PH)	2315	2230	186
P_2H_4 (ν_1)	2280	2265	96
P-OH ν(OH)	2875	2650–2800	186
H_2O (ν_1(in phase))	2970	2960	169
H_2O (ν_3(transversal))	3230	3200	169
H_2O (ν_3(longitudinal))	3410	3360	169
H_2O (ν_1(out of phase))	3510	3460	169
Residue (300 K)			
Assignment	Position with ^{16}O (cm^{-1})	Position with ^{18}O (cm^{-1})	Reference
ν(P-O)	930–1040	910–1030	186
δ(PH_2)	1080–1115	1050–1115	186
ν(P=O)	1150–1330	1140–1300	186
δ(O=P-OH)	1530–1700	1530–1730	186
P-OH ν(OH)	2170	2160	186
ν(PH)	2270	2270	186
P-OH ν(OH)	2450–2720	2450–2680	186
ν(OH)	2780–3500	2780–3300	186

Note. ν_L defines the lattice mode.
*Fermi resonance

Table 5.S2. Infrared assignments for phosphine (PH_3) – water (H_2O) ices at 5 K prior to the irradiation, after the irradiation, and of the residues at 300 K.

Pristine ice, before irradiation (5 K)			
Assignment	Position with ^{16}O (cm^{-1})	Position with ^{18}O (cm^{-1})	Reference
H_2O (ν_L)	770	740	169
PH_3 (ν_2)	983	983	187
PH_3 (ν_4)	1101	1103	187
H_2O (ν_2)	1650	1640	169
PH_3 (ν_1/ ν_3)	2319	2314	187
H_2O (ν_1(in phase))	3040	3090	169
H_2O (ν_3(transversal))	3220	3250	169
H_2O (ν_3(longitudinal))	3380	3375	169
H_2O (ν_1(out of phase))	3550	3440	169
New peaks after irradiation (5 K)			
Assignment	Position with ^{16}O (cm^{-1})	Position with ^{18}O (cm^{-1})	Reference
ν(P-O)	950	970	186
δ(PH_2)	1045	1090	186
ν(P=O)	1140–1300	1140	186
δ(O=P-OH)	1710	1670	186
P-OH ν(OH)	2170	2160	186
P_2H_4 (ν_1)	2280	2275	96
ν(OH)	2900	2910	186
Residue (300 K)			
Assignment	Position with ^{16}O (cm^{-1})	Position with ^{18}O (cm^{-1})	Reference
ν(P-O)	790-950	780-930	186
δ(PH_2)	1040	1050	186
ν(P=O)	1120–1320	1100–1300	186
δ(O=P-OH)	1550–1670	1530–1640	186
ν(PH)	2230	2240	186
P-OH ν(OH)	2700	2460-2660	186
ν(OH)	2950-3000	2750-3300	186

Note. ν_L defines the lattice mode.

Table 5.S3. SIMS calibration data of pure pyrophosphoric acid, phosphoric acid, and phosphorous acid scaled to the intensity of the most intense signal.

Positive Ions		Negative Ions	
Pyrophosphoric Acid, $H_4P_2O_7$			
$H_5P_2O_7^+$	17.1	$H_3P_2O_7^-$	45.2
$H_4PO_4^+$	100	$HP_2O_6^-$	93.0
$H_2PO_3^+$	18.9	$H_2PO_4^-$	8.2
$H_4PO_2^+$	5.2	PO_3^-	100
$H_2PO_2^+$	9.8	PO_2^-	16.9
PO_2^+	13.3		
PO^+	10.2		
Phosphoric Acid, H_3PO_4			
$H_4PO_4^+$	100	$H_2PO_4^-$	23.8
$H_2PO_3^+$	28.1	PO_3^-	100
$H_4PO_2^+$	1.1	PO_2^-	2.0
$H_2PO_2^+$	9.3		
PO_2^+	4.3		
PO^+	20.7		
Phosphorous Acid, H_3PO_3			
$H_4PO_3^+$	100	$H_2PO_3^-$	17.7
$H_2PO_3^+$	17.5	PO_3^-	100
$H_4PO_2^+$	7.4	PO_2^-	37.8
$H_2PO_2^+$	72.6		
PO_2^+	1.4		
PO^+	72.3		

Table 5.S4. SIMS analysis of the residues formed at 5000 nA irradiation currents showing the raw ion counts and accounting for overlapping ion counts from various oxoacids (corrected ion counts) exploiting the calibration experiments.

	PH_3/CO_2		PH_3/H_2O		$PH_3/C^{18}O_2$		$PH_3/H_2{}^{18}O$	
Positive Ions	Ion Counts ($\times 10^5$)	Corrected Ion Counts ($\times 10^5$)	Ion Counts ($\times 10^5$)	Corrected Ion Counts ($\times 10^5$)	Ion Counts ($\times 10^5$)	Corrected Ion Counts ($\times 10^5$)	Ion Counts ($\times 10^5$)	Corrected Ion Counts ($\times 10^5$)
$H_5P_2O_7^+$	1.8	0	1.4	0	0.22	0	0.07	0
$H_4PO_4^+$	11.5	0.9	9.3	1.0	3.3	21	5.9	5.5
$H_4PO_3^+$	3.3	0	0.9	0	0.4	0	0.3	0
$H_2PO_3^+$	5.7	2.9	6.0	4.0	1.0	0.2	2.6	0.9
$H_2PO_2^+$	6.1	2.6	3.6	2.1	4.7	4.1	10.4	9.6
Negative Ions	Ion Counts ($\times 10^5$)	Corrected Ion Counts ($\times 10^5$)	Ion Counts ($\times 10^5$)	Corrected Ion Counts ($\times 10^5$)	Ion Counts ($\times 10^5$)	Corrected Ion Counts ($\times 10^5$)	Ion Counts ($\times 10^5$)	Corrected Ion Counts ($\times 10^5$)
$H_3P_2O_7^-$	4.0	0	6.1	0	0.3	0	0.3	0
$HP_2O_6^-$	52.8	44.5	29.9	17.4	0.8	0.3	0.1	0
$H_2PO_4^-$	3.0	2.2	5.1	4.0	4.1	4.0	1.6	1.5
$H_2PO_3^-$	1.1	0	0.8	0	0.8	0	0.5	0
PO_3^-	37.9	13.2	35.0	0.5	17.8	0	7.4	0
PO_2^-	9.9	5.8	10.5	6.3	3.8	1.6	1.9	0.5

5.4.3 SIMS Analysis

After each experiment, the wafer was removed and stored in an air-tight container under inert nitrogen atmosphere. The residue on the wafer was analyzed utilizing a time-of-flight secondary-ion mass spectrometry instrument (TOF-SIMS 5-300, ION-TOF) equipped with a reflectron mass analyzer, a 30 keV Bi_n liquid metal primary ion source (Bi-LMIG), and a low-energy electron flood gun. Spectra were acquired with Bi_3^+ in bunched mode with a focus of 2–3 mm, a beam current of 0.25 pA, and a total dose of 1.25×10^8 ions. Data were acquired from a 500 μm^2 analysis area. The positive and negative ions from the sputtered residue were recorded (Tables 5.S3 & 5.S4), and the residues were analyzed and compared with fragment assignments from calibrated phosphorus oxoacids adjusted for the mass shifts since our studies utilized ^{18}O-labelled precursors.

5.4.4 GC×GC−TOFMS

The gas chromatographic analysis was carried out by a GC×GC Pegasus IV D instrument coupled to a time-of-flight mass spectrometer ((TOF-MS), LECO Corp.). The TOF-MS system operated at a storage rate of 150 Hz, with a 25–700 amu mass range, a detector voltage of 1.5 to 1.8 kV, and a solvent delay of 12 min. The ion source and transfer temperatures were set to 503 K. The column set consisted of an Agilent J&W DB 5MS Ultra Inert primary column (30 m × 0.25 mm inner diameter (ID), 0.25 µm film thickness) Press-

Tight (Restek Corp.) connected to an Agilent DB Wax secondary column (1.40 m × 0.1 mm ID, 0.1 μm film thickness). Helium was used as carrier gas at a constant flow rate $\bar{u}$ = 1 mL min^{-1}. Sample volumes of 1 μL were injected in the splitless mode into an ultra inert, single taper w/glass wool splitless inlet liner (Agilent) at an injector temperature of 503 K. All samples and reference compounds were analyzed with the identical temperature program. The primary oven was operated as follows: 313 K for 1 min, temperature increase of 5 K min^{-1} to 473 K and held for 15 min. The secondary oven used the same temperature program with a constant temperature offset of 303 K. A modulation period of 5 seconds was applied for the liquid nitrogen cooled thermal modulator. Data were acquired and processed with LECO Corp. ChromaTOF software. Compound identification was performed by comparison with the chromatographic retention in both dimensions and mass spectra of authentic standards. The derivatization reagents including *N*,*O*-bis(trimethylsilyl)-trifluoroacetamide (BSTFA) and trimethylsilyl chloride (TMCS), the internal standard methyl laurate, hexane, and water as well as phosphonic acid ($HPO(OH)_2$), phosphoric acid (H_3PO_4), pyrophosphoric acid ($H_4P_2O_7$), and sodium triphosphate ($Na_5P_3O_{10}$) were purchased from Sigma Aldrich. Sample-handling glassware was wrapped in aluminum foil and heated at 773 K for 3 h prior to usage to eliminate possible contamination. Eppendorf tips were sterile and the water used for extraction, standard solutions, reagent solutions, and blanks were of high-performance liquid chromatography grade. The residues were extracted with 10 × 50 μL water from their silver wafers and transferred into conical reaction vials (1 mL V-Vial, Wheaton). The aqueous extracts were dried under a gentle stream of nitrogen and silylated with an excess of 50 μL BSTFA and 10 μL TMCS for 2 h at 353 K in the presence of the internal standard methyl laurate in hexane (5 μL, 10^{-5} M). The derivatized mixtures were transferred into GC vials for their subsequent GC×GC–TOFMS analysis. Procedural blanks (Figures 5.S2 & 5.S3) were run in sequence to each sample in order to monitor background interferences.

Compound identification was performed by comparison with the chromatographic retention in both dimensions of authentic standards and mass spectra. Comparison with previously reported data on TMS derivatives of phosphorus oxoacids[26,27,211] let us identify multiple oxoacids. Table 5.S6 summarizes the analytes' retention times in the first and second chromatographic dimension as well as the corresponding mass spectra of the

analyzed residue and standard. The mass spectra of all three phosphorus oxoacids are characterized by the molecular ion $[M]^+$ peak, the fragment ion $[M-15]^+$ formed by the loss of a methyl group as well as silicon-containing fragments at m/z 45 [CH_3SiH_2], 73 [$(CH_3)_3Si$], 75 [$(CH_3)_3SiH_2$], 133 [$(CH_3)_3Si_2O_2$], 147 [$(CH_3)_5Si_2O$], and 207 [$(CH_3)_5Si_3O_3$]. The phosphorus oxoacids detected in the residues were found to contain ^{18}O isotopes, whereas the standard samples used for identification were made of the natural isotopic composition dominated by ^{16}O. Esterfication, necessary to increase the volatility of our target compounds in the gas chromatographic analysis, resulted in a shift of the tautomeric equilibria of phosphonic and phosphinic acid towards their more active pyramidal forms (Figure 5.S1).

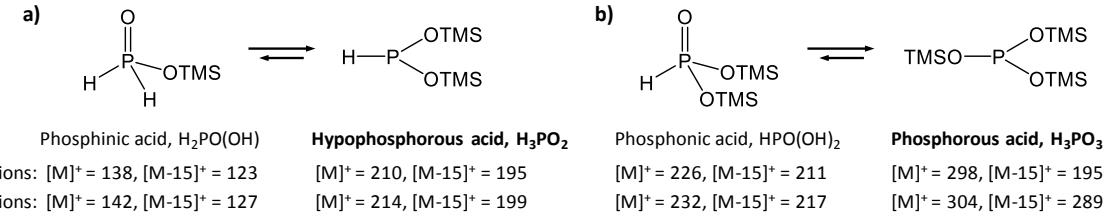

Figure 5.S1. Tautomeric forms of trimethylsilyl (TMS) derivatives of H_3PO_2 (a) and H_3PO_3 (b). The characteristic molecular ion peak $[M]^+$ as well as $[M-15]^+$ of the ^{18}O-TMS derivatives of hypophosphorous acid and phosphorous acid, respectively, revealed the formation of both phosphorus oxoacids in the residues of the irradiated phosphine-doped interstellar ice analogues.

Table 5.S5. Identified phosphorus oxoacids as trimethylsilyl (TMS) derivatives by GC×GC-TOFMS.

Compound	R_{t1} [a]	R_{t2} [b]	MS-fragmentation / ^{18}O sample		MS-fragmentation / ^{16}O standard	
	[min]	[sec]	$[M^{+\bullet}]$	Other important ions, m/z	$[M^{+\bullet}]$	Other important ions, m/z
Hypophosphorous acid (+I)	12.40	2.7	214	199, 73	210	195, 73
Phosphonic acid (+III)	13.24	1.6	304	289, 207, 147, 133, 75	298	283, 207, 147, 133, 75
Phosphoric acid (+V)[c]	18.59	1.6	322	307, 291, 147, 133, 73, 45	314	299, 283, 211, 147, 133, 73, 45
Phosphoric acid (+V)[d]			320	305, 289, 147, 133, 73, 45		

[a] GC×GC retention time 1st dimension. [b] GC×GC retention time 2nd dimension. [c] $[M^{+\bullet}]$ = 322 corresponds to $H_3P^{18}O_4$ and [d] $[M^{+\bullet}]$ = 320 to $H_3P^{18}O_3{}^{16}O$.

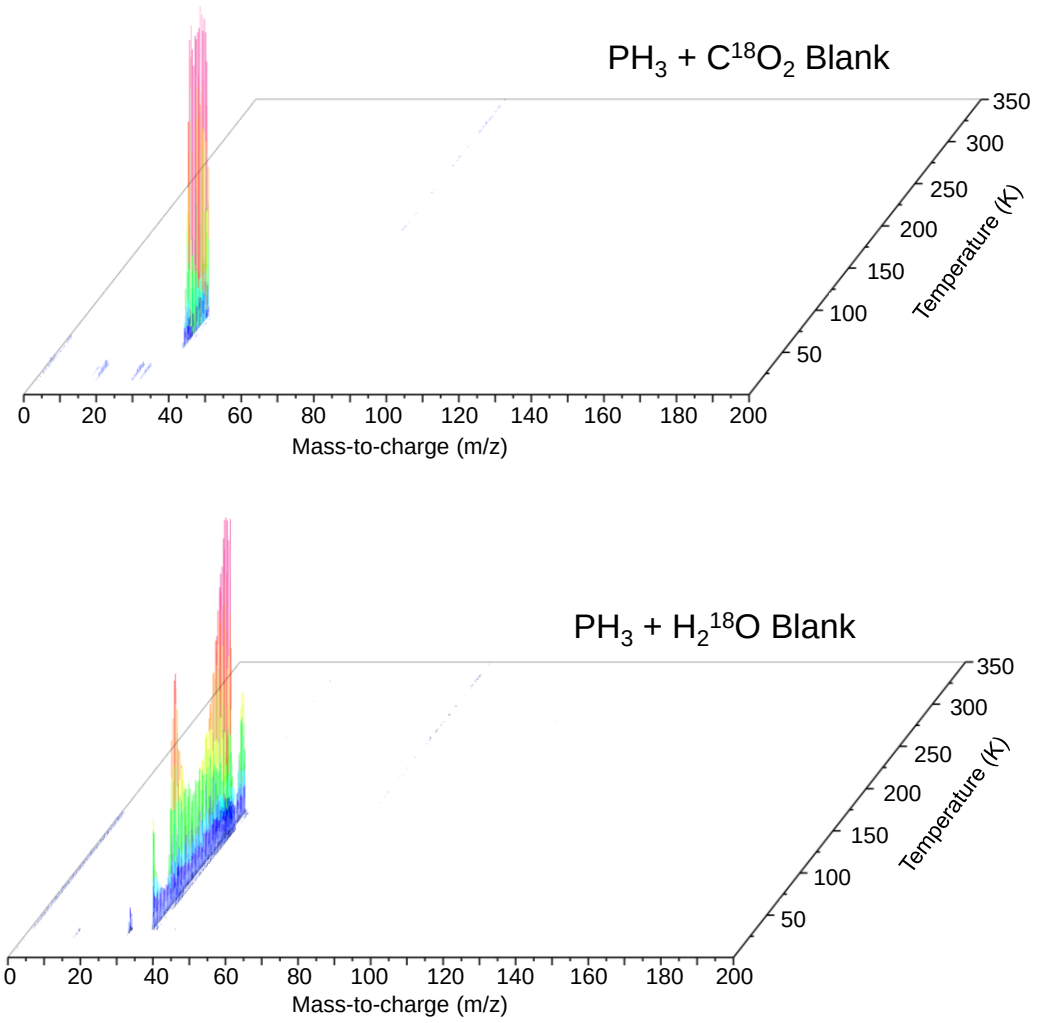

Figure 5.S2. PI-ReTOF-MS data as a function of temperature during TPD for the unirradiated ice mixtures of $PH_3/C^{18}O_2$ (top) and $PH_3/H_2{}^{18}O$ (bottom) at 10.86 eV photoionization energy. The strong signal at m/z = 34 results from PH_3, while H_2O and CO_2 have higher ionization energies than 10.86 eV and thus are not observed. It shall be highlighted that no oxoacids are observed in these blank experiments.

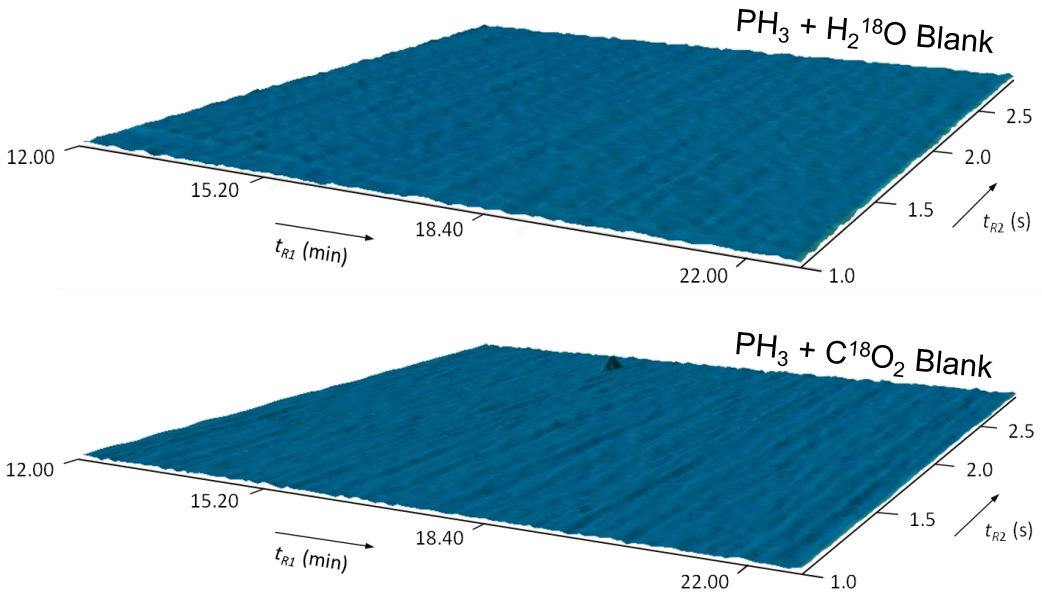

Figure 5.S3. GC×GC-TOFMS chromatogram of the blanks from the mixtures of $PH_3/C^{18}O_2$ (top) and $PH_3/H_2{}^{18}O$ (bottom). Mass-to-charges (m/z) of 214 (×100) and 304 (×150) were selected for the above representation (*z*-axis = 600,000).

5.4.5 Theoretical

For the theoretical calculations (Table 5.S6), the geometries of neutral molecules and cations were optimized by the hybrid density functional B3LYP[85-88] with the cc-pVTZ basis set and thus obtained the harmonic frequencies. Their coupled cluster[89-92] CCSD(T)/cc-pVDZ, CCSD(T)/ccpVTZ, and CCSD(T)/cc-pVQZ energies were then calculated and extrapolated to completed basis set limits,[213] CCSD(T)/CBS, with B3LYP/cc-pVTZ zero-point energy corrections. The energies are accurate within 0.08 eV.[214] The adiabatic ionization energies were computed by taking the energy difference between the ionic and the neutral states that correspond to similar conformation. At this level of theory, the adiabatic ionization energies are within 0.05 eV. The GAUSSIAN09 program[95] was utilized in the electronic structure calculations.

Table 5.S6. Calculated enthalpies of formation at 0 K for distinct isomers of phosphorus oxoacids.

Structure	Formula	Name	$\Delta_f H$ (eV)[a]
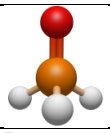	H_3PO	Phosphine oxide	−3.63
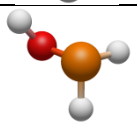	H_2POH	Hydroxyphosphine	−3.60
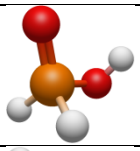	$H_2P(O)OH$	Phosphinic acid	−6.76
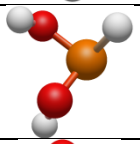	$HP(OH)_2$	Hypophosphorous acid	−6.39
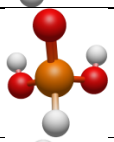	$HPO(OH)_2$	Phosphonic acid	−10.04
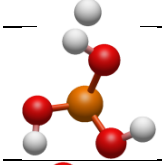	$P(OH)_3$	Phosphorous acid	−9.52
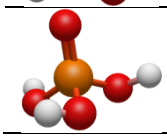	$PO(OH)_3$	Phosphoric acid	−13.13

[a]CCSD(T)/CBS

5.4.6 Reaction Mechanisms

Having identified four monophosphorus oxoacids [hydroxyphosphine (H_3PO: PH_2OH(-I)), phosphinic acid (H_3PO_2: $H_2P(O)OH$(+I)), phosphonic acid (H_3PO_3: $HP(O)(OH)_2$(+III)), phosphoric acid (phosphoric acid (H_3PO_4(+V))] along with pyrophosphoric acid ($H_4P_2O_7$(+V)) with phosphorus in four distinct oxidation states ranging from –I to +V, we are discussing now possible formation pathways. For simplicity in the following discussion, the ^{18}O label is dropped. It should be noted that although the FTIR analysis provided evidence on the emergence of functional groups associated with phosphorus oxoacids even at 5 K, the FTIR data were unable to identify individual

oxoacids due to overlapping absorptions of the functional groups. Therefore, kinetic profiles linked to the formation of individual phosphorus oxoacids could not be provided. However a few important conclusions can be drawn. First, based on the PI-ReTOF-MS data recorded at 100 nA, 1,000 nA, and 5,000 nA, the yields of PH_2OH(−I) and $H_2P(O)OH$(+I) depend on the irradiation current and hence dose. Recall that in the PH_3–H_2O system, $H_2P(O)OH$(+I) is absent in the 100 nA experiment, but emerges at 1,000 nA. This observation suggests a sequential formation of phosphorus oxoacids via stepwise reaction of oxygen atoms starting with phosphine (PH_3). Considering the water- and carbon dioxide-rich ices, the radiolysis of water and carbon dioxide can generate electronically excited oxygen atoms in strongly endoergic reactions;[160,161,215,216] water can also decompose via the formation of atomic hydrogen and hydroxyl radicals (OH). The required energy for the bond dissociation can be supplied by the energetic electrons.

$$CO_2(X\,^1\Sigma_g^+) \rightarrow CO(X\,^1\Sigma^+) + O(^1D) \qquad \Delta_R G = 7.59\ \text{eV} \qquad (5.S1)$$

$$H_2O(X\,^1A_1) \rightarrow H(^2S) + OH(X\,^2\Pi_\Omega) \qquad \Delta_R G = 4.83\ \text{eV} \qquad (5.S2)$$

$$H_2O(X\,^1A_1) \rightarrow H_2(X\,^1\Sigma_g^+) + O(^1D) \qquad \Delta_R G = 6.74\ \text{eV} \qquad (5.S3)$$

Simultaneously, the energetic electrons can also lead to a phosphorus–hydrogen bond rupture in phosphine leading to phosphino (PH_2) radicals (reaction 5.S4).[187]

$$PH_3(X\,^1A_1) \rightarrow PH_2(X\,^2B_1) + H(^2S) \qquad \Delta_R G = 3.51\ \text{eV} \qquad (5.S4)$$

In the water–phosphine system, the formation of PH_2OH may proceed via a barrier-less recombination of the phosphino (PH_2) radical with the hydroxyl (OH) radical. Alternatively, electronically excited oxygen atoms can insert without barrier into the phosphorus–hydrogen bond leading to PH_2OH as well (reaction 5.S6). It is important to note that electronically excited oxygen atoms can also add without barrier to the phosphorus atom of phosphine yielding phosphine oxide (H_3PO) (reaction 5.S7), which can then undergo hydrogen migration to form PH_2OH.[207,208,217] Schmidt et al. suggested

that a barrier between 3.01 and 3.73 eV separated both isomers;[218] this energy can be supplied by the energetic electrons as well. Recall that the formation of phosphine oxide could not be proven or disproven in our study. We would like to stress that Stief et al. also probed the gas phase kinetics of ground state atomic oxygen with phosphine over a temperature range of 208 K to 423 K revealing that ground state oxygen preferentially adds to the phosphorus atom (31, 32);[219,220] unfortunately, neither products were identified, nor the role of intersystem crossing from the triplet to the singlet surface were probed.

$$PH_2(X\,^2B_1) + OH(X\,^2\Pi_\Omega) \rightarrow PH_2OH(X\,^1A') \qquad \Delta_R G = -5.27\ \text{eV} \qquad (5.S5)$$

$$PH_3(X\,^1A_1) + O(^1D) \rightarrow PH_2OH(X\,^1A') \qquad \Delta_R G = -8.27\ \text{eV} \qquad (5.S6)$$

$$H_3PO(X\,^1A_1) \rightarrow PH_2OH(X\,^1A') \qquad \Delta_R G = 0.03\ \text{eV} \qquad (5.S7)$$

Once PH_2OH is formed, the addition of another electronically excited oxygen atom to the phosphorus atom produces $H_2P(O)OH$ (reaction 5.S8). Successive insertions of electronically excited oxygen atoms in phosphorus–hydrogen bonds may lead via $HP(O)(OH)_2$ (reaction 5.S9) to H_3PO_4 (reaction 5.S10). Essentially, in this reaction sequence, up to four oxygen atoms are required to oxidize phosphine to ultimately phosphoric acid via stepwise oxidation. The release of up to four oxygen atoms requires 27.0 eV and 30.4 eV to be generated from water and carbon dioxide, respectively. Therefore, thermal reactions cannot lead to the oxoacids at 5 K, but cosmic ray triggered non-equilibrium chemistry is required to supply the required oxygen atoms (and possibly the hydroxyl radicals) for the oxidation process.

$$PH_2OH(X\,^1A') + O(^1D) \rightarrow H_2P(O)OH(X\,^1A') \qquad \Delta_R G = -7.68\ \text{eV} \qquad (5.S8)$$

$$H_2P(O)OH(X\,^1A') + O(^1D) \rightarrow H_2P(O)(OH)_2(X\,^1A') \qquad \Delta_R G = -7.81\ \text{eV} \qquad (5.S9)$$

$$H_2P(O)(OH)_2(X\,^1A') + O(^1D) \rightarrow H_3PO_4(X\,^1A) \qquad \Delta_R G = -7.62\ \text{eV} \qquad (5.S10)$$

5.4.7 Conversion Yield

The infrared analysis indicates that 76 ± 8 % of the phosphine reacted in the 10:1 CO_2:PH_3 ice; this was determined by utilizing the comparative area of the ν_2 and ν_4 bands of phosphine. Similarly, the ν_2, $2\nu_2 + \nu_3$, and $\nu_1 + \nu_3$ bands of carbon dioxide show that 28 ± 1 % of CO_2 was destroyed after the irradiation. This equates to $8 \pm 2 \times 10^{16}$ molecules of phosphine and $3 \pm 1 \times 10^{17}$ molecules of carbon dioxide destroyed by irradiation. Since each irradiated carbon dioxide molecule liberates only one oxygen atom, the ratio of available reactive phosphorus-to-oxygen atoms is thus 1.0 : 3.4 ± 0.8. If all of the reacted phosphine became incorporated into one of the three simplest oxoacids, the $8 \pm 2 \times 10^{16}$ molecules produced suggest that $2.1 \pm 0.8 \times 10^{-4}$ molecules were formed per eV of irradiation. The formation of H_3PO_4 is limited by the number of oxygen atoms generated, and at most $7 \pm 2 \times 10^{16}$ molecules of H_3PO_4 could form, which corresponds to a generation of $1.7 \pm 0.6 \times 10^{-4}$ H_3PO_4 molecules eV^{-1}. The ν_2 and ν_L bands of water were analyzed for the 10:1 H_2O : PH_3 ice, and 62 ±2 % of phosphine was found to have reacted, while only 37 ± 5 % of the water was destroyed. This is equivalent to $6 \pm 2 \times 10^{16}$ phosphine molecules and $8 \pm 3 \times 10^{17}$ water molecules. In this case, much more oxygen was available compared to phosphorus, with a 1 : 12 phosphorus-to-oxygen atom ratio, and thus phosphorus will always be the limiting atom in the formation of the oxoacids. Here, the upper yields of $6 \pm 2 \times 10^{16}$ molecules of phosphorus oxoacids are formed at $1.6 \pm 0.6 \times 10^{-4}$ molecules eV^{-1}.

Using reagent standards, the quantity of phosphoric acid (H_3PO_4) in the residues can be determined via GC×GC-TOFMS and compared to the infrared spectra to establish a reaction yield. The CO_2:PH_3 ices produced 5 nmol (3×10^{15} molecules) of phosphoric acid, while only 1 nmol (6×10^{14} molecules) was detected from the H_2O:PH_3 ice, which results in $7 \pm 3 \times 10^{-6}$ molecules of H_3PO_4 per eV in the CO_2:PH_3 ice and $2 \pm 1 \times 10^{-6}$ H_3PO_4 molecules eV^{-1} in the H_2O:PH_3 ice. Thus, phosphoric acid represents 4 % of the reacted phosphine in CO_2:PH_3, while a 1 % yield was found in the H_2O:PH_3 system. As phosphoric acid was the most abundant compound detected in the residues, this indicates that most of the phosphorus sublimed during the TPD, for example as diphosphane as detected experimentally.

CHAPTER 6

ALKYL PHOSPHONIC ACIDS FROM ICES OF PHOSPHINE, WATER, AND METHANE

This chapter is based on the paper: A. M. Turner, M. J. Abplanalp, A. Bergantini, R. Frigge, C. Zhu, B.-J. Sun, A. H. H. Chang, C. Meinert, R. I. Kaiser, "Synthesis of Alkyl phosphonic Acids in Interstellar Analogue Ices—A Promising Extraterrestrial Origin of Prebiotic Phosphorus Compounds", prepared for submission.

The discovery of alkylphosphonic acids in the Murchison meteorite has provided an extraterrestrial carrier for organic phosphorus compounds that would be soluble and bioavailable to Earth's first organisms. While modern biomolecules utilize P(+V) for their phosphate moieties, the limited bioavailability of phosphate minerals in neutral or acidic media containing iron and calcium ions on early Earth led to the hypothesis that the more soluble P(+III) compounds such as the alkylphosphonic acids could have served as the initial source of biological phosphorus. The origin of these alkylphosphonic acids has remained a topic of vigorous debate, with previous studies attempting to explain their formation via aqueous processing of iron-nickel phosphide minerals from meteorites. Here, we provide via a combined experimental and computational study a plausible alternative route to alkylphosphonic acids in ice mixtures of phosphine (PH_3), water (H_2O), and methane (CH_4) exposed to ionizing radiation, thus simulating the chemical processes of the icy mantles of interstellar ice grains in interstellar clouds. By utilizing tunable photoionization reflectron time-of-flight mass spectrometry (PI-ReTOF-MS) and two-dimensional gas chromatography time-of-flight mass spectrometry (GC×GC-TOF-MS), we report for the first time the detection of the three simplest alkylphosphonic acids carrying methyl (CH_3), ethyl (C_2H_5), and propyl (C_3H_7) functional groups in processed interstellar ice analogue samples. This discovery opens a previously overlooked avenue into the formation of molecules of astrobiological significance by demonstrating the facile synthesis of phosphorus-containing molecules in interstellar ices in form of alkylphosphonic acids, which might become incorporated into comets and asteroids prior their delivery to Earth.

6.1 Introduction

While phosphates (PO_4^{3-}) along with their P(+V) derivatives present the ubiquitous form of phosphorus for contemporary terrestrial minerals and biomolecules, the increased solubility of reduced oxidation states like P(+III) under Earth's early, oxygen-poor atmospheric conditions have been proposed as the initial source of prebiotic phosphorus available for the first terrestrial microorganisms.[5] Phosphorus-bearing biomolecules include ribonucleic/deoxyribonucleic acid (RNA/DNA), adenosine diphosphate/triphosphate (ADP/ATP), and phospholipids; in each case a phosphate group is chemically bonded to a carbon atom of a sugar—ribose (RNA, ADP/ATP), deoxyribose (DNA)—or of glycerol (phospholipids). The Murchison meteorite, a carbonaceous chondrite carrying key classes of exogenously synthesized organic molecules like amino acids and sugars,[139] contains phosphorus as phosphide (−III) and phosphate (+V) minerals.[142] Schreibersite, an iron-nickel phosphide ($(Fe,Ni)_3P$) mineral found in meteorites, has been studied as a possible source of phosphite ($H_2PO_3^-$, P(+III)) minerals contained in ancient Archean carbonaceous deposits and, given the 10^3-fold greater solubility of phosphite over phosphate minerals, as the ultimate origin of soluble prebiotic phosphorus.[201] While a purely terrestrial hypothesis might state that no "phosphorus problem" exists and that organisms could have scavenged the limited phosphorus from geologic phosphates,[5] an extraterrestrial view advocates that meteoric minerals were delivered to Earth during the heavy bombardment period and, after aqueous processing, formed soluble phosphites that were available to the first organisms.[201] An alternative to these hypotheses considers chemical reactions essential to produce complex, biologically-relevant organic molecules in astrophysical environments such as in interstellar ices in deep space prior to their delivery to Earth.[187,206]

A notable class of molecules that possesses these characteristics of an impending abiotic synthesis in extraterrestrial ices are alkyl phosphonic acids ($R–P(O)(OH)_2$) with 'R' signifying an alkyl group (C_nH_{2n+1}); these molecules represent the *only* phosphorus-containing organic compounds of extraterrestrial origin identified thus far.[7] Alkyl phosphonic acids, which carry methyl (CH_3), ethyl (C_2H_5), isopropyl/*n*-propyl (C_3H_7), and

n-butyl (C_4H_9) chains, were identified in the Murchison meteorite and exhibit the carbon-phosphorus bond that Cooper et al. noted would be critical to survive aqueous alternation on the parent body.[7] Thus, alkyl phosphonic acids represent both a soluble and bioavailable source of phosphorus that could persist on an aqueously altered body prior to their delivery to Earth as well as the potential for the formation of phosphate esters in extraterrestrial bodies without aqueous alternation. While phosphorus-bearing minerals like schreibersite have been investigated as a source of alkyl phosphonic acids,[6,17,20,143] the unique potential of an alternative formation scenario—the synthesis of alkyl phosphonic acids in phosphorus-doped ices condensed on interstellar grains in cold molecular clouds through interaction with ionizing radiation—has not been fully explored yet. Functional groups, which might be linked to alkyl phosphonic acids, were detected in processed phosphine (PH_3)-rich ices, but previous infrared spectroscopic studies could not identify any discrete alkyl phosphonic acids[206] since the absorptions of functional groups of complex organic molecules often overlap.[186] The organic chemistry of carbonaceous chondrites such as Murchison is consistent with icy bodies possessing at least partially interstellar organic matter.[139] In addition, interstellar analogue ices have shown the potential to yield complex organic molecules of biochemical relevance from fundamental biomolecules like amino acids[52] to simple sugars.[74] These interstellar compounds can be incorporated eventually into planetesimals, comets, and asteroids.[7] Phosphine (PH_3) presents a promising phosphorus-source for these interstellar ices as phosphine has been observed in the circumstellar envelope of the carbon-star IRC+10216[37] from which it can be ejected to the interstellar medium and eventually become incorporated into cold molecular clouds and hence icy grains. Furthermore, phosphine has been contemplated as the carrier of the phosphorus signal detected in comet 67P/Churyumov-Gerasimenko in the framework of the *Rosetta* mission.[41] Likewise, interstellar analogue ices of phosphine and water exposed to ionizing radiation generate a homologues series of phosphorus oxoacids including phosphonic acid (H_3PO_3), phosphoric acid (H_3PO_4), and pyrophosphoric acid ($H_4P_2O_7$).[221] Therefore, the addition of organic carbon to these interstellar ice analogues could provide the critical reactant

necessary to establish the plausible formation of alkyl phosphonic acids in extraterrestrial ices.

In this *Report*, we present compelling evidence on the synthesis of the three simplest alkyl phosphorus oxoacids—methyl (CH_3), ethyl (C_2H_5), and propyl (C_3H_7) phosphonic acid—formed in interstellar ice analogues containing phosphine (PH_3), water (H_2O), and methane (CH_4) exposed to energetic electrons as a proxy for secondary electrons generated during the interaction of galactic cosmic rays with interstellar ices at temperatures of 5 K.[160] By exploiting reflectron time-of-flight mass spectrometry (ReTOF-MS) coupled with tunable photoionization (PI) and isotopic experiments of mixtures with $H_2{}^{18}O$ and $^{13}CH_4$, the present study represents the very first discovery of individual alkyl phosphonic acids in processed interstellar ice analogues in cold molecular clouds synthesized abiotically upon interaction with ionizing radiation. Since molecular clouds represent nurseries of stars and planetary systems, the detection of these alkyl phosphonic acids suggests that these molecules could have been at least partially delivered to our Solar System from their interstellar nurseries via circumstellar disks thus defining where in deep space phosphorus-bearing molecular precursors relevant to the origins of life might be synthesized.

The experiments were carried out in an ultrahigh-vacuum vessel at base pressures of typically 8×10^{-11} Torr by exposing ice mixtures of phosphine (PH_3), water ($H_2O/H_2{}^{18}O$), and methane ($CH_4/^{13}CH_4$) to energetic electrons at interstellar temperatures of 5 K (*Supplementary Information*). These studies replicate the processing of polar interstellar ices by galactic cosmic ray-initiated electron cascades for a few 10^6 years covering a representative life-time of cold molecular clouds.[54] Taking advantage of interstellar model ices—sometimes referred to as analogue ices—signifies an endorsed methodology in the astrophysics community to reveal the underlying reaction mechanisms and products such as alkyl phosphonic acids in interstellar ices. The chemical modification of the ices was probed on line and *in situ* via Fourier transform infrared spectroscopy (FTIR). After the irradiation, the ices were annealed to 320 K to sublime the molecules via temperature programmed desorption (TPD). During the TPD process,

individual molecules were ionized at distinct photoionization energies in the gas phase via single photon vacuum ultraviolet (VUV) photoionization and mass resolved by a reflectron time-of-flight mass spectrometer (PI-ReTOF-MS) to identify the synthesized alkyl phosphorus oxoacids and their structural isomers selectively. The solid residues that remained at room temperature were analyzed after derivatization exploiting two dimensional gas chromatography coupled with reflectron time-of-flight mass spectrometry (GC×GC-TOF-MS).

6.2 Results & Discussion

6.2.1 Infrared Spectroscopy

Infrared spectroscopy of irradiated ices represents a valuable tool to identify small, individual molecules and functional groups of phosphorus-bearing molecules.[202] The use of water-rich ices (PH_3:H_2O:CH_4 = 1:10:2) in our experiments is appropriate for analogue ices since water serves as a major constituent of interstellar ices.[53] However, as a strong infrared absorber, the water-rich ice obscures several newly emerging infrared absorptions, and the only products observed were diphosphine (P_2H_4) (ν_1 (2274 cm^{-1}), ν_3 (1067 cm^{-1})) and the ν(P–O) (1014 cm^{-1}) and ν(P=O) (1153 cm^{-1}) fundamentals; both latter assignments were verified via the shift of the peak positions using $H_2{}^{18}O$ (Table 6.S4). Previous infrared studies on irradiated ices of phosphine (PH_3), water (H_2O), and a hydrocarbon mixture of methane, ethane (C_2H_6), propane (C_3H_8), and butane (C_4H_{10}) utilized water-depleted ices.[206] Here, exposure to ionizing radiation led to several functional groups associated with alkyl phosphorus oxoacids including P–O, P=O, O–H, O=P–OH, P–CH_3, and P–O–CH_3. These results indicate that functional groups of alkyl phosphorus oxoacids result from the exposure of ices to ionizing radiation at 5 K, but since the infrared absorptions of individual alkyl phosphorus oxoacids fall in a similar range and, hence, overlap, infrared spectroscopy alone does not allow an identification of discrete and unique organic molecules such as alkyl phosphorus oxoacids.[203]

6.2.2 PI-ReTOF-MS

To probe individual alkyl phosphorus oxoacid isomers selectively, PI-ReTOF-MS was utilized. Here, the subliming alkyl phosphorus oxoacids were photoionized at discrete photon energies and identified according to their mass-to-charge (m/z) ratios. This requires the knowledge of the ionization energies for the alkyl phosphorus oxoacids along with their structural isomers (Figures 6.1 & 6.S6). Isomers for each molecular formula can be divided into two groups: isomers carrying the P=O functional group with ionization energies larger than 10 eV and isomers not containing the P=O moiety holding ionization energies less than 9 eV. Therefore, we selected first a photoionization energy of 10.49 eV to photoionize all isomers; thereafter, a photoionization energy of 9.93 eV was chosen to photoionize only the isomers without the P=O moiety. The mass spectra of the subliming molecules were recorded as a function of temperature and are compiled in Figure 6.S7; the sublimation temperatures, ion count intensities, and mass-to-charge ratios of the $H_2{}^{16}O/H_2{}^{18}O$ and $^{12}CH_4/^{13}CH_4$ bearing samples were analyzed to determinate the number of oxygen and carbon atoms based on their mass shifts (Table 6.S3).

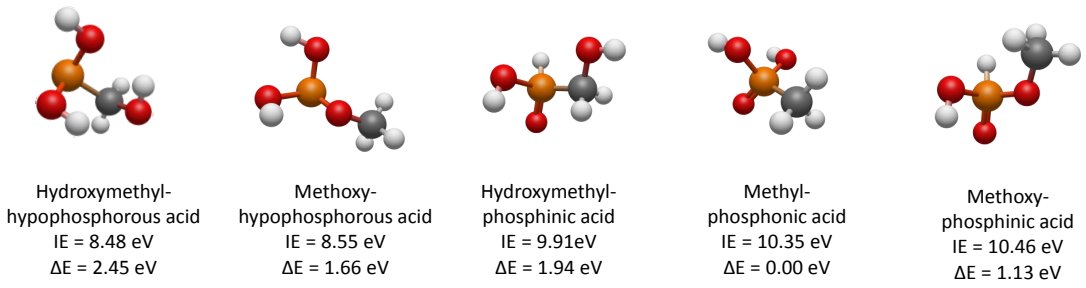

Figure 6.1. Adiabatic ionization energies (IE) and relative energies (ΔE) for distinct H_5CPO_3 isomers calculated at the CCSD(T)/CBS with B3LYP/ccpVTZ level of theory.

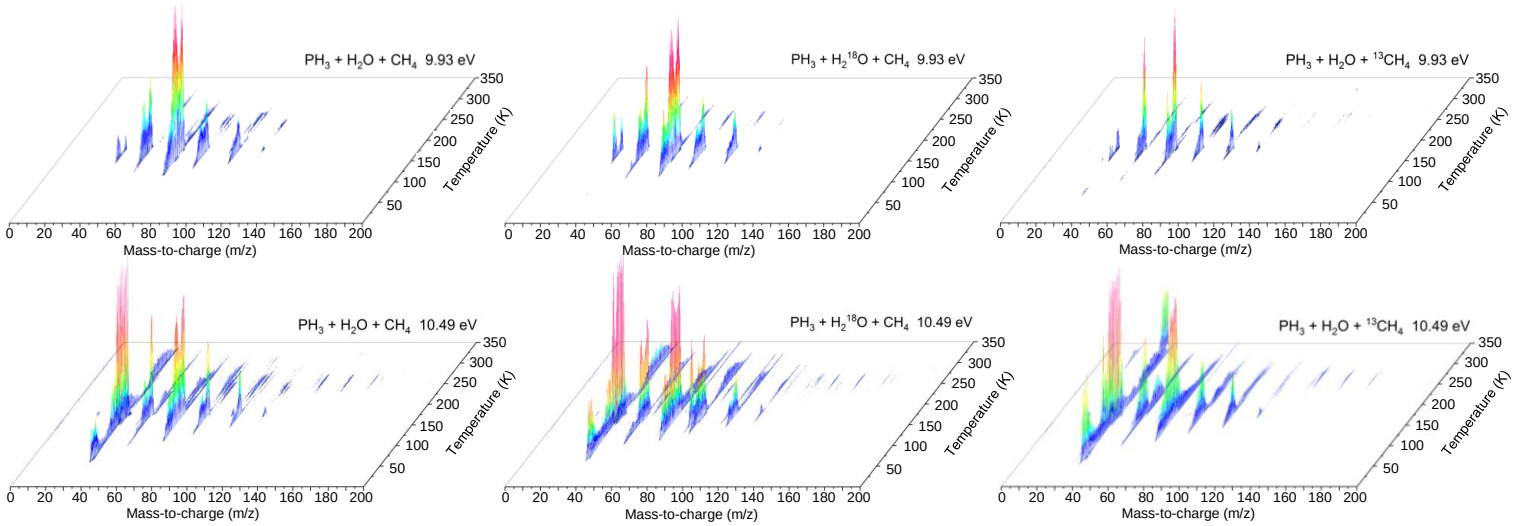

Figure 6.2. PI-ReTOF-MS data recorded at photon energies of 9.93 eV (top) and 10.49 eV (bottom) as a function of temperature of the newly formed products subliming into the gas phase from the irradiated $PH_3/H_2O/CH_4$ (left), $PH_3/H_2{}^{18}O/CH_4$ (center), and $PH_3/H_2O/{}^{13}CH_4$ (right) ices.

Considering the main focus of our work—the search for individual alkyl phosphonic acids—we are focusing first on ions linked to the molecular formula H_5CPO_3, which includes the methylphosphonic acid isomer ($CH_3P(O)(OH)_2$). In the $PH_3/H_2O/CH_4$ ices, this should lead to the observation of ion counts at m/z = 96 ($H_5CPO_3^+$) upon photoionization of the subliming molecules. Using ^{18}O labeling ($PH_3/H_2{}^{18}O/CH_4$), the signal should shift by 6 amu to m/z = 102 ($H_5CP^{18}O_3^+$) while ^{13}C labeling ($PH_3/H_2O/{}^{13}CH_4$) is anticipated to increase the ion counts by 1 amu to m/z = 97 ($H_5{}^{13}CPO_3^+$). The TPD profiles (Figure 6.3) recorded at a photoionization energy of 10.49 eV reveal clear signal at m/z = 96, 102, and 97 demonstrating that molecules with the molecular formulas H_5CPO_3, $H_5CP^{18}O_3$, and $H_5{}^{13}CPO_3$ are subliming from the irradiated $PH_3/H_2O/CH_4$, $PH_3/H_2{}^{18}O/CH_4$, and $PH_3/H_2O/{}^{13}CH_4$ ices, respectively (Figure 6.3). It should be stressed that blank studies—experiments conducted under identical conditions, but without irradiating the ices—do not depict any ion counts at these mass-to-charge ratios demonstrating that any signal at m/z = 96, 102, and 97 is linked to the processing of the ice samples by ionizing radiation. Let us inspect the TPD profiles in detail.

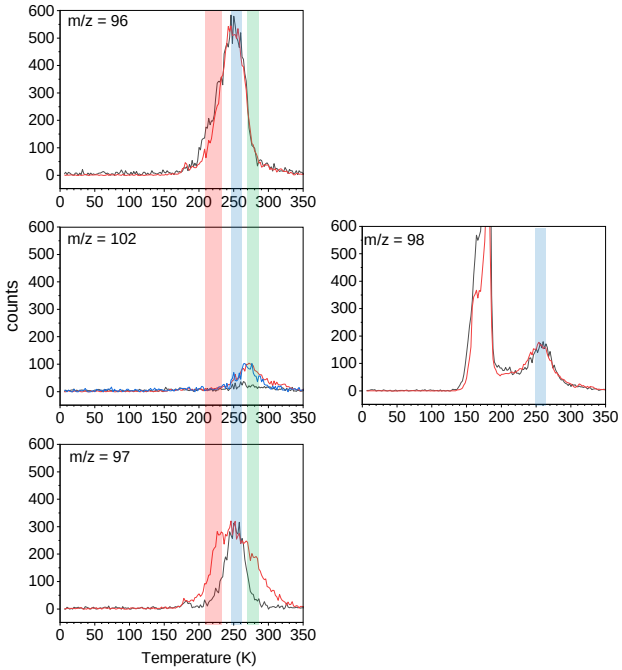

Figure 6.3. Temperature programmed desorption (TPD) profiles of photoionized H_5CPO_3 isomers along with their ^{18}O and ^{13}C substituted counterparts ($H_5CP^{18}O_3$, $H_5{}^{13}CPO_3$) recorded at m/z = 96, 102, and 97 subliming from the processed $PH_3 + H_2O + CH_4$ (top), $PH_3 + H_2{}^{18}O + CH_4$ (center), and $PH_3 + H_2O + {}^{13}CH_4$ (bottom) ices. The TPD profiles are shown for photon energies of 9.93 eV (black line), 10.35 eV (blue line), and 10.49 eV (red line). Colored bands indicate distinct sublimation events.

For the non-isotopically labeled ices ($PH_3/H_2O/CH_4$) at a photon energy of 10.49 eV, the signal at m/z = 96 appears as a single peak (Figure 6.3; red line). Ions at this mass-to-charge ratio can be linked to parent ions of the H_5CPO_3 isomers—potentially the desired methylphosphonic acid ($CH_3P(O)(OH)_2$)—and also to parent ions associated with H_6CP_2O isomers. The carrier(s) can be distinguished based on ^{18}O labeling. Here, H_5CPO_3 isomers (m/z = 96) would shift signal by 6 amu to m/z = 102 ($H_5CP^{18}O_3$), whereas the presence of H_6CP_2O isomers would only result in a shift by 2 amu to m/z = 98 ($H_6CP_2{}^{18}O$) due to the presence of three versus one oxygen atoms, respectively. A comparison of the TPD profile at m/z = 96 in the $PH_3/H_2O/CH_4$ ices with those recorded at m/z = 102 and 98 in the $PH_3/H_2{}^{18}O/CH_4$ ices reveals that the majority of the signal at m/z = 96 can be explained by H_6CP_2O isomers (70 %) (m/z = 98, red line), whereas close to 30 % of the ions originate from H_5CPO_3 isomers (m/z = 102, red line). A closer look at the TPD profile of m/z = 97 recorded for the $PH_3/H_2O/^{13}CH_4$ system at 10.49 eV reveals the presence of a single carbon atom. Further, as indicated in Figure 6.3, three sublimation events can be inferred from the TPD profile. The sublimation event peaking at 250 K agrees nicely with the sublimation event of the H_6CP_2O isomers (m/z = 96), whereas the sublimation peaking at 280 K correlates with the $H_5CP^{18}O_3$ isomers (m/z = 102); the sublimation starting at 180 K at m/z = 97 suggests hitherto unidentified less polar molecule(s). Therefore, the data recorded at a photon energy of 10.49 eV suggest that the sublimation event peaking at 280 K can be associated with the formation of H_5CPO_3 isomers. To assign the H_5CPO_3 isomer(s), additional experiments were conducted at photon energies of 9.93 eV and 10.35 eV (Figure 6.3). This is best visualized for the TPD trace at m/z = 102 for the $PH_3/H_2{}^{18}O/CH_4$ ices. Here, the TPD profiles for $H_5CP^{18}O_3{}^+$ overlap for 10.49 eV (red line) and 10.35 eV (blue line). No signal at m/z = 102 was observed at 9.93 eV (black line) indicating that the hydroxymethyl-hypophosphorous acid ($HOCH_2P(OH)_2$), methoxy-hypophosphorous acid ($CH_3OP(OH)_2$), and hydroxymethyl-phosphinic acid ($HOCH_2PH(O)OH$) isomers can be eliminated as products because their ionization energies are below 9.93 eV and hence signal should be observed at 9.93 eV upon photoionization if present. The 10.35 eV experiment can discriminate between the two remaining $H_5CP^{18}O_3$ isomers: methylphosphonic acid ($CH_3P(O)(OH)_2$) and methoxyphosphinic acid ($CH_3OPH(O)OH$) since the latter cannot be photoionized at this energy (IE = 10.46 eV).

Consequently, the signal at m/z = 102 recorded at 10.35 eV (blue line) confirms the synthesis of the methylphosphonic acid isomer via its molecular parent at m/z = 102 ($CH_3P(^{18}O)(^{18}OH)_2$). Note that besides methylphosphonic acid—the main target of this study—additional molecules were detected (*Supplementary Information*, Figure 6.S7). For the phosphorus oxoacids, hydroxyphosphine (H_2POH) and phosphinic acid ($H_2P(O)OH$) were probed revealing consistent results with ices of phosphine and water.[221] Besides methylphosphonic acid, methylphosphine oxide (CH_3PH_2O) and methoxyphosphine oxide (CH_3OPH_2O) were detected as well thus exposing the synthesis of a homologous series of three methyl-substituted phosphorus oxoacids: methylphosphine oxide (CH_3PH_2O), methoxyphosphine oxide (CH_3OPH_2O), and methylphosphonic acid ($CH_3P(O)(OH)_2$).

6.2.3 GC×GC-TOF-MS

Besides subliming into the gas phase, phosphorus bearing molecules may persist within the solid residues remaining after the ice sublimation in the course of the TPD phase to 320 K. These residues were solvated and analyzed utilizing GC×GC-TOF-MS (Figure 6.4, Tables 6.S1 & 6.S2). Phosphorus oxoacids and alkyl phosphonic acids were detected through a comparison of the dual retention times (R_{t1}×R_{t2}) on both columns along with the mass spectra of the trimethylsilyl derivatives based on the molecular ion (M^+) and the methyl loss channel ($M-15^+$) with known standards. Data were recorded for the residues formed from the $PH_3/H_2{}^{18}O/CH_4$ ices along with those remaining in the $PH_3/H_2O/{}^{13}CH_4$ ices.

First, trimethylsilylated derivatives of phosphonic acid (H_3PO_3) and of phosphoric acid (H_3PO_4) were identified with the molecular ion (M^+) at m/z = 226 and 314, respectively, along with the methyl loss pathways at m/z = 211 and 299, respectively in the solvated residues formed from the $PH_3/H_2O/{}^{13}CH_4$ ices. The molecular ion and methyl loss fragment for phosphoric acid ($H_3P^{18}O_4$) were also detected in the $PH_3/H_2{}^{18}O/CH_4$ system at m/z = 322 and 307, respectively. The mass shifts by 8 amu from 314 to 322 (M^+) and 299 to 307 ($M-15^+$) verify the presence of four oxygen atoms. For phosphonic acid (H_3PO_3), the fully ^{18}O labelled form ($H_3P^{18}O_3$) could not be observed since phosphonic acid is known to undergo a facile oxygen exchange upon hydrolysis. Instead, $H_3P^{16}O^{18}O_2$ could be monitored through its ($M-15^+$) ion at m/z = 215. Note that the phosphonic acid (H_3PO_3) calibration standard revealed

that the $(M-15)^+$ signal was more pronounced than the molecular ion (M^+) by a factor of about 30; therefore, the molecular ion peak was difficult to detect.

Second, three alkyl phosphonic acids were detected in the solvated residues. Methylphosphonic acid ($^{13}CH_3P(O)(OH)_2$) was observed via m/z = 241 (M^+) and 226 ($M-15^+$) in the solvated $PH_3/H_2O/^{13}CH_4$ residues. The mass shift by 1 amu compared to the methylphosphonic acid ($CH_3P(O)(OH)_2$) standard indicates the presence of only one carbon atom. In the solvated $PH_3/H_2{}^{18}O/CH_4$ residues, this signal shifts by 6 amu to m/z = 246 and 231 demonstrating that three oxygen atoms are present in this molecule. Ethylphosphonic acid ($C_2H_5P(O)(OH)_2$) and n-propylphosphonic acid ($C_3H_7P(O)(OH)_2$) were also detected in both solvated residues via their methyl loss fragments at m/z = 241 and 256 ($PH_3/H_2O/^{13}CH_4$) and 245 and 259 ($PH_3/ H_2{}^{18}O/CH_4$), respectively. Mass shifts compare to the standards by 6 amu indicate the presence of three oxygen atoms ($PH_3/ H_2{}^{18}O/CH_4$), whereas a mass increase by 2 amu and 3 amu ($PH_3/H_2O/^{13}CH_4$) verify two and three carbon atoms as predicted for the ethyl- and n-propylphosphonic acids, respectively. Therefore, based on a cross correlation of the retention times and the mass shifts in the ^{13}C and ^{18}O labelled ices, the formation of methyl, ethyl, and n-propylphosphonic acid could be established.

Third, the signal for methylphosphate ($^{13}CH_3OP(O)(OH)_2$) was detected in the solvated $PH_3/H_2O/^{13}CH_4$ residues through m/z = 257 and 242 for the molecular ion and methyl loss fragment, respectively. For the $PH_3/H_2{}^{18}O/CH_4$ system, only the $M-15^+$ signal was detected at m/z = 249 once again due to the lower intensity of the parent compared to the fragment. Likewise, in the $PH_3/H_2{}^{18}O/CH_4$ system, signal shifts by 8 amu from m/z = 241 to 249 indicating the presence of four oxygen atoms. Additionally, these mass spectra can be uniquely assigned to methylphosphate and not the hydroxymethyl-phosphonic acid isomer ($HOCH_2P(O)(OH)_2$) because methylphosphate acquires two trimethylsilyl groups during derivatization while three trimethylsilyl groups derivatize hydroxymethyl-phosphonic acid. This detection signifies the formation of a P(+V)–O–C bond as present in contemporary phosphorus-containing biomolecules.

Finally, it is important to quantify the yields of the phosphorus oxoacids and of the alkyl phosphonic acids. These are presented here for the $PH_3/H_2O/^{13}CH_4$ system considering the partial $^{16}O/^{18}O$ exchange as discussed above. For methyl-, ethyl, and n-propylphosphonic

acid, 280 ± 13 ng, 10 ± 2 ng, and 2.5 ± 0.6 ng were determined, which results in an alkyl phosphonic acid molar ratio of 150±6 : 5±1 : 1. This enhanced formation of methylphosphonic acid compared to ethylphosphonic acid is consistent with the analysis of the Murchison meteorite. Note that propyl- and butylphosphonic acid were detected in Murchison but were not quantified. Regarding the phosphorus oxoacids, 7.6 ± 0.1 μg of phosphoric acid (H_3PO_4) and 40 ± 5 ng of phosphonic acid (H_3PO_3) translate into a molar ratio of 150 ± 10 : 1. A comparison of these data with a detailed infrared spectroscopy analysis (*Supplementary Information*) indicates that 46 ± 9 % and 0.3 ± 0.1 % of the reacted phosphine was converted to phosphoric acid (H_3PO_4) and phosphonic acid (H_3PO_3), respectively. Likewise, conversion yields to methyl-, ethyl, and n-propylphosphonic acid were determined to be 1.7 ± 0.3 %, 0.05 ± 0.01 %, and 0.012 ± 0.002 %, respectively.

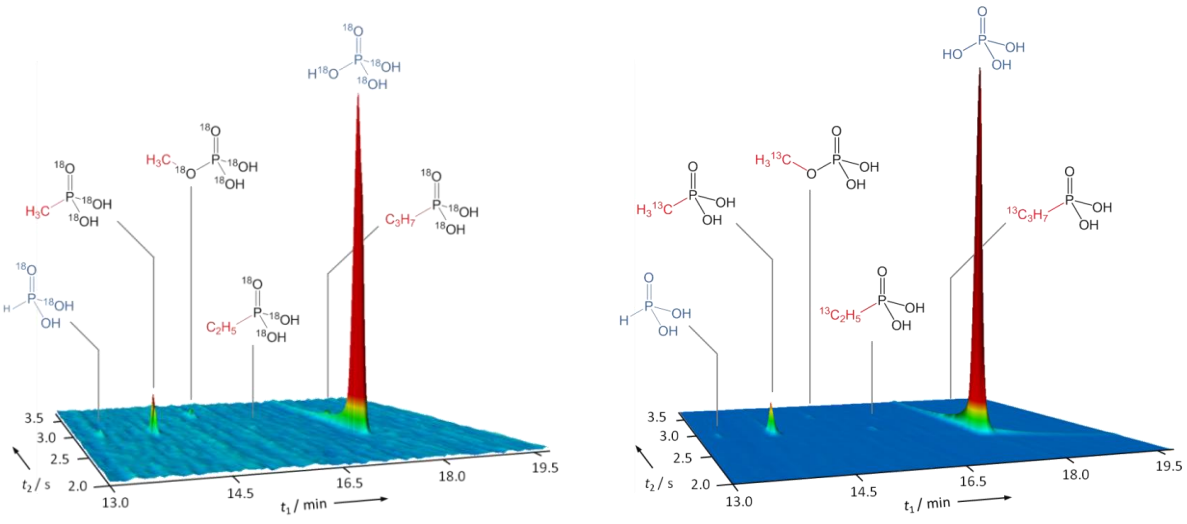

Figure 6.4. Organophosphorus compounds detected in the room temperature residues irradiated ices composed of $PH_3/H_2{}^{18}O/CH_4$ (left) and $PH_3/H_2O/{}^{13}CH_4$ (right) by multidimensional gas chromatography. Further details and scaled chromatograms provided in the *Supplementary Information* (Figures 6.S1 & 6.S2).

6.3 Conclusions

The present study provides compelling evidence on the facile synthesis of the three simplest alkyl phosphonic acids—methylphosphonic acid ($CH_3P(O)(OH)_2$), ethylphosphonic acid ($C_2H_5P(O)(OH)_2$), and n-propylphosphonic acid ($C_3H_7P(O)(OH)_2$)—upon interaction of ionizing radiation with phosphine-bearing interstellar analogue ices. The detection of these P(+III) compounds endorses the hypothesis that alkyl phosphonic acids—the *only* known organic phosphorus-containing molecules of extraterrestrial origin as detected in the Murchison meteorite and potential source of bioavailable phosphorus to Earth's first organisms—can be synthesized abiotically within mantles of interstellar icy grains as present in molecular clouds. The tentative identification of methylphosphonic acid ($CH_3P(O)(OH)_2$) further signifies the presence of P(+V) and the P–O–C backbone found in contemporary biomolecules. If confirmed, given the capacity for P(+V)–O–C bond formation in interstellar ice analogues of phosphine, water, and methane, the replacement of methane in these ice mixtures with sugars such as ribose or with glycerol would feasibly produce fundamental building blocks of biomolecules such as of RNA and DNA. In fact, recent studies demonstrated the favorable phosphorylation of sugars in microdroplets of aqueous phosphoric acid,[26] and the linkage of sugars with phosphoric acid in ices exposed to ionizing radiation would reasonably provide alternative phosphorylation routes in deep space. Alkyl phosphonic acids serve as a soluble reduced-oxidation state phosphorus-containing compound that Gulick[5] proposed as a prebiotic source of phosphorus, while methylphosphate demonstrates the ability of P(+V)–O–C linkages to form in interstellar ices and acts as a prototype for larger biomolecules carrying this moiety. Considering that molecular clouds signify nurseries of stars and planetary systems, the detection of alkyl phosphonic acids advocates that these molecules could have been at least partially delivered to our Solar System from their interstellar nurseries via circumstellar disks and incorporated in asteroids and comets prior to their delivery to Earth thus defining where in deep space phosphorus-bearing molecular precursors relevant to the *Origins of Life* might be synthesized.

6.4 Experimental Summary

Experiments were performed in an ultra-high vacuum chamber by depositing ices of phosphine (PH_3), water ($H_2O/H_2{}^{18}O$), and methane ($CH_4/{}^{13}CH_4$) with a ratio in the ice of 1:10:2 onto a polished silver mirror mounted to a copper cold finger capable of temperatures as low as 5 K.[69] The ice mixtures were irradiated with 5 keV electrons for 1 hour at 2.0 × 10^{12} electrons cm^{-1} s^{-1} and then heated at 1 K min^{-1} to 320 K. FTIR spectroscopy monitored the ices on line and *in situ* from 6000 to 500 cm^{-1}.[206] PI-ReTOF-MS probed the subliming molecules at photoionization energies of 10.49 eV, 10.35 eV, and 9.93 eV (*Supplementary Information*).[69] The residues that remained on the silver substrates at room temperature were extracted, derivatized with *N*,*O* bis(trimethylsilyl)-trifluoroacetamide (BSTFA) and trimethylsilyl chloride (TMCS), and, using helium as a carrier gas, passed through an Agilent J&W DB 5MS Ultra Inert primary column (10 m/13 m × 0.25 mm inner diameter (ID), 0.12 μm film thickness) connected to a DB Wax secondary column (1.4 m × 0.1 mm ID, 0.1 μm film thickness).[221] This two-dimensional gas chromatography utilized TOF-MS for detection. The theoretical calculations used the GAUSSIAN09 program to obtain the ionization energies and relative energies of the structural isomers at the CCSD(T)/CBS with B3LYP/ccpVTZ level of theory.[95]

6.5 Supplementary Information

6.5.1 Experimental Details

Experiments were performed in a stainless steel ultra-high vacuum chamber capable of achieving pressures as low as 8 × 10^{-11} Torr using magnetically suspended turbomolecular pumps (Osaka) backed by oil-free scroll pumps (Anest Iwata).[222] A polished silver mirror was mounted to a rotatable low-oxygen high-conductivity copper cold head that could reach temperatures as low as 5 K using a two-stage closed-cycle helium refrigerator (Sumitomo Heavy Industries, RDK-415E). A gaseous mixture of phosphine (PH_3, 99.9995 %) and methane (CH_4, 99.999 %) was deposited onto the cold silver target via a glass capillary array while water (H_2O, HPLC grade) was simultaneously deposited using a second array to form an ice with a 10:2:1 H_2O:CH_4:PH_3 composition ratio. Isotopically labeled water ($H_2{}^{18}O$, 99 atom % ^{18}O; Sigma Aldrich) and methane

($^{13}CH_4$, 99 atom % ^{13}C; Sigma Aldrich) were utilized in duplicate experiments to observe mass shifts of products. The thickness of the ice was determined using laser interferometry to be 750 ± 50 nm,[120] while the composition ratio utilized the integrated absorption coefficients of the infrared vibrational bands taken from a Nicolet 6700 Fourier Transform Infrared Spectrometer (FTIR) from 6000 to 500 cm^{-1} (*Infrared & Conversion Yields*).[206] The ices were irradiated with 5 keV electrons for one hour at 2.0 × 10^{12} electrons cm^{-1} s^{-1}, and the CASINO simulation[82] calculated the average penetration depth to be 270 nm with a maximum penetration depth of 630 nm, which is less than the ice thickness, and resulted in an average dose of 27 ± 6 eV $molecule^{-1}$. After irradiation, the ices were annealed using a controlled temperature programmed desorption (TPD) scheme at 1 K min^{-1} to 320 K and then held constant for one hour. Blank experiments were also performed following the same procedures but without the electron irradiation. The subliming molecules were detected using photoionization reflectron time-of-flight mass spectrometry (PI-ReTOF-MS, Jordan TOF Products, Inc.).[69] The experiments were performed at two distinct vacuum ultraviolet (VUV) photoionization energies generated via four-wave mixing: the first at 10.49 eV ($\omega_{VUV} = 3\omega_1$) using the third harmonic (ω_1, 354.6 nm) of a neodymium-doped yttrium aluminum garnet laser (Nd:YAG, Spectra Physics, PRO-250, 30 Hz) and xenon as the non-linear medium. The second photoionization energy at 9.93 eV ($\omega_{VUV} = 2\omega_1 - \omega_2$) was prepared by combining the output from the Nd:YAG laser's second harmonic (ω_1, 532 nm) and from a second Nd:YAG laser, which used 532 nm to pump a Rhodamine 610/640 dye solution to produce 607 nm, which after undergoing a tripling process (ω_2, 202 nm) was mixed with ω_1 using krypton as the non-linear medium. The VUV photons were separated from the other photons using a lithium fluoride biconvex lens (ISP Optics) and passed 1 mm above the ice mixture. The ReTOF-MS analyzed any ionized molecules by correlating the arrival time with mass-to-charge ratios with an amplified signal from a fast preamplifier (Ortec 9305) and 4 ns bin width triggered at 30 Hz (Quantum Composers, 9518). The three experimental ice mixtures were $PH_3/H_2O/CH_4$, $PH_3/H_2{}^{18}O/CH_4$, and $PH_3/H_2O/{}^{13}CH_4$. Each was irradiated with 5 keV electrons and then heated from 5 K to 320 K at 1 K min^{-1}. The subliming molecules were photoionized using 10.49 and 9.93 eV photons for detection

with the ReTOF-MS. An additional experiment at 10.35 eV was performed for the $PH_3/H_2{}^{18}O/CH_4$ mixture, while the $PH_3/H_2O/CH_4$ mixture was also subjected to a non-irradiation "blank" experiment at 10.49 eV photoionization energy. The blank experiment found no products at all, which confirms that irradiation is necessary for reactions.

6.5.2 GC×GC-TOFMS Analysis

Sample-handling glassware was wrapped in aluminum foil and heated at 773 K for 5 h prior to usage. Eppendorf tips were sterile and the water used for extraction, standard solutions, and blanks had been prepared by a Millipore Super-Q water filter system (4 ppb total organic carbon). The derivatization reagent N,O-bis(trimethylsilyl) trifluoroacetamide (BSTFA) with 1% trimethylsilyl chloride (TMCS), the internal standard methyl laurate, hexane, as well as phosphorus standards (methylphosphonic acid, ethylphosphonic acid, n-propylphosphonic acid, phosphonic acid ($HPO(OH)_2$), and phosphoric acid (H_3PO_4)) were purchased from Sigma Aldrich. The residues were extracted with 10 × 50 µL water from their silver wafers and transferred into conical reaction vials (1 mL V-Vial, Wheaton). The aqueous extracts were dried under a gentle stream of nitrogen and silylated with an excess of 50 µL BSTFA / TMCS (99 : 1) for 90 min at 338 K. The mixtures were cooled to room temperature and subsequently dried under a gentle stream of nitrogen. A final volume of 30 µL of the internal standard methyl laurate in hexane was added to each reaction vial, mixed with a vortex mixer and transferred into GC vials prior their analyses by two-dimensional gas chromatography time-of-flight mass spectrometry (GC×GC-TOFMS). Procedural blanks were run in sequence to each sample in order to monitor significant background interferences. The multidimensional analysis was carried out by a GC×GC Pegasus IV D instrument coupled to a time-of-flight mass spectrometer (LECO Corp.). The MS system operated at a storage rate of 150 Hz, with a 25–400 amu mass range, a detector voltage of 1.5 kV, and a solvent delay of 12 min. Ion source and injector temperatures were set to 503 K. The column set consisted of a DB-5ms Ultra Inert column (30 m × 0.25 mm, 0.25 µm film thickness) in the first dimension and a DB Wax in the second dimension (1.4 m × 0.1 mm, 0.1 µm film thickness, Agilent J&W). Helium was used as carrier gas at a constant flow of 1 mL min^{-1}. All samples and

standard compounds were injected with an identical temperature program in the splitless mode. The temperature of the primary column was held at 313 K for 1 min then increased to 488 K at a rate of 5 K min^{-1} followed by an isothermal hold for 4 min. The secondary oven used a temperature off-set of 288 K. A modulation period of 4 s was applied. All standard compounds used to produce calibration curves were injected 3 times and each residue sample 6 times in order to accurately calculate peak areas with reliable statistical error bars. Data were processed using the LECO Corp. Chroma TOFTM software. Compound identification was performed by comparison with the chromatographic retention in both dimensions and mass spectra of authentic standards (Tables 6.S1 & 6.S2, Figures 6.S1–6.S5).

Table 6.S1. Identified alkylphosphonic acids and phosphorus oxoacids as trimethylsilyl (TMS) derivatives by GC×GC-TOF-MS.

Compound	R_{t1} [a] [min]	R_{t2} [b] [sec]	PH_3/ $H_2{}^{18}O$/ CH_4		PH_3/H_2O/$^{13}CH_4$		Standards (^{12}C/^{16}O)	
			$[M^{+\bullet}]$	$[M-15]^{+\bullet}$	$[M^{+\bullet}]$	$[M-15]^{+\bullet}$	$[M^{+\bullet}]$	$[M-15]^{+\bullet}$
Phosphonic acid	13.24	2.92	n.d.	215[c]	226	211	226	211
Methylphosphonic acid	14.20	2.92	246	231	241	226	240	225
Methylphosphate	15.28	3.43	n.d.	249	257	242	256[d]	241[d]
Ethylphosphonic acid	16.12	3.16	n.d.	245	n.d.	241	254	239
n-Propylphosphonic acid	17.52	3.00	n.d.	259	n.d.	256	268	253
Phosphoric acid	17.48	2.68	322	307	314	299	314	299

[a]GC×GC retention time 1st dimension. [b]GC×GC retention time 2nd dimension. [c]Corresponds to the daughter ion of $H_3P^{16}O^{18}O_2$. [d]Standards commercially unavailable.

Table 6.S2. Quantities of identified alkylphosphonic acids and phosphorus oxoacids in different ice mixtures, and the irradiation yield (molecules eV^{-1}).

Compound	Molecular Formula	PH_3/ H_2O/ $^{13}CH_4$ (nmol)[a]	yield (molecules eV^{-1})
Phosphonic acid	$HPO(OH)_2$	0.53 ± 0.06	$1.4 \pm 0.5 \times 10^{-7}$
Methylphosphonic acid	$CH_3P(O)(OH)_2$	2.90 ± 0.13	$7.4 \pm 2.5 \times 10^{-7}$
Methylphosphate	$CH_3OP(O)(OH)_2$	0.09 ± 0.01	$2.3 \pm 0.8 \times 10^{-8}$
Ethylphosphonic acid	$C_2H_5P(O)(OH)_2$	0.09 ± 0.02	$2.3 \pm 1.2 \times 10^{-8}$
n-Propylphosphonic acid	$C_3H_7P(O)(OH)_2$	0.02 ± 0.004	$5 \pm 2 \times 10^{-9}$
Phosphoric acid	H_3PO_4	78 ± 1	$2.0 \pm 0.7 \times 10^{-5}$

The data are mean values from two-dimensional gas chromatographic analyses (n = 6) based on $[M-15]^{+\bullet}$; errors shown are 1 σ standard deviations.

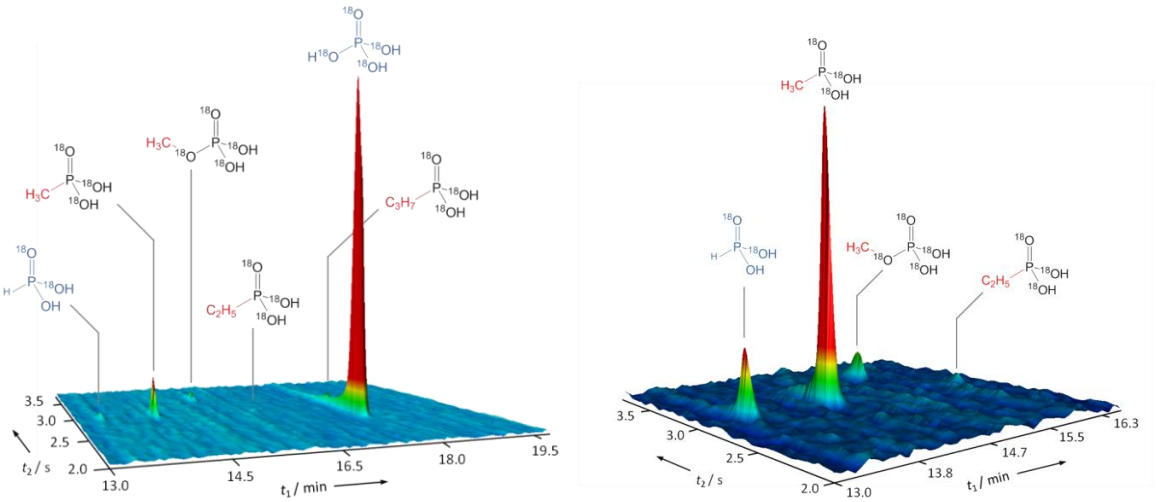

Figure 6.S1. Organophosphorus compounds detected in the room temperature residues irradiated ices composed of $PH_3/H_2{}^{18}O/CH_4$ by multidimensional gas chromatography. Atomic mass units m/z 215 (×20), 231 (×10), 247 (×20), 245 (×20), 259 (×30), and 307 were selected for the above representation with z-scaling = 160,000. Right: Partial GC×GC chromatogram of detected organophosphorus compounds. Atomic mass units m/z 213, 215, 229, 231, 241, 243 (×10), 245 (×10) were selected with z-scaling = 14,000.

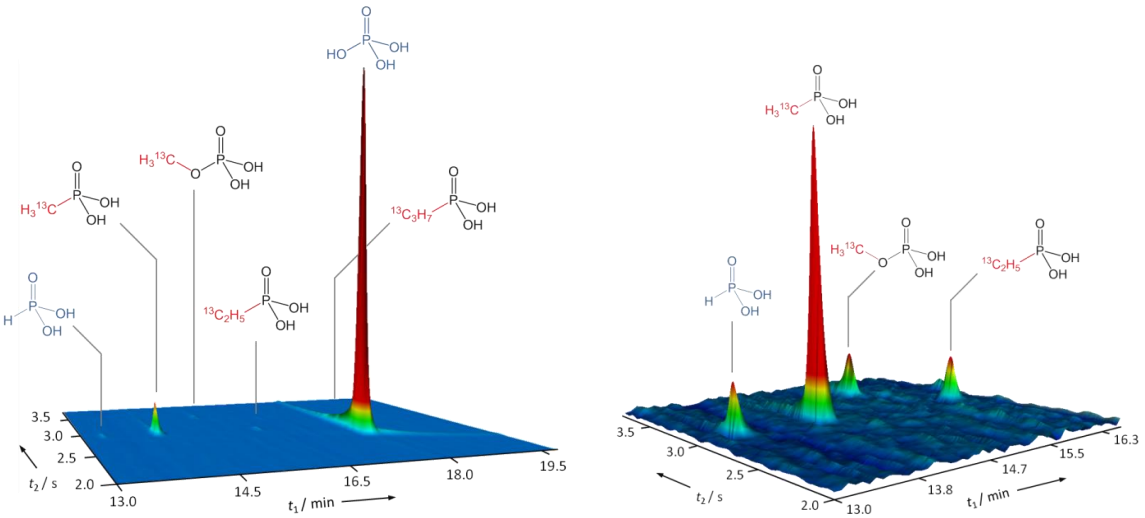

Figure 6.S2. Organophosphorus compounds detected in the room temperature residues irradiated ices composed of $PH_3/H_2O/{}^{13}CH_4$ by multidimensional gas chromatography. Atomic mass units m/z 211×5, 226×5, 242×10, 241×10, 256, and 299 were selected for the above representation with z-scaling = 260,000. Right: Partial GC×GC chromatogram of detected organophosphorus compounds. Atomic mass units m/z 211 (×5), 226, 242 (×10), 241 (×10) were selected with z-scaling = 13,000.

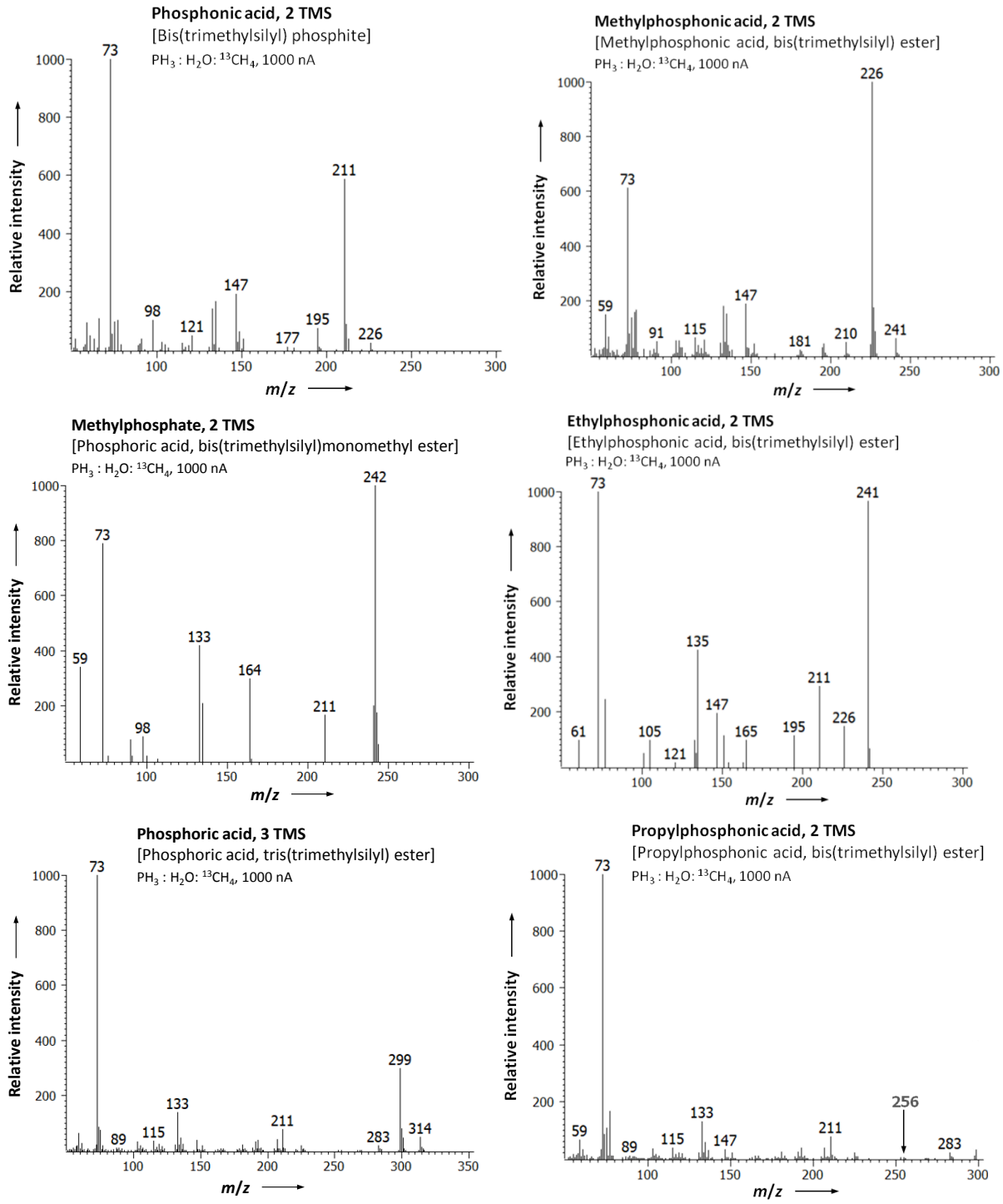

Figure 6.S3. Time-of-flight mass spectra of silylated phosphorus compounds identified in the residue from irradiated ices of $PH_3/H_2O/^{13}CH_4$. The $[M-15]^+$ ion has been used for mass spectral deconvolution.

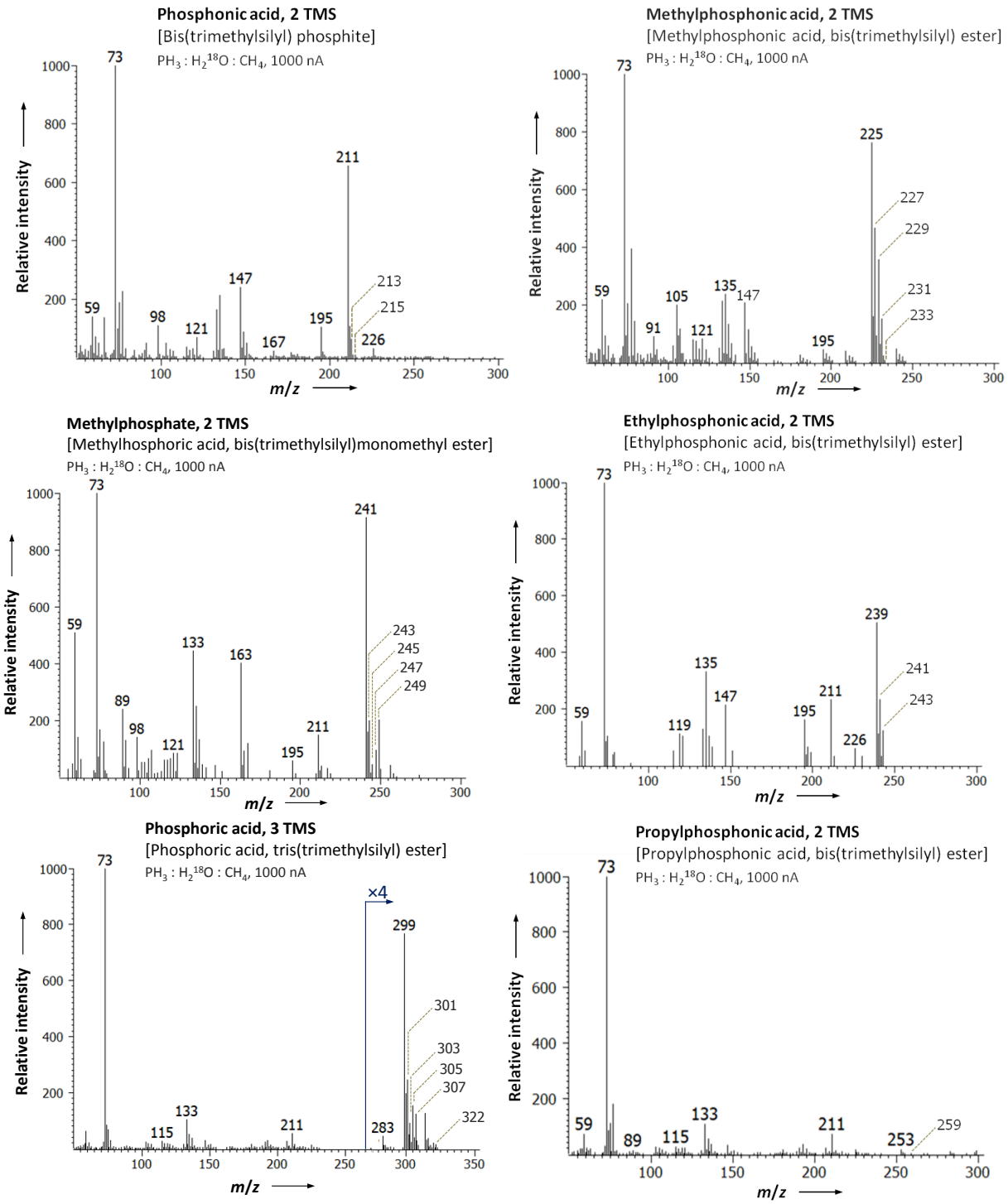

Figure 6.S4. Time-of-flight mass spectra of silylated phosphorus compounds in the residue from irradiated ices of $PH_3/H_2{}^{18}O/CH_4$. The $[M–15]^+$ ion has been used for mass spectral deconvolution.

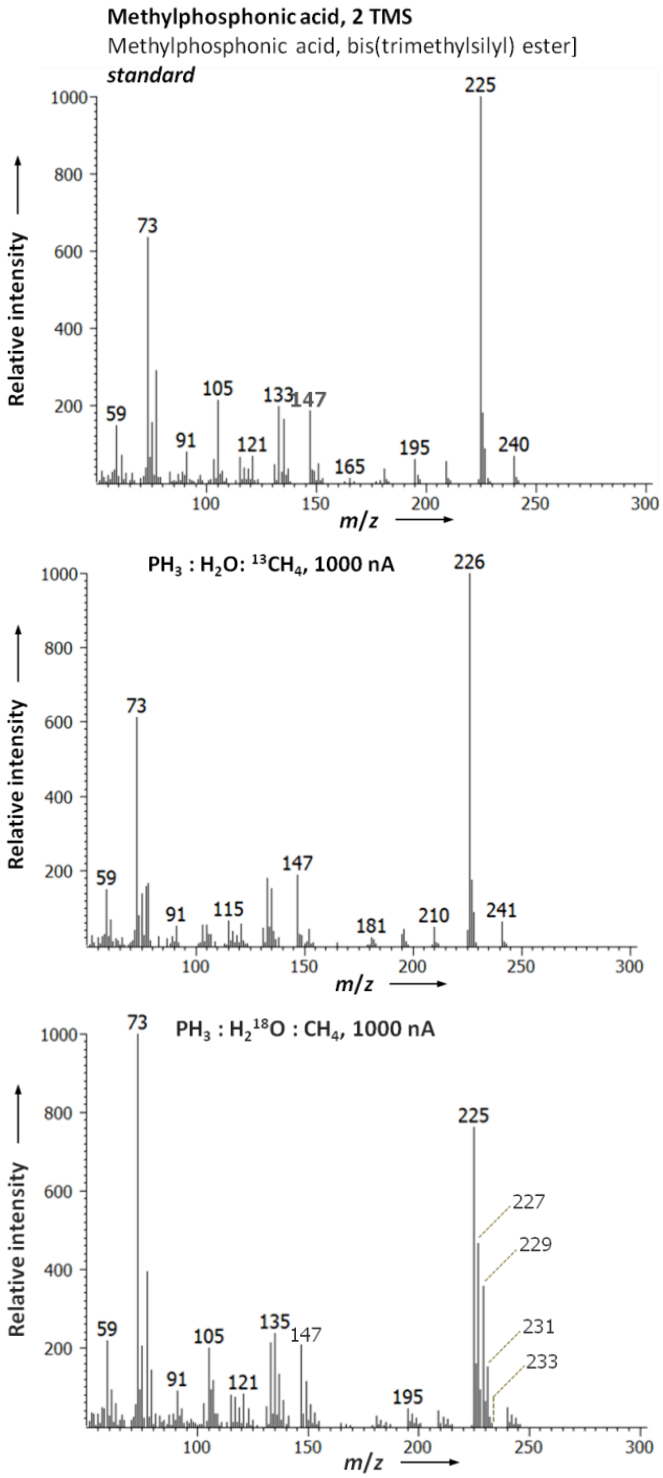

Figure 6.S5. Time-of-flight mass spectra of silylated methylphosphonic acid identified in residues of ices $PH_3/H_2{}^{18}O/\ CH_4$ (bottom) and $PH_3/H_2O/{}^{13}CH_4$ (center) to the reference standard (top) derivatized and analyzed identically. The $[M–15]^+$ ion has been used for mass spectral deconvolution.

6.5.3 Theoretical Methods

For the theoretical calculations (Figure 6.S6), the geometries of neutral molecules and cations were optimized by the hybrid density functional B3LYP[85-88] with the cc-pVTZ basis set and thus obtained the harmonic frequencies. Their coupled cluster[89-92] CCSD(T)/cc-pVDZ, CCSD(T)/ccpVTZ, and CCSD(T)/cc-pVQZ energies were then calculated and extrapolated to completed basis set limits,[213] CCSD(T)/CBS, with B3LYP/cc-pVTZ zero-point energy corrections. The adiabatic ionization energies were computed by taking the energy difference between the ionic and the neutral states that correspond to similar conformation. At this level of theory, the adiabatic ionization energies are within 0.08 eV. The GAUSSIAN09 program[95] was utilized in the electronic structure calculations.

6.5.4 PI-ReTOF-MS Results

The detection of subliming molecules via photoionization reflectron time-of-flight mass spectrometry (PI-ReTOF-MS) with molecular formulas consistent with methyl phosphorus oxoacids include H_5CPO (m/z = 64), H_5CPO_2 (m/z = 80), H_5CPO_3 (m/z = 96), and H_5CPO_4 (m/z = 112) (Figure 6.S7). Isomers can be determined by tuning the photon energy to exclude specific isomers as described above in *Experimental Details*. The results for H_5CPO_4, H_5CPO_2, and H_5CPO are presented below, while section 6.2.2 discusses the results of H_5CPO_3 with the methylphosphonic acid isomer being the main topic of the preset investigation.

H_5CPO_4. H_5CPO_4 has two structural isomers (m/z = 112, 113 (^{13}C), 120 (^{18}O)): methylphosphate ($CH_3OP(O)(OH)_2$) (**XVII**) and hydroxylmethyl-phosphonic acid ($HOCH_2P(O)(OH)_2$) (**XVI**). Signal at m/z = 112 ($PH_3/H_2O/CH_4$) and 113 ($PH_3/H_2O/^{13}CH_4$) can also contribute from H_7CP_3 isomers like methyltriphosphane ($CH_3P_3H_4$), whereas ion counts at m/z = 120 ($PH_3/H_2{}^{18}O/CH_4$) originate from $H_5CP^{18}O_4$. However, the lack of any ion counts at m/z = 120 at photon energies of 10.49 eV, which is above the adiabatic ionization energy of both H_5CPO_4 isomers, leads to the conclusion that the H_5CPO_4 isomers are either not formed or that their vapor pressure is too low to be detected in the gas phase.

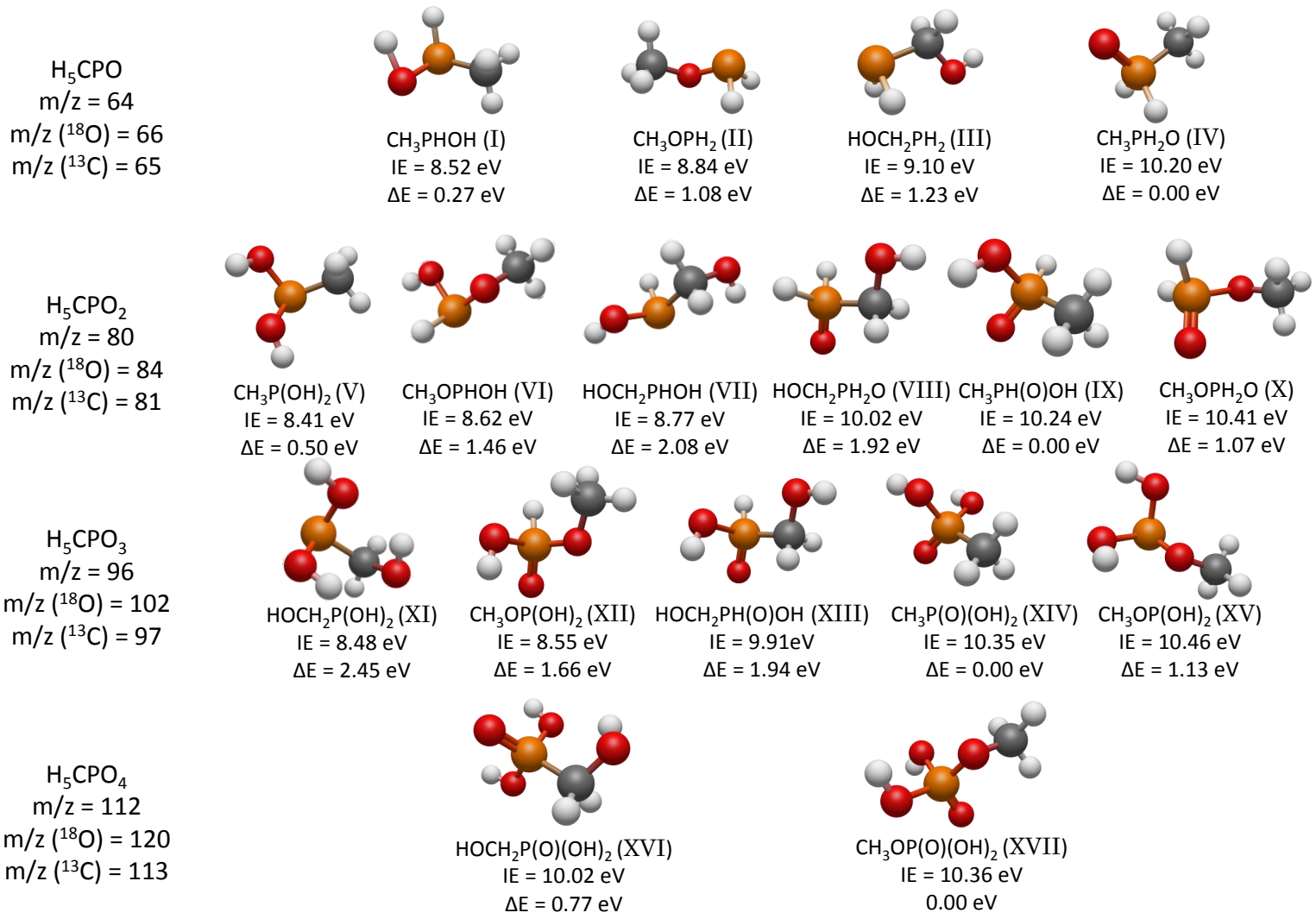

Figure 6.S6. Calculated ionization energies (IE) and relative isomeric energies (ΔE) for the isomers of H_5CPO, H_5CPO_2, H_5CPO_3, and H_5CPO_4

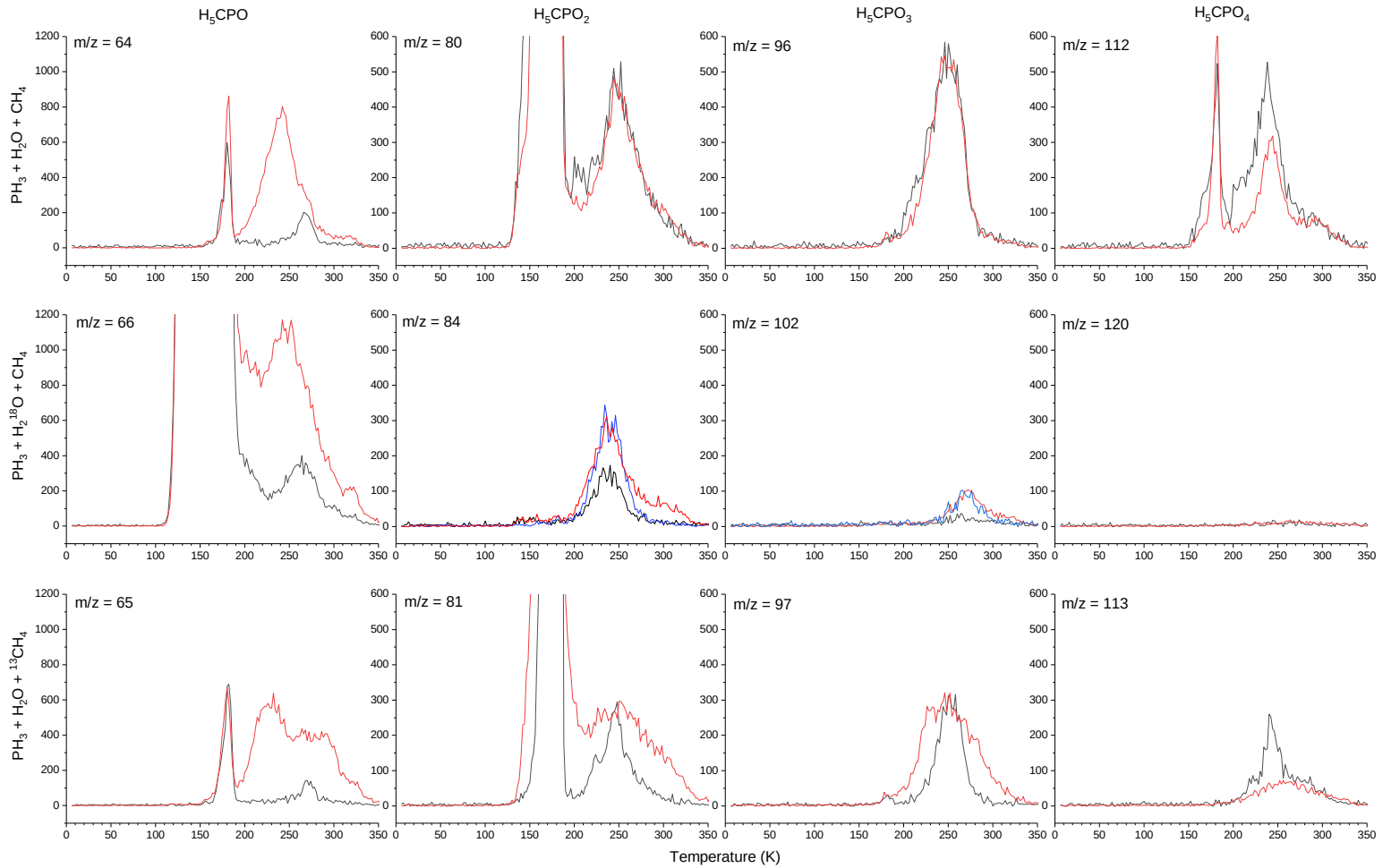

Figure 6.S7. Temperature programmed desorption profiles showing ion counts as a function of temperature for $PH_3 + H_2O + CH_4$ (top), $PH_3 + H_2{}^{18}O + CH_4$ (center), and $PH_3 + H_2O + {}^{13}CH_4$ (bottom) associated with the mass-to-charge ratios (m/z) of H_5CPO (m/z = 64, 66 (^{18}O), 65 (^{13}C)), H_5CPO_2 (m/z = 80, 84 (^{18}O), 81 (^{13}C)), H_5CPO_3 (m/z = 96, 102 (^{18}O), 97 (^{13}C)), and H_5CPO_4 (m/z = 112, 120 (^{18}O), 113 (^{13}C)). Temperatures increased to 320 K and were held constant after. The signals are shown for 9.93 eV (black), 10.35 eV (blue), and 10.49 eV (red) photoionization energy.

H_5CPO_2. The molecular formula H_5CPO_2 (m/z = 80, 81 (^{13}C), 84 (^{18}O)) may account for six isomers. Three isomers have ionization energies above 9.93 eV: methoxyphosphine oxide (CH_3OPH_2O) (**X**), hydroxymethylphosphine oxide ($HOCH_2PH_2O$) (**VIII**), and methylphosphinic acid ($CH_3PH(O)OH$) (**IX**). The remaining three isomers hold ionization energies below 9.93 eV: methoxy-hydroxyphosphine (CH_3OPHOH) (**VI**), hydroxymethyl-hydroxyphosphine ($HOCH_2PHOH$) (**VII**), and methyl-hypophosphorous acid ($CH_3PH(OH)_2$) (**V**) (Figure 6.S6). The TPD profiles show three sublimation events peaking at about 160 K and 250 K and depicting a shoulder at about 300 K. Note that signal at m/z = 80 could also originate from H_6CP_2 isomers such as methyldiphosphine ($CH_3P_2H_3$). This should be mirrored in signal at m/z = 81 in the $PH_3/H_2O/^{13}CH_4$ system ($^{13}CH_3P_2H_3$). Indeed, a comparison of the TPD profiles and of the early sublimation event peaking at 160 K in particular of m/z = 80 and n/z = 81 suggests the presence of methyldiphosphine ($CH_3P_2H_3$) and ^{13}C-methyldiphosphine ($^{13}CH_3P_2H_3$), respectively, which is absent in the $PH_3/H_2{}^{18}O/CH_4$ system at m/z = 84. Considering the late sublimation event at 250 K, which can be detected in all systems even when lowering the photon energy to 9.93 eV indicates that at least one isomer with an ionization energy less than 9.93 eV is formed (**V**, **VI**, and/or **VII**). Likewise, the shoulder at 300 K disappears in the $PH_3/H_2{}^{18}O/CH_4$ system when lowering the photon energy to 10.35 eV. Therefore, a second isomer must have an ionization energy between 10.49 eV and 10.35 eV, i.e. methoxyphosphine oxide (CH_3OPH_2O) (**X**).

Table 6.S3. PI-ReTOF-MS products detected from irradiation of the PH_3 + H_2O + CH_4 ice mixture and confirmed using $H_2{}^{18}O$ and $^{13}CH_4$.

Molecular Formula	m/z	Molecular Formula	m/z
H_5CP^+	48	$H_6CP_2O^+$	96
H_3PO^+	50	$H_5CPO_3^+$	96
$H_6C_3O^+$	58	$P_3H_5^+$	98
$H_7C_2P^+$	62	$H_7CP_3^+$	112
H_5CPO^+	64	$H_4P_3O^+$	113
$P_2H_4^+$	66	$H_5P_3O^+$	114
$H_7C_2PO^+$	78	$H_5CP_3O^+$	128
$H_6CP_2^+$	80	$H_5P_2O_4^+$	131
$H_7C_2PO^+$	80	$H_6C_2P_2O_3^+$	140
$H_5CPO_2^+$	80	$H_7CP_2O_4^+$	145
$H_4P_2O^+$	82	$H_9C_2P_2O_4^+$	159
$H_9C_3PO^+$	92	$H_6P_3O_4^+$	163
$H_8C_2P_2^+$	94	$H_8CP_3O_4^+$	177

H_5CPO. The simplest of the one-carbon phosphorus oxoacids, H_5CPO (m/z = 64, 65 (^{13}C), 66 (^{18}O)) can have four isomers: methylhydroxyphosphine (CH_3PHOH) (**I**), methoxyphosphine (CH_3OPH_2) (**II**), hydroxymethylphosphine ($HOCH_2PH_2$) (**III**), and methylphosphine oxide (CH_3PH_2O) (**IV**). Three notable sublimation events are seen at 10.49 eV at m/z = 64 with peaks at 170 K, 240 K, and 270 K (Figure 6.S7), although the 170 K peak is obscured in the $PH_3/H_2{}^{18}O/CH_4$ system by the intense signal at m/z = 66 for diphosphine (P_2H_4). The sublimation events at 170 K ($PH_3/H_2O/CH_4$ and $PH_3/H_2O/{}^{13}CH_4$ systems) and 270 K remain at 9.93 eV ionization energy, while the 240 K event vanishes. This confirms the formation and sublimation of methylphosphine oxide (CH_3PH_2O, IE = 10.20) (**IV**) via the sublimation event at 240 K and the possibility of at least two of the other three isomers that all have ionization energies less than 9.93 eV (**I**, **II**, **III**).

6.5.5 Infrared & Conversion Yields

The reactant ratio of the ice was determined using the vibrational modes and absorption coefficients (*A*) for phosphine (ν_2, 983 cm^{-1}, A = 5.1 × 10^{-17} cm $molecules^{-1}$ and ν_4, 1103 cm^{-1}, A = 7.1 × 10^{-17} cm $molecules^{-1}$), methane (ν_3, 3006 cm^{-1}, A = 6.6 × 10^{-18} cm $molecules^{-1}$ and ν_4, 1300 cm^{-1}, A = 1.3 × 10^{-18} cm $molecules^{-1}$), and water (ν_L, 765 cm^{-1}, A = 2.7 × 10^{-17} cm $molecules^{-1}$ and ν_2, 1642 cm^{-1}, A = 9.8 × 10^{-17} cm $molecules^{-1}$).[120,206] For this determination, the refractive index and density of phosphine (*n* = 1.51, 0.90 g cm^{-3}), [83,120] methane (*n* = 1.34, 0.45 g cm^{-3}),[168] and water (*n* = 1.29, 0.94 g cm^{-3})[80,169] were also utilized. After irradiation, only 33 ± 4 % of the phosphine remained, while 69 ± 3 % of methane and 75 ± 10 % of water did not react. Although two-thirds of phosphine reacted, the initial ratios of 1:10:2 (PH_3:H_2O:CH_4) indicate that approximately equal amounts of phosphine and methane were destroyed while four times as much water reacted. Quantitatively, 180 ± 40 nmol (1.1 ± 0.3 × 10^{17} molecules) of phosphine and 160 ± 40 nmol (9 ± 2 × 10^{16} molecules) of methane were consumed while 650 ± 150 nmol (4.0 ± 0.9 × 10^{17} molecules) of water reacted. The 1:1:4 (PH_3:CH_4:H_2O) reaction ratio is similar the stoichiometric ratio of methylphosphate ($CH_3OP(O)(OH)_2$) or methylphosphonic acid ($CH_3P(O)(OH)_2$) in excess oxygen, and thus assuming the exclusive formation of either of these products, about 170 nmol (1 × 10^{17} molecules) could be produced with 4.3 ± 1.5 ×

10^{-4} molecules eV^{-1} efficiency. Compared to this theoretical value, the GC×GC-TOFMS analysis (Table S4) detected 2.90 ± 0.13 nmol of methylphosphonic acid (1.7 % yield) and 78 ± 1 nmol of phosphoric acid (46 % yield) in the $PH_3/H_2O/^{13}CH_4$ system. This is equivalent to 7.3 ± 2.5 × 10^{-7} molecules eV^{-1} of methylphosphonic acid and 2.0 ± 0.7 × 10^{-5} molecules ev^{-1} of phosphoric acid. When accounting for the quantities of phosphonic acid (0.53 nmol, 0.3 ± 0.1 % yield), methylphosphate (0.09 nmol, 0.05 ± 0.1 % yield), ethylphosphonic acid (0.09 nmol, 0.05 ± 0.1 % yield), and n-propylphosphonic acid (0.02 nmol, 0.012 ± 0.002 % yield), nearly half of the reacted phosphorus can be accounted for by these compounds in the residue. In terms of irradiation efficiency, phosphonic acid, methylphosphate, ethylphosphonic acid, and n-propylphosphonic acid yielded 1.4 ± 0.5 × 10^{-7} molecule eV^{-1}, 2.3 ± 0.8 × 10^{-8} molecule eV^{-1}, 2.3 ± 1.2 × 10^{-8} molecule eV^{-1}, and 5 ± 2 × 10^{-9} molecule eV^{-1}, respectively. Much of the remaining phosphorus sublimed during TPD as diphosphine, triphosphane, and methylphosphine. Thus, methylphosphonic acid was found to be the second most abundant product of the residue after phosphoric acid and several times more abundant than non-methylated phosphonic acid.

Table 6.S4. Infrared absorption peaks before and after irradiation for $PH_3 + H_2O/H_2{}^{18}O + CH_4/^{13}CH_4$.

Pristine ice, before irradiation (5 K)			
Assignment	Position with $^{16}O/^{12}C$ (cm^{-1})	Position with $^{18}O/^{12}C$ (cm^{-1})	Position with $^{16}O/^{13}C$ (cm^{-1})
H_2O (ν_L)	764	731	775
PH_3 (ν_2)	983	982	982
PH_3 (ν_4)	1103	1104	1105
CH_4 (ν_4)	1300	1300	1293
H_2O (ν_2)	1644	1647	1648
PH_3 (ν_1/ν_3)	2311	2305	2315
CH_4 (ν_3)	3006	3006	2997
H_2O (ν_1/ν_3)	3224	3198	3231
CH_4 ($\nu_1 + \nu_4$)	4200	4199	4192
CH_4 ($\nu_3 + \nu_4$)	4297	4296	4281
New peaks after irradiation (5 K)			
ν(P–O)	1014	1034	1008
P_2H_4 (ν_3)	1067	1072	1070
ν(P=O)	1153	1132	1155
P_2H_4 (ν_1)	2275	n.d.	2280

6.5.6 Comment on Methylphosphate Detection

Although methylphosphate was not detected on the Murchison meteorite, Cooper et al. note that the C–P bond of the alkylphosphonic acids provides substantial stability compared to the phosphate ester bond of methylphosphate, so much so that some phosphonic acids have been shown to persist through heating in hot hydrochloric acid.[7] However, acids are known to hydrolyze esters,[223] and the use of hydrochloric acid in the sample preparation of the Murchison meteorite may have destroyed any alkyl phosphates originally present in the meteorite. Therefore, our detection of methylphosphate provides evidence that organic phosphates can also be synthesized in interstellar ices alongside organic phosphonates and subsequently incorporated into the early solar system, but these may not have been detected on the Murchison meteorite yet possibly due to the sample preparation.

6.5.7 Reaction Mechanisms

Having established the synthesis of methylphosphonic acid via PI-ReTOF-MS and GC×GC–TOFMS, we now consider possible formation mechanisms toward this product. It should be noted that these reactions were carried out in the condensed (ice) phase, but not under single collision conditions in the gas phase. Therefore, it is *not* feasible (neither in our lab nor worldwide) to determine the efficiency of each proposed elementary reaction (oxidation step) involved in the formation of methylphosphonic acid, for instance. This would require pulse-probe experiments with femtosecond (few 10 fs pulses) electron pulses penetrating the ice sample. These experiments do not exist yet. However, based on the molecular structures of the reactants and products ($CH_3P(O)(OH)_2$), we identify two potential routes essentially involving the oxidation of methylphosphine (CH_3PH_2) (route I) or the reaction of methane with phosphonic acid $HP(O)(OH)_2$ (route II).

Reaction Mechanisms – Route I: Previous studies[187] on the irradiation of phosphine with methane (CH_4) and deuterated methane (CD_4) ice mixtures demonstrated that radical recombination of the phosphino (PH_2) radical with the methyl radical (CH_3) was the dominant pathway (77%) toward the formation of methylphosphine (CH_3PH_2)

compared to carbene (CH_2) insertion into phosphine (8%) or phosphinidene insertion into methane (15%) in processed methane-phosphine ices.

$$CH_4 \rightarrow CH_3 + H(^2S) \qquad \Delta_R G = +439 \text{ kJ mol}^{-1} \qquad (6.S1)$$

$$PH_3 \rightarrow PH_2 + H(^2S) \qquad \Delta_R G = +399 \text{ kJ mol}^{-1} \qquad (6.S2)$$

$$CH_3 + PH_2 \rightarrow CH_3PH_2 \qquad \Delta_R G = -291 \text{ kJ mol}^{-1} \qquad (6.S3)$$

$$CH_4 + PH_3 \rightarrow CH_3PH_2 + 2\,H \qquad \Delta_R G = +547 \text{ kJ mol}^{-1} \qquad (6.S4)$$

The net reaction forming methylphosphine and two hydrogen atoms from methane and phosphine requires 547 kJ mol^{-1} (5.67 eV), which cannot be achieved thermally at 5 K and thus must be initiated by external sources of energy, such as through non-equilibrium chemistry initiated by the implanted electrons.[203]

Having formed methylphosphine (CH_3PH_2), oxidation of the phosphorus may convert methylphosphine to methylphosphonic acid ($CH_3P(O)(OH)_2$). This formally requires three oxygen atoms. Upon interaction of water (H_2O) with ionizing radiation, the water molecules can undergo unimolecular decomposition via, for instance, reactions 6.S5 and 6.S6. The simplest way to reach methylphosphonic acid is the stepwise oxidation of methylphosphine by three singlet oxygen atoms as compiled schematically in equation 6.S7.

$$H_2O \rightarrow H(^2S) + OH(X\,^2\Pi_\Omega) \qquad \Delta_R G = +466 \text{ kJ mol}^{-1} \qquad (6.S5)$$

$$H_2O \rightarrow H_2 + O(^1D) \qquad \Delta_R G = +650 \text{ kJ mol}^{-1} \qquad (6.S6)$$

$$CH_3PH_2 + 3\,O(^1D) \rightarrow CH_3P(O)(OH)_2 \qquad \Delta_R G = -2140 \text{ kJ mol}^{-1} \qquad (6.S7)$$

Reaction Mechanisms – Route II: Route II involves the initial oxidation of phosphine to phosphonic acid (H_3PO_3) via successive addition/insertion of oxygen atoms from the decomposition of water (equation 6.S6) to phosphine (equation 6.S8).

$$PH_3 \xrightarrow{+O} H_2POH \xrightarrow{+O} HP(OH)_2 \xrightarrow{+O} HP(O)(OH)_2 \qquad \Delta_R G = -2180 \text{ kJ mol}^{-1} \qquad (6.S8)$$

Having formed phosphonic acid, methane and phosphonic acid can decompose to produce the methyl (equation 6.S1) and phosphonyl radical (equation 6.S10), which can undergo barrierless radical recombination to form methylphosphonic acid (equation 6.S11).

$$HP(O)(OH)_2 \rightarrow P(O)(OH)_2 + H(^2S) \quad (6.S10)$$

$$CH_3 + P(O)(OH)_2 \rightarrow CH_3P(O)(OH)_2 \quad (6.S11)$$

It must be noted that these are proposed reactions schemes and the actual formation route to methylphosphonic acid may be even a combination of routes I or II. Ideally, the reaction mechanisms would be derived by fitting concentration profiles of reactants, intermediates, and products through a set of coupled differential equations,[224,225] but these require accurate measurements of the infrared absorption bands for the products and intermediates of the reaction. Considering similar absorptions of the functional groups for a variety of the products, the overlapping absorption bands prevent a determination of accurate temporal concentration profiles.

CHAPTER 7
CONCLUSION

These experiments of irradiated ices of phosphine, water, and methane have demonstrated the potential for interstellar ices to produce phosphorus oxoacids and alkyl phosphonic acids (Figure 7.1), which have been discovered on the Murchison meteorite. The systematic approach presented in this dissertation revealed that irradiated pure phosphine ices form larger phosphanes, up to octaphosphane (P_8H_{10}). Even when diluted by a factor of ten in a water matrix, the major products of phosphine-containing ices are consistently diphosphine (P_2H_4) and triphosphane (P_3H_5). Ice mixtures of phosphine and methane, though, demonstrate that methane preferentially reacts with phosphine rather than producing larger hydrocarbons, and these reactions occur predominantly via recombination of the phosphino (PH_2) and methyl (CH_3) radicals. While infrared spectroscopy provides a valuable tool to calculate the fraction of reactants consumed from irradiation and the assignment of simple molecules along with functional groups, the limitations of infrared spectroscopy become apparent when investigating larger, poorly studied molecules such as alkyl phosphanes and their oxygenated counterparts because the absorption bands only identify functional groups and not discrete molecules. In these cases, mass spectrometry techniques such as PI-ReTOF-MS are crucial to accurately assign not only discrete compounds but also, using tunable photoionization, the isomers of these compounds. However, the reactions of phosphine and water also revealed a limitation of ReTOF-MS—in order for molecules to be detected, they must sublime at temperatures lower than room temperature. Major products of phosphine and water, such as phosphoric acid (H_3PO_4), are solids are room temperature and were not observed by ReTOF-MS in the gas phase. The solids produced by the experiments were thus analyzed using SIMS or GC×GC and found the following phosphorus oxoacids: phosphonic acid (H_3PO_3), phosphoric acid (H_3PO_4), and pyrophosphoric acid ($H_4P_2O_7$) (Figure 7.2). The addition of methane produced methylphosphonic acid as verified by both PI-ReTOF-MS and GC×GC. In addition to ethyl- and propylphosphonic acid, methylphosphate was also assigned based on its mass spectrum. Thus, ices composed of simple, astrochemically

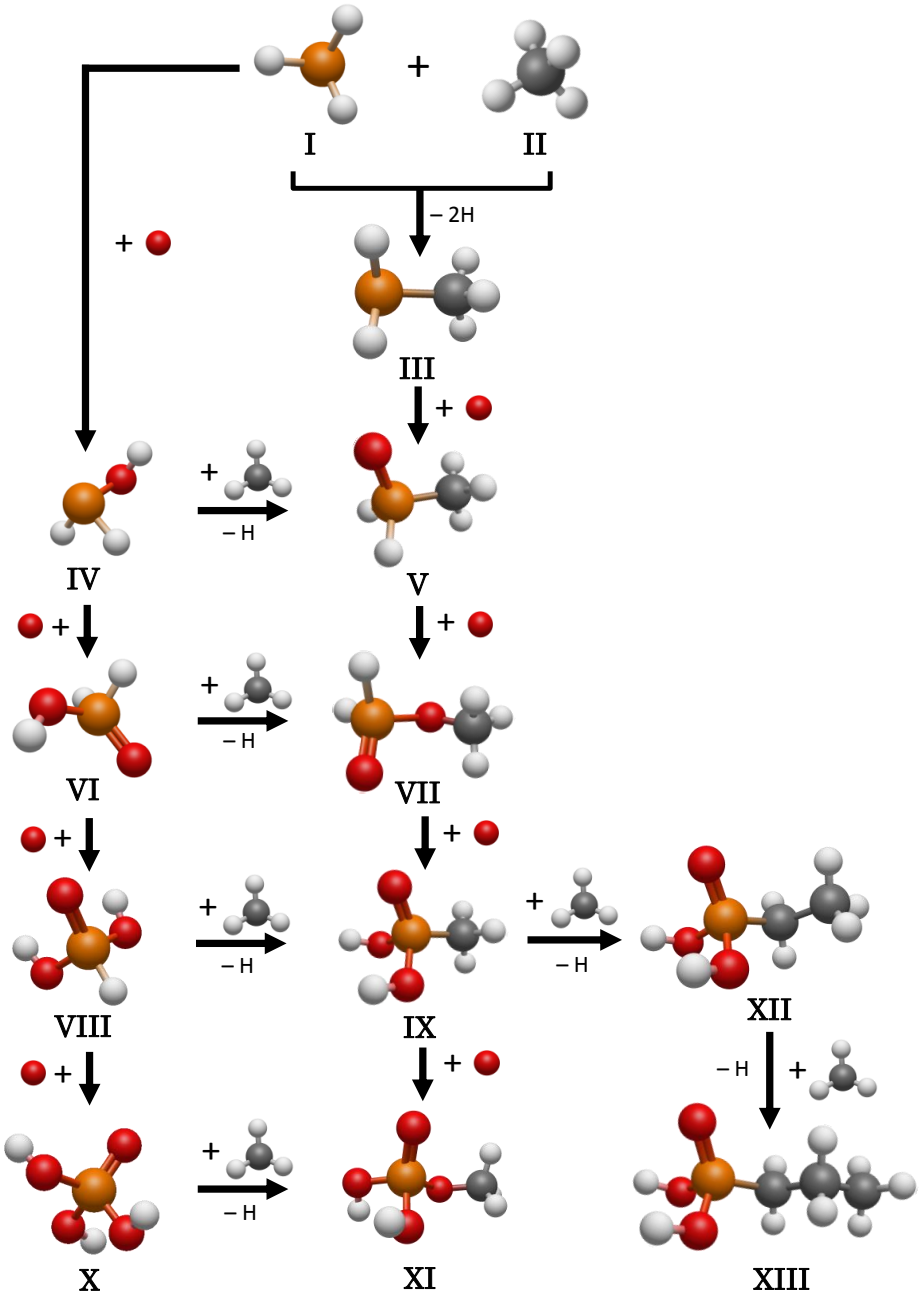

Figure 7.1. Schematic showing reactions of phosphine, methane, and oxygen (from water or carbon dioxide) leading to higher order products. **I.** phosphine **II**. methane **III**. methylphosphine **IV**. hydroxyphosphine V. methylphosphine oxide **VI**. phosphinic acid **VII**. methoxyphosphine oxide **VIII**. phosphonic acid **XI**. methylphosphonic acid X**.** phosphoric acid **XI**. methylphosphate **XII**. ethylphosphonic acid **XIII**. n-propylphosphonic acid

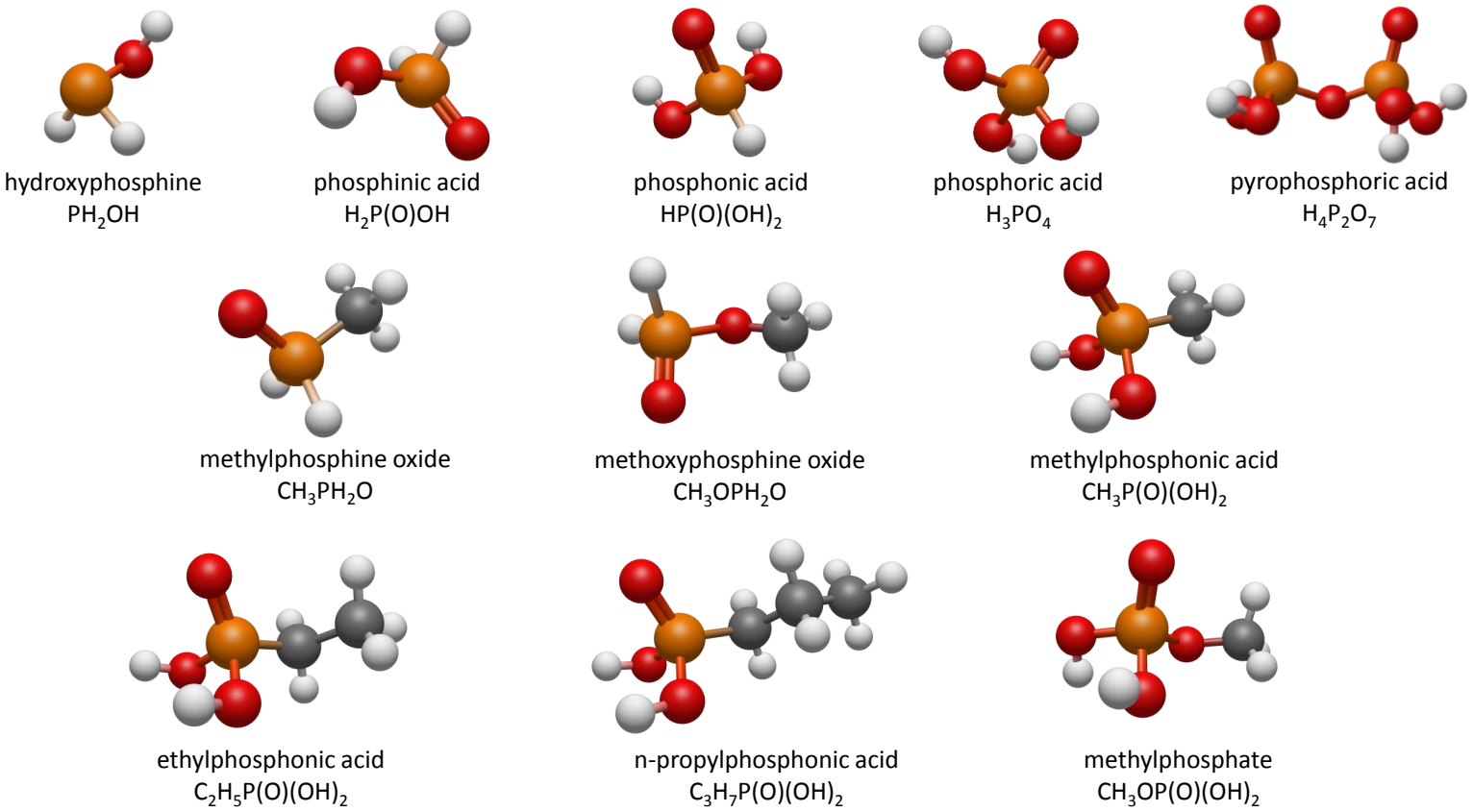

Figure 7.2. Phosphorus oxoacids and alkyl phosphorus oxoacids that were detected from either PI-ReTOF-MS or GC×GC-TOF-MS.

relevant compounds—phosphine, water, and methane—that are exposed to electron irradiation, which mimics the secondary electrons generated by galactic cosmic rays, produce methylphosphonic acid—the simplest of the only phosphorus-containing organic compounds of extraterrestrial origin yet discovered—and methylphosphate, which contains the biologically-present P(+V)–O–C bond and serves as a prototype for potentially more complex molecules that could be in interstellar ices.

Given the capacity for phosphine-doped ices to form methylphosphonic acid and methylphosphate, the outlook for phosphine-based astrochemical research would lie toward the formation of larger, more complex molecules that approach true biomolecules. For example, recent results from my colleague Cheng Zhu in the Kaiser research group has found glycerol phosphate—a biomolecule noted for its role in the glycerol phosphate shuttle—was synthesized from ices containing phosphine and methanol. Such an irradiation may also produce phosphoglycerate and 3-phosphorglyceric acid, both important for glycolysis and related to the three and four carbon sugars utilized in primitive metabolic systems. While phosphine and water ices satisfactorily form phosphates upon irradiation, the replacement of methane from my ices with other sources of carbon—especially those with the potential to form sugars such as ribose—provide the opportunity to demonstrate that molecules similar to the backbone of RNA/DNA and the ribose-phosphate group of ADP/ATP can be synthesized in interstellar ices. Figure 7.3 encapsulates the process by which simple astrophysically relevant compounds combine to form biomolecules. Phosphorus is contained in many of these structures, although notably absent in proteins and fats. After linkages to glycerol or ribose are investigated, the addition of nitrogen is necessary to create a truly complete phosphorus-containing biomolecule. Given our recent discovery that ices containing phosphine and methanol can produce glycerol phosphate, the addition of ammonia (NH_3) to these ices can potentially form the entire hydrophilic head of a phospholipid. The discovery of an ice mixture that produced purine, the heterocyclic aromatic component of nucleotides and ADP/ATP, would be a breakthrough toward synthesizing other phosphorus-containing biomolecules. Besides ammonia and methane, other ice mixtures to consider for purine synthesis might to include methylamine (CH_3NH_2), hydrogen

cyanide (HCN), and methyl cyanide (CH_3CN), all of which are gas phase detections in the interstellar medium.[115,226,227]

While much of this dissertation has been guided toward the eventual formation of alkyl phosphonic acids with additional interest in phosphates (e.g. phosphoric acid and methylphosphate) due to the astrobiological implications of these molecules, this research also contributes to the astrochemical understanding of extraterrestrial phosphorus, which continues to be enhanced by new discoveries such as the detection of phosphine oxide (PO) and phosphine nitride (PN) in several oxygen-rich circumstellar envelopes.[228] The presence of phosphine in the gas giants and phosphorus signal attributed to phosphine in comet 67P/Churyumov-Gerasimenko points to the possibility that phosphine was a component of the early solar system, and thus the scientific community must consider the role of phosphine whenever new phosphorus-based compounds are discovered in comets and meteorites. Furthermore, given that the discoverers of Murchison's alkyl phosphonic acids take the view that these compounds were not *formed* by aqueous alteration of the meteorite's parent body—a view inconsistent with research using schreibersite—but instead *survived* this aqueous alternation due to the stability of the C–P bond, which labile species such as phosphate esters would be less likely to survive,[7] one must also consider that the alkyl phosphonic acids may provide clues to other phosphorus-containing molecules that were formed alongside the alkyl phosphonic acids but did not persist after aqueous processing. Not only is their survival on aqueously processed parent bodies in doubt, but also the analysis methods may have destroyed the phosphate esters. These phosphate esters, which have the P(+V)–O–C moiety included in compounds such as methylphosphate and nearly all biomolecules, may also have formed from the interstellar medium before the birth of the solar system and thus would be present on small solar system bodies if conditions are suitable for their survival. Their intact delivery to an early Earth would offer prebiotic compounds for the first organisms. Thus, experiments that successfully synthesize alkyl phosphonic acids in astrophysical environments, such as ice mixtures of phosphine, water, and methane, also contribute broader results to the scientific community by suggesting additional products that may have been present in the early solar system. These successful experiments represent the first steps to discovering how life

incorporated phosphorus by discovering the possible compounds available to the first life on Earth. This dissertation demonstrates that irradiated phosphine-doped ices signify one such successful experiment and should serve as an impetus for future research to continue progressing toward the discovery of the keys to life.

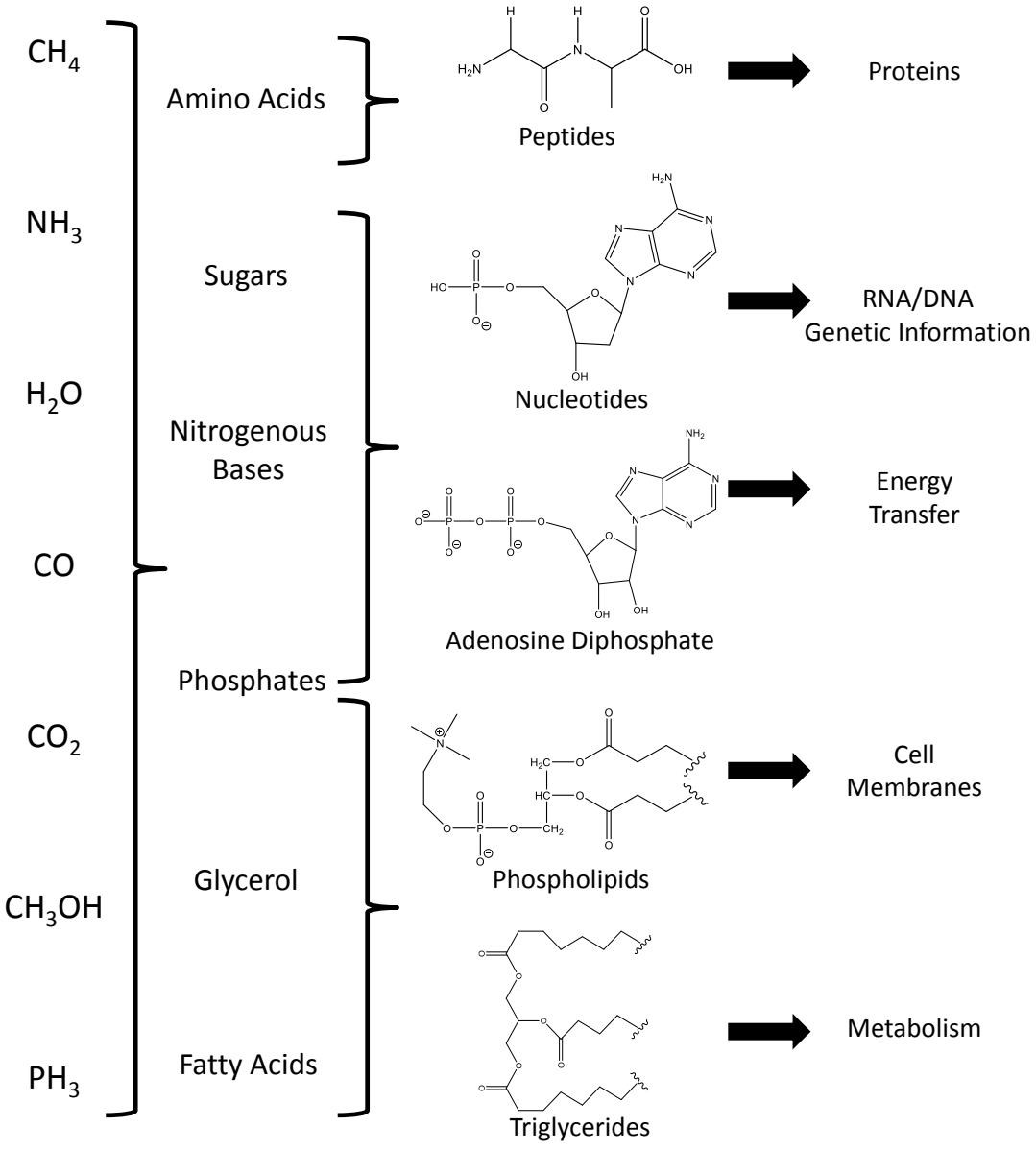

Figure 7.3. Scheme illustrating (from left to right) how simple interstellar molecules synthesize to form classes of biomolecules, which themselves combine to form more complex molecules, and these molecules' roles in biology. The simple molecules on the left collectively react to form the next set of more complex classes of molecules, although each simple molecule may not contribute to each of the molecular classes in the second column.

APPENDIX
LIST OF EXPERIMENTS

Table A.1. List of experiments performed including the components of the ice mixture, irradiation current, and the analytical techniques used. Blank experiments were also performed but not included in this list.

Molecular source of:			Irradiation (nA)	Analytical techniques utilized			
Phosphorus	Oxygen	Organic Carbon		IR + QMS	ReTOF-MS PIEs* (eV)	SIMS	GC×GC-TOF-MS
PH_3			100	×	10.49		
PH_3			1000	×			
PH_3			5000	×			
PH_3	H_2O		100	×			
PH_3	H_2O		1000	×			
PH_3	H_2O		5000	×			
PH_3	$H_2{}^{18}O$		100	×	9.93/10.86	×	
PH_3	$H_2{}^{18}O$		1000	×	9.93/10.86	×	
PH_3	$H_2{}^{18}O$		5000	×	10.86	×	×
PH_3	CO_2		100	×			
PH_3	CO_2		1000	×			
PH_3	CO_2		5000	×			
PH_3	$C^{18}O_2$		100	×	9.93/10.86	×	
PH_3	$C^{18}O_2$		1000	×	10.86	×	
PH_3	$C^{18}O_2$		5000	×	10.86	×	×
PH_3		CH_4	100	×	10.49		
PH_3		CH_4	1000	×			
PH_3		CH_4	5000	×			
PH_3		CD_4	100	×	10.49		
PH_3	H_2O	CH_4	1000	×	9.93/10.49		
PH_3	$H_2{}^{18}O$	CH_4	1000	×	9.93/10.35/10.49		×
PH_3	H_2O	$^{13}CH_4$	1000	×	9.93/10.49		×
PH_3	H_2O	CH_4, C_2H_6, C_3H_8, C_4H_{10}	100	×			
PH_3	H_2O	CH_4, C_2H_6, C_3H_8, C_4H_{10}	1000	×			
PH_3	H_2O	CH_4, C_2H_6, C_3H_8, C_4H_{10}	5000	×			
PH_3	CO_2	CH_4	100	×			
PH_3	CO_2	CH_4	1000	×			
PH_3	CO_2	CH_4	5000	×			
PH_3	CO_2	CH_4, C_2H_6, C_3H_8, C_4H_{10}	100	×			
PH_3	CO_2	CH_4, C_2H_6, C_3H_8, C_4H_{10}	1000	×			
PH_3	CO_2	CH_4, C_2H_6, C_3H_8, C_4H_{10}	5000	×			

*Photoionization energies

GLOSSARY

abiotic not derived from living organisms

absorption coefficient a measure of the rate of decrease in the intensity of (infrared) light as it travels through a medium

adiabatic ionization energy the minimum about of energy required to remove an electron from a neutral molecule

alkyl phosphonic acid organic oxoacid of general formula $RP(O)(OH)_2$, R = C_xH_{2x+1}; the only organic phosphorus-containing compounds of extraterrestrial origin

Archean Eon geologic period occurring 2.5 to 4 billion years ago

Avogadro constant equal to approximately 6.02×10^{23} mol^{-1}

barrierless not requiring activation energy

carbonaceous chondrite a granular, stony meteorite containing a notable proportion of carbon, organic matter, and water

circumstellar envelope a roughly spherical shell around a star not gravitationally bound to the star and mixes with the interstellar medium at great distances; for older stars, eventually become a protoplanetary nebula

coherent relating to light in which wavelengths are in phase in space and time

column density the number of units per area along a line of sight

deformation mode a vibration that changes bond angles while bond lengths remain the same

endoergic relating to a process that absorbs energy

exoergic relating to a process that releases energy

exogenous in terms of astrobiology, relating to a source outside of Earth

Fermi resonance a phenomenon when two vibrations with the same symmetry undergo a transition of similar energy that results in a change of expected infrared peak frequency and intensity

four wave mixing a phenomenon in non-linear optics in which two or three wavelengths of light generate new wavelengths

galactic cosmic ray high energy atomic nuclei originating from outside the solar system

Hadean Eon geologic period ending 4 billion years ago

harmonic light with a frequency that is a positive integer multiple of the frequency of an original wave, with the first harmonic used to describe the original fundamental frequency

Heavy Bombardment Period an event 3.8 to 4.1 billion years ago during which a large number of meteorites impacted Earth and other planets

homologous chemical compounds having the same functional group but differing in composition by a fixed group of atoms

interstellar medium matter that exists between star systems

IRC +10216 Also known as CW Leonis, a carbon star in the constellation Leo

isomers molecules with the same molecular formula but different chemical structure, ex: HCN vs. HNC

isotopes atoms of the same element that differ by the number of neutrons, ex: ^{16}O vs. ^{18}O

isotopologues molecules that differ in their isotopic composition, ex: H_2O vs. D_2O (^1H_2O vs ^2H_2O)

isotopomers molecules that have the same number of each isotope of each element but in different positions, ex: $^{13}CH_3COH$ vs. $CH_3{}^{13}COH$

isovalency relating to species with the same number of valence electrons and as a result, similar chemistries

laser interferometry the use of superimposed lasers causing interference from which information, in this case ice thickness, can be extracted

lattice mode a vibration mode of the lattice of a solid

non-equilibrium chemistry reactions that occur when the reactants are not initially present in a Boltzmann distribution; also referred to as non-thermal chemistry

nonlinear medium a material in which the dielectric polarization of light responds nonlinearly to the electric field

picoammeter an ammeter capable of measuring currents in the range of picoamperes (pA)

prebiotic occurring before the emergence of life

phosphane a saturated compound of phosphorus and hydrogen with formula P_xH_{x+2}

phosphinic acid a molecule with formula $H_2P(O)OH$ or H_3PO_2, thus containing P(I); commonly referred to as *hypophosphorous acid*, which is properly the isomer with formula $HP(OH)_2$

phosphorus oxoacid a molecule that contains at least one phosphorus and oxygen atom, and at least one hydrogen bound to an oxygen that forms an ion by loss of one or more protons; ex: H_3PO_3 and H_3PO_4

phosphonic acid a molecule with formula $HP(O)(OH)_2$ or H_3PO_3, thus containing P(III); commonly referred to as *phosphorous acid*, which is properly the isomer with formula $P(OH)_3$

phosphoric acid a molecule with formula $P(O)(OH)_3$ or H_3PO_4 , thus containing P(V), which is the geologically and biologically ubiquitous form of phosphorus

pyrophosphoric acid a molecule with formula $(OH)_2(O)P{-}O{-}P(O)(OH)_2$ or $H_4P_2O_7$ including two P(V) atoms bridged by an oxygen; also called *diphosphoric acid*

refractive index the ratio of the speed of light in a vacuum to its speed in a particular medium

schreibersite an iron-nickel phosphide mineral with formula $(Fe,Ni)_3P$ that is rare on Earth but more common in meteorites

Strecker synthesis reactions converting an aldehyde or ketone to an amino acid utilizing potassium cyanide and ammonium chloride followed by hydrolysis

vacuum ultraviolet ultraviolet light with wavelength less than 200 nm (or photon energy greater than 6.2 eV); the name derives from its absorption in atmosphere and so vacuum (or a specialized gas) is necessary to transmit these wavelengths

67P/ Churyumov-Gerasimenko a comet visited by the ESA space probe *Rosetta* and the *Philae* lander from 2014 to 2016

REFERENCES

1. Miller, S. L.; Urey, H. C. *Science* **1959**, *130*, 245.
2. Miller, S.; Urey, H. *Science* **1953**, *117*, 528.
3. Parker, E. T.; Cleaves, H. J.; Callahan, M. P., et al. *Origins of Life and Evolution of Biospheres* **2011**, *41*, 201.
4. Pasek, M. A.; Sampson, J. M.; Atlas, Z. *Proceedings of the National Academy of Sciences* **2014**, *111*, 15468.
5. Gulick, A. *American Scientist* **1955**, *43*, 479.
6. Pasek, M. A.; Harnmeijer, J. P.; Buick, R., et al. *Proceedings of the National Academy of Sciences* **2013**, *110,* 10089.
7. Cooper, G. W.; Onwo, W. M.; Cronin, J. R. *Geochimica Et Cosmochimica Acta* **1992**, *56*, 4109.
8. de Graaf, R. M.; Visscher, J.; Schwartz, A. W. *Nature* **1995**, *378*, 474.
9. de Graaf, R. M.; Visscher, J.; Schwartz, A. W. *Journal of Molecular Evolution* **1997**, *44*, 237.
10. De Graaf, R.; Visscher, J.; Schwartz, A. W. *Origins of Life and Evolution of the Biosphere* **1998**, *28*, 271.
11. De Graaf, R.; Visscher, J.; Xu, Y., et al. *Journal of Molecular Evolution* **1998**, *47*, 501.
12. Schwartz, A. *Origins of Life and Evolution of the Biosphere* **1997**, *27*, 505.
13. Guélin, M.; Cernicharo, J.; Paubert, G.; Turner, B. *Astronomy & Astrophysics* **1990**, *230*, L9.
14. Agúndez, M.; Cernicharo, J.; Guélin, M. *Astrophysical Journal Letters* **2007**, *662*, L91.
15. Gorrell, I. B.; Wang, L. M.; Marks, A. J., et al. *Chemical Communications* **2006**, 1643.
16. Bryant, D. E.; Kee, T. P. *Chemical Communications* **2006**, 2344.
17. Pasek, M. A.; Lauretta, D. S. *Astrobiology* **2005**, *5*, 515.
18. Pasek, M. A.; Kee, T. P.; Bryant, D. E., et al. *Angewandte Chemie* **2008**, *120*, 8036.
19. Kee, T. P.; Bryant, D. E.; Herschy, B., et al. *Life* **2013**, *3*, 386.
20. La Cruz, N. L.; Qasim, D.; Abbott-Lyon, H., et al. *Physical Chemistry Chemical Physics* **2016**, *18*, 20160.
21. Bryant, D. E.; Greenfield, D.; Walshaw, R. D., et al. *Geochimica Et Cosmochimica Acta* **2013**, *109*, 90.
22. Pasek, M. A. *Geoscience Frontiers* **2017**, *8*, 329.
23. Bryant, D. E.; Marriott, K. E.; Macgregor, S. A., et al. *Chemical Communications* **2010**, *46*, 3726.
24. Gull, M.; Mojica, M. A.; Fernández, F. M., et al. *Scientific Reports* **2015**, *5*, 17198.
25. Pasek, M. A.; Dworkin, J. P.; Lauretta, D. S. *Geochimica Et Cosmochimica Acta* **2007**, *71*, 1721.
26. Nam, I.; Lee, J. K.; Nam, H. G.; Zare, R. N. *Proceedings of the National Academy of Sciences* **2017**, *114*, 12396.
27. Gibard, C.; Bhowmik, S.; Karki, M., et al. *Nature Chemistry* **2017**, *10,* 212.
28. Tenenbaum, E.; Woolf, N.; Ziurys, L. *Astrophysical Journal Letters* **2007**, *666*, L29.
29. Turner, B.; Bally, J. *Astrophysical Journal Letters* **1987**, *321*, L75.
30. Ziurys, L. *Astrophysical Journal Letters* **1987**, *321*, L81.
31. Milam, S.; Halfen, D.; Tenenbaum, E., et al. *Astrophysical Journal* **2008**, *684*, 618.
32. Guélin, M.; Muller, S.; Cernicharo, J., et al. *Astronomy & Astrophysics* **2000**, *363*, L9.
33. Halfen, D.; Clouthier, D.; Ziurys, L. M. *Astrophysical Journal Letters* **2008**, *677*, L101.
34. Agundez, M.; Cernicharo, J.; Guelin, M. *Astronomy & Astrophysics* **2014**, *570*.
35. Tenenbaum, E.; Ziurys, L. *Astrophysical Journal Letters* **2008**, *680*, L121.
36. Agundez, M.; Cernicharo, J.; Pardo, J., et al. *Astronomy & Astrophysics* **2008**, *485*, L33.
37. Agundez, M.; Cernicharo, J.; Decin, L., et al. *Astrophysical Journal Letters* **2014**, *790*.

38. Ridgway, S.; Wallace, L.; Smith, G. *Astrophysical Journal* **1976**, *207*, 1002.
39. Larson, H.; Fink, U.; Smith, H.; Davis, D. *Astrophysical Journal* **1980**, *240*, 327.
40. Pasek, M. A.; Mousis, O.; Lunine, J. I. *Icarus* **2011**, *212*, 751.
41. Altwegg, K.; Balsiger, H.; Bar-Nun, A., et al. *Science Advances* **2016**, *2*, e1600285.
42. Glindemann, D.; Bergmann, A.; Stottmeister, U.; Gassmann, G. *Naturwissenschaften* **1996**, *83*, 131.
43. Devai, I.; Delaune, R. D. *Organic Geochemistry* **1995**, *23*, 277.
44. Bernstein, M. P.; Dworkin, J. P.; Sandford, S. A., et al. *Nature* **2002**, *416*, 401.
45. Holtom, P.; C., B.; A., O., et al. *Astrophysical Journal* **2005**, *626*, 940.
46. Meinert, C.; Filippi, J.; de Marcellus, P., et al. *ChemPlusChem* **2012**, *77*, 186.
47. Munoz Caro, G. M.; Meierhenrich, U. J.; Schutte, W. A., et al. *Nature* **2002**, *416*, 403.
48. Lafosse, A.; Bertin, M.; Domaracka, A., et al. *Physical Chemistry Chemical Physics* **2006**, *8*, 5564.
49. Kaiser, R. I.; Maity, S.; Jones, B. M. *Angewandte Chemie International Edition* **2015**, *54*, 195.
50. Bennett, C.; Kaiser, R. I. *Astrophysical Journal* **2007**, *661*, 899.
51. Maity, S.; Kaiser, R. I.; Jones, B. M. *Faraday Discussions* **2014**, *168*, 485.
52. Kaiser, R. I.; Stockton, A. M.; Kim, Y. S., et al. *Astrophysical Journal* **2013**, *765*, 111.
53. Boogert, A. A.; Gerakines, P. A.; Whittet, D. C. *Annual Review of Astronomy and Astrophysics* **2015**, *53*, 541.
54. Kaiser, R. I. *Chemical Reviews* **2002**, *102*, 1309.
55. Langmuir, I. *Procedings of the National Academy of Sciences* **1919**, *5*, 252.
56. Parker, D. S.; Wilson, A. V.; Kaiser, R. I., et al. *Journal of the American Chemical Society* **2012**, *134*, 13896.
57. Parker, D.; Mebel, A.; Kaiser, R. *Chemical Society Reviews* **2014**, *43*, 2701.
58. Housecroft, C. E. S., A. G. *Inorganic Chemistry*; Limited Second Edition ed.; Pearson: Harlow, UK, 2005.
59. Berthollet, C. L. *Mem Acad Sci* **1785**, *99*, 319.
60. Gengembre, P. *Hist Mem Acad Roy Sci* **1785**, *10*, 651.
61. Thenard, P. *Acad Sci Paris* **1844**, *18*, 652.
62. de Bruyn, C. A. L. *Recueil des Travaux Chimiques des Pays-Bas* **1895**, *14*, 85.
63. Kim, Y.; Gilje, J. W.; Seff, K. *Journal of the American Chemical Society* **1977**, *99*, 7057.
64. Fujii, T.; Selvin, C. P.; Sablier, M.; Iwase, K. *Journal of Physical Chemistry A* **2002**, *106*, 3102.
65. Baudler, M.; Glinka, K. *Chemical Reviews* **1994**, *94*, 1273.
66. Baudler, M.; Schmidt, L. *Naturwissenschaften* **1957**, *44*, 488.
67. Baudler, M.; Ständeke, H.; Borgardt, M.; Strabel, H. *Naturwissenschaften* **1965**, *52*, 345.
68. Shackelford, J. F.; Alexander, W. *CRC Materials Science and Engineering Handbook*; CRC press, 2000.
69. Jones, B. M.; Kaiser, R. I. *Journal of Physical Chemistry Letters* **2013**, 1965.
70. Bennett, C. J.; Brotton, S. J.; Jones, B. M., et al. *Analytical Chemistry* **2013**, *85*, 5659.
71. Jones, B. M.; Kaiser, R.; Strazzulla, G. *Astrophysical Journal* **2014**, *781*, 85.
72. Kaiser, R. I.; Maity, S.; Jones, B. M. *Physical Chemistry Chemical Physics* **2014**, *16*, 3399.
73. Jones, B. M.; Kaiser, R. I.; Strazzulla, G. *Astrophysical Journal* **2014**, *788*, 170.
74. Kaiser, R. I.; Maity, S.; Jones, B. M. *Angewandte Chemie International Edition* **2015**, *54*, 195.
75. Maity, S.; Kaiser, R. I.; Jones, B. M. *Physical Chemistry Chemical Physics* **2015**, *17*, 3081.
76. Maksyutenko, P.; Muzangwa, L. G.; Jones, B. M.; Kaiser, R. I. *Physical Chemistry Chemical Physics* **2015**, *17*, 7514.
77. Maity, S.; Kaiser, R.; Jones, B. M. *Astrophysical Journal* **2014**, *789*, 36.

78. Fulvio, D.; Sivaraman, B.; Baratta, G., et al. *Spectrochimica Acta Part A: Molecular and Biomolecular Spectroscopy* **2009**, *72*, 1007.
79. Hudgins, D.; Sandford, S.; Allamandola, L.; Tielens, A. *Astrophysical Journal Supplement* **1993**, *86*, 713.
80. Westley, M.; Baratta, G.; Baragiola, R. *Journal of Chemical Physics* **1998**, *108*, 3321.
81. Brunetto, R.; Caniglia, G.; Baratta, G.; Palumbo, M. *Astrophysical Journal* **2008**, *686*, 1480.
82. Hovington, P.; Drouin, D.; Gauvin, R. *Scanning* **1997**, *19*, 1.
83. Francia, M. D.; Nixon, E. R. *Journal of Chemical Physics* **1973**, *58*, 1061.
84. VonDrasek, W. A.; Okajima, S.; Hessler, J. P. *Appl. Opt.* **1988**, *27*, 4057.
85. Becke, A. D. *Journal of Chemical Physics* **1992**, *96*, 2155.
86. Becke, A. D. *Journal of Chemical Physics* **1992**, *97*, 9173.
87. Becke, A. D. *Journal of Chemical Physics* **1993**, *98*, 5648.
88. Lee, C.; Yang, W.; Parr, R. G. *Physical Review B* **1988**, *37*, 785.
89. Purvis III, G. D.; Bartlett, R. J. *Journal of Chemical Physics* **1982**, *76*, 1910.
90. Hampel, C.; Peterson, K. A.; Werner, H.-J. *Chemical Physics Letters* **1992**, *190*, 1.
91. Knowles, P. J.; Hampel, C.; Werner, H. J. *Journal of Chemical Physics* **1993**, *99*, 5219.
92. Deegan, M. J.; Knowles, P. J. *Chemical Physics Letters* **1994**, *227*, 321.
93. Kaiser, R. I.; Sun, B. J.; Lin, H. M., et al. *Astrophysical Journal* **2010**, *719*, 1884.
94. Kostko, O.; Zhou, J.; Sun, B. J., et al. *Astrophysical Journal* **2010**, *717*, 674.
95. Frisch, M. J. *GAUSSIAN 09, Revision D.01* Gaussian, Inc., Wallingford CT**, 2013**.
96. Durig, J.; Shen, Z.; Zhao, W. *Journal of Molecular Structure: THEOCHEM* **1996**, *375*, 95.
97. Ding, F. J.; Zhang, L. F. *Journal of Molecular Structure: THEOCHEM* **1996**, *369*, 167.
98. GRAMS/AI-Spectroscopy-Software; 7.02 ed.; Thermo Scientific: 2002.
99. Berkowitz, J.; Curtiss, L.; Gibson, S., et al. *Journal of Chemical Physics* **1986**, *84*, 375.
100. Elbel, S.; Tom Dieck, H.; Becker, G.; Ensslin, W. *Inorganic Chemistry* **1976**, *15*, 1235.
101. Fehlner, T. *Journal of the American Chemical Society* **1968**, *90*, 6062.
102. Haring, R.; Haring, A.; Klein, F., et al. *Nuclear Instruments and Methods in Physics Research* **1983**, *211*, 529.
103. De Vries, A.; Haring, R.; Haring, A., et al. *Journal of Physical Chemistry* **1984**, *88*, 4510.
104. Gerakines, P.; Schutte, W.; Ehrenfreund, P. *Astronomy & Astrophysics* **1996**, *312*, 289.
105. Farenzena, L.; Iza, P.; Martinez, R., et al. *Earth, Moon, and Planets* **2005**, *97*, 311.
106. Zheng, W.; Jewitt, D.; Osamura, Y.; Kaiser, R. I. *Astrophysical Journal* **2008**, *674*, 1242.
107. Schlegel, H. B.; Skancke, A. *Journal of the American Chemical Society* **1993**, *115*, 7465.
108. Hilbig, R.; Wallenstein, R. *Applied Optics* **1982**, *21*, 913.
109. Brunetto, R.; Caniglia, G.; Baratta, G. A.; Palumbo, M. E. *Astrophysical Journal* **2008**, *686*, 1480.
110. McKean, D.; Schatz, P. *Journal of Chemical Physics* **1956**, *24*, 316.
111. Sennikov, P.; Raldugin, D.; Nabiev, S. S., et al. *Spectrochimica Acta Part A: Molecular and Biomolecular Spectroscopy* **1996**, *52*, 453.
112. Milam, S. N., *Following Carbon's Evolutionary Path: From Nucleosynthesis to the SOlar System,* University of Arizona, 2007.
113. Johnson III, R. D. *NIST Computational Chemistry Comparison and Benchmark Database, NIST Standard Reference Database Number 101, Release 17b., http://cccbdb.nist.gov/* **2015**.
114. Cottrell, T. L. *The Strengths of Chemical Bonds*; Academic Press: New York,, 1954.
115. Kaifu, N.; Morimoto, M.; Nagane, K., et al. *Astrophysical Journal* **1974**, *191*, L135.
116. Fourikis, N.; Takagi, K.; Morimoto, M. *Astrophysical Journal* **1974**, *191*, L139.
117. Kim, Y. S.; Kaiser, R. I. *Astrophysical Journal* **2011**, *729*.
118. Lafont, S.; Lucas, R.; Omont, A. *Astronomy & Astrophysics* **1982**, *106*, 201.

119. Halfen, D. T.; Clouthier, D. J.; Ziurys, L. M. *Astrophysical Journal* **2014**, *796*.
120. Turner, A. M.; Abplanalp, M. J.; Chen, S., et al. *Physical Chemistry Chemical Physics* **2015**, *17*, 27227.
121. Westley, M.; Baratta, G.; Baragiola, R. *Journal of Chemical Physics* **1998**, *108*, 3321.
122. Babar, S.; Weaver, J. *Applied Optics* **2015**, *54*, 477.
123. Goodman, A. M. *Applied Optics* **1978**, *17*, 2779.
124. Satorre, M.; Domingo, M.; Millán, C., et al. *Planetary and Space Science* **2008**, *56*, 1748.
125. Li, H. H. *Journal of Physical and Chemical Reference Data* **1976**, *5*, 329.
126. R.H. Staley, J. L. B. *Journal of the American Chemical Society* **1974**, *96*, 6252.
127. Hodges, R. V.; McDonnell, T.; Beauchamp, J. *Journal of the American Chemical Society* **1980**, *102*, 1327.
128. Kim, H.-W.; Chechla, A. A.; Kim, B. *Journal of Molecular Structure: THEOCHEM* **2007**, *802*, 105.
129. Bennett, C. J.; Jamieson, C. S.; Osamura, Y.; Kaiser, R. I. *Astrophysical Journal* **2006**, *653*, 792.
130. Bennett, C. J.; Kaiser, R. I. *Astrophysical Journal* **2007**, *660*, 1289.
131. Gordon, M. S.; Boatz, J.; Gano, D. R.; Friedrichs, M. G. *Journal of the American Chemical Society* **1987**, *109*, 1323.
132. Kaiser, R.; Eich, G.; Gabrysch, A.; Roessler, K. *Astrophysical Journal* **1997**, *484*, 487.
133. Fueno, T.; Bonacic-Koutecky, V.; Koutecky, J. *Journal of the American Chemical Society* **1983**, *105*, 5547.
134. Adriaenssens, T.; Ughi, G. J.; Dubois, C., et al. *EuroIntervention* **2014**, 20130911-03.
135. Chase, M. W. *NIST-JANAF Thermochemical Tables, Journal of Physical Chemistry Reference Data* **1998**.
136. Ehrenfreund, P.; Charnley, S. B. *Annual Review of Astronomy and Astrophysics* **2000**, *38*, 427.
137. Bahr, D.; Fama, M.; Vidal, R.; Baragiola, R. *Journal of Geophysical Research: Planets* **2001**, *106*, 33285.
138. Baragiola, R.; Vidal, R.; Svendsen, W., et al. *Nuclear Instruments and Methods in Physics Research Section B: Beam Interactions with Materials and Atoms* **2003**, *209*, 294.
139. Cronin, J. R.; Chang, S. C. In *The Chemistry of Life's Origin*; Greenberg, J., Mendoza-Gomez, C., Pirronello, V., Eds.; Kluwer: Dordrecht, The Netherlands, 1993, p 209.
140. Botto, O.; Bada, J.; Ehrenfreund, P. In *Proceedings of Asteroids, Comets, Meteors - ACM 2002*; Warmbein, B., Ed.; ESA Publications Division: Berlin, Germany, 2002.
141. Kvenvolden, K.; Lawless, J.; Pering, K., et al. *Nature* **1970**, *228*, 923.
142. Fuchs, L. H. In *Meteorite Research*; Springer: 1969, 683.
143. Pasek, M. A. *Proceedings of the National Academy of Sciences* **2008**, *105*, 853.
144. Elsila, J.; De Leon, N.; Buseck, P.; Zare, R. *Geochimica et Cosmochimica Acta* **2005**, *69*, 1349.
145. Spencer, M. K.; Hammond, M. R.; Zare, R. N. *Proceedings of the National Academy of Sciences* **2008**, *105*, 18096.
146. Remusat, L.; Guan, Y.; Wang, Y.; Eiler, J. M. *Astrophysical Journal* **2010**, *713*, 1048.
147. Charnley, S.; Ehrenfreund, P.; Kuan, Y. *Spectrochimica Acta A* **2001**, *57*, 685.
148. Gibb, E.; Whittet, D.; Boogert, A.; Tielens, A. *Astrophysical Journal Supplement* **2004**, *151*.
149. Nilsson, H.; Stenberg Wieser, G.; Behar, E., et al. *Science* **2015**, *347*, aaa0571.
150. Capaccioni, F.; Coradini, A.; Filacchione, G., et al. *Science* **2015**, *347*, aaa0628.
151. Bennett, C. J.; Chen, S. H.; Sun, B. J., et al. *Astrophysical Journal* **2007**, *660*, 1588.
152. Shimoyama, A.; Ogasawara, R. *Origins of Life and Evolution of the Biosphere* **2002**, *32*, 165.
153. Alexander, C.; Bowden, R.; Fogel, M., et al. *Science* **2012**, *337*, 721.
154. Walsh, K.; Morbidelli, A.; Raymond, S., et al. *Nature* **2011**, *475*, 206.

155. Fedoseev, G.; Cuppen, H. M.; Ioppolo, S., et al. *Monthly Notices of the Royal Astronomical Society* **2015**, *448*, 1288.
156. Chuang, K.-J.; Fedoseev, G.; Ioppolo, S., et al. *Monthly Notices of the Royal Astronomical Society* **2015**, *455*, 1702.
157. Rubin, M.; Altwegg, K.; Balsiger, H., et al. *Science* **2015**, *348*, 232.
158. Schulz, R.; Hilchenbach, M.; Langevin, Y., et al. *Nature* **2015**, *518*, 216.
159. Jones, B. M.; Bennett, C. J.; Kaiser, R. I. *Astrophysical Journal* **2011**, *734*.
160. Bennett, C. J.; Jamieson, C.; Mebel, A. M.; Kaiser, R. I. *Physical Chemistry Chemical Physics* **2004**, *6*, 735.
161. Zheng, W.; Jewitt, D.; Kaiser, R. I. *Astrophysical Journal* **2006**, *648*, 753.
162. Jamieson, C. S.; Kaiser, R. I. *Chemical Physics Letters* **2007**, *440*, 98.
163. Mottl, M. J.; Glazer, B. T.; Kaiser, R. I.; Meech, K. J. *Chemie der Erde-Geochemistry* **2007**, *67*, 253.
164. Bennett, C. J.; Osamura, Y.; Lebar, M. D.; Kaiser, R. I. *Astrophysical Journal* **2005**, *634*, 698.
165. Heavens, O. S. *Annals of the New York Academy of Sciences* **1965**, *122*, 638.
166. Zhou, L.; Maity, S.; Abplanalp, M., et al. *Astrophysical Journal* **2014**, *790*.
167. Roder, H. *Journal of Physical and Chemical Reference Data* **1978**, *7*, 949.
168. Bouilloud, M.; Fray, N.; Bénilan, Y., et al. *Monthly Notices of the Royal Astronomical Society* **2015**, *451*, 2145.
169. Hagen, W.; Tielens, A.; Greenberg, J. *Chemical Physics* **1981**, *56*, 367.
170. Hudson, R. L.; Gerakines, P. A.; Moore, M. *Icarus* **2014**, *243*, 148.
171. Van Nes, G.; Vos, A. *Acta Crystallographica Section B: Structural Crystallography and Crystal Chemistry* **1978**, *34*, 1947.
172. Yaws, C.; Chen, D. *Thermophysical Properties of Chemicals and Hydrocarbons, vol* **2008**.
173. Snyder, R.; Schachtschneider, J. *Spectrochimica Acta* **1963**, *19*, 85.
174. Shimanouchi, T. *Tables of Molecular Vibrational Frequencies Consolidated Volume I; National Bureau of Standards: Washington, DC* **1972**.
175. Abplanalp, M. J.; Kaiser, R. I. *Astrophysical Journal* **2016**, *827*, 132.
176. Murphy, W.; Fernandez-Sanchez, J.; Raghavachari, K. *Journal of Physical Chemistry* **1991**, *95*, 1124.
177. Strazzulla, G.; Johnson, R. E. In *Comets in the Post-Halley Era: In Part Based on Reviews Presented at the 121st Colloquium of the International Astronomical Union, Held in Bamberg, Germany, April 24–28, 1989*; Newburn, R. L., Neugebauer, M., Rahe, J., Eds.; Springer Netherlands: Dordrecht, 1991, p 243.
178. Chapman, A.; Thirlwell, L. *Spectrochimica Acta* **1964**, *20*, 937.
179. Brun, G. Revue de Chimie Minerale **1970**, *7*, 413.
180. Ahmadi, I.; Rahemi, H.; Tayyari, S. *Journal of the Korean Chemical Society* **2005**, *49*, 129.
181. Kim, Y. S.; Bennett, C. J.; Chen, L. H., et al. *Astrophysical Journal* **2010**, *711*, 744.
182. Charnley, S. B.; Millar, T. J. *Monthly Notices of the Royal Astronomical Society* **1994**, *270*, 570.
183. Wakelam, V.; Cuppen, H.; Herbst, E. In *Astrochemistry & Astrobiology*; Smith, I. W. M., Cockell, C. S., Leach, S., Eds.; Springer Berlin Heidelberg: 2013, p 115.
184. Turner, B. E.; Tsuji, T.; Bally, J., et al. *Astrophysical Journal* **1990**, *365*, 569.
185. Gillett, F.; Forrest, W. *Astrophysical Journal* **1974**, *187*, 37.
186. Socrates, G. *Infrared and Raman Characteristic Group Frequencies, Third Edition*; John Wiley & Sons, Ltd.: New York, 2004.
187. Turner, A. M.; Abplanalp, M. J.; Kaiser, R. I. *Astrophysical Journal* **2016**, *819*, 97.
188. Kim, H.-W.; Zeroka, D. *Journal of Molecular Structure: THEOCHEM* **2001**, *571*, 59.
189. Bennett, C. J.; Kaiser, R. I. *Astrophysical Journal* **2005**, *635*, 1362.

190. Ennis, C. P.; Bennett, C. J.; Kaiser, R. I. *Physical Chemistry Chemical Physics* **2011**, *13*, 9469.
191. de Barros, A.; da Silveira, E.; Bergantini, A., et al. *Astrophysical Journal* **2015**, *810*, 156.
192. Zondlo, M. A.; Onasch, T. B.; Warshawsky, M. S., et al. *Journal of Physical Chemistry B* **1997**, *101*, 10887.
193. Maté, B.; Medialdea, A.; Moreno, M. A., et al. *Journal of Physical Chemistry B* **2003**, *107*, 11098.
194. Horn, A.; Banham, S.; McCoustra, M. *Journal of the Chemical Society, Faraday Transactions* **1995**, *91*, 4005.
195. Abplanalp, M. J.; Kaiser, R. I. *Astrophysical Journal* **2017**, *836*, 195.
196. Buchwald, V. *Philosophical Transactions of the Royal Society A* **1977**, *286*, 453.
197. Sears, D. W. *Earth and Planetary Science Letters* **1978**, *41*, 128.
198. Horsman, G. P.; Zechel, D. L. *Chemical Reviews* **2016**, *117*, 5704.
199. Bryant, D. E.; Greenfield, D.; Walshaw, R. D., et al. *International Journal of Astrobiology* **2009**, *8*, 27.
200. Pasek, M.; Herschy, B.; Kee, T. P. *Origins of Life and Evolution of the Biosphere* **2015**.
201. Pasek, M. A.; Harnmeijer, J. P.; Buick, R., et al. *Proceedings of the National Academy of Sciences* **2013**, *110*, 10089.
202. Abplanalp, M. J.; Förstel, M.; Kaiser, R. I. *Chemical Physics Letters* **2016**, *644*, 79.
203. Abplanalp, M. J.; Gozem, S.; Krylov, A. I., et al. *Proceedings of the National Academy of Sciences* **2016**, 201604426.
204. Pasek, M. A.; Gull, M.; Herschy, B. *Chemical Geology* **2017**, *475*, 149.
205. Keefe, A. D.; Miller, S. L. *Journal of Molecular Evolution* **1995**, *41*, 693.
206. Turner, A. M.; Abplanalp, M. J.; Blair, T. J., et al. *Astrophysical Journal Supplement* **2018**, *234*, 6.
207. Withnall, R.; Andrews, L. *Journal of Physical Chemistry* **1988**, *92*, 4610.
208. Withnall, R.; Andrews, L. *Journal of Physical Chemistry* **1987**, *91*, 784.
209. Zinbo, M.; Sherman, W. R. *Tetrahedron letters* **1969**, *10*, 2811.
210. Butts, W. C.; Rainey, W. T. *Analytical chemistry* **1971**, *43*, 538.
211. Little, J. L. *Journal of Chromatography A* **1999**, *844*, 1.
212. Harvey, D.; Horning, M. *Journal of Chromatography A* **1973**, *76*, 51.
213. Peterson, K. A.; Woon, D. E.; Dunning Jr, T. H. *Journal of Chemical Physics* **1994**, *100*, 7410.
214. Peterson, K. A.; Dunning Jr, T. H. *Journal of Physical Chemistry* **1995**, *99*, 3898.
215. Zheng, W.; Kim, Y. S.; Kaiser, R. I. *Physical Chemistry Chemical Physics* **2011**, *13*, 15749.
216. Zheng, W.; Jewitt, D.; Kaiser, R. I. *Astrophysical Journal* **2006**, *639*, 534.
217. Hamilton, P. A.; Murrells, T. P. *Journal of Physical Chemistry* **1986**, *90*, 182.
218. Schmidt, M. W.; Yabushita, S.; Gordon, M. S. *Journal of Physical Chemistry* **1984**, *88*, 382.
219. Nava, D. F.; Stief, L. J. *Journal of Physical Chemistry* **1989**, *93*, 4044.
220. Stief, L.; Payne, W.; Nava, D. *Journal of Chemical Physics* **1987**, *87*, 2112.
221. Turner, A. M.; Bergantini, A.; Abplanalp, M., et al. *Nature Communicatins* **2018**, submitted.
222. Jones, B. M.; Kaiser, R. I. *Journal of Physical Chemistry Letters* **2013**, *4*, 1965.
223. Morrison, R.; Boyd, R.; Englewood Cliffs, NJ: Prentice Hall: 1992.
224. Kim, Y. S.; Kaiser, R. I. *Astrophysical Journal* **2010**, *725*, 1002.
225. Kim, Y.; Kaiser, R. *Astrophysical Journal* **2012**, *758*, 37.
226. Snyder, L. E.; Buhl, D. *Astrophysical Journal* **1971**, *163*, L47.
227. Solomon, P.; Jefferts, K.; Penzias, A.; Wilson, R. *Astrophysical Journal Letters* **1971**, *168*, L107.
228. Ziurys, L. M.; Schmidt, D. R.; Bernal, J. J. *Astrophysical Journal*, **2018**, *856*, 169.

PUBLICATION LIST

First Authorship

1. A. M. Turner, M. J. Abplanalp, S. Y. Chen, Y. T. Chen, A. H. H. Chang, R. I. Kaiser, *A Photoionization Mass Spectroscopic Study on the Formation of Phosphanes in Low Temperature Phosphine Ices*, Physical Chemistry Chemical Physics, 17, 27281-27291 (2015).

2. A. M. Turner, M. J. Abplanalp, R. I. Kaiser, *Probing the Carbon-phosphorus Bond Coupling in Low-temperature Phosphine (PH_3)-Methane (CH_4) Interstellar Ice Analogues*, The Astrophysical Journal 819, 97 (2016).

3. A. M. Turner, M. J. Abplanalp, R. I. Kaiser, *Mechanistic Studies on the Radiolytic Decomposition of Perchlorates on the Martian Surface*, The Astrophysical Journal, 820, 127 (2016).

4. A. M. Turner, M. J. Abplanalp, T. J. Blair, R. Dayuha, R. I. Kaiser, *An Infrared Spectroscopic Study* t*oward the Formation of Alkyl phosphonic Acids and their Precursors in Extraterrestrial Environments*. The Astrophysical Journal Supplement, 234, 6 (2018).

5. A. M. Turner, A. Bergantini, M. J. Abplanalp, C. Zhu, S. Góbi, B.-J. Sun, K.-H. Chao, A. H. H. Chang, C. Meinert, R. I. Kaiser, *An Interstellar Origin of Phosphorus Oxoacids*. Submitted for publication.

6. A. M. Turner, M. J. Abplanalp, A. Bergantini,R. Frigge, C. Zhu, B.-J. Sun, A. H. H. Chang, C. Meinert, R. I. Kaiser, *Synthesis of Alkyl phosphonic Acids in Interstellar Analogue Ices—A Promising Extraterrestrial Origin of Prebiotic Phosphorus Compounds*. Prepared for submission.

Co-authorship

1. L. Zhou, S. Maity, M. J. Abplanalp, A. M. Turner, R. I. Kaiser, *On the Radiolysis of Ethylene Ices by Energetic Electrons and Implications to the Extraterrestrial Hydrocarbon Chemistry,* The Astrophysical Journal, 790, 38 (2014).

2. B. M. McMurtry, A. M. Turner, S. E. J. Saito, R. I Kaiser, *On the Formation of Niacin (Vitamin B3) and Pyridine Carboxylic Acids in Interstellar Model Ices,* Chemical Physics, 472, 173 (2016).

3. B. M. McMurtry, S. E. J. Saito, A. M. Turner, H. K. Chakravarty, R. I Kaiser, *On the Formation of Benzoic Acid and Higher Order Benzene Carboxylic Acids in Interstellar Model Ice Grains*, The Astrophysical Journal, 831, 174 (2016).

4. S. Góbi, A. Bergantini, A. M. Turner, R.I. Kaiser, *Electron Radiolysis of Ammonium Perchlorate: A Reflectron Time-of- Flight Mass Spectrometric Study,* Journal of Physical Chemistry A, 121, 3879-3890 (2017).

5. M. J. Abplanalp, S. Góbi, A. Bergantini, A. M. Turner, R. I. Kaiser, *On The Synthesis of Chocolate Flavovoids (Propanols, Butanals) in the Interstellar Medium,* ChemPhysChem, doi: 10.1002/cphc.201701350, (2018).

6. C. Zhu, A. M. Turner, M. J. Abplanalp, R. I. Kaiser, *Formation of High Order Carboxylic Acids (RCOOH) in Interstellar Analogous Ices of Carbon Dioxide (CO_2) and Methane (CH_4).* The Astrophysical Journal Supplement, 234, 15 (2018).

7. C. Zhu, R. Frigge, A. M. Turner, R. I. Kaiser, B.-J. Sun, S.-Y. Chen, A. H. H. Chang, *First Identification of Phosphino Formic Acid (H_2PCOOH)—A Previously 'Unstable' Molecule*, Chemical Communications, Submitted for publication.

8. R. Frigge, C. Zhu, A. M. Turner, M. J. Abplanalp, A. Bergantini, B.-J. Sun, Y.-L. Chen, A. H. H. Chang, R. I. Kaiser, *A Vacuum Ultra Violet Photoionization Study on the Formation of N-Methyl Formamide ($HCONHCH_3$) in Deep Space—A Potential Interstellar Molecule with a Peptide Bond,* The Astrochemical Journal. Submitted for publication.

9. R. Frigge, A. M. Turner, M. J. Abplanalp, B.-J. Sun, Y.-L. Chen, A. H. H. Chang, R. I. Kaiser, *A Vacuum Ultraviolet Photoionization Study on the Formation of Methylamine (CH_2NH) and Ethylenediamine ($NH_2CH_2CH_2NH_2$) in Low Temperature Interstellar Model Ices Exposed to Ionizing Radiation*, The Astrophysical Journal. Submitted for publication.

Conference Presentations

1. A. M. Turner, T. J. Blair, R. Dayuha, R. I. Kaiser, *Formation of alkyl phosphonic acids using phosphine ices*, Experimental Laboratory Astrophysics Workshop (ICE-2013), Kauai, HI, February 25-27, 2013 [poster]

2. A. M. Turner, R. I. Kaiser, R. Dayuha, *Formation of alkyl phosphonic acids using phosphine ices*, ACS 246rd National Meeting, Indianapolis, IN, September 8^{-1}2, 2013 [poster]

3. A. M. Turner, M. J. Abplanalp, R. I. Kaiser, *Production of Open-Chain Phosphanes and Alkyl-Phosphanes in Astrochemical Ice Analogues*, Experimental Laboratory Astrophysics Workshop (ICE-2015), Kauai, HI, February 23-26, 2015 [oral]

4. A. M. Turner, R. I. Kaiser, M. J. Abplanalp, *Laboratory synthesis of alkyl phosphanes in astrochemical ice analogs*, Pacifichem 2015, Honolulu, HI, December 15-20, 2015 [poster]

5. A. M. Turner, R. I. Kaiser, *Toward the formation of alkyl phosphonic acids in phosphine ices*, AAS Division for Planetary Sciences 48th /European Planetary Science Congress 11th Annual Meeting, Pasadena, CA, October 16-21, 2016 [oral]

6. A. M. Turner, R. I. Kaiser, *Investigating the formation of alkyl phosphonic acids in phosphine ices*, ACS 253rd National Meeting, San Francisco, CA, April 2-6, 2017 [oral]